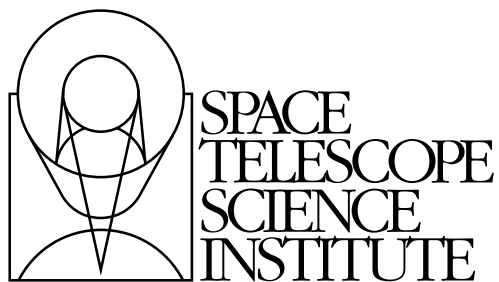

Version 3.0
December 2010

Cosmic Origins Spectrograph Instrument Handbook for Cycle 19



Space Telescope Science Institute
3700 San Martin Drive
Baltimore, Maryland 21218
help@stsci.edu

User Support

For prompt answers to any question, please contact the STScI Help Desk.

- Send e-mail to: help@stsci.edu.
- Phone: 410-338-1082.
- Within the USA, you may call toll free: 1-800-544-8125.

World Wide Web

Information and other resources are available on the STScI COS World Wide Web site:

<http://www.stsci.edu/instruments/cos>

COS Handbook History

Version	Date	Editors
3.0	December 2010	Dixon, W. V.
2.0	January 2010	Dixon, W. V., and Niemi, S.-M.
1.0	December 2007	Soderblom, D. R.

Additional Contributors

Please see the acknowledgments.

Citation

In publications, please refer to this document as
Dixon, W. V., et al. 2010, Cosmic Origins Spectrograph Instrument
Handbook, Version 3.0 (Baltimore: STScI)

Send comments or corrections to:
Space Telescope Science Institute
3700 San Martin Drive
Baltimore, Maryland 21218
E-mail: help@stsci.edu



Table of Contents

Acknowledgments	ix
Chapter 1:	
Introduction	1
1.1 Purpose of This Handbook	1
1.2 Document Conventions	2
1.3 COS FAQ	2
Chapter 2: Special Considerations for Cycle 19	3
2.1 Observing below 1150 Å with G130M	3
2.2 Time-Dependent Sensitivity Changes	3
2.3 SNAP Programs with COS	4
2.4 Should I Use COS or STIS?	4
Chapter 3: An Introduction to COS	7
3.1 The Location of COS in the HST Focal Plane	7
3.2 The COS User Coordinate System	7
3.3 The Optical Design of COS	10
3.3.1 External Shutter	10
3.3.2 The Apertures and Aperture Mechanism	11
3.3.3 Gratings and Mirrors: The Optics Select Mechanisms	12
3.3.4 Detectors	15
3.4 Size of a Resolution Element	15
3.5 Basic Instrument Operations	16
3.5.1 Target Acquisitions	16
3.5.2 Observing Modes: Spectroscopic and Imaging	16
3.5.3 Observing Modes: TIME-TAG and ACCUM	16
3.5.4 Typical Observing Sequences	17
3.6 COS Quick Reference Guide	17

Chapter 4: Description and Performance of the COS Detectors	20
4.1 The FUV XDL Detector.....	20
4.1.1 XDL Properties	20
4.1.2 XDL Spectrum Response.....	21
4.1.3 XDL Background Rate	21
4.1.4 XDL Read-out Format	22
4.1.5 Stim Pulses.....	23
4.1.6 Pulse-height Distributions.....	23
4.1.7 Gain Sag.....	24
4.1.8 Non-linear Photon Counting Effects (Dead Time).....	25
4.1.9 Structures in the Dark Images.....	25
4.2 The NUV MAMA Detector	26
4.2.1 MAMA Properties	26
4.2.2 MAMA Spectrum Response.....	27
4.2.3 MAMA Background Rate.....	27
4.2.4 MAMA Read-out Format	27
4.2.5 MAMA Dead Time.....	28
Chapter 5: The COS Line-Spread Function	29
5.1 Mid-Frequency Wavefront Errors	29
5.2 First Results.....	30
5.3 Non-Gaussian Wings in the MAMA PSF	31
5.4 Quantifying the Resolution	31
5.5 Impact on Equivalent Width Measurements.....	32
Chapter 6: Spectroscopy with COS	35
6.1 The Capabilities of COS	35
6.1.1 First-Order Sensitivity	36
6.1.2 Observing below 1150 Å	38
6.1.3 Second-Order Sensitivity	39
6.1.4 Time-Dependent Sensitivity Changes	40
6.1.5 Zero-Order Image	40
6.1.6 Spectroscopic Resolving Power.....	40
6.1.7 Spatial Resolution and Field of View	41
6.1.8 Photometric (Flux) Precision	42
6.1.9 Wavelength Accuracy.....	42
6.1.10 Internal Scattered Light	43

6.1.11 Vignetting of the NUV Channel	44
6.2 TIME-TAG vs. ACCUM Mode	45
6.2.1 TIME-TAG Mode	45
6.2.2 ACCUM Mode	46
6.3 Valid Exposure Times	47
6.4 Estimating the BUFFER-TIME in TIME-TAG Mode	47
6.4.1 Faint Targets (BUFFER-TIME > Exposure Time)	48
6.4.2 Bright Targets (BUFFER-TIME < 110 Seconds)	48
6.4.3 Very Bright Targets (BUFFER-TIME < 80 Seconds)	49
6.4.4 BUFFER-TIME and AUTO-ADJUST	49
6.5 Spanning the Gap with Multiple CENWAVE Settings	49
6.6 FUV Single-Segment Observations	50
6.7 Internal Wavelength Calibration Exposures	50
6.7.1 Concurrent Wavelength Calibration with TAGFLASH	51
6.7.2 AUTO Wavecalcs (when TAGFLASH is not used)	51
6.7.3 GO Wavecalcs (User-specified)	53
6.7.4 No-Cal Wavecalcs	53
6.8 Fixed-Pattern Noise	53
6.8.1 COS Flat Fielding	53
6.8.2 Use of Optional Parameter FP-POS	55
6.8.3 A Simple Example	57
6.9 COS Spectroscopy of Extended Sources	57
6.10 Wavelength Settings and Ranges	58
Chapter 7: Imaging with COS	61
7.1 Introduction to COS Imaging	61
7.2 Sensitivity	63
7.3 Image Characteristics	64
Chapter 8: Target Acquisitions	66
8.1 Introduction	66
8.2 Target Acquisition Overview	67
8.3 ACQ/SEARCH Acquisition Mode	68
8.3.1 Description	68
8.3.2 Performance	70
8.3.3 Effect of NUV Detector Background	71

8.4 ACQ/IMAGE Acquisition Mode	72
8.4.1 Description	72
8.4.2 Performance	73
8.5 ACQ/PEAKXD Acquisition Mode	74
8.5.1 Description	74
8.5.2 Performance	74
8.5.3 Effects of FUV Detector Distortions	74
8.6 ACQ/PEAKD Acquisition Mode	75
8.6.1 Description	75
8.6.2 Performance	75
8.7 Exposure Times	76
8.7.1 Imaging Acquisitions	76
8.7.2 Dispersed-Light Acquisitions	77
8.8 Centering Accuracy and Data Quality	77
8.8.1 Centering Accuracy and Photometric Precision	78
8.8.2 Centering Accuracy and Wavelength Accuracy	78
8.8.3 Centering Accuracy and Spectroscopic Resolution	79
8.9 Recommended Parameters for all COS TA Modes	79
8.10 Special Cases	81
8.10.1 Early Acquisitions and Preliminary Images	81
8.10.2 Offset Target Acquisitions	81
8.10.3 Acquisition Failure Actions and Diagnostics	81
Chapter 9: Bright-Object Protection	82
9.1 Introduction	82
9.2 Screening Limits	83
9.3 Screening versus Data-Rate Limits	83
9.4 Source V or Flux Limits	84
9.5 Policies and Procedures	87
9.6 On-Orbit Protection Procedures	90
Chapter 10: Overheads and Orbit	
Usage Determination	92
10.1 Observing Overheads	92
10.2 Generic Observatory Overheads	93
10.3 Spectral Element Movement Overheads	94
10.4 Acquisition Overheads	95

10.5 Science Exposure Overheads.....	95
10.6 First Exposure Overhead Adjustment	96
10.7 Examples of Orbit Estimates	97
10.7.1 FUV Acquisition plus TIME-TAG.....	97
10.7.2 NUV Acquisition plus TIME-TAG	98
10.7.3 NUV plus FUV TIME-TAG.....	98
10.7.4 FUV TIME-TAG with BOA and FLASH=NO	99
10.7.5 FUV TIME-TAG with Multiple FP-POS	101

Chapter 11: Exposure-Time

Calculator (ETC)	102
11.1 The COS Exposure Time Calculators	102
11.2 Imaging Observations of Red Objects	103
11.3 Sensitivity, Count Rate, and S/N.....	104
11.4 Detector and Sky Backgrounds.....	104
11.4.1 Detector dark background.....	104
11.4.2 Earthshine	106
11.4.3 Zodiacal Light.....	106
11.4.4 Geocoronal Airglow Emission.....	108
11.4.5 Tabular Sky Backgrounds.....	109
11.5 Extinction Correction	111
11.6 Examples.....	112
11.6.1 A Flat-spectrum Source	112
11.6.2 An Early-type Star	113
11.6.3 A Solar-Type Star with an Emission Line	113
11.6.4 A Faint QSO	114

Chapter 12: Data Products

and Data Reduction	115
12.1 Overview.....	115
12.2 COS Data Files.....	116
12.3 Additional COS Files.....	117

Chapter 13:

The COS Calibration Program	118
13.1 Introduction.....	118
13.2 Ground Testing and Calibration	119

13.3 SMOV4 Testing and Calibration.....	119
13.4 Cycle 17 Calibration Program.....	120
13.5 Cycle 18 Calibration Program.....	122
13.6 Cycle 19 Calibration Plans.....	122
Chapter 14: Spectroscopic	
Reference Material	123
14.1 Introduction.....	123
14.2 Using the Information in this Chapter.....	124
14.2.1 Grating Parameters.....	124
14.2.2 Wavelength Ranges.....	124
14.2.3 Grating Sensitivities and Effective Areas.....	124
14.2.4 Signal-to-Noise Plots.....	124
14.3 Gratings.....	127
14.4 Line-Spread Functions.....	152
Appendix A: Spectrograph Design	
Parameters	157
A.1 FUV Channel.....	157
A.2 NUV Gratings.....	158
Glossary	160
Index	165

Acknowledgments

The technical and operational information contained in this handbook is the summary of the experience gained by members of the STScI COS Team and by the COS IDT at the University of Colorado in Boulder.

Current and former members of the STScI COS Team include Alessandra Aloisi (lead), Tom Ake, Rossy Diaz, Van Dixon, Tom Donaldson, Linda Dressel, Scott Friedman, Parviz Ghavamian, Paul Goudfrooij, Phil Hodge, Mary Beth Kaiser, Tony Keyes, Claus Leitherer, Matt McMaster, Melissa McGrath, Derck Massa, Sami Niemi, Cristina Oliveira, Rachel Osten, Charles Proffitt, David Sahnou, Ken Sembach, Brittany Shaw, Ed Smith, David Soderblom, Katya Verner, Nolan Walborn, Alan Welty, and Brian York. All of these individuals contributed to this volume, as did Russ Makidon.

The COS IDT includes James Green (Principal Investigator), Cynthia Froning (Project Scientist), Steven Penton, Steven Osterman (Instrument Scientist), Stéphane Béland, Eric Burgh, Charles Danforth, Kevin France, and Brian Keeney, all of whom provided information and assistance. COS co-investigators are Dennis Ebbets (Ball Aerospace), Sara R. Heap (GSFC), Claus Leitherer (STScI), Jeffrey Linsky (University of Colorado), Blair D. Savage (University of Wisconsin-Madison), Ken Sembach (STScI), J. Michael Shull (University of Colorado), Oswald Siegmund (University of California, Berkeley), Theodore P. Snow (University of Colorado), John Spencer (Southwest Research Institute), and John T. Stocke (University of Colorado). K. Brownsberger, J. Morse, and E. Wilkinson have also been part of the COS IDT and have made significant contributions.

The prime contractor for COS is Ball Aerospace, Boulder, Colorado. The XDL detector was built at UC Berkeley by O. Siegmund, J. McPhate, J. Vallergera, and B. Welsh.

The Editor thanks Susan Rose (Senior Technical Editor) for her contributions to the production of this handbook.

References and Additional Information

This document relies heavily on information provided by the COS team in Boulder. The primary documents used are

Morse, J. 2004, Cosmic Origins Spectrograph Science Operations Requirements Document (referred to as OP-01);

Wilkinson, E. 2002, COS Calibration Requirements and Procedures, rev. B. (referred to as AV-03); and

Wilkinson, E. 2008, COS Prelaunch Calibration Data (referred to as AV-04).

We also used the *STIS Instrument Handbook* (Kim Quijano et al. 2007, v8.0).

Introduction

In this chapter...

1.1 Purpose of This Handbook / 1

1.2 Document Conventions / 2

1.3 COS FAQ / 2

1.1 Purpose of This Handbook

The *COS Instrument Handbook* describes the design, performance, operation, and calibration of COS. It is meant to be the principal reference manual for users of the Cosmic Origins Spectrograph. This handbook is written and maintained at STScI. While it presents the best available information about COS, tabulated parameters are likely to evolve as we learn more about its on-orbit performance.

The handbook is designed for readers who are

- preparing a Phase I proposal to observe with *HST*;
- writing a Phase II program once a proposal has been accepted; or
- analyzing data from observations that have already been made.

This handbook is not meant to be the primary reference for COS data reduction or analysis; that information is provided in the [COS Data Handbook](#). For quick reference, information on COS data products is provided in [Chapter 12](#).

1.2 Document Conventions

This document follows the usual STScI conventions:

- Terms, words, or phrases that are to be entered by the user in a literal way in an HST proposal are shown in a typewriter or Courier font, such as “COS/FUV” or “TIME-TAG”
- Names of software packages or commands (such as **calcos**) are shown in boldface.
- Wavelengths in this handbook and in COS data products are always as measured in vacuum and are quoted in Ångstroms (Å).

1.3 COS FAQ

Table 1.1: COS Frequently-Asked Questions

Question	Answer
Should I use COS or STIS? Does COS have an imaging mode?	Section 2.4 Chapter 7
What detectors are available? What apertures? What gratings? What are their properties?	Chapter 4 Section 3.3.2 Tables 6.1, 6.4, 6.5
What do COS images look like? What do COS spectra look like? Do the spectra have gaps?	Figure 7.1 Figures 4.2, 4.5 Section 6.5
What is the difference between ACCUM and TIME-TAG mode? How do I calculate the BUFFER-TIME for TIME-TAG exposures? How do I obtain wavelength-calibration exposures?	Section 6.2 Section 6.4 Section 6.7
What are the science impacts of the COS line-spread function? What is the COS sensitivity below 1150 Å? Which COS gratings suffer from second-order contamination?	Chapter 5 Figure 6.3 Section 6.1.3
How accurate is COS absolute/relative photometry? How accurate are the COS wavelength scale and zero point?	Section 6.1.8 Section 6.1.9
How do I plan a successful target acquisition?	Chapter 8
What are the bright-object limits? How do I confirm that my target/field is safe to observe?	Table 9.1 Section 9.5
How much time should I request for my observations?	Chapter 10

Special Considerations for Cycle 19

In this chapter...

2.1 Observing below 1150 Å with G130M / 3
2.2 Time-Dependent Sensitivity Changes / 3
2.3 SNAP Programs with COS / 4
2.4 Should I Use COS or STIS? / 4

2.1 Observing below 1150 Å with G130M

Two new G130M central-wavelength settings, 1055 and 1096 Å, will be available for Cycle 19. They span the 900-1300 Å bandpass, providing both effective area and spectral resolution greater than those of the G140L grating at comparable wavelengths, though their resolution is substantially lower than that of the G130M modes currently in use. These new cenwave settings have $R \sim 3000-1000$ (decreasing with increasing wavelength), with an effective area of 20 cm² between 900 and 1050 Å, increasing rapidly to > 1000 cm² at 1150 Å. Using the new G130M settings with only detector segment B turned on will allow COS to observe, in the 900-1085 Å range, targets that are too bright at longer wavelengths. (In this configuration, the spectral wavelengths will not be corrected for mechanism drift or zero-point offsets.) See [Section 6.1.2](#) for details.

2.2 Time-Dependent Sensitivity Changes

The throughput of some COS modes—the bare-aluminum NUV G225M and G285M gratings and the FUV channels—has declined with time more rapidly than was initially expected ([Section 6.1.4](#)), and the FUV detector is beginning to show evidence of gain sag in regions exposed to the bright Lyman α airglow line ([Section](#)

4.1.7). Even so, the COS FUV sensitivity is still outstanding, and COS will remain the instrument of choice for most spectroscopic observations of faint FUV targets.

The figures and tables in this handbook were constructed using projected instrumental sensitivities for the middle of Cycle 18 (2011 April). Observers are reminded to use the COS Exposure Time Calculator (ETC; see [Chapter 11](#)) to design their proposals; it will be updated with sensitivity curves appropriate for Cycle 19 in time for the Phase II proposal deadline. One exception: both this handbook and the Phase I version (19.1) of the COS ETC use projected values for the NUV dark rate appropriate for the middle of Cycle 19 (2012 April).

2.3 SNAP Programs with COS

The COS photon-counting detectors can be harmed by exposure to bright light. Because all COS observations must be checked at STScI by an Instrument Scientist to confirm that both the intended target and all nearby objects lie within safe-brightness limits, the total number of targets accepted for all COS and STIS MAMA SNAP programs will be limited to 150 per cycle. For more information on this and other policies pertaining to *HST* observing, please see the [Call for Proposals](#).

2.4 Should I Use COS or STIS?

With the installation of COS and the repair of STIS, *HST* has two spectrographs with significant overlap in spectral range and resolving power. Each has unique capabilities, and the decision of which to use will be driven by the science goals of the program and the nature of the target to be observed.

In the far-UV (from about 1100 to 1800 Å), the throughput of the COS FUV channel exceeds that of the STIS FUV MAMA by factors of 10 to 30, and the combination of the spectroscopic resolving power ($\sim 20,000$) and wavelength coverage (300 to 370 Å per setting) of the medium-resolution COS FUV modes results in a discovery space (throughput times wavelength coverage) for observations of faint FUV point sources that is at least 10 times greater for most targets than that of STIS modes with comparable resolution, and is as much as 70 times greater for faint, background-limited point sources.

In the near-UV (approximately 1700 to 3200 Å), COS and STIS have complementary capabilities. To accommodate the NUV detector format, the COS NUV spectrum is split into three non-contiguous stripes, each of which covers a relatively small range in wavelength. Obtaining a full NUV spectrum of an object requires several set-ups and exposures (6 or more for the medium-resolution gratings and 4 for G230L). When broad NUV wavelength coverage is needed, obtaining a single STIS spectrum may be more efficient than taking separate COS spectra. Users should also consider that the STIS NUV modes have produced a large set of existing observations, while the COS NUV modes have so far seen limited use. As a result, the calibration of the STIS NUV

modes is likely to be superior to that of comparable COS modes for the foreseeable future.

Because the background count rate for COS/NUV is substantially lower than for STIS, COS will often be superior for faint sources, even when more exposures are required to span the full wavelength coverage. In particular, STIS has significantly higher dark rate in the NUV. As of September 2010, the mean dark rate of the STIS NUV MAMA was about 3.4×10^{-3} counts pixel⁻¹ s⁻¹, about twice the typical pre-SM4 value. The COS dark rate has been increasing with time, but even if current trends continue, the projected mean value of 7.3×10^{-4} counts pixel⁻¹ s⁻¹ for April 2012 will still be several times lower than the rate for STIS. Observers are advised to perform detailed calculations using both the COS and STIS ETCs and to consider carefully the relative instrument overheads to determine which combination of instruments and modes is best for their science.

For observations of extended sources, the spatial resolution offered by STIS must be weighed against the superior sensitivity of COS. One of the primary design goals of STIS was to provide spatially-resolved spectra in the UV, optical, and near-IR. The STIS long slits, when used with the first-order gratings, allow spatially-resolved observations that exploit the intrinsically high resolution of *HST* over the full width of the detectors (approximately 0.05 arcsec per 2-pixel spatial resolution element over a length of 25 arcsec with the NUV and FUV MAMAs, and ~ 0.1 arcsec per 2-pixel spatial-resolution element over a length of 52 arcsec with the CCD).

COS was optimized for point-source observations. While COS has relatively large entrance apertures (2.5 arcsec diameter), flux from regions more than 0.5 arcsec from the aperture center is significantly vignetted. These large apertures also mean that objects extended in the dispersion direction will yield spectra with lower spectral resolution. In addition, the optical design of the FUV channel limits the achievable spatial resolution; measured values of the FWHM in the spatial dimension vary between about 0.25 and 1.5 arcsec, depending on grating and wavelength ([Section 6.1.7](#)). The COS NUV channel uses a different optical design and has a spatial resolution comparable to that of the STIS first-order NUV modes (~ 0.05 arcsec), with somewhat better sampling; however, for sources extending more than 1 arcsec in the spatial direction, the various NUV spectral segments will begin to overlap.

The line-spread functions (LSFs) of both instruments exhibit non-Gaussian wings due to mid-frequency zonal (polishing) errors in the Optical Telescope Assembly (OTA). Using STIS, one can minimize their effects through the use of narrow apertures. On COS, narrow apertures are not available. The broad wings of the COS LSF, especially in the short wavelengths of the FUV band, can affect the detectability of faint, narrow features and blend closely-spaced lines. Studies that require accurate knowledge of the line profile will require full consideration of the COS LSF ([Chapter 5](#)). The non-Gaussian wings of the COS LSF should have only modest impact on science programs targeting broad lines and continuum sources.

Both COS detectors and the STIS MAMA detectors are prohibited from observing objects that exceed specific brightness levels (see [Chapter 9](#) in this handbook and Sections 13.8 and 14.8 of the *STIS Instrument Handbook*). Some brightness limits have been established for the health and safety of the instrument, while others are

practical limits that are set to ensure good data quality. Because STIS is less sensitive than COS, the brightness limits for STIS tend to be significantly less stringent. In the NUV range, the STIS G230LB and G230MB gratings can also be used with the STIS CCD, which has no bright-object limitations. STIS also has a number of small and neutral-density apertures that can be used with the MAMA detectors to attenuate the light of a too-bright object. COS has only a single neutral-density filter that attenuates by a factor of about 200 but also degrades the spectral resolution by a factor of 3 to 5. In most cases, some combination of STIS gratings and apertures will be a better choice for observing a UV-bright object than COS with its neutral-density filter. Users are advised to compare results from the COS and STIS ETCs to decide on an appropriate strategy for their target.

The STIS high-dispersion echelle modes E140H and E230H have resolving powers of $\sim 114,000$ (or even $R \sim 200,000$ with the 0.1×0.03 aperture and specialized data reduction; see Section 12.6, “Improving the Sampling of the Line Spread Function,” of the *STIS Instrument Handbook*), significantly higher than the best COS resolution. Also, STIS can obtain spectra in the optical and near-IR at wavelengths up to 10,200 Å, while the maximum wavelength observable by COS is about 3,200 Å.

Both STIS and COS can perform observations in TIME-TAG mode, whereby the time of each photon’s arrival is recorded. STIS is capable of a much finer time resolution (125 microseconds vs. 32 milliseconds for COS), although few programs require such a high sampling rate. Due to its lower sensitivity, STIS may be able to observe a target in TIME-TAG mode that is too bright for TIME-TAG observations with COS. On the other hand, TIME-TAG data acquired with the COS FUV detector includes information on the pulse-height distribution, while TIME-TAG data acquired with the STIS and COS MAMAs do not. Pulse-height information can be valuable in identifying and rejecting background counts in the spectra of faint sources.

An Introduction to COS

In this chapter...

3.1 The Location of COS in the HST Focal Plane / 7
3.2 The COS User Coordinate System / 7
3.3 The Optical Design of COS / 10
3.4 Size of a Resolution Element / 15
3.5 Basic Instrument Operations / 16
3.6 COS Quick Reference Guide / 17

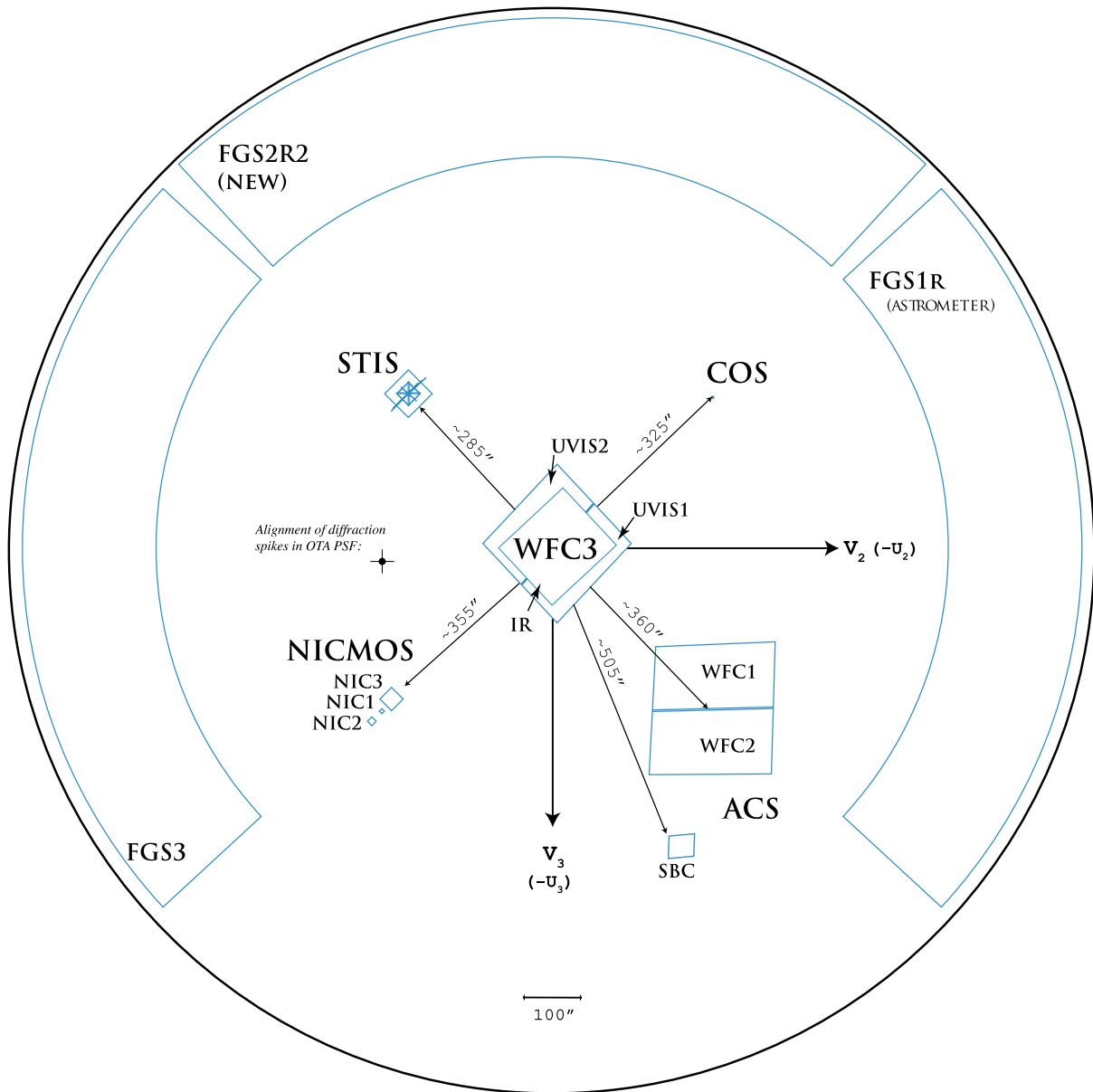
3.1 The Location of COS in the HST Focal Plane

The location of the COS aperture in the *HST* focal plane is shown in [Figure 3.1](#). Note the relative orientation of the *HST* V_2 and V_3 axes (the V_1 axis is along *HST*'s optical axis), as well as the relative locations and orientations of the other instruments. The COS aperture lies ~ 325 arcsec from the V_1 axis in the $+V_2, -V_3$ quadrant.

3.2 The COS User Coordinate System

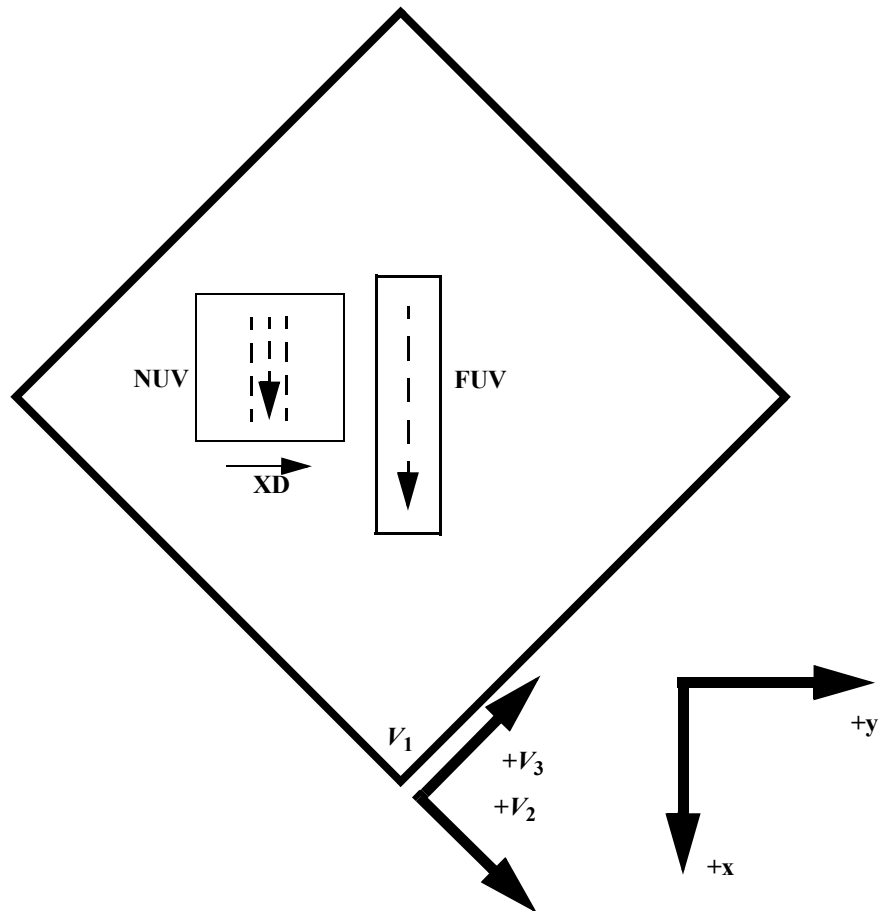
[Figure 3.2](#) presents a schematic layout of the COS focal plane. In this figure, the x and y axes denote the COS user coordinate system. In this system, x lies along the wavelength (dispersion) axis and increases with increasing wavelength for both the FUV and NUV channels. For the NUV channel, y increases with increasing wavelength in the cross-dispersion (XD) direction. All references to COS (including POS TARG specifications in APT, the [Astronomer's Proposal Tool](#), detector pixel coordinates, and science header keywords) employ the user coordinate system.

Figure 3.1: A Schematic View of the *HST* Focal Plane



This drawing shows the entire *HST* focal plane and the apertures of the scientific instruments. The view is from the rear of the telescope looking forward toward the sky, the opposite of the sense of [Figure 3.2](#).

Figure 3.2: Schematic Layout of the COS Detectors

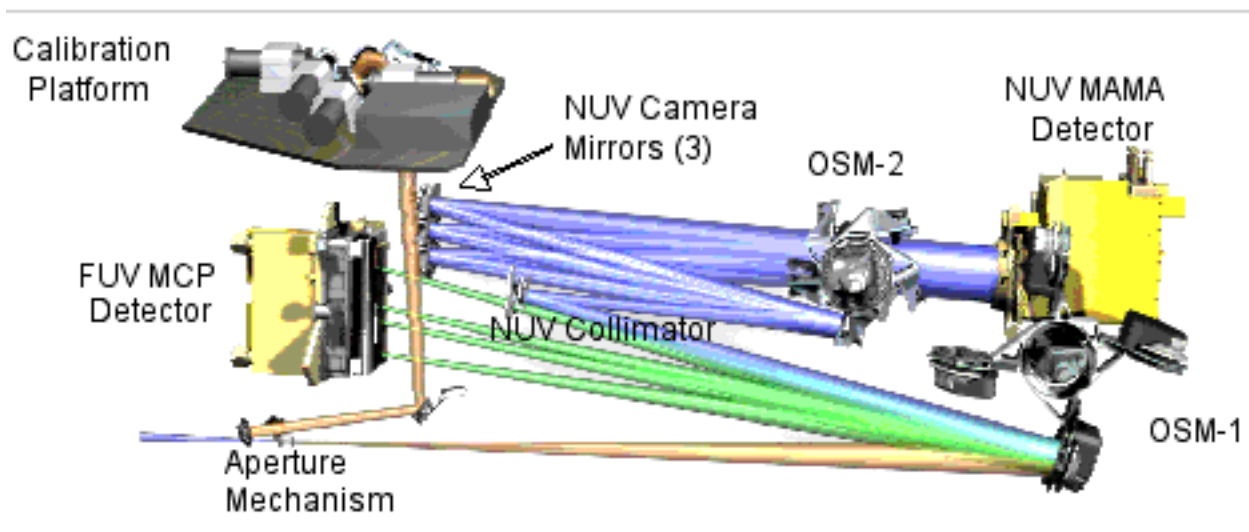


This view is from the front of the telescope looking aft. The dashed arrows show the direction of increasing wavelength for the two detectors, and “XD” indicates the direction of increasing wavelength for the NUV cross-dispersion direction. The x and y axes denote the COS user coordinate system. For both the FUV and NUV channels, wavelength increases in the $+x$ or $(+V_2, -V_3)$ direction. Note that this diagram is purely schematic and it is intended to show only relative directions. This diagram does **not** show the locations of apertures. The bottom corner of this square (at V_1) corresponds to the center of the WF3 camera (see [Figure 3.1](#)).

3.3 The Optical Design of COS

In most spectrographs, the light from the telescope is focused on a slit, and the instrument's optics then re-image the slit onto the detector. In such a design, the slit width and how the slit is illuminated determine the resolving power and line-spread function (LSF). COS is different: it is essentially a slitless spectrograph with an extremely small field of view. In this section, the light from the *HST* Optical Telescope Assembly (OTA) is followed as it progresses through COS to each optical element and mechanism. The optical path and mechanism locations are shown in [Figure 3.3](#).

Figure 3.3: The COS optical path and the locations of the mechanisms



The optical path is drawn to scale, with all elements in proportion and in their correct relative locations.

3.3.1 External Shutter

The external shutter is located at the front of the COS enclosure. When closed, the shutter blocks all external light from entering the COS instrument and prevents light from the COS internal lamps from exiting the instrument. The opening and closing of the external shutter does not define the duration of an exposure, as the shutter may be opened before an exposure begins to allow for target acquisition and bright-object checking.

3.3.2 The Apertures and Aperture Mechanism

After passing through the external shutter, the light from the OTA first encounters one of the COS entrance apertures (Table 3.1), which are mounted on the Aperture Mechanism (ApM). Selecting among these apertures can involve movement of the Aperture Mechanism.

Table 3.1: COS Entrance Apertures.

Aperture	Full name	Purpose	Size (mm)
PSA	Primary Science Aperture	science aperture	0.700 circular
BOA	Bright Object Aperture	science aperture with ND2 filter	0.700 circular
WCA	Wavelength Calibration Aperture	wavecals with Pt-Ne lamp	0.020 × 0.100
FCA	Flat-Field Calibration Aperture	flat field with deuterium lamp	0.750 × 1.750

Primary Science Aperture

The Primary Science Aperture (PSA) is a 2.5 arcsec (700 μm) diameter field stop. It is located, not at the *HST* focal surface, but near the point of the circle of least confusion. This aperture transmits $\geq 95\%$ of the light from a well-centered, aberrated point-source image delivered by the *HST* optics. The PSA is expected to be used for observing in almost all instances. The PSA is in place, ready to use, at the start of a new visit. Note that, when the PSA is in place, the WCA (see below) is also in place and available for use.

Wavelength Calibration Aperture

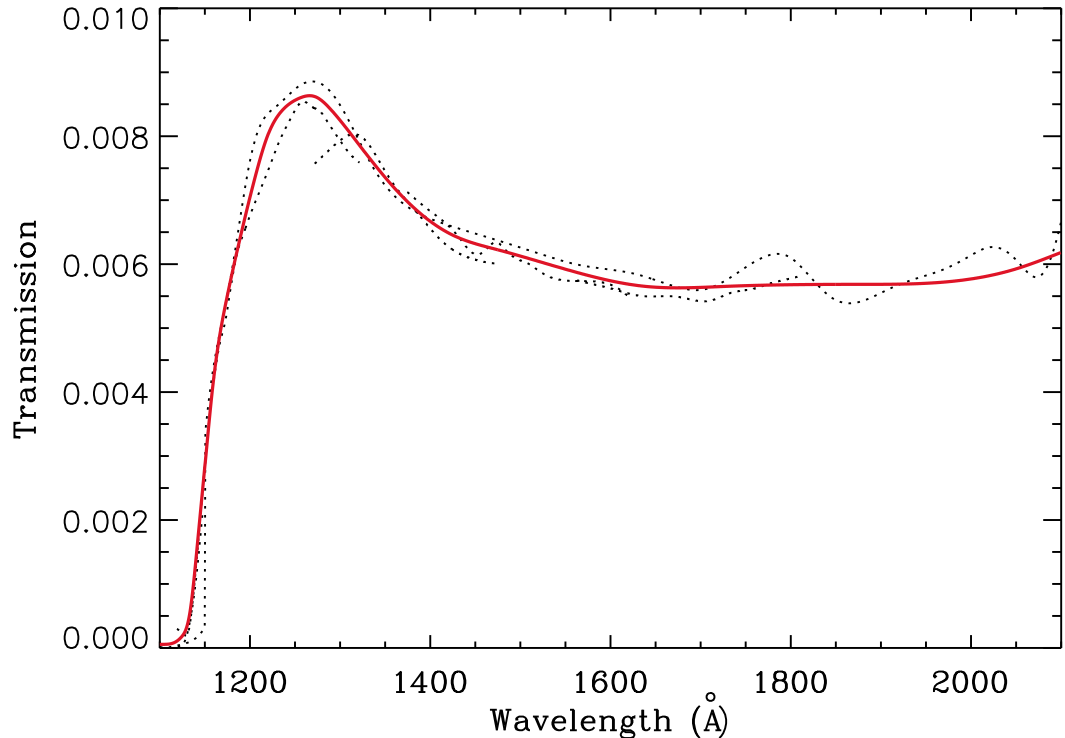
The Wavelength Calibration Aperture (WCA) is offset from the PSA by 2.5 mm (about 9 arcsec) in the cross-dispersion direction. Light from external sources cannot illuminate the detector through the WCA; instead the WCA is illuminated by one of two Pt-Ne wavelength-calibration (wavecal) lamps. The wavecal spectrum is used by **calcos** to assign wavelengths to the science spectra obtained through either the PSA or BOA. The Pt-Ne lamps are also used during acquisitions to provide a reference point from which the center of the target aperture is computed. As noted above, both the PSA and WCA are available for use at the same time and no additional motion of the Aperture Mechanism is needed to obtain a wavecal exposure.

Bright Object Aperture

Like the PSA, the Bright Object Aperture (BOA) is 2.5 arcsec (700 μm) in diameter, but has a neutral-density (ND2) filter immediately behind it. Its attenuation varies with wavelength (Figure 3.4) but is about a factor of 200 at 2000 \AA . The BOA is offset from the PSA by 3.7 mm (about 13 arcsec) in the cross-dispersion direction. For scientific observations, the aperture block is shifted, via movement of the Aperture Mechanism, to place the BOA in the position normally occupied by the PSA. Thus,

spectra obtained through either the PSA or BOA use the same optical path and detector region (for a given channel), and so may employ the same flat-field calibrations. Moving the BOA into place for scientific use shifts the WCA as well, precluding simultaneous use of the WCA for a wavecal exposure. The Aperture Mechanism must be moved to obtain a wavecal exposure when the BOA is used.

Figure 3.4: Transmission of the COS BOA as a Function of Wavelength



Dashed lines represent the ratio of BOA to PSA spectra of the standard star LDS749b obtained using all three FUV gratings. The thick red curve is a spline fit to the dashed curves.

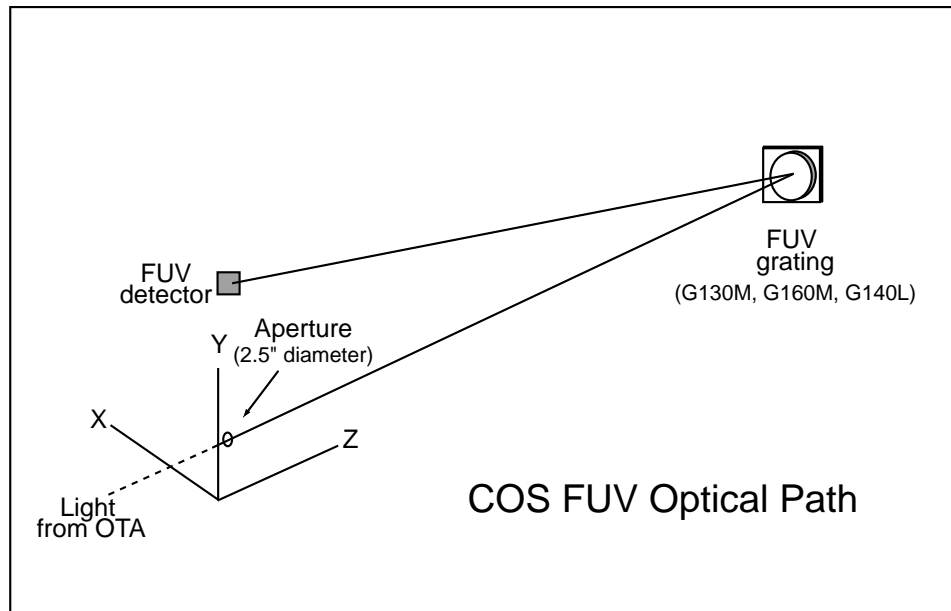
Flat-field Calibration Aperture

The Flat-field Calibration Aperture (FCA) is used only for calibration and is not available to observers. The FCA is used to obtain flat-field exposures using one of the two deuterium hollow-cathode flat-field calibration lamps.

3.3.3 Gratings and Mirrors: The Optics Select Mechanisms

After passing through one of the COS apertures, light next encounters the Optics Select Mechanism 1 (OSM1), a rotating mechanism that can bring one of four optical elements into the beam. One of these, NUV Collimating Mirror (NCM1), is a flat mirror that directs the beam to the NUV channel. The other three elements are gratings for the FUV channel. Note that the FUV and NUV channels cannot be used simultaneously.

Figure 3.5: The COS FUV Optical Path

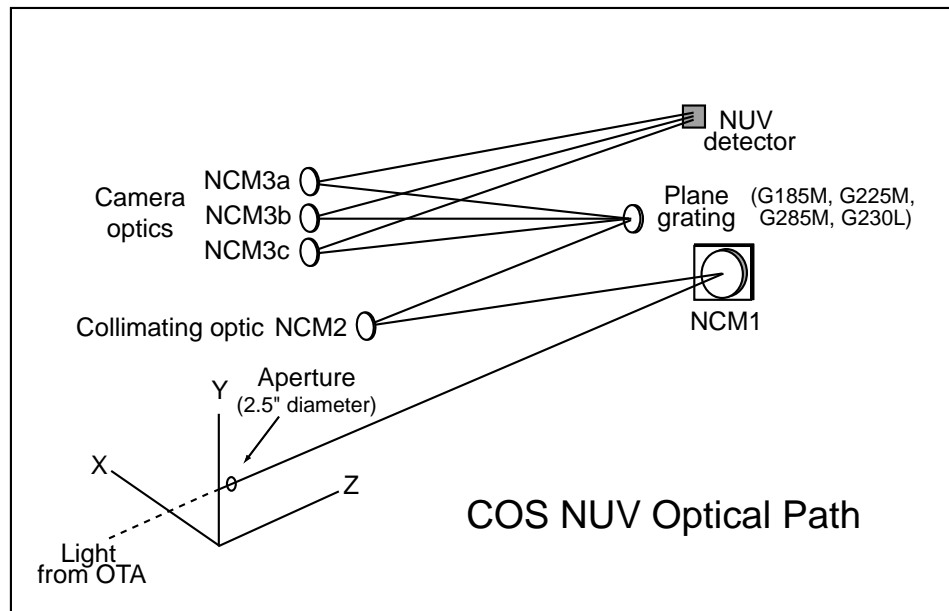


FUV Channel Optical Design

The COS FUV optical path is illustrated schematically in [Figure 3.5](#). To maximize throughput, a single optical element (one of three FUV gratings) is used to disperse the light, focus it onto the detector, and remove the spherical aberration introduced by the *HST* primary mirror. Given the location of OSM1 in the *HST* optical path, it is possible for the FUV gratings to disperse, focus, and correct the beam optimally only for a point source that is centered in the aperture. Performance is degraded when the source is moved away from the aperture center; however, this degradation is low for displacements up to about 0.4 arcsec (see [Section 8.8](#)).

The COS FUV channel provides spectra from 900 to 2150 Å at low and moderate spectral resolution ([Section 6.1](#)). The FUV detector is described fully in [Chapter 4](#), but it is important to note that it consists of two independent segments with a small physical gap between them. Wavelengths falling in the gap are not recorded. Though the gap prevents a single continuous spectrum from being obtained in one setting, the missing wavelengths can be recovered by shifting the grating, as described in [Section 6.5](#). The gap can be made useful: in some configurations, the geocoronal Lyman- α line can be placed there, eliminating the local high count rates that this emission line can cause.

Figure 3.6: The COS NUV Optical Path



OSM2 and the NUV Channel

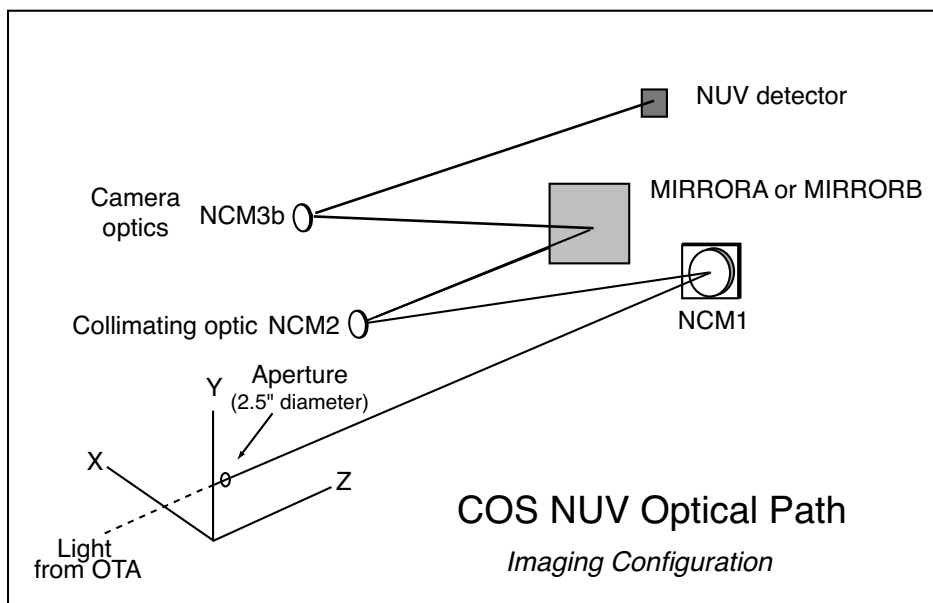
The COS NUV channel, illustrated schematically in [Figure 3.6](#), provides coverage from about 1650 to 3200 Å at low and moderate spectral resolution. If the NUV channel is to be used, OSM1 is turned to place mirror NCM1 in the beam, directing it to the NUV Collimating Mirror 2 (NCM2), which collimates the light, and then to Optics Select Mechanism 2 (OSM2). OSM2 holds five optical elements: four plane diffraction gratings plus a mirror for target acquisitions or imaging.

To accommodate the NUV detector format, dispersed light from the NUV gratings is imaged onto the detector by three parallel mirrors (NCM3a, 3b, 3c). For the medium-dispersion gratings, the spectra appear as three non-contiguous 35-40 Å stripes on the MAMA detector, providing 105-120 Å wavelength coverage per exposure. The low-dispersion grating provides ~ 400 Å per stripe. The layout of the stripes is shown in [Figure 4.5](#). The gratings can be shifted via slight rotations of OSM2 to cover the entire NUV wavelength band. The NCM3 mirrors are spaced such that several correctly-chosen exposures will produce a complete spectrum, from the low end of the short-wavelength stripe to the high end of the long-wavelength stripe.

Imaging with the NUV Mirror

For imaging observations, OSM2 is turned to place a mirror in the light path, rather than a grating ([Figure 3.7](#)). When used in direct specular reflection, this mirror is designated as MIRRORA. For bright targets, the flux can be attenuated by adjusting OSM1 so that the order-sorting filter in front of the mirror reflects the light onto the detector. This configuration is referred to as MIRRORB. COS imaging is described in [Chapter 7](#).

Figure 3.7: COS NUV Optical Path for Imaging Observations



3.3.4 Detectors

The FUV and NUV channels employ separate detectors. The FUV detector is a photon-counting, cross delay line (XDL) device, similar to the *FUSE* detectors. Its two segments are separated by a small gap, as discussed above. The NUV detector is also a photon-counting device, a MAMA (multi-anode micro-channel array) similar to that used by STIS. The COS detectors are more fully described in [Chapter 4](#).

3.4 Size of a Resolution Element

Throughout this document, we assume that a resolution element (resel) spans 6×10 pixels on the FUV detector and 3×3 pixels on the NUV detector ([Table 3.3](#)). These values were determined before launch; even then, it was known that the true size of a resel would vary with wavelength. Preliminary analysis of in-flight data suggests that the FUV resel is somewhat larger than previously assumed (see the discussion of the line-spread function in [Chapter 5](#)), while the NUV resel is smaller. We will continue to refine our analysis of the instrument parameters. In the mean time, keep in mind that the [COS Exposure Time Calculator](#) (ETC) uses the pre-flight resel sizes in all of its calculations. Users who adopt a larger or smaller resel should adjust the ETC results accordingly.

3.5 Basic Instrument Operations

3.5.1 Target Acquisitions

The COS entrance apertures are 2.5 arcsec in diameter. To ensure that the target is centered in the aperture, a target-acquisition procedure must be performed at the beginning of each visit. For moving targets, acquisition should be repeated at the beginning of each orbit.

The COS flight software provides two methods for acquiring and centering a target in the aperture. The first method obtains a direct image of the aperture with the NUV channel and moves the telescope to the center of light. The second method centers the target using its dispersed spectrum and can be performed with either the NUV or FUV channel. For both methods, a target's center of light can be computed from a single exposure or from a series of exposures that map out a grid on the sky. Acquisitions are described in [Chapter 8](#).

3.5.2 Observing Modes: Spectroscopic and Imaging

While COS was designed as a spectrograph, the NUV channel can be used for imaging observations. With a plate scale of 23.5 mas per pixel, COS provides the highest spatial sampling of any instrument aboard *HST*. The image is corrected for the telescope's spherical aberration, but is degraded by zonal (polishing) errors on its primary and secondary mirrors (see [Chapter 5](#)). The NUV imaging count-rate limit of 50 counts per second per pixel ([Table 9.1](#)) corresponds to a *Galex* NUV magnitude of 17.6.

3.5.3 Observing Modes: TIME-TAG and ACCUM

COS provides two spectral observing modes, TIME-TAG and ACCUM. In TIME-TAG mode, the position, arrival time, and (for FUV) pulse height of each detected photon are recorded in the memory buffer. In ACCUM mode, only the location of arriving photons is recorded.

TIME-TAG mode is preferred, because it allows for more sophisticated data reduction. For example, an observer may compare data from the night and day sides of the orbit or compute the count rate of an object whose intensity varies on short time scales. TIME-TAG observations through the PSA allow the taking of occasional wavelength-calibration spectra during an exposure. These spectra are used by the COS data-reduction pipeline **calcos** to correct drifts in the spectrum due to small motions of the optics selection mechanism. ACCUM mode is designed for observations of targets too bright for TIME-TAG mode. Because the lower information content of ACCUM data reduces their utility for archival researchers, its use must be justified for each target.

Both TIME-TAG and ACCUM modes may be used with either the FUV or NUV channel. For more information comparing TIME-TAG and ACCUM, see [Section 6.2](#).

3.5.4 Typical Observing Sequences

In the majority of cases, the following sequence of events will produce high-quality data:

- Acquire the object using ACQ/ IMAGE. This should take about seven minutes. See the examples in [Chapter 10](#).
- Obtain spectra in TIME-TAG mode using multiple FP-POS settings and FLASH=YES so the spectra can be corrected for grid-wire shadows and OSM drifts. The COS ETC provides a means of calculating essential parameters such as the BUFFER-TIME.
- Obtain more spectra during additional orbits to achieve the desired signal-to-noise ratio.

3.6 COS Quick Reference Guide

Table 3.2: COS Instrument Characteristics

Property	FUV channel	NUV channel
Entrance apertures	2.5 arcsec round: clear (PSA) or attenuated (BOA)	
Detector plate scale	0.1 arcsec per pixel 1 arcsec per resel (G130M cross-dispersion)	23.5 mas per pixel 70.5 mas per resel (imaging mode)

Table 3.3: COS Detector Characteristics

		FUV XDL	NUV MAMA
Photocathode		CsI (opaque)	Cs ₂ Te (semi-transparent)
Window		None	MgF ₂ (re-entrant)
Wavelength range		< 900 – 2150 Å	1650 – 3200 Å
Active area		85 × 10 mm (two)	25.6 × 25.6 mm
Pixel format (full detector)		16384 × 1024 (two)	1024 × 1024
Image size recorded per spectrum		16384 × 128 (two, ACCUM) 16384 × 1024 (two, TIME-TAG)	1024 × 1024
Pixel size		6 × 24 μm	25 × 25 μm
Spectral resolution element size (= resel)		6 × 10 pix	3 × 3 pix
Quantum efficiency		~26% at 1335 Å ~12% at 1560 Å	~10% at 2200 Å ~8% at 2800 Å
Typical dark-count rate (away from SAA) ¹		1.25 cnt s ⁻¹ cm ⁻² 1.8 × 10 ⁻⁶ cnt s ⁻¹ pix ⁻¹ 1.1 × 10 ⁻⁴ cnt s ⁻¹ resel ⁻¹	117 cnt s ⁻¹ cm ⁻² 7.3 × 10 ⁻⁴ cnt s ⁻¹ pix ⁻¹ 6.6 × 10 ⁻³ cnt s ⁻¹ resel ⁻¹
Detector global count rate limit ²	TIME-TAG mode	30,000 cnt s ⁻¹ (but counts lost at rates above ~21,000 cnt s ⁻¹)	
	ACCUM mode	~60,000 cnt s ⁻¹ per segment	~170,000 cnt s ⁻¹
Local count-rate limit ²		~1.67 cnt s ⁻¹ pix ⁻¹ ~100 cnt s ⁻¹ resel ⁻¹	~200 cnt s ⁻¹ pix ⁻¹ ~1800 cnt s ⁻¹ resel ⁻¹
Screening limits for bright objects		see Table 9.1	
Dead-time constant		7.4 μsec	280 nsec

1. FUV dark rates were measured in 2010 September; NUV values are projections to the middle of Cycle 19 (2012 April).

2. Count rates higher than these limits will trigger a detector shut-down. Bright-object screening limits are lower. See [Chapter 9](#).

Table 3.4: COS Calibration Accuracies

Property	FUV channel	NUV channel
Wavelength zero point: M gratings	15 km s ⁻¹	15 km s ⁻¹
Wavelength zero point: L gratings	150 km s ⁻¹	175 km s ⁻¹
Wavelength scale	15 km s ⁻¹	15 km s ⁻¹
Absolute photometry	5%	5%
Relative photometry (same object at a different time)	2%	2%
Flat field quality (spectral S/N) per resel, using standard techniques	35:1 ¹	100:1
Flat field quality (spectral S/N) per resel, goal	100:1	100:1

1. S/N of 100:1 is possible; see [Section 6.8.1](#).

Table 3.5: Useful Figures and Tables

Topic	Source	Content
Usage planning	Table 6.1	COS grating parameters
	Table 6.4	FUV grating wavelength ranges
	Table 6.5	NUV grating wavelength ranges
	Table 9.1	COS count-rate screening limits
	Table 11.3	Earthshine and zodiacal light fluxes
	Table 11.4	Strengths of airglow lines
Aperture parameters and PSFs	Figure 3.1	<i>HST</i> focal plane and COS aperture
	Figure 3.4	BOA transmission
	Figure 5.1	Model LSFs for the COS FUV Channel
	Figure 5.2	Model LSFs for the COS NUV Channel
	Figure 5.3	Resolving Power of FUV Gratings
	Figure 7.4	Cross section of the COS imaging PSF
	Figure 8.5	Relative transmission of the COS PSA in the NUV
Effective Area	Figure 6.1	FUV spectroscopy
	Figure 6.2	NUV spectroscopy
	Figure 7.3	NUV imaging
Acquisitions	Figure 8.2	Point-source images with all apertures and mirrors
	Figure 8.1	Example of 3 × 3 spiral search pattern
	Figure 8.3	ACQ/IMAGE exposure times
	Figure 8.4	Dispersed-light exposure times
Detector characteristics	Figure 4.1	FUV XDL detector schematic layout
	Figure 4.5	NUV MAMA detector layout
	Table 11.1	Detector background count rates
Overheads and observing parameters	Table 6.3	TAGFLASH exposure durations
	Table 10.1	Generic observatory overhead times
	Table 10.2	Overhead times for OSM1 movements
	Table 10.3	Overhead times for OSM2 movements
	Table 10.4	Science exposure overhead times
Celestial backgrounds	Figure 11.1	Sky background versus wavelength
	Figure 11.2	Moon, Earth and zodiacal-light background levels
	Figure 11.3	Galactic extinction model
Data quality	Figure 6.8	FUV flat-field example
	Figure 6.9	NUV flat-field example

Description and Performance of the COS Detectors

In this chapter...

4.1 The FUV XDL Detector / 20

4.2 The NUV MAMA Detector / 26

4.1 The FUV XDL Detector

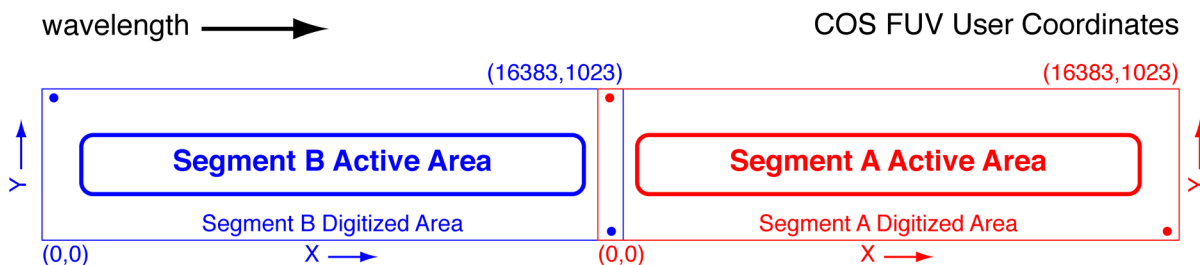
4.1.1 XDL Properties

The COS FUV detector is a windowless cross delay line (XDL) device that is similar to the detectors used on the *Far Ultraviolet Spectroscopic Explorer (FUSE)*. The XDL is a photon-counting micro-channel plate (MCP) detector with two independently-operable segments. Each segment has an active area of 85×10 mm; they are placed end to end and separated by a 9-mm gap. When the locations of detected photons are digitized, they are placed into an array of 16384×1024 pixels, though the active area of the detector is considerably smaller. The long dimension of the array is in the direction of dispersion; increasing pixel number (the detector's x axis in user coordinates) corresponds to increasing wavelength. The XDL format is shown schematically in [Figure 4.1](#).

The FUV XDL is optimized for the 1150-to-1775 Å bandpass, with a cesium iodide photocathode on the front MCP. The front surfaces of the MCPs are curved with a radius of 826 mm to match the curvature of the focal plane. When photons strike the photocathode, they produce photoelectrons that are amplified by a stack of MCPs. The charge cloud that comes out of the MCP stack, several millimeters in diameter, lands on the delay-line anode. There is one anode for each detector segment, and each anode

has separate traces for the dispersion (x) and cross-dispersion (y) axes. The location of an event in each axis is determined by measuring the relative arrival times of the collected charge pulse at each end of the delay-line anode for that axis. The results of this analog measurement are digitized to 14 bits in x and 10 bits in y . In TIME-TAG mode, the total charge collected from the event, called the pulse height, is saved as a 5-bit number.

Figure 4.1: The FUV XDL Detector.



This diagram is drawn to scale, and the slight curvature at the corners is also present on the masks of the flight detectors. Wavelength increases in the direction of the increasing x coordinate. The red and blue dots show the approximate locations of the stim pulses on each segment. The numbers in parentheses show the pixel coordinates at the corner of the segment's digitized area; the two digitized areas overlap in the region of the inter-segment gap.

The detector electronics generate pulses that emulate counts located near the corners of the anode, outside the active area of the MCPs. These “stim pulses” (see [Section 4.1.5](#)) provide a means of tracking and correcting thermal distortions.

The XDL's quantum efficiency is improved by the presence of a series of wires, called the quantum-efficiency (DQE) grid, placed above the detector (*i.e.*, in the light path). These wires create shadows in the spectrum that are flagged by **calcos** during data reduction. The XDL also includes an ion-repeller grid that reduces the background rate by preventing low-energy thermal ions from entering the open-faced detector. They act as a 95% transmission neutral-density filter.

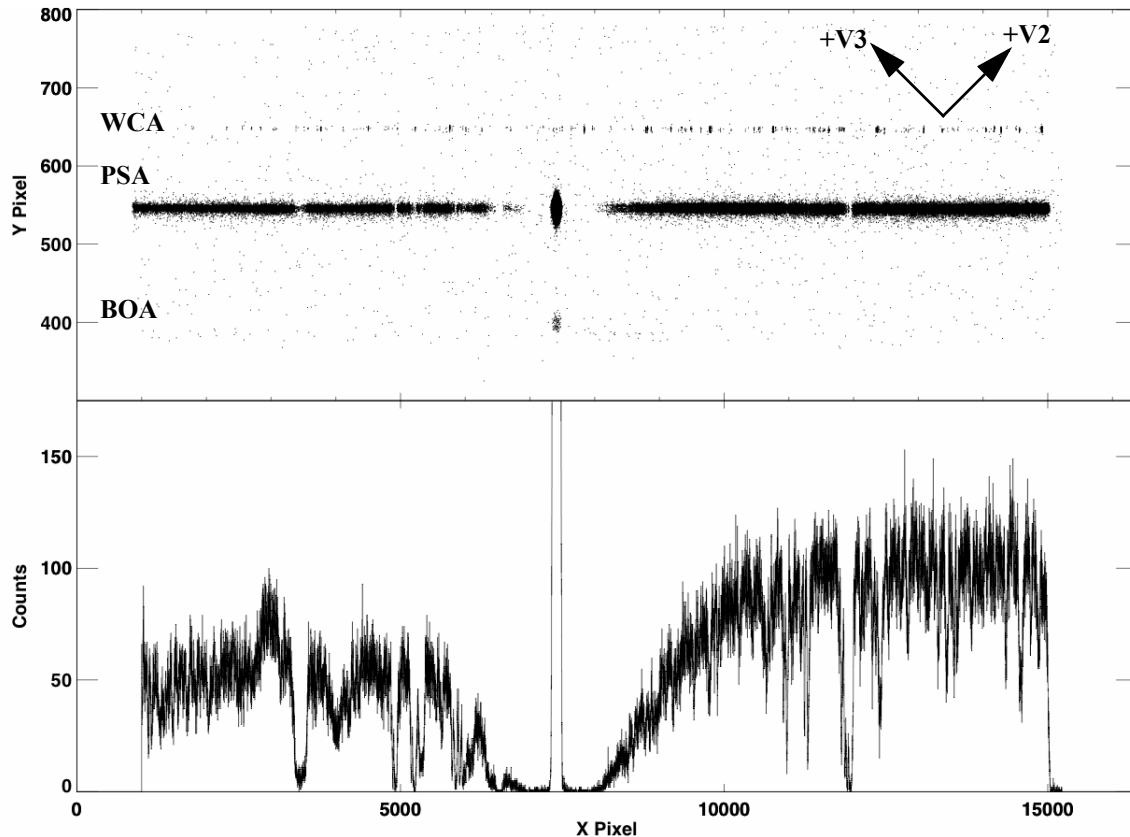
4.1.2 XDL Spectrum Response

COS is considerably more sensitive than STIS and earlier-generation *HST* instruments at comparable spectral resolutions in the FUV. Effective areas for the COS FUV gratings are shown in [Figure 6.1](#). The time-dependent changes in the sensitivity of the COS FUV channel are discussed in [Section 6.1.4](#).

4.1.3 XDL Background Rate

The XDL detectors have extremely low dark rates, on the order of 10^{-6} counts/s/pixel; see [Section 11.4.1](#).

Figure 4.2: Example of a COS FUV Spectrum



Upper panel: A stellar spectrum obtained with segment B of the COS FUV detector using the G130M grating at a central wavelength of 1309 \AA . The wavelength calibration (WCA) spectrum is on top, and the stellar spectrum (PSA) is below. As noted in [Section 3.3.2](#), both the PSA and BOA are open to the sky when the COS shutter is open, so Lyman- α airglow through the BOA is also visible below the PSA (near $Y = 400$). The *HST* +V2 and +V3 axes are over plotted. Note that the size of the active area of the MCP is smaller than the overall digitized area (16384×1024). Lower panel: the extracted stellar spectrum from the PSA.

4.1.4 XDL Read-out Format

The FUV channel creates one spectral stripe on each detector segment for the science spectrum and another for the wavelength-calibration spectrum. The aperture not being used for science may also create a spectrum. If so, it will appear below the science spectrum if the PSA is being used, or above it in the case of a BOA observation. Since the non-target aperture is usually observing blank sky, it will normally be visible only if Lyman α falls in the spectral range. [Figure 4.2](#) shows an example of an FUV spectrum obtained on orbit with segment B. The upper panel shows the two-dimensional image; the lower panel shows the extracted PSA spectrum. Note the difference in the x and y axis scales in the upper figure.

Although the gap between the two FUV detector segments prevents the recording of an uninterrupted spectrum, it can be made useful. For example, when the G140L

grating is used with a central wavelength of 1280 Å, the bright Lyman α airglow feature falls in the gap. For suggestions on spanning the gap, see [Section 6.5](#).

Should a high count rate on one of the segments be a safety concern, the detector can be operated in single-segment mode, whereby the high voltage on one segment is lowered to a value that prevents it from detecting light. This adjustment is required for central wavelength 1105 Å on G140L, since the zero-order light falling on segment B is too bright.

4.1.5 Stim Pulses

The signals from the XDL anodes are processed by Time-to-Digital Converters (TDCs). Each TDC contains a circuit that produces two alternating, periodic, negative-polarity pulses that are capacitively coupled to both ends of the delay-line anode. These stim pulses emulate counts located near the corners of the anode, beyond the active area of the detector. Stim pulses provide a means for **calcos** to correct the temperature-dependent shift and stretch of the image during an exposure, and they provide a first-order check on the dead-time correction. They are recorded in both TIME-TAG and ACCUM modes.

Four stim-pulse rates are available: 0 (i.e., off), 2, 30, and 2000 Hz per segment. These rates, which are only approximate, are *not* user selectable. Exposures longer than 100 sec will use the 2 Hz rate, those between 10 and 100 sec use 30 Hz, and those shorter than 10 seconds use 2000 Hz.

4.1.6 Pulse-height Distributions

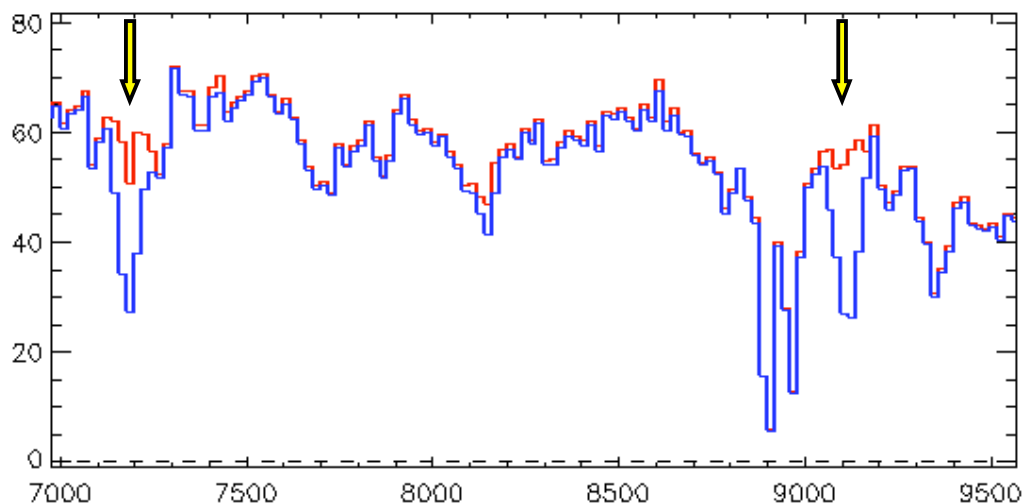
The XDL detectors convert each ultraviolet photon into a shower of electrons, for which the detector electronics calculate the x and y coordinates and the total charge, or pulse height. The pulse height is a property of the MCP in the region where the photon landed; it is not related to the energy of the incident photon. The pulse height distribution (PHD) is a histogram of the pulse heights for all events detected during an exposure. The PHD is peaked at the average gain of the MCPs with a width determined by the MCP characteristics. Background events, both internal and cosmic-ray-induced, tend to have a falling exponential PHD, with most events being at very low values. On-board charge-threshold discriminators filter out very large and small pulses to reduce the background and improve the signal-to-noise ratio. In TIME-TAG mode, the pulse height is recorded for each detected photon event. By rejecting low pulse-height events, **calcos** further reduces the background rate. In ACCUM mode, only the integrated pulse-height distribution is recorded ([Section 6.2.2](#)), so pulse-height filtering is not possible.

4.1.7 Gain Sag

Prolonged exposure to light causes the XDL detectors to become less efficient at photon-to-electron conversion, a phenomenon called “gain sag.” As a result, the peak of the PHD slowly decreases. As it approaches the minimum threshold imposed by **calcos**, target photons may be rejected as background events. As it falls still farther, target photons may be permanently lost. Gain sag appears first in regions of the detector that are illuminated by bright airglow lines, but eventually affects the entire spectrum. Figure 4.3 shows the effect of gain sag on the COS XDL detectors. The data were obtained in 2010 September using the grating setting G160M/1623/FP=4. The blue curve was constructed using only photon events with pulse heights in the range 4-30 (the limits used by **calcos** in late 2010). The red curve includes all photon events. Arrows mark two regions that suffer gain sag: the region near pixel 7200 is illuminated by Lyman α when grating setting G130M/1309/FP=3 is used, and that near pixel 9100 is illuminated by Lyman α when the setting is G130M/1291/FP=3. Note that the red curve lies slightly above the blue curve, even in regions where the gain sag is small; changing the pulse-height thresholds alters the effective sensitivity of the instrument.

To combat these effects, we have developed short, medium, and long-term solutions. In the short term, we will flag low-gain pixels and exclude them when combining spectra taken at multiple FP-POS positions (see Section 6.8.2), and we will implement time- and position-dependent pulse-height thresholds within **calcos**. These pipeline improvements should be implemented in early 2011. In the medium term, we are investigating the possibility of raising the high-voltage level of the XDL detectors. This technique was successfully employed by *FUSE*, which used detectors similar to those of COS. In the long term, it is possible to move the spectrum in the cross-dispersion direction onto a previously-unused portion of the detector by offsetting the aperture mechanism.

Figure 4.3: Gain Sag in the FUV XDL Detector



Spectra showing the effects of gain sag on segment B. Raw counts are plotted against raw X pixel number in this G160M/1623/FP=4 observation, binned by 20 pixels. The blue curve includes only photon events with pulse heights in the range 4-30. The red curve includes all photon events. The spectral features marked with arrows are not astrophysical, but represent the effect of gain sag on regions of the detector illuminated by Lyman α when other gratings are employed.

4.1.8 Non-linear Photon Counting Effects (Dead Time)

The electronics that control the COS detectors have a finite response time t , called the dead time, that limits the rate at which photon events can be processed. If two photons arrive within time t , the second photon will not be processed. For the FUV channel, three factors limit the detected count rate. The first is the Fast Event Counter (FEC) for each segment, which has a dead time of 300 ns. The FEC dead time matters only at count rates well above what is usable, introducing a 1% error at a count rate of 33,500 per segment per second.

The second factor is the time required to digitize a detected event. For a given true count rate C , the detected count rate D is:

$$D = \frac{C}{1 + C \cdot t}$$

where t is the dead-time constant. For the FUV XDL detector, $t = 7.4 \mu\text{sec}$, so the apparent count rate deviates from the true count rate by 1% when $C = 1,350$ counts/s and by 10% when $C = 15,000$ counts/s. Note that, when the effect is near the 10% level, then the FUV detector is near its global count-rate limit (see [Table 9.1](#)), so non-linear effects are relatively small.

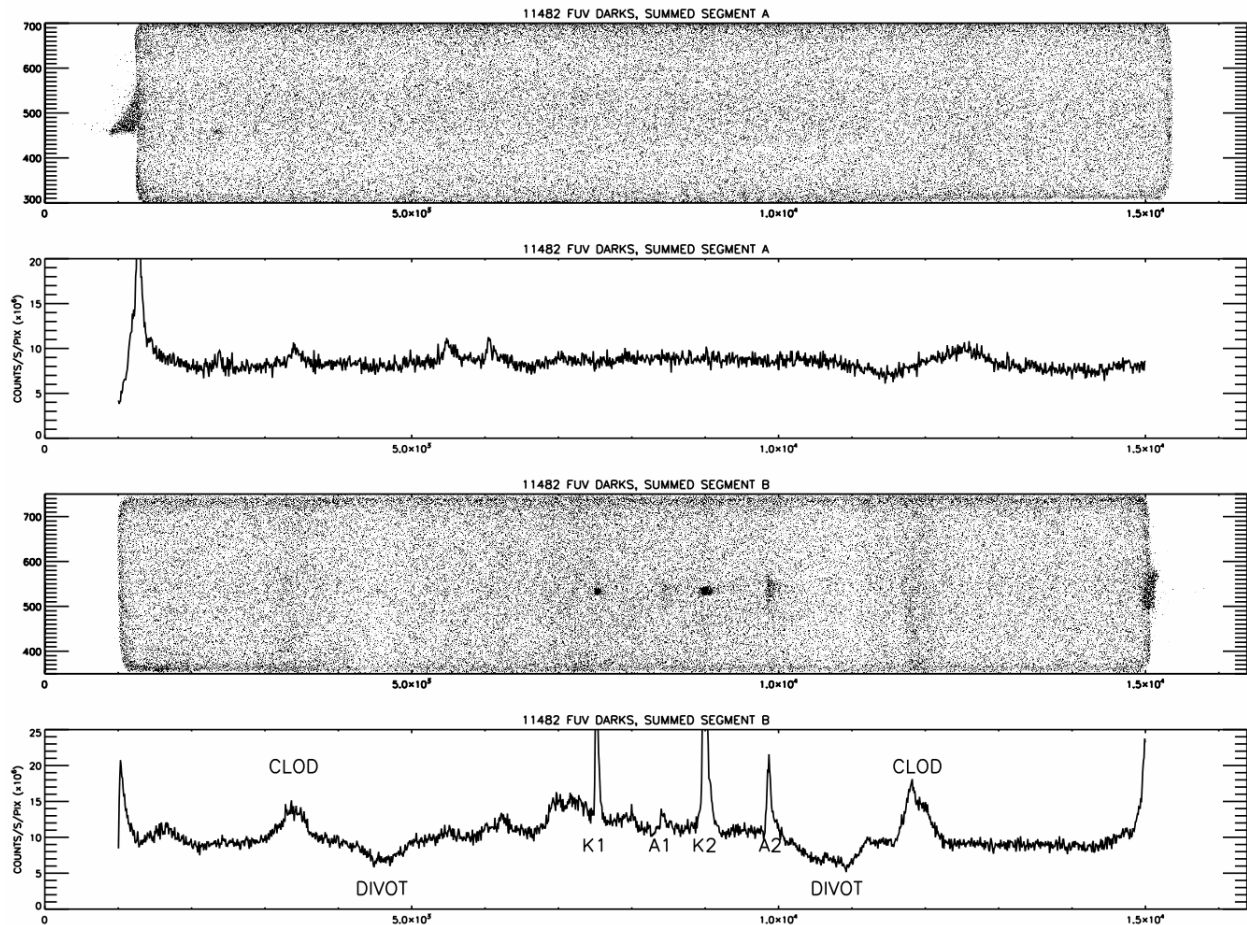
Finally, the Detector Interface Board (DIB) combines the count streams from the two FUV segments and writes them to a single data buffer. The DIB is limited to processing about 250,000 counts/s in ACCUM mode and only 30,000 counts/s in TIME-TAG mode (the highest rate allowed for TIME-TAG mode). The DIB interrogates the A and B segments alternately; because of this, a count rate that is high in one segment but not the other could cause a loss of data from both segments. Tests have shown that the DIB is lossless up to a combined rate for both segments of 20,000 counts/s, and the loss is 100 counts/s at a rate of 40,000 counts/s. Thus, this effect is less than 0.3% at the highest allowable rates. Furthermore, information in the engineering data characterizes this effect.

While dead-time corrections are automatically made in the **calcos** pipeline, they are not (at present) included in the ETC, which will over-predict count rates for bright targets.

4.1.9 Structures in the Dark Images

Deep FUV detector dark images show that the dark rate varies as a function of position on the detector and proximity to the South Atlantic Anomaly (SAA). [Figure 4.4](#) shows the sum of a large number of dark exposures for both segments. While segment A appears relatively featureless, segment B exhibits several regions with higher count rates. In most cases, these features will have a negligible effect on the extracted spectra, since they are quite faint, only a few times the typical background rate ([Section 11.4.1](#)). In TIME-TAG mode, these features are nearly eliminated by the default pulse-height filtering used by **calcos** when the data are processed. They cannot be removed from ACCUM mode exposures, however, because pulse-height information is not available. Since ACCUM mode is used only for bright targets, these features should constitute a negligible fraction of the total counts.

Figure 4.4: FUV Detector Dark Features.



Summed raw dark frames from program 11482. Each segment is displayed as an image and as a projection onto the x axis (units are counts/s/pixel $\times 10^6$). While segment A appears relatively featureless, segment B shows four pseudo-emission lines, known as arcs and knots (and labeled A and K, respectively), as well as a pair of divot/clod features, which result when their large pulse heights cause photons to be mis-registered. No pulse-height screening is employed here; when the default TIME-TAG screening is used, the Segment B features are significantly reduced.

4.2 The NUV MAMA Detector

4.2.1 MAMA Properties

The COS NUV detector is a Multi-Anode Micro-channel Array (MAMA) identical to that used for the NUV in STIS. (In fact, it is the STIS NUV flight spare.) The COS MAMA has a semi-transparent cesium telluride photocathode on a magnesium fluoride window and is sensitive to photons with wavelengths from 1150 to 3200 Å.

The NUV optics focus light through the MgF₂ window onto the Cs₂Te photocathode. A photoelectron generated by the photocathode then falls onto a curved-channel micro-channel plate (MCP), which generates a cloud of electrons. The active area of the coded anode array is 25.6 mm square and is divided into 1024 × 1024 pixels on 25 μm centers. The spatial resolution at 2500 Å is 35 μm FWHM.

4.2.2 MAMA Spectrum Response

The inherent spectral response of the COS NUV MAMA is essentially identical to that of the STIS NUV MAMA. However, the overall optical train of COS differs from STIS, so the throughputs are different ([Figure 6.2](#)).

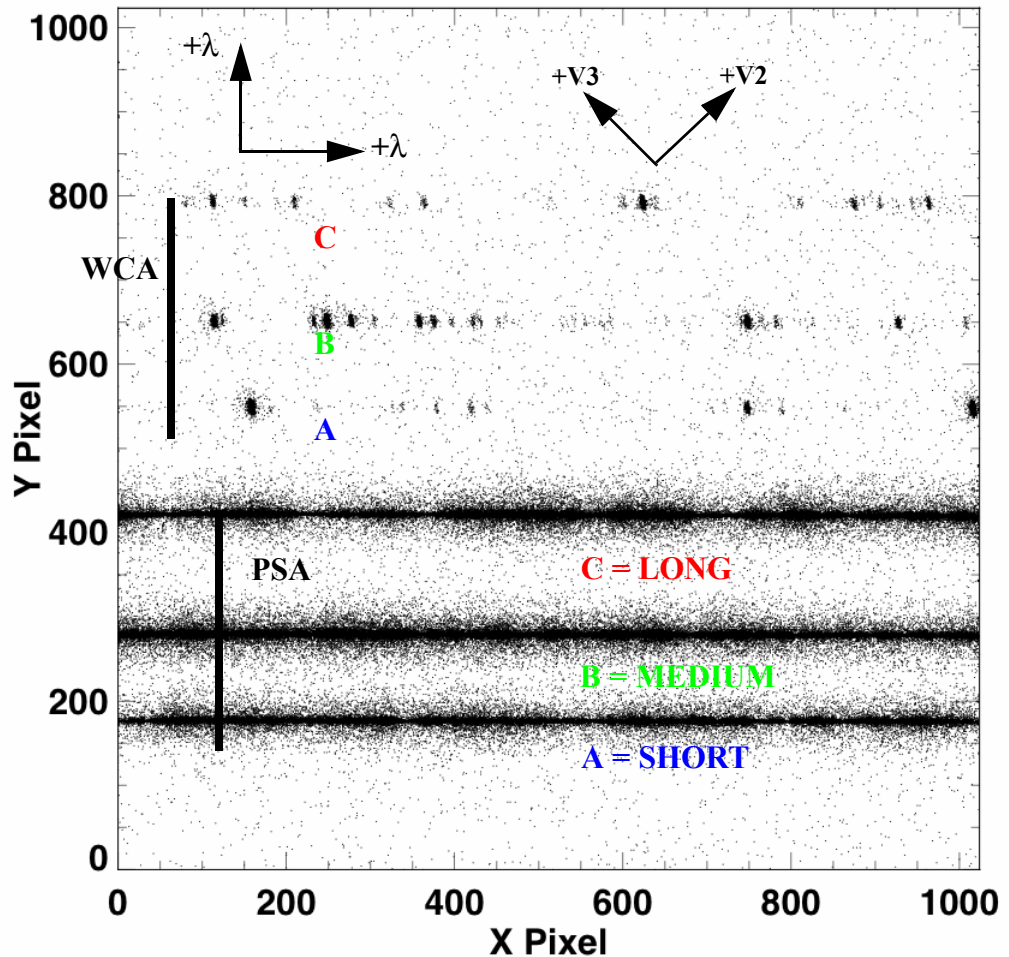
4.2.3 MAMA Background Rate

A sum of dark exposures taken away from the SAA shows a relatively featureless background, with slight enhancements at two of the corners. Although the early dark data showed a rate that was lower than had been measured on the ground, the rate has steadily increased since launch. As of 2010 September, the rate is approximately 3.6×10^{-4} counts/s/pixel, which is close to the prelaunch prediction; see [Section 11.4.1](#). If the current trend continues, then the mean NUV dark rate will increase to about 7.3×10^{-4} counts/s/pixel by 2012 April.

4.2.4 MAMA Read-out Format

The NUV channel creates six spectral stripes on the MAMA detector, three for the science data and three for the wavelength-calibration data. Stripes are separated by ~2.8 mm (center to center) in the cross-dispersion direction, and there is a gap of 3.7 mm between the reddest science stripe and the bluest calibration stripe. The NUV detector is read out as a 1024 × 1024 array, but in all other respects the data are handled in the same way as for the FUV detector. As noted, no pulse-height information is provided for MAMA data. An NUV spectrum obtained in TAGFLASH mode is shown in [Figure 4.5](#).

Figure 4.5: Example of a COS NUV Spectrum.



A COS NUV spectrum obtained in `TIME-TAG` mode with `FLASH=YES`. The stellar spectrum (labeled PSA) is on the bottom, and the wavelength-calibration spectrum (labeled WCA) on the top; each has three stripes. From bottom to top, these stripes are designated A, B, and C, as illustrated. Wavelength increases to the right and toward the top of the chip. The *HST* +V2 and +V3 axes are also shown. The SHORT, MEDIUM, and LONG designations are used in Phase II with the `ACQ/PEAKXD` command and the `STRIPE` Optional Parameter.

4.2.5 MAMA Dead Time

The dead time for the COS NUV MAMA is 280 nsec, the same as for the STIS NUV MAMA. The 1% level of non-linearity is reached for $C = 36,000$ counts/s.

The COS Line-Spread Function

In this chapter...

5.1 Mid-Frequency Wavefront Errors / 29
5.2 First Results / 30
5.3 Non-Gaussian Wings in the MAMA PSF / 31
5.4 Quantifying the Resolution / 31
5.5 Impact on Equivalent Width Measurements / 32

5.1 Mid-Frequency Wavefront Errors

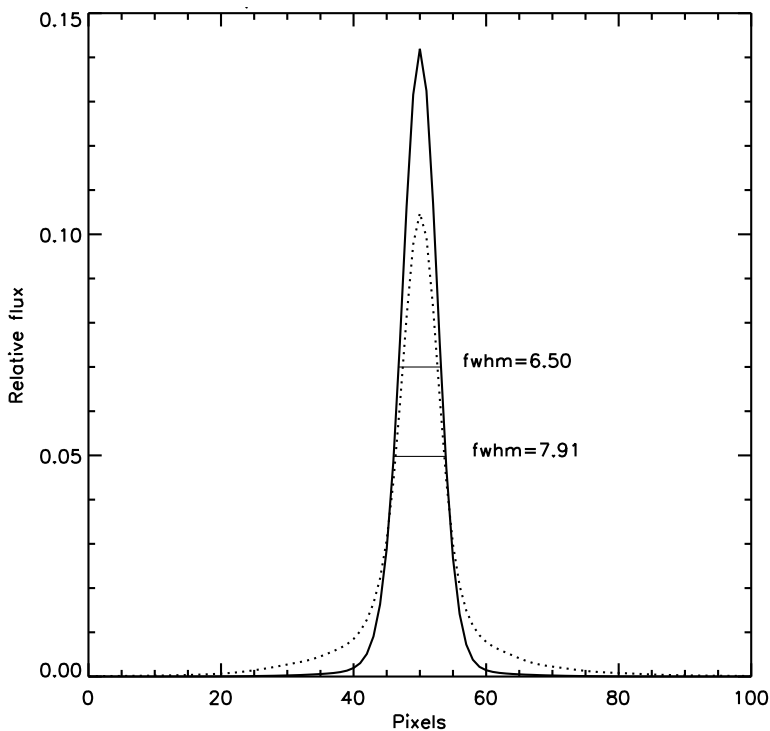
Analysis of SMOV data indicates that the COS on-orbit spectroscopic line-spread function (LSF) differs from that observed during pre-launch ground testing. While the COS optics successfully correct for the spherical aberration of the *HST* primary mirror, mid-frequency wavefront errors (MFWFEs) due to zonal (polishing) errors in the *HST* primary and secondary mirrors result in an LSF with extended wings and a core that is slightly broader and shallower than expected. These extended wings limit the detectability of faint, narrow spectral features. The effect is larger at shorter wavelengths, and it may have consequences for some COS FUV science. The most severely impacted programs are likely to be those that

- rely on models of the shapes of narrow lines;
- search for very weak lines;
- aim to measure line strengths in complex spectra with overlapping or nearly overlapping lines; or
- require precise estimates of residual intensity in very strong or saturated lines.

5.2 First Results

Initial results from an analysis of the on-orbit COS LSF are reported by Ghavamian et al. (2009) in [COS ISR 2009-01](#). They find that model LSFs incorporating *HST* MFWFEs are required to reproduce the absorption features observed in stellar spectra obtained with COS. [Figure 5.1](#) shows two model LSFs computed for grating G130M at 1309 Å. The solid line represents a model incorporating the spherical aberration of the *HST* Optical Telescope Assembly (OTA); it is well-fit by a Gaussian with FWHM = 6.5 pixels. The dotted line represents a model that also includes the MFWFEs. It has a FWHM of 7.9 pixels, slightly larger than that of the solid curve, and broad non-Gaussian wings, which can complicate the detection of nearby narrow features. Plots of model LSFs for all of the COS gratings are presented in [Chapter 14](#), and tabular versions are available on the [COS Web site](#).

Figure 5.1: Model Line-Spread Functions for the COS FUV Channel

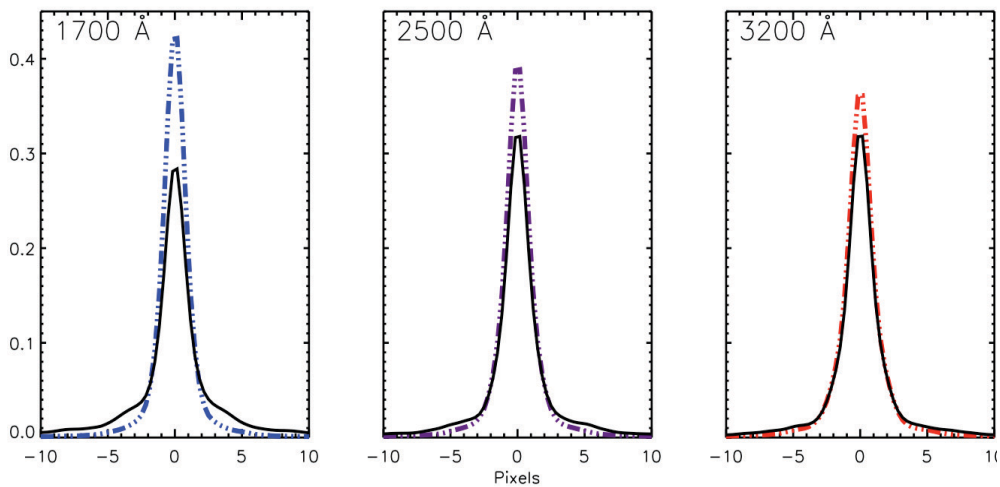


Model LSFs for G130M at 1309 Å, normalized to a sum of unity. The solid line represents a model LSF that incorporates the spherical aberration of the OTA; it is well-fit by a Gaussian with FWHM = 6.5 pixels. The dotted line represents a model that also includes the *HST* mid-frequency wave-front errors. It shows a larger FWHM and broad, non-Gaussian wings.

5.3 Non-Gaussian Wings in the MAMA PSF

While most NUV observations should be minimally affected by the MFWFEs, they will reflect the point-spread function of the COS MAMA detector, which exhibits faint, extended wings that are unrelated to the telescope optics. While the telescope-induced wings weaken as wavelength increases, the detector wings become stronger with increasing wavelength. Figure 5.2 shows model NUV detector LSFs with and without the MFWFEs at various wavelengths. Beyond 2500 Å, the detector wings dominate.

Figure 5.2: Model LSFs for the COS NUV Channel



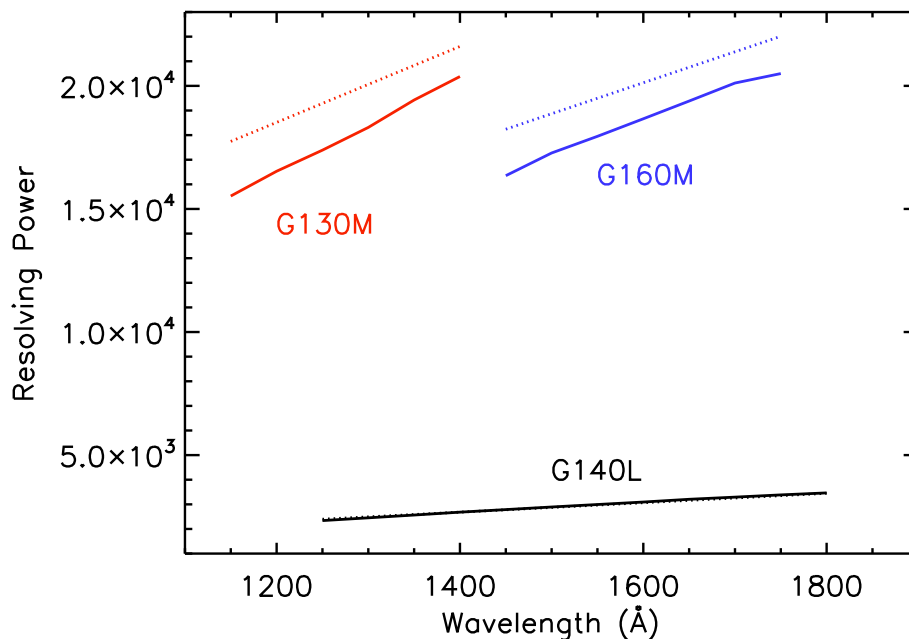
LSFs including the MFWFEs are plotted as solid lines, those without as dotted lines.

5.4 Quantifying the Resolution

When a substantial fraction of the power in an LSF is transferred to its extended wings, traditional measures of resolution, such as the FWHM of the line core, can be misleading. For example, an observer assuming that the resolution $R = 16,000$ quoted for the G130M grating represents the FWHM of a Gaussian would mistakenly conclude that COS can resolve two closely-spaced narrow absorption features, when in fact it cannot. Nevertheless, the FWHM is a convenient tool, and we use it to describe the COS gratings in tables throughout this handbook. When using these tables, keep in mind that the quoted resolution R is computed from the empirically-determined FWHM of the line core, and careful modeling may be needed to determine the feasibility of a particular observation or to analyze its result.

Figure 5.3 shows the resolving power of the FUV gratings for two cases: the first assumes a Gaussian LSF of FWHM = 6.5 pixels, with no MFWFEs from the *HST* OTA (dotted lines); the second is an LSF model with the MFWFEs included (solid lines). In the latter case, the FWHM of the LSF is calculated directly from the line profile by taking the width at half the peak (from Table 1 of COS ISR 2009-01). The MFWFEs reduce the resolving power of the G130M and G160M gratings by ~20%. The G140L profile is least affected by the MFWFEs, due to its lower dispersion. Preliminary measurements of the resolution of the G130M grating at $\lambda < 1200 \text{ \AA}$ are presented in Section 6.1.6.

Figure 5.3: Resolving Power of FUV Gratings



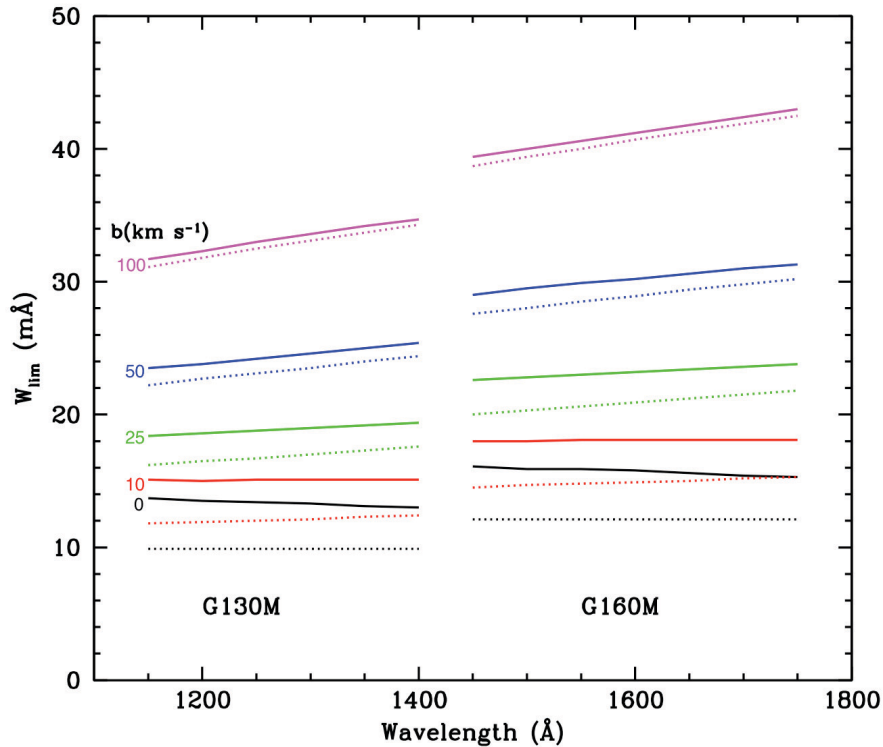
The resolving power ($R = \lambda/\text{FWHM}$) for the three gratings of the COS FUV channel for observations through the PSA aperture. The dotted lines are the pre-launch prediction using a Gaussian FWHM of 6.5 pixels. The solid lines are the values predicted by the LSF model with the on-orbit MFWFEs included. (The dotted and solid lines for G140L nearly overlap.)

5.5 Impact on Equivalent Width Measurements

Two aspects of the COS LSF make the detection of weak spectral features more difficult: the line core is wider, and light is shifted from the core into the wings. Together, these factors increase the limiting equivalent width for absorption features in COS spectra. Figure 5.4 shows the limiting equivalent widths as a function of wavelength for a 3σ FUV detection of absorption features at S/N = 10 per pixel. A series of Gaussian spectral features with nominal Doppler parameters of $b = 0, 10, 25, 50$ and 100 km/s have been convolved with both a Gaussian instrumental LSF and the

modeled on-orbit COS LSF for the G130M and G160M gratings. The results are similar for the NUV gratings, although the effect of the MFWFEs would be more moderate for the long-wavelength G285M grating.

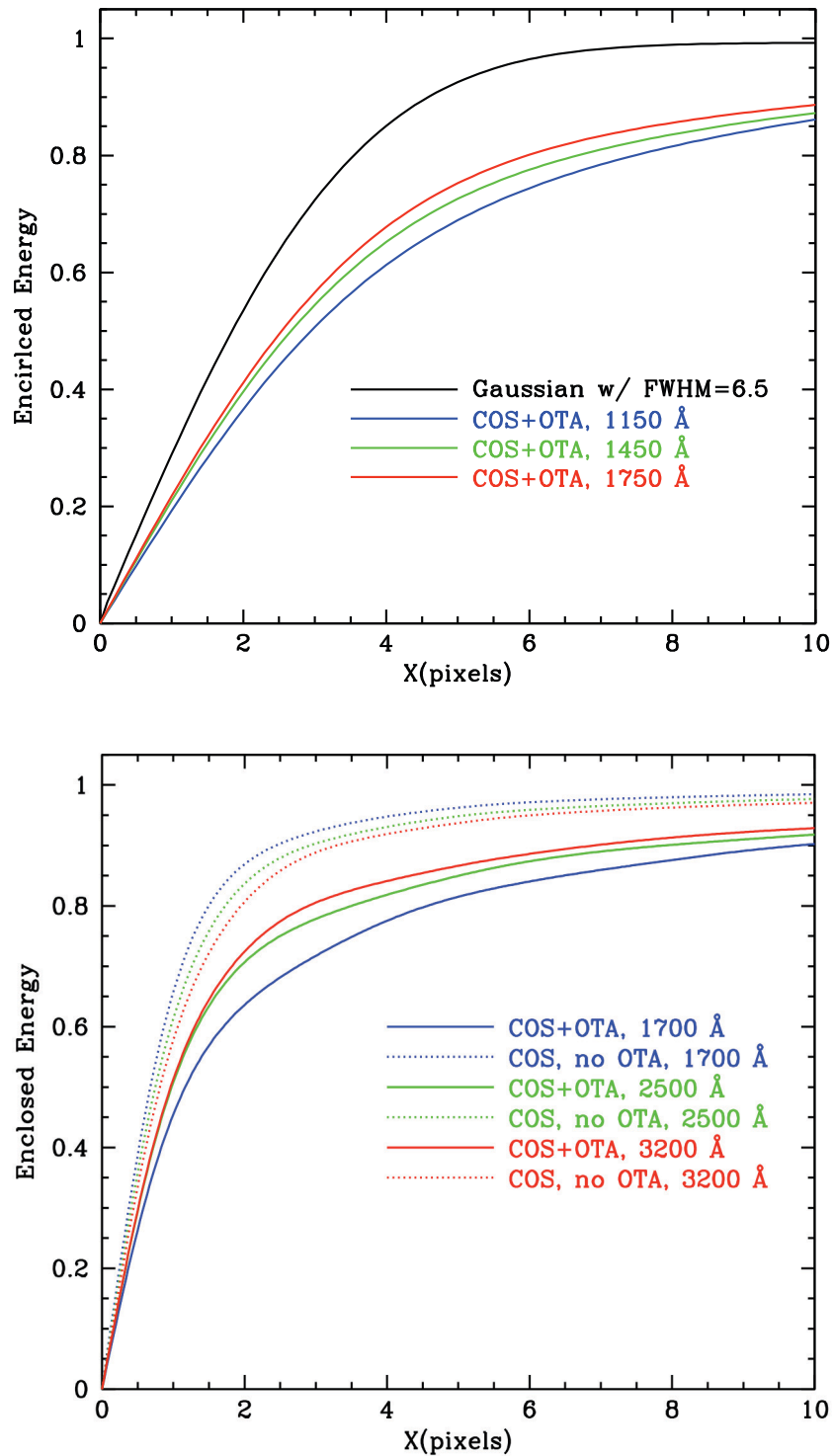
Figure 5.4: Limiting Equivalent Width of FUV Medium-Resolution Gratings



Limiting equivalent width as a function of wavelength for 3σ detections of absorption features at a S/N of 10 per pixel. Solid lines represent the full on-orbit LSFs including MFWFEs. Dashed lines represent Gaussian LSFs without MFWFEs. The colors correspond to features with intrinsic Doppler parameters $b = 0$ km/s (black), 10 km/s (red), 25 km/s (green), 50 km/s (blue) and 100 km/s (magenta).

Figure 5.5 shows the fraction of enclosed energy within the LSF, measured from the center of the profile, for both the FUV and NUV channels. The differences between the modeled on-orbit LSFs (MFWFEs included) and the Gaussian LSFs without MFWFEs are apparent in both spectroscopic channels. Though inclusion of the MFWFEs at longer NUV wavelengths widens the FWHM of the on-orbit LSF models only slightly, the wider wings decrease noticeably the spectral purity and the contrast level of the observed spectra.

Figure 5.5: Enclosed Energy Fraction of the COS Line-Spread Function



The enclosed energy fraction of the COS LSF for an unresolved spectral feature as measured from the center of the profile (collapsed along the cross-dispersion direction). A Gaussian with FWHM = 6.5 Å matches typical FUV results from ground tests (top panel). For the NUV (bottom panel), model profiles with and without the effects of the OTA MFWFEs are shown.

Spectroscopy with COS

In this chapter...

6.1 The Capabilities of COS / 35
6.2 TIME-TAG vs. ACCUM Mode / 45
6.3 Valid Exposure Times / 47
6.4 Estimating the BUFFER-TIME in TIME-TAG Mode / 47
6.5 Spanning the Gap with Multiple CENWAVE Settings / 49
6.6 FUV Single-Segment Observations / 50
6.7 Internal Wavelength Calibration Exposures / 50
6.8 Fixed-Pattern Noise / 53
6.9 COS Spectroscopy of Extended Sources / 57
6.10 Wavelength Settings and Ranges / 58

6.1 The Capabilities of COS

The two detectors and seven diffraction gratings (three for FUV, four for NUV) of COS enable high-sensitivity spectroscopy at low and moderate resolution across the FUV and NUV bands. The bandpass and resolution of each grating are presented in [Table 6.1](#).

For each exposure, the observer selects a detector (FUV or NUV); a grating, central wavelength, and FP-POS setting; one of the two 2.5 arcsec apertures (PSA or BOA); and a data-taking mode (TIME-TAG or ACCUM). [Chapter 14](#) provides detailed specifications for each grating and aperture. Note that the two channels cannot be used simultaneously, as the NUV channel is fed by a mirror on the FUV optics select mechanism (OSM1).

Table 6.1: COS Grating Parameters

Grating	Approximate Wavelength Range (Å)	Bandpass per Exposure and FUV Gap ¹ (Å)	Inferred PSA Resolving Power $R = \lambda/\text{FWHM}^2$	Approximate BOA Resolving Power	Dispersion (mÅ pixel ⁻¹)
FUV Channel					
G130M	900 – 1236	295 / 16	3000 – 1000 ³	—	9.97
	1150 – 1450	292 / 14.3	16,000 – 21,000	5900	9.97
G160M	1405 – 1775	360 / 18.1	16,000 – 21,000	4400	12.23
G140L	< 900 – 2150	> 1150 / 112	1500 – 4000	1100	80.3
NUV Channel					
G185M	1700 – 2100	3 × 35	16,000 – 20,000	3500	37
G225M	2100 – 2500	3 × 35	20,000 – 24,000	4600	33
G285M	2500 – 3200	3 × 41	20,000 – 24,000	5000	40
G230L	1650 – 3200 ⁴	(1 or 2) × 398	2100 – 3900	500	390

1. Width of gap between FUV detector segments; see [Section 6.5](#).
2. Empirically-determined FWHM of the LSF, which is not Gaussian. R increases approximately linearly with wavelength.
3. R falls with increasing wavelength.
4. Some shorter wavelengths are recorded in second-order light. They are listed in [Table 6.5](#).

6.1.1 First-Order Sensitivity

COS is considerably more sensitive than STIS and earlier-generation *HST* instruments at comparable spectral resolutions, particularly in the far ultraviolet. Effective areas for targets observed through the PSA are shown in [Figure 6.1](#) and [Figure 6.2](#). Note that the COS sensitivity changes with time ([Section 6.1.4](#)); plots and tables in this handbook are based on predictions for mid-Cycle 18 (2011 April). Please consult the [COS Web pages](#) for updated information.



While the figures and tables in this handbook can be used to derive accurate estimates of count rates, exposure times, and the like, we recommend the use of the COS ETC in all cases, because it properly computes instrument throughput, accounts for detector and astronomical backgrounds, and checks for violations of local and global count-rate limits.

Figure 6.1: Effective Areas for the FUV Channel through the PSA

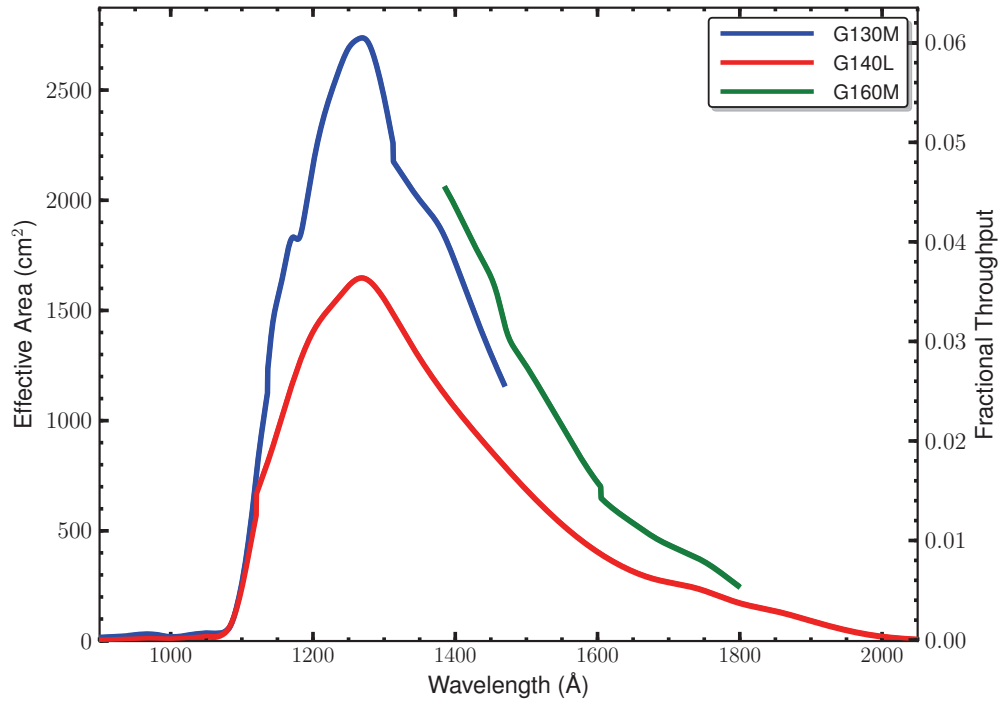


Figure 6.2: Effective Areas for the NUV Channel through the PSA

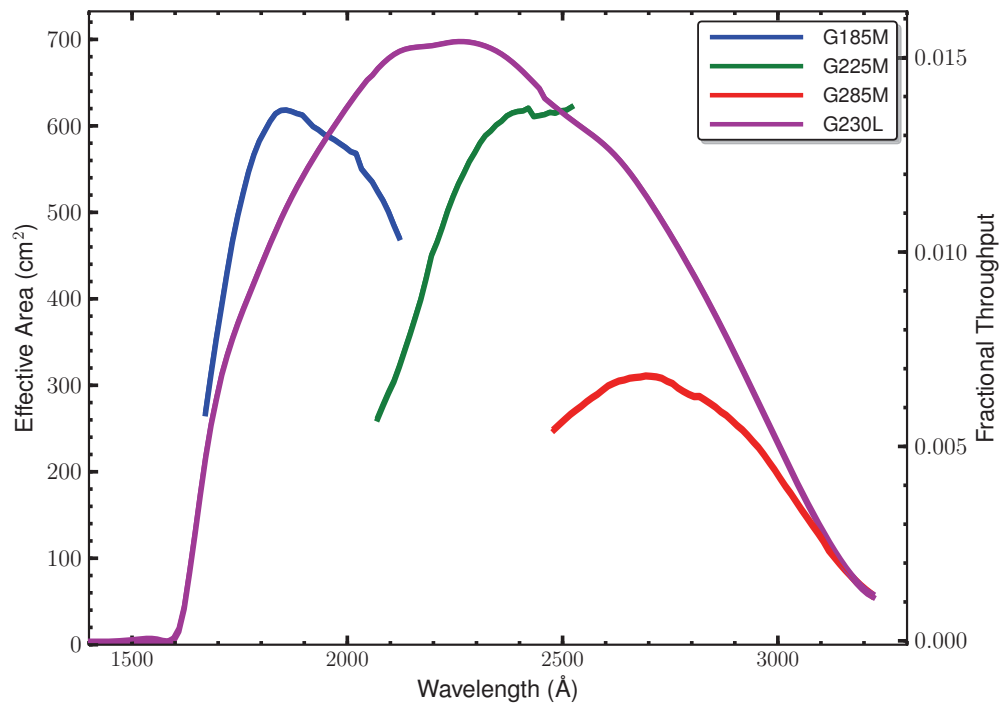
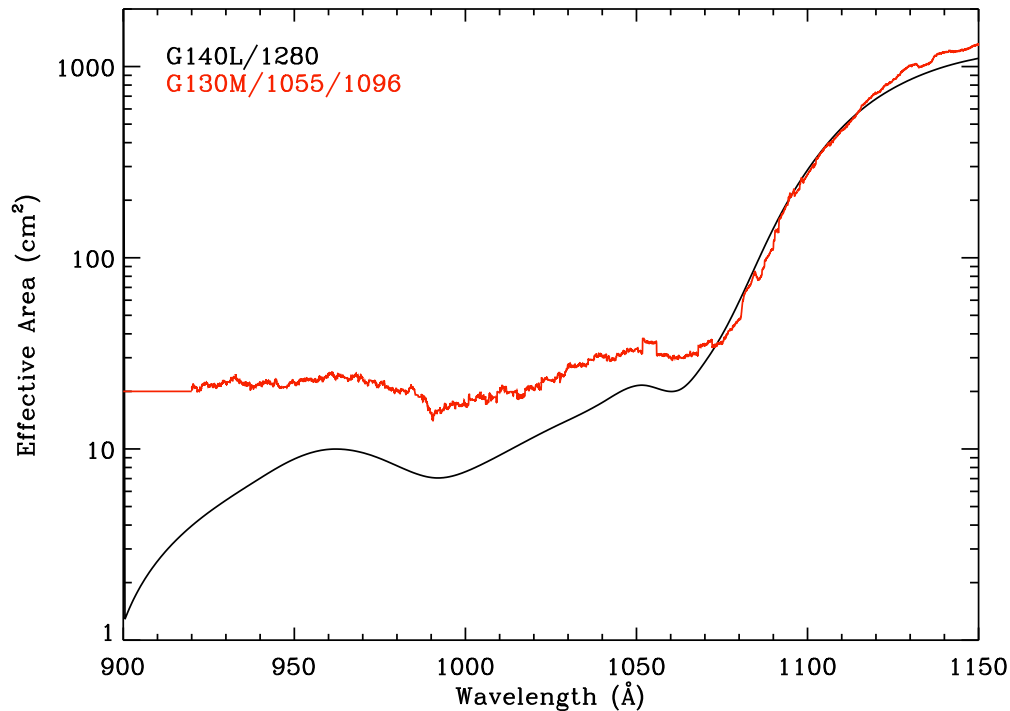


Figure 6.3: Effective Area at Wavelengths below 1150 Å



Effective areas of the new G130M modes (red) and G140L (black). Below 920 Å, G130M is not well characterized, so the effective area is assumed to be constant.

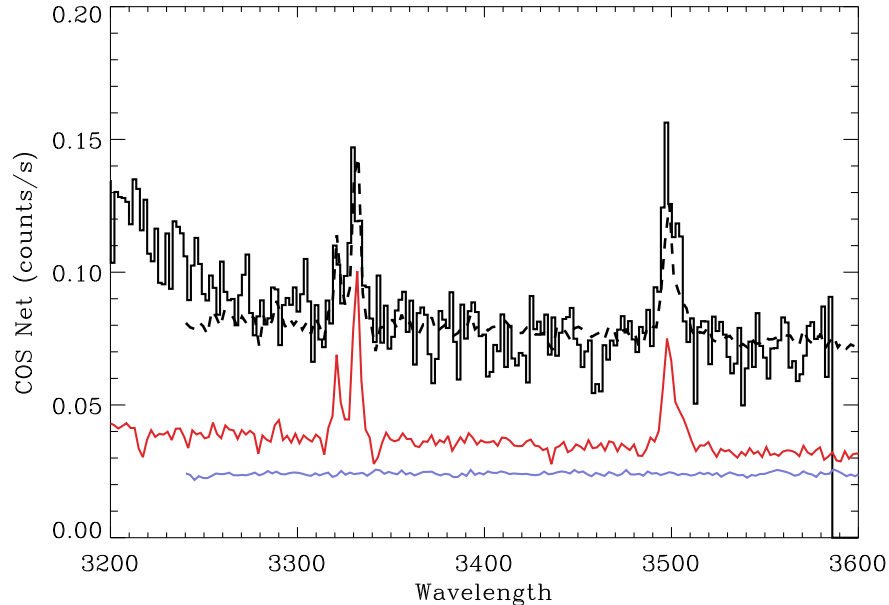
6.1.2 Observing below 1150 Å

Figure 6.3 presents the effective areas of the G130M and G140L gratings at wavelengths below 1150 Å. From this figure, we can draw two fundamental conclusions: First, COS can obtain useful spectra at wavelengths between 900 and 1150 Å. Second, the contrast between the throughput at 1070 and 1150 Å is roughly a factor of 100.

When G140L is used with CENWAVE=1280, wavelengths as long as 1200 Å can fall on detector segment B. For many targets, the count rate at 1150 Å will exceed the local bright limit, while the count rate at shorter wavelengths is perfectly safe. Consequently, turning segment A off and using FP-POS=4 is the recommended approach for observing bright objects below 1150 Å with the G140L grating.

When grating G130M is used with CENWAVE=1055, detector B records wavelengths shortward of ~ 1050 Å, depending on the FP-POS setting employed (Section 14.3). Using this grating mode with segment A turned off further reduces the danger of high count rates at longer wavelengths. Note that both the sensitivity and resolving power (Section 6.1.6) of G130M are greater than those of G140L in this wavelength range.

Figure 6.4: Second-Order Light in G230L Spectrum



Black curve is stripe B of the G230L CENWAVE = 3360 spectrum of NGC 6833. Blue curve is an FOS spectrum over the same wavelength range (units are Ångstroms). Red curve is an FOS spectrum of the 1600 - 1800 Å region, plotted as $f(2\lambda)$. The FOS spectra have been rescaled by arbitrary amounts for display purposes. The dashed curve, a combination of the two FOS spectra, reasonably reproduces the COS spectrum.

6.1.3 Second-Order Sensitivity

Because the MAMA detector is sensitive to wavelengths as short as 1150 Å, NUV spectra longward of 2300 Å are vulnerable to contamination from second-order light. To mitigate this problem, the COS NUV optics were designed to provide peak reflectivities between 1600 and 2000 Å. Gratings G225M and G285M are coated with bare aluminum, which when oxidized has poor reflectivity below 1800 Å. After six reflections (two MgF₂ mirrors in the *HST* OTA and four bare-Al optics in COS), light from below 1250 Å is attenuated by 99%. Mounted directly on gratings G230L and G285M are order-sorting filters that block most light from below 1700 Å.

For G230L, stripes B and C are still affected by second-order flux. When CENWAVE=3360, stripe B is contaminated by second-order light beyond 3200 Å. In a spectrum of the planetary nebula NGC 6833 obtained with CENWAVE=3360, second-order light accounts for roughly 40% of the flux at 3320 Å and more than 50% at 3500 Å (Figure 6.4). Above 1700 Å, stripe C is more sensitive to second-order light than first-order by design (Table 6.5), but on-orbit observations reveal that first-order light is detectable at a level of 5% from wavelengths greater than 3700 Å at all central-wavelength settings.

In the FUV channel, second-order light is present at long wavelengths ($\lambda > 2150$ Å) in spectra taken with G140L CENWAVE=1280 FUV. These photons are rejected by the COS pipeline during processing but available in the “net counts” column of the `*x1d*.fits` files.

6.1.4 Time-Dependent Sensitivity Changes

Observations of *HST* primary spectrophotometric standard stars show that there is a significant time dependence of the COS sensitivity for some spectrographic modes. The reflectivity of the G225M and G285M NUV gratings, which are coated with bare aluminum (rather than MgF₂ over aluminum like the other gratings), showed a time-dependent degradation before launch that has continued on orbit, decreasing at a rate of ~3% and ~10% per year respectively, independent of wavelength.

Throughout 2009, the FUV modes showed a wavelength-dependent sensitivity decline, falling ~3% per year below 1400 Å and as much as 11% per year at 1800 Å. In 2010, this decline has slowed to ~5% per year, independent of wavelength. The cause of the FUV decline is still under investigation, but it may be a property of the detector photocathode. For details, see [COS ISR 2010-15](#).

Calcos includes a time-dependent sensitivity calibration, and regular monitoring of standard stars is used to update the sensitivity reference files periodically. At the time of this writing, the ETC reflects the best estimate of the sensitivity for the middle of Cycle 18, but it will be updated with Cycle 19 predictions in time for the Cycle 19 Phase II proposal deadline.

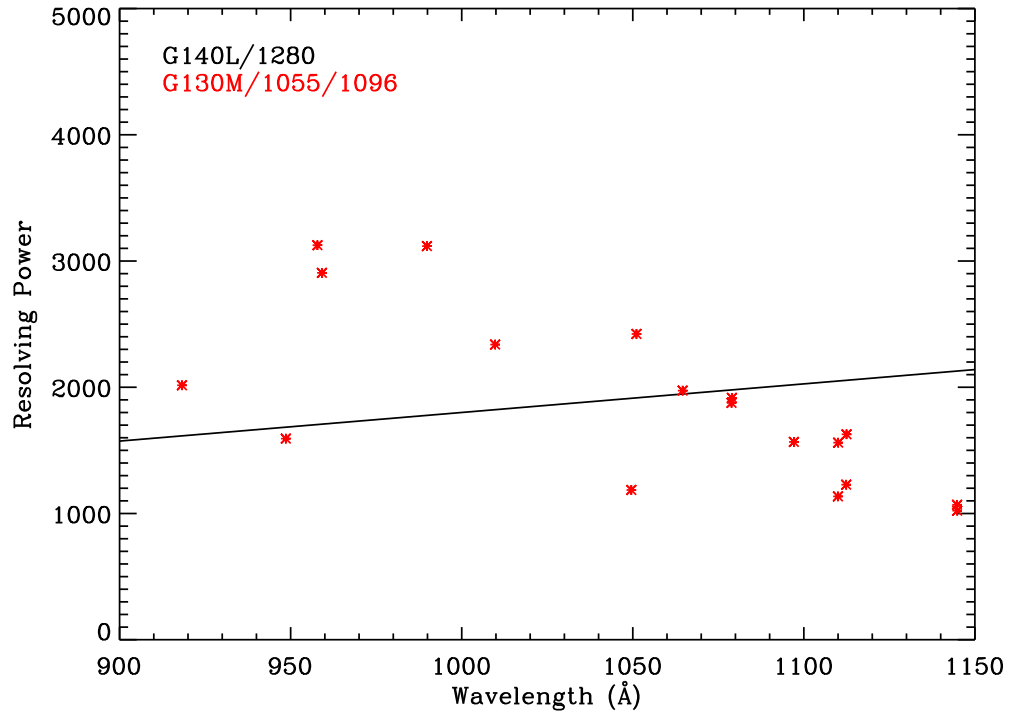
6.1.5 Zero-Order Image

The 1105 Å central-wavelength setting of grating G140L places the zero-order image from the grating on segment B of the FUV detector, violating detector count-rate limits, while a useful first-order spectrum falls onto segment A. For this central wavelength, observations can be made only in single-segment mode, with the high voltage for segment B reduced ([Section 6.6](#)). After final alignment of COS on-orbit, the zero-order image was also found to fall on segment B for the 1230 Å setting with FP-POS=4. In Cycle 18, CENWAVE=1230 was replaced with CENWAVE=1280 to keep the zero-order image off the detector. Two-segment observations are allowed for all FP-POS settings with CENWAVE=1280.

6.1.6 Spectroscopic Resolving Power

The spectroscopic resolving power ($R = \lambda/\text{FWHM}$) of each COS grating is listed in [Table 6.1](#) and plotted as a function of wavelength for the FUV gratings in [Figure 5.3](#). These values correspond to the FWHM of the model line-spread functions (LSFs) that are described in [Chapter 5](#) and presented in [Chapter 14](#). Measured FWHM values for the new central-wavelength settings of G130M are presented in [Figure 6.5](#). (The decrease in resolving power with increasing wavelength apparent in this figure is predicted by the LSF models.) Because the COS LSF is not a Gaussian, simple rules relating R to the detectability of narrow spectral features may not apply. Careful modeling of the LSF may be required to determine the feasibility of an observation.

Figure 6.5: Resolving Power of G130M and G140L below 1150 Å



Resolving power ($R = \lambda/\text{FWHM}$) of the new G130M modes (red) and G140L (black). Values for G130M are derived from observed spectral features. Values for G140L are extrapolated from wavelengths longer than 1200 Å, which are themselves based on model LSFs.

6.1.7 Spatial Resolution and Field of View

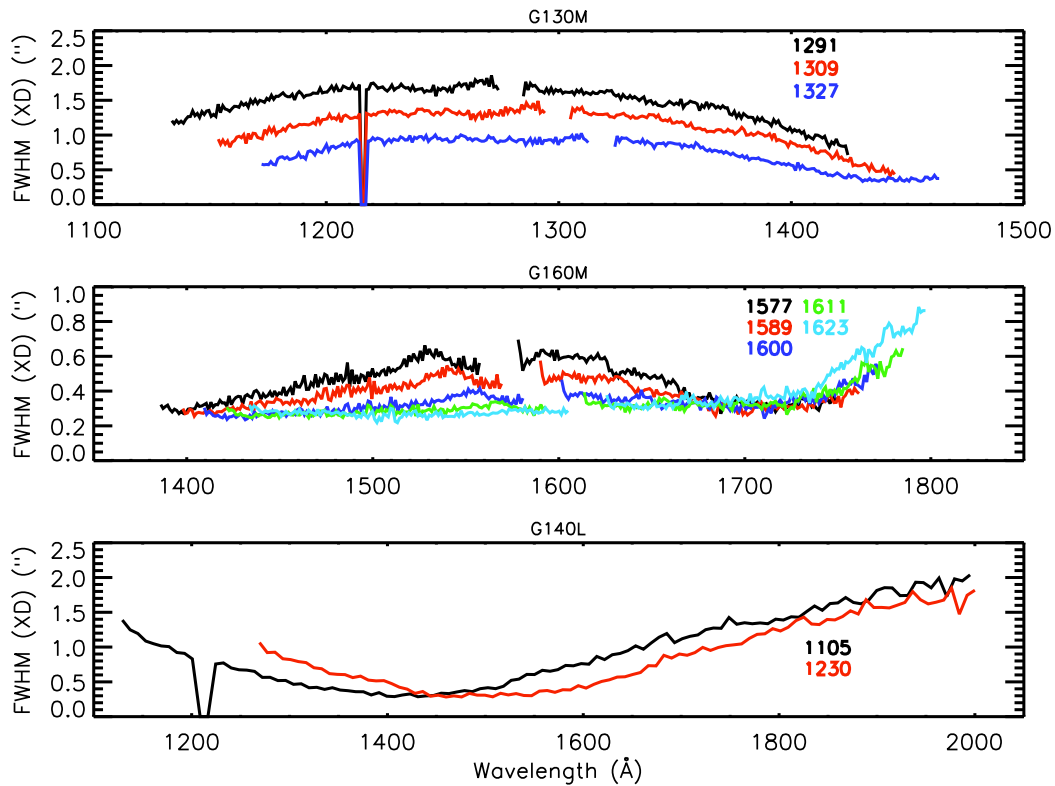
The spatial resolution of COS is affected by the mid-frequency wavefront errors (MFWFEs) via the non-Gaussian wings they introduce (Chapter 5). The NUV channel corrects for the telescope’s spherical aberration, but not for the MFWFEs. In spectroscopic mode, ground tests showed that COS can separate the NUV spectra of two equally-bright objects that are separated by 1 arcsec in the cross-dispersion direction.

The situation in the FUV is more complex, because of the uncorrected astigmatism in the cross-dispersion direction. Figure 6.6 shows the strong dependence of the spectral width on both the wavelength and central-wavelength setting for each of the FUV gratings. At wavelengths for which the profile width is large, the spectra of two objects separated by less than the profile width in the XD direction would be combined.

The COS field of view is determined by the entrance apertures, which are 2.5 arcsec in diameter, but the aberrated light entering the aperture means that objects up to 2 arcsec from the center of the aperture will contribute to the recorded spectra.

For additional information, please see “FUV Spectroscopic Performance” (COS ISR 2010-09, Ghavamian et al. 2010) and “NUV Spectroscopic Performance” (COS ISR 2010-08, Béland et al. 2010).

Figure 6.6: Cross-Dispersion Profile Widths for FUV Gratings



Variation in the width of the FUV spatial profile. The widths are obtained via Gaussian fits to the cross-dispersion profiles of a point source observed through the PSA. (Empirically-determined FWHM values may be slightly smaller.) Widths are plotted as a function of wavelength for each of the central-wavelength settings. Dips in the G130M and G140L spectra mark airglow features.

6.1.8 Photometric (Flux) Precision

Based on measurements made during SMOV, we estimate that the absolute flux calibration of COS is accurate to about 5% in the FUV. In the NUV, the calibration is accurate to about 2% for the medium-resolution gratings; it is slightly less accurate in some parts of the G230L bandpass. Time-dependent sensitivity corrections should be accurate to about 2%.

6.1.9 Wavelength Accuracy

The wavelength-accuracy requirements for each of the COS gratings and the error budget to achieve them are shown in [Table 6.2](#). To compute the error budget, the allowed uncertainty was divided equally between internal and external sources. Internal sources include the accuracy of the wavelength scale, the dispersion relation, aperture offsets, distortions, and drifts. The external tolerance budget is dominated by target mis-centering in the aperture. For more on this subject, see [Section 8.8.2](#).

Table 6.2: Wavelength Calibration Uncertainties

Grating	Error goal (1σ)		Internal error (1σ)	External error (1σ)	Plate scale ¹
	km s ⁻¹	pixels	pixels	arcsec	pixel arcsec ⁻¹
G130M	15	5.7 – 7.5	3.0 – 4.0	0.09 – 0.12	45.1
G160M	15	5.8 – 7.2	3.1 – 3.8	0.10 – 0.12	44.6
G140L	150	7.5 – 12.5	4.0 – 6.6	0.12 – 0.21	47.1
G185M	15	7.2 – 10.0	1.2 – 1.7	0.03 – 0.04	41.85
G225M	15	9.7 – 13.3	1.6 – 2.3	0.04 – 0.06	41.89
G285M	15	9.7 – 14.7	1.6 – 2.6	0.05 – 0.07	41.80
G230L	175	8.3 – 15.5	1.4 – 2.6	0.03 – 0.07	42.27

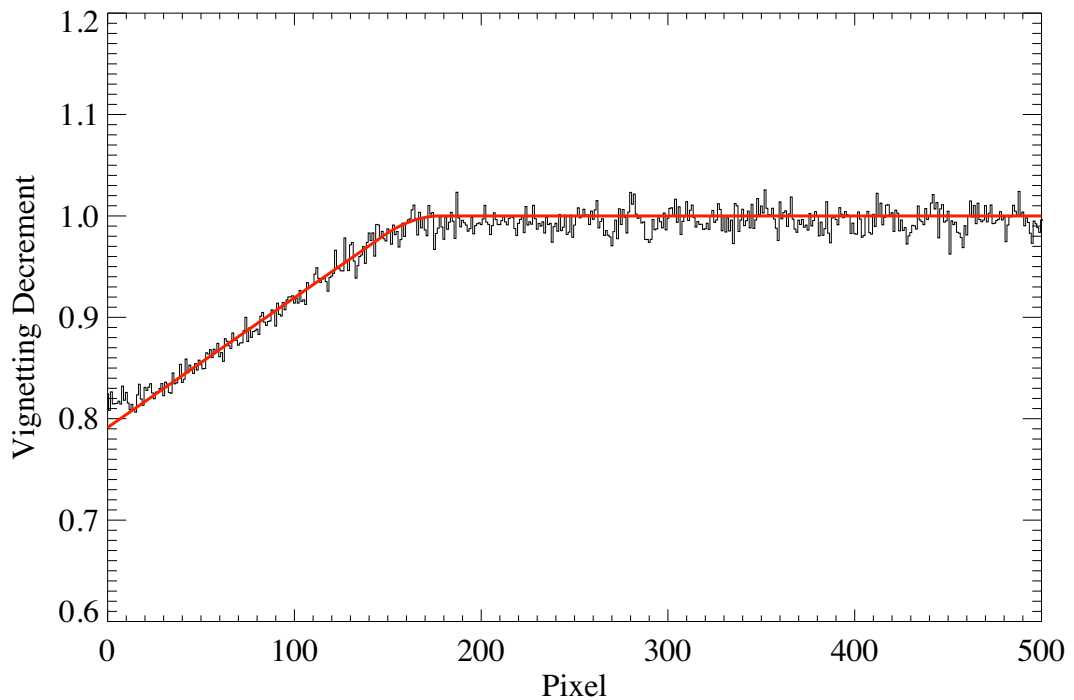
1. The plate scale is shown to indicate the centering precision required during acquisition. These pre-launch values, determined from ray traces, are for the along-dispersion direction. Plate scales measured from on-orbit data are presented in [Chapter 14](#).

The COS grating mechanisms (OSM1 and OSM2) continue to move after reaching their commanded positions. Though small, the drift is significant enough to degrade spectral resolution, especially during the first few minutes after a grating motion. To measure and remove this effect, the TAGFLASH operating technique was developed. In this mode, the wavelength calibration lamp is turned on periodically during TIME-TAG science observations with the PSA so that spectral drifts can be removed during data processing. Because the wavelength calibration spectrum is recorded on the detector well away from the science spectrum, one does not contaminate the other. TAGFLASH is the default mode for TIME-TAG observations with the PSA; it is described further in [Section 6.7.1](#).

6.1.10 Internal Scattered Light

The internal scattered-light level within COS is quite low. In ground-test measurements, light scattered along the dispersion axis represents less than 1% of the nearby continuum. On orbit, the COS LSF dominates the internal scattered light ([Chapter 5](#)). The extended wings of the LSF can fill in the cores of saturated absorption features that would otherwise appear black. This effect can be modeled using the synthetic line profiles presented in [Chapter 14](#).

Figure 6.7: Vignetting Profile for NUV M Gratings



Vignetting profile of the medium-resolution gratings as a function of pixel location showing the linear decrease in throughput near the low-pixel edge of the NUV detector. The red line shows the best fit to the profile obtained from observations of the white dwarf G191-B2B.

6.1.11 Vignetting of the NUV Channel

After on-orbit alignment of COS in *HST*, fluxes of external targets in the PSA were found to be depressed at the short wavelength ends of the NUV stripes. For the medium-resolution gratings, the reduction is about 20% at the first pixel and rises linearly to expected levels over approximately the next 160 pixels (Figure 6.7). For G230L, the reduction is about 15% at the first pixel and extends about 110 pixels. (The slope is the same as in Figure 6.7; it is as though the ramp were shifted by 50 pixels.) The depression is thought to be due to vignetting of the beam at the NUV camera mirrors that image the spectrum on the detector. The vignetting correction, performed by **calcos**, is the same for all stripes and grating settings and is not included in the COS Exposure Time Calculator (ETC). Ongoing studies suggest that the vignetting changes with time. Users are advised to consult the [COS web pages](#), where additional information will be posted as it becomes available.

6.2 TIME-TAG vs. ACCUM Mode

COS exposures may be obtained in either a time-tagged photon-address mode (TIME-TAG), in which the position, arrival time, and pulse height (for FUV observations) of each detected photon are saved in an event stream, or in accumulation (ACCUM) mode, in which only the positions of the photon events are recorded.

6.2.1 TIME-TAG Mode

In TIME-TAG mode, each photon is kept as a separate event in a list in COS memory. Each entry in that list contains the (x, y) coordinates of the photon together with the pulse height of the charge cloud generated by it (for FUV observations). Time markers are inserted in the list every 32 msec by the instrument electronics. When data are processed by the ground system, arrival times are assigned to the events according to the time marker preceding the event.

COS observations should be obtained in TIME-TAG whenever possible, because it provides significant opportunities for temporal sampling, exclusion of poor quality data, and, for the FUV, improved thermal correction (by tracking the stim-pulse positions as a function of time) and background removal (by using the pulse-height information). TIME-TAG mode should always be used for exposures that will generate count rates of 21,000 counts sec^{-1} or less from the entire detector (including both detector segments for the FUV). At count rates between 21,000 and 30,000 counts sec^{-1} , TIME-TAG may be used to obtain properly flux-calibrated data, but the loss of some continuous time periods within extended exposures will occur (see the discussion under BUFFER-TIME below). At present, TIME-TAG should not be used for count rates greater than 30,000 counts sec^{-1} . ACCUM mode should be used for such high count-rate targets.

We recommend that TIME-TAG mode always be used with FLASH=YES (the so-called TAGFLASH mode) unless circumstances prevent it (see [Section 6.7.1](#)).

Doppler Correction for TIME-TAG Mode

No on-board corrections are made for shifts in the spectrum due to the orbital motion of *HST* while in TIME-TAG mode; this is done later in pipeline processing.

Pulse-height Data for TIME-TAG

In FUV TIME-TAG mode, the pulse height of each photon event is recorded, along with the position and arrival time. Pulse heights are stored as 5-bit words, so their values range from 0 to 31. Post-observation pulse-height screening is useful for rejecting unwanted background events and can often improve the signal-to-noise ratio in the extracted science spectrum. Pulse-height information is not provided by the NUV detector.

6.2.2 ACCUM Mode

In ACCUM mode, an image of the detector is stored in a 16-bit memory buffer. As each photon arrives from the detector, the location in the buffer at coordinates (x, y) is incremented by one. Each location can hold at most 65,535 counts; the next event will cause the value to roll over to zero. To conserve memory, only a 16384×128 region of each segment is stored. Timing and pulse-height information is not saved, preventing the application of the data-correction techniques available in TIME-TAG mode.

ACCUM mode is designed for bright targets whose high count rates would fill the on-board buffer memory too rapidly if the data were taken in TIME-TAG mode. In some instances, it may be possible to observe a relatively bright object in TIME-TAG mode if the BOA is used instead of the PSA, although the BOA degrades the spectroscopic resolution. Observers wishing to use ACCUM mode will be asked to justify doing so when submitting their Phase II program.

Observing Efficiencies with ACCUM

FUV ACCUM images do not include the entire detector. To conserve memory, photons are collected only from the stim regions and that portion of the detector actually illuminated by the target (1/8 of the full detector area, or 128 pixels in y). Each FUV ACCUM image fills one-half of the total COS memory, so it is possible to acquire two FUV images before dumping the on-board buffer.

NUV ACCUM images cover the entire detector. Because they are smaller, up to nine of them can be stored in the memory buffer. Unlike TIME-TAG mode, no data may be acquired during an ACCUM readout. NUV ACCUM mode is thus most efficient when repeated identical observations are stored in memory, then read out all at once. (Within APT, the [Astronomer's Proposal Tool](#), one may easily schedule multiple iterations of an exposure using the `Number_of_Iterations` parameter.)

Doppler Correction for ACCUM Mode

In ACCUM mode, the COS flight software adjusts the pixel coordinates of detected events to correct for the orbital motion of *HST*. The correction (always by an integral number of pixels) is updated whenever *HST*'s velocity with respect to the target changes enough to shift the spectrum by an additional pixel. This is done via a small table, computed on the ground, that lists the time of each pixel shift, based on the orbital motion and the dispersion of the grating in use.

Note that ACCUM mode exposures longer than 900 seconds that use the G130M or G160M gratings may blur the FUV spectra by 1 to 2 pixels (about 1/6 to 1/3 of a resolution element) since shifts are performed in pixel, not wavelength, space.

Pulse-Height Distribution Data for ACCUM Mode Observations

Some pulse-height information is available for FUV ACCUM observations. A pulse-height histogram, consisting of 256 bins (128 bins for each detector segment) of 32 bits each, is dumped for every ACCUM mode image obtained with the FUV detector. (Why 128 bins? In ACCUM mode, individual pulse heights are stored as 7-bit words, so their values range from 0 to 127.) Pulse-height data are not provided for NUV exposures.

6.3 Valid Exposure Times

The minimum COS exposure duration is 0.1 seconds (but `FLASH=YES` `TIME-TAG` exposures impose a longer minimum; see [Section 6.7.1](#)). The maximum is 6,500 seconds. Between these extremes, COS exposure times must be integer multiples of 0.1 seconds. If the observer specifies an exposure time that is not a multiple of 0.1 seconds, its value is rounded *down* to the next lower integral multiple of 0.1 seconds, (or set to 0.1 seconds if a smaller value is specified). Exposure times larger than about 3,000 seconds are normally appropriate only for visits with the CVZ special requirement, because the visibility period of a typical orbit is ~50 minutes. See the *HST Primer* for information about *HST*'s orbit and visibility periods.

For `TARGET=WAVE` exposures, `DEF` (default) must be entered as the exposure time. The value appropriate for the optical configuration will be chosen from a table established at STScI for best performance. At present, `TARGET=WAVE` flash durations are identical to those given in [Table 6.3](#).

6.4 Estimating the BUFFER-TIME in TIME-TAG Mode

COS maintains two on-board data buffers, each with a capacity of 9 MBytes (2.35×10^6 counts). The time set aside to fill one of these buffers is called the `BUFFER-TIME`. COS uses the `BUFFER-TIME` to establish the pattern and timing of memory dumps during a `TIME-TAG` exposure: For the first `BUFFER-TIME` of an exposure, counts are recorded in the first COS data buffer. At the end of this time, data recording switches to the second data buffer, and the first buffer is read out while the second is being filled.

For all external `TIME-TAG` observations, a value of the `BUFFER-TIME` must be specified in the Phase II proposal. The `BUFFER-TIME` is 2.35×10^6 counts divided by the anticipated count rate in photons per second. The `BUFFER-TIME` calculation should include counts from the detector dark current and stim pulses (for FUV) as well as the detected photon events, factoring in the instrument quantum efficiency and dead time. We recommend use of the COS ETC to compute an accurate value of the `BUFFER-TIME`. **Give yourself a margin of error of about 50%; i.e., multiply the ETC `BUFFER-TIME` by 2/3.**

If the `BUFFER-TIME` is overestimated, the buffer may fill before input switches to the other buffer. Subsequently-arriving photons will be lost, leaving a gap in the data. The pipeline will correct the exposure times for any such gaps, so flux calibrations will be correct, but the overall S/N will be lower than expected. If `BUFFER-TIME` is underestimated, input will switch to the second buffer before the first buffer is full. No data will be lost, but the resulting drain on spacecraft resources could preclude other activities, including parallel observations.

6.4.1 Faint Targets (BUFFER-TIME > Exposure Time)

For faint targets, the predicted BUFFER-TIME may be considerably longer than the exposure time. In such cases, set BUFFER-TIME equal to the exposure time. In orbits with multiple science exposures, you can minimize overheads – and squeeze out a few more seconds of observing time – by setting the BUFFER-TIME for each exposure to the exposure time minus 100 seconds. The buffer takes about 110 seconds to empty, so most of the data will be read out before the exposure is completed, leaving only a fraction for the end of the exposure. This allows the next exposure to begin sooner. You can test the effects of such trade-offs by trying them out within APT.

6.4.2 Bright Targets (BUFFER-TIME < 110 Seconds)

It takes 110 seconds to empty a COS data buffer. A BUFFER-TIME of 110 seconds corresponds to a count rate of 21,000 counts per second. If the count rate exceeds this value, then the second data buffer will be filled before the first buffer has been completely read out. In this situation, you have two options: You can shorten your exposure, or you can accept gaps in the recorded data stream. In either case, **calcos** will compute the actual exposure time and will calculate fluxes correctly, but the total number of collected counts, and hence the S/N, will be limited by the 21,000 counts per second rate.

- Option A: You wish to receive all the data and are willing to shorten the exposure time. In this case, use $2/3$ of the BUFFER-TIME returned by the ETC. If the BUFFER-TIME is less than 111 seconds, APT will issue a warning and truncate the exposure time at $2 \times \text{BUFFER-TIME}$ to ensure that all data are recorded.
- Option B: You can tolerate data drop-outs, but want control of the total exposure time. In this case, choose a BUFFER-TIME of 111 seconds. You will lose some fraction of the data during each BUFFER-TIME interval (see example below), but APT will not truncate your exposure.

As an example, suppose that $2/3 \times (\text{BUFFER-TIME returned by the ETC})$ is 100 seconds, and you want an exposure time of 360 seconds.

- With Option A, you would specify BUFFER-TIME=100. Because it takes longer than that to read out the buffer, APT limits you to an exposure time of $2 \times 100 = 200$ sec. In this case, COS records all the events that arrived during the exposure.
- With Option B, you would specify BUFFER-TIME=111. Since the COS buffer may be full after the first 100 seconds, the last 11 seconds of data may not be recorded and are lost each time the buffer fills. With this option you will get a series of data blocks as follows: **100**, *11*, **100**, *11*, **100**, *11*, **27**, where the bold numbers represent periods when the data are recorded, and the italic numbers represents periods when the data are lost. The COS shutter remains open for the full 360 seconds, and the data are properly flux calibrated by the pipeline.

6.4.3 Very Bright Targets (BUFFER-TIME < 80 Seconds)

The minimum allowed value of the BUFFER-TIME is 80 seconds. This value corresponds to a count rate of 30,000 counts per second over the entire detector, the maximum rate at which the flight electronics are capable of processing counts. If 2/3 of the ETC BUFFER-TIME is less than 80 seconds, then the source is very bright and should be observed in ACCUM mode. If your exposure is less than 80 seconds in length, set BUFFER-TIME=80. The buffer will be read out immediately after the exposure ends, and there will be no idle time.



The software and parameters that control dumps of the data buffer have been designed to avoid any loss of data from an observation. The duration and timing of data dumps depend on several factors, and observers are urged to experiment with APT to optimize the efficiency of their observations.

6.4.4 BUFFER-TIME and AUTO-ADJUST

If you use the AUTO-ADJUST feature in APT to set your exposure times, do it first, then adjust the BUFFER-TIME of each exposure according to the rules above.

6.5 Spanning the Gap with Multiple CENWAVE Settings

Single exposures for both the FUV and NUV channels have gaps in the spectra due to the physical layout of the detectors and optics.

The FUV detector consists of two segments whose active areas are separated by a gap approximately 9 mm wide. The optical image of the spectrum is continuous across the segments, but the wavelengths that fall in the gap are not recorded. These wavelengths can be brought onto the active area of the detector by choosing one of the alternate central-wavelength settings listed in [Table 6.4](#).

For the FUV M gratings, the gap (14-18 Å) is about twice the size of the difference in central wavelength shifts (9 Å). Thus the missing wavelengths are recovered by a second exposure two central-wavelength settings from the original exposure. For the G140L grating, both central wavelengths are needed to obtain a complete spectrum from below 1100 Å to Lyman α .

For the NUV channel, dispersed light from the gratings is imaged onto the detector by three camera mirrors, resulting in three non-contiguous spectral stripes being recorded at once. The gaps between the stripes are approximately 64 Å for the G185M and G225M gratings, 74 Å for G285M, and 700 Å for G230L ([Table 6.5](#)). To acquire a complete medium-resolution spectrum requires six settings with G185M, six with G225M, and eight with G285M. A full spectrum with G230L requires all four central wavelength settings. Such a complete spectrum can probably be acquired more efficiently with STIS, but COS may be a better choice when a limited number of specific wavelengths is desired.

6.6 FUV Single-Segment Observations

The FUV detector segments are operated and read out independently. For all FUV gratings, segment A detects the longer-wavelength light and segment B the shorter wavelengths. Normally, both segments are used for a science exposure, but there are circumstances in which operating with one detector segment at the nominal high voltage and the other effectively turned off may be beneficial. The `SEGMENT` optional parameter allows this choice. STScI strongly recommends use of both segments (the default for all but the G140L 1105 Å setting) unless special circumstances exist. Such circumstances include

- Sources with unusual spectral energy distributions at FUV wavelengths (bright emission lines or rapidly increasing/decreasing continuum slopes), for which the count rate on one detector segment exceeds the bright-object protection limit, while the other segment is safe for observing. In some cases, this problem may be mitigated by adjusting the central wavelength or `FP-POS` setting.
- Sources for which the count rate on one detector segment is high but safe, while the other segment has a relatively low count rate. If the science to be done were on the low count-rate segment, operating just that segment would reduce data losses due to dead-time effects and increase the S/N of the resulting spectrum.

The optional parameter `SEGMENT` (=BOTH (default), A, or B) specifies which segment of the FUV detector to use for an observation. A value of `BOTH` will activate both segments. If `A` is selected, only segment A of the detector will be activated for photon detection, and the spectrum will contain data from only the long-wavelength half of the detector. If `B` is selected, only the short-wavelength segment B of the detector will be activated and used to generate data. Wavelength and flat-field calibration procedures remain the same for a particular segment whether the other segment is operating or not.

If grating G140L is specified with the 1105 Å wavelength setting, then the value must be `SEGMENT=A`. Switching from two-segment to single-segment operation (or back again) incurs a substantial overhead time; see [Table 10.4](#).

6.7 Internal Wavelength Calibration Exposures

Three types of internal wavelength calibration exposures may be inserted in the observation sequence by the scheduling system or by the observer:

1. `FLASH=YES` (so-called TAGFLASH) lamp flashes (`TIME-TAG` observing with the PSA only),
2. `AUTO` wavecal, and
3. User-specified wavecal.

Note that *all* wavelength-calibration exposures are taken in TIME-TAG mode. Wavelength calibration exposure overheads are higher when the BOA is used for science observation, because the aperture mechanism must be moved to place the WCA in the wavelength-calibration beam.

While it is possible to suppress the taking of any wavelength-calibration spectra, doing so significantly lessens the archival quality of COS data and must be justified on a case-by-case basis.

6.7.1 Concurrent Wavelength Calibration with TAGFLASH

The Optional Parameter FLASH indicates whether or not to “flash” the wavelength calibration lamp during TIME-TAG exposures utilizing the PSA. These flashes provide data used by the **calcos** pipeline to compensate for drifts of the Optics Select Mechanisms. In this mode, when the external shutter is open to observe an external target, the wavecal lamp is turned on briefly at the beginning of and at intervals throughout the exposure. Light from the science target and the internal wavelength calibration source is recorded simultaneously on different portions of the detector. Other than the flash at the start, the timing of flashes is determined by the elapsed time since the last OSM motion. As a result, flashes may occur at different times in different exposures. The grating-dependent flash durations (Table 6.3) and the flash intervals are defined and updated as necessary by STScI. Observers may not specify either flash duration or interval. When flashing is enabled, the exposure time must be at least as long as a single flash.

TIME-TAG sequences with FLASH=YES provide the highest on-target exposure time, as no on-target time is lost to wavelength-calibration exposures. We thus strongly recommend use of Optional Parameter FLASH=YES with all TIME-TAG observations through the PSA. (Since FLASH=YES is the default for TIME-TAG spectroscopic exposures, the observer need not specify it.) FLASH=YES may not be specified for ACCUM mode or when the BOA is selected.

6.7.2 AUTO Wavecals (when TAGFLASH is not used)

For ACCUM, BOA, or FLASH=NO TIME-TAG exposures, a separate wavelength calibration exposure will be automatically scheduled by APT for each set of external spectrographic science exposures using the same spectral element, central wavelength, and FP-POS value. These AUTO wavecals are always obtained in TIME-TAG mode with the external shutter closed. This automatic wavelength calibration exposure will be added before the first associated science exposure and after each subsequent science exposure if more than 40 minutes of visibility time has elapsed since the previous wavelength calibration exposure and if the same spectrograph set-up has been in use over that time. The calibration exposure will often use some science target orbital visibility. The calibration lamp configuration and exposure time will be based on the grating and central wavelength of the science exposure. Utilization of a GO wavecal (see below) resets the 40 minute interval timer. Insertion of a FLASH=YES exposure in the time-line does not affect the 40-minute clock.

Table 6.3: TAGFLASH Exposure Durations

Grating	Central Wavelength (Å)	Flash duration (s)	Grating	Central Wavelength (Å)	Flash duration (s)
G130M	all	12	G225M (cont.)	2357	12
G160M	all	12		2373	22
G140L	all	7		2390	7
G185M	1786	12		2410	7
	1817	12	G285M	2617	12
	1835	12		2637	12
	1850	22		2657	7
	1864	32		2676	22
	1882	17		2695	22
	1890	12		2709	12
	1900	22		2719	7
	1913	17		2739	7
	1921	12		2850	22
	1941	12		2952	7
	1953	17		2979	17
	1971	17		2996	17
	1986	12		3018	22
2010	12	3035		27	
G225M	2186	7	3057	32	
	2217	12	3074	32	
	2233	7	3094	32	
	2250	22	G230L	2635	7
	2268	12		2950	7
	2283	12		3000	7
	2306	12		3360	12
	2325	12	MIRRORA	...	7
	2339	12	MIRRORB	...	27

AUTO wavecals may not be turned off by the observer. If there is a science requirement to turn off AUTO wavecals, specific permission must be sought from the STScI Contact Scientist.

FLASH=NO observations will be less efficient than FLASH=YES observations in terms of on-target utilization of orbital visibility and in the quality of their wavelength calibration due to possible OSM residual motions.

6.7.3 GO Wavecals (User-specified)

Observers may request additional wavelength-calibration exposures, called GO wavecals, by selecting `TARGET=WAVE`, `EXPTIME=DEF`, and `FLASH=NO`. The exposure must be made in `TIME-TAG` mode. GO wavecals use the same calibration lamp configuration and exposure times as the automatic wavelength calibrations discussed above. The default modes of operation automatically secure needed wavelength-calibration information to go with your science data, so GO wavecals are rarely required.

6.7.4 No-Cal Wavecals

The COS Pt-Ne wavelength-calibration lamps produce no lines on FUV segment B in the following observing modes:

- G130M, central wavelength 1055 Å, all FP-POS settings;
- G130M, central wavelength 1096 Å, all FP-POS settings;
- G140L, central wavelength 1280 Å, all FP-POS settings.

To these data, **calcos** assigns the wavelength shifts derived from the segment A spectrum. If no segment A data are present, no shift is assigned.

6.8 Fixed-Pattern Noise

The signal-to-noise ratio (S/N) of COS observations is improved through two techniques, flat fielding and coadding spectra taken at different central wavelengths or FP-POS settings. Flat fielding removes the high-frequency, pixel-to-pixel detector variations by dividing the data by a high S/N flat-field response image. FP-POS exposures smooth out the detector variations by combining in wavelength space data taken at different positions on the detector.

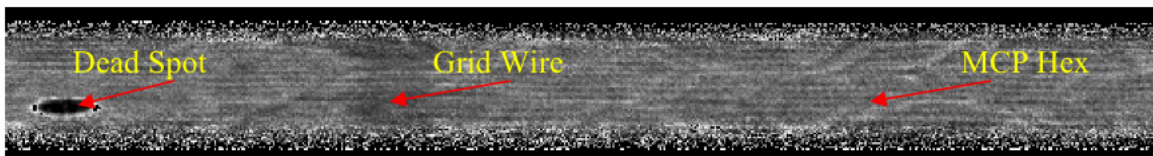
6.8.1 COS Flat Fielding

The internal flat-field calibration system consists of two deuterium lamps and the flat-field calibration aperture (FCA). The system was designed such that light from the lamps follows nearly the same optical path as that from an external target. The FCA is placed near the usual location of the PSA, and the lamp beam illuminates the gratings and mirrors from this slightly offset position.

The deuterium lamps are not bright enough to map out the flat field at FUV wavelengths, so the FUV flats are constructed from on-orbit observations of bright white dwarfs. A preliminary FUV flat is shown in [Figure 6.8](#). The dark, vertical stripe is a shadow cast by a grid wire in front of the detector ([Section 4.1.1](#)). A detector dead spot and the hexagonal pattern of the fiber bundles in the micro-channel plate are also visible. Although significant structure is present in the FUV flats, it is reproducible and can be removed during data reduction.

The COS FUV detector can achieve a S/N of about 18 per resel (6×10 pixels) with a single grating setting. By using multiple FP-POS settings, it is possible to reach S/N = 35 per resel. Using high S/N data obtained during SMOV at four FP-POS settings of the G160M grating at a central wavelength 1600 Å, and using a data-reduction technique that estimates the flat field from the data itself, we have demonstrated the capability of the FUV detector to achieve S/N > 100 per resel in special circumstances. At the time of this writing, a flat-field calibration file is not yet available for FUV data. Characterization of the FUV flat field is ongoing. Observers are advised to check the [COS Web pages](#) for the latest developments.

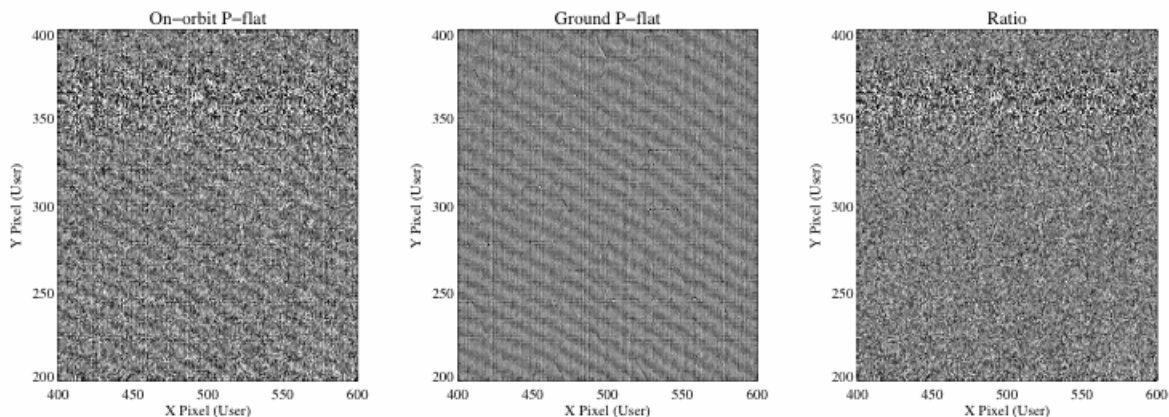
Figure 6.8: Section of a Flat-Field Image for the FUV XDL



A section of the FUV flat field showing representative detector features and a grid wire.

The NUV flat field used by **calcos** was built from a combination of external PSA deuterium lamp exposures taken on the ground and internal FCA observations taken on the ground and on orbit. [Figure 6.9](#) presents a comparison between two NUV flat-field frames, one obtained on orbit and one on the ground. Each image was divided by a low-order polynomial to isolate the high-order fringe pattern characteristic of the NUV detector. Their ratio is consistent with the noise in the on-orbit image, indicating that the ground image can be used to flat-field data taken on orbit. Pre-flight ground tests with COS show that the NUV MAMA can deliver S/N up to about 50 without using a flat field. Using a flat field, S/N of 100 or more per resolution element should be routinely achievable.

Figure 6.9: Flat-Field Exposures for the NUV MAMA



6.8.2 Use of Optional Parameter FP-POS

Fixed-pattern noise in the COS detectors limits the S/N that can be achieved in a single exposure to ~18 per resolution element for the FUV and 50 for the NUV. To achieve higher S/N ratios, one can obtain a series of exposures, each slightly offset in the dispersion direction, causing spectral features to fall on a different part of the detector. For STIS and GHRS, these motions are known as FP-SPLITS. For COS, these motions are specified by the FP-POS optional parameter.

Four FP-POS offset positions are available: a nominal position (0), two positions toward longer wavelengths (-2 and -1), and one position toward shorter wavelengths (+1). Positions -2, -1, 0, and +1 are designated respectively as FP-POS=1, 2, 3, and 4. The nominal position, FP-POS=3, is the default and is the setting used to define the wavelength range associated with the grating central wavelengths (Table 6.4 and Table 6.5). In pipeline processing, **calcos** creates individual calibrated spectra for each FP-POS exposure, then aligns and combines them into a merged spectral product, using only good-quality data at each wavelength.

The optical mechanism on which the grating is mounted is rotated by one step for each adjacent FP-POS position. The amount that a particular spectral feature moves in the dispersion direction on the detector is approximately 250 pixels per step for the FUV channel and 52 pixels for the NUV. The corresponding wavelength shifts for each grating are given in Chapter 14. There is a preferred direction for moving the grating mechanism; overheads are reduced if FP-POS exposures are obtained in increasing order (see Section 10.3). When moving to a new grating or central-wavelength setting, you may select any FP-POS position without paying an additional overhead penalty. Thus, the most efficient order is FP-POS=1, 2, 3, 4, as it requires no backward motion of the grating mechanism.

A wavelength calibration exposure will be obtained each time the FP-POS changes. For FLASH=YES exposures, the time-since-grating-move clock is not reset by an FP-POS movement; however, there will always be at least one lamp flash during each individual FP-POS exposure. For FLASH=NO exposures, a separate wavelength calibration exposure will be taken for each FP-POS position change.

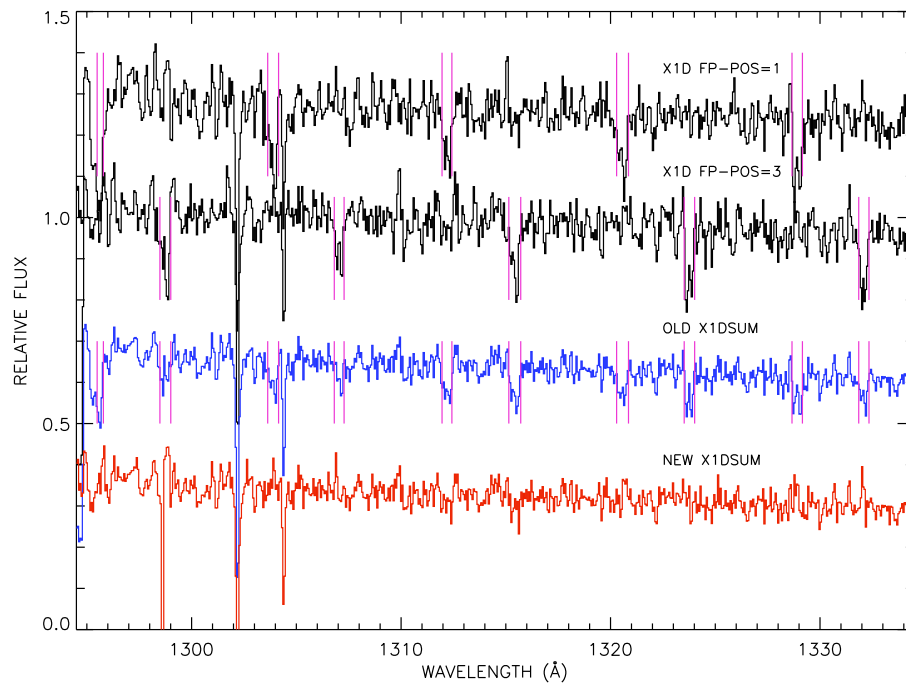
FP-POS and gap coverage in the FUV

The two segments of the COS FUV detector have a gap between them (Section 6.5). If you require a spectrum that covers all available wavelengths at medium resolution, the best strategy is to use the grating at one FP-POS setting but at four consecutive central wavelengths. For example, use of G130M at central wavelengths 1300, 1309, 1318, and 1327 Å, all with FP-POS=3, will efficiently cover the full range available with G130M and will provide the equivalent of four FP-POS positions. To construct a complete FUV medium-resolution spectrum, we recommend using G130M at its four shortest central wavelengths plus G160M at its four longest wavelengths. The pipeline does not combine spectra with different central wavelengths, but a tool to do so is under development.

Requirements for Use of Multiple FP-POS or CENWAVE Settings

Because the use of multiple FP-POS settings results in spectra with significantly higher S/N ratios, proposers who do not intend to use multiple FP-POS settings must justify their observing strategy in their Phase I proposals. In general, COS observations that do not employ two or more FP-POS or CENWAVE settings will not be approved without strong justification that such is required for the scientific objectives of the program. Otherwise, grid wires and other detector artifacts may compromise the archival value of the data.

Figure 6.10: Use of Multiple FP-POS Settings to Improve S/N Ratio



On-orbit FUV observations of a white dwarf. The black curves represent single exposures at two FP-POS settings. Grid-wire shadows are marked with purple lines. The blue curve represents a simple sum of these spectra. It shows twice as many grid-wire shadows as the individual exposures, but they are half as deep. To produce the red curve, spectral regions affected by grid-wire shadows are masked before the spectra are combined. This technique is employed by **calcos** versions 2.6b and later to construct summed extracted spectra (`x1dsum` files).

6.8.3 A Simple Example

To illustrate how these techniques can improve the S/N of COS spectra, [Figure 6.10](#) presents on-orbit spectra of the white dwarf WD 0320-539. The black curves represent single exposures at two FP-POS settings, taken with segment A of the FUV detector. The regularly-spaced absorption features are shadows cast by the grid wires; only the O I λ 1302 and Si II λ 1304 lines are astrophysical. Summing the spectra from multiple FP-POS settings reduces the depth of the grid-wire features (blue spectrum), but doubles their number. The red spectrum is the result of masking the grid-wire shadows in each spectrum before combining them. Between 1305 and 1330 Å, the two black curves have S/N = 18.6 per resel, the blue has 28.1, and the red has 33.8. Masking the grid wires nominally improves the S/N by 20% in this case, but the real improvement is in the removal of large, systematic features. This technique is employed by **calcos** versions 2.6b and later to produce `x1dsum` files ([Section 12.2](#)).

6.9 COS Spectroscopy of Extended Sources

COS spectra of extended objects could have significantly lower resolution than those of point sources, depending on the spatial distribution of the source. For example, measurements of Lyman α airglow lines, which uniformly fill the COS aperture, show $R = 1450$ for G130M and $R = 165$ for G140L. Filled-aperture observations of SNR N132D confirm $R \sim 1500$ for both FUV M gratings (France et al. 2009, *ApJ*, 707, L27). In the NUV, the situation is much worse, because a source that fills the aperture will lead to cross-contamination among the three spectral stripes on the MAMA detector.

A similar but more favorable situation arises in the case of multiple point sources that fall within the aperture. COS was designed to resolve two point sources that are one arcsec apart in the cross-dispersion direction, and ground tests confirm that it is possible. However, a point source that is more than 0.4 arcsec from the center of the PSA will not have all of its light transmitted; see [Section 8.8.1](#).

The optional Parameter `EXTENDED` (default = NO) sets a science header keyword to inform the **calcos** pipeline that the target is an extended source. The keyword may be used in the future to activate special data-reduction procedures, although none are currently in the pipeline. No aspect of on-board data-taking is affected by this parameter.

6.10 Wavelength Settings and Ranges

Table 6.4 and Table 6.5 show the wavelength ranges recorded on the detectors for each valid combination of grating and central-wavelength setting at the default FP-POS=3 position (Section 6.8.2). The wavelength ranges spanned at other FP-POS settings may be estimated using the FP-POS step values provided in Chapter 14. Note, however, that uncertainties in the positioning of the Optics Select Mechanisms (Section 3.3.3) correspond to about half of an FP-POS step. These wavelength ranges are subject to change as the instrumental calibration evolves. The most recent measurements are available from the [COS Web site](#).

Table 6.4: Wavelength Ranges for FUV Gratings for FP-POS=3

Grating	Central wavelength setting (Å) ¹	Recorded wavelengths ²	
		Segment B	Segment A
G130M	1055	899 – 1040	1055 – 1196
	1096	940 – 1080	1096 – 1236
	1291	1134 – 1274	1291 – 1431
	1300	1144 – 1283	1300 – 1441
	1309	1154 – 1294	1309 – 1450
	1318	1163 – 1303	1319 – 1460
	1327	1172 – 1313	1328 – 1469
G160M	1577	1386 – 1559	1577 – 1751
	1589	1397 – 1571	1589 – 1762
	1600	1409 – 1581	1601 – 1774
	1611	1420 – 1594	1612 – 1786
	1623	1432 – 1606	1625 – 1798
G140L	1105	HV OFF	1118 – 2251 ³
	1280	<900 – 1165	1280 – 2391 ³

1. The central wavelength is (approximately) the shortest wavelength recorded on segment A.
2. All wavelength ranges quoted here are approximate, due to uncertainties in the position of the OSM1 mechanism.
3. G140L spectra are flux calibrated up to 2150 Å. At longer wavelengths, second-order light may be present.

Table 6.5: Wavelength Ranges for NUV Gratings for FP-POS=3

Grating	Central wavelength setting (Å) ¹	Recorded wavelengths		
		Stripe A	Stripe B	Stripe C
G185M	1786	1670 – 1705	1769 – 1804	1868 – 1903
	1817	1701 – 1736	1800 – 1835	1899 – 1934
	1835	1719 – 1754	1818 – 1853	1916 – 1951
	1850	1734 – 1769	1833 – 1868	1931 – 1966
	1864	1748 – 1783	1847 – 1882	1945 – 1980
	1882	1766 – 1801	1865 – 1900	1964 – 1999
	1890	1774 – 1809	1872 – 1907	1971 – 2006
	1900	1783 – 1818	1882 – 1917	1981 – 2016
	1913	1796 – 1831	1895 – 1930	1993 – 2028
	1921	1804 – 1839	1903 – 1938	2002 – 2037
	1941	1825 – 1860	1924 – 1959	2023 – 2058
	1953	1837 – 1872	1936 – 1971	2034 – 2069
	1971	1854 – 1889	1953 – 1988	2052 – 2087
	1986	1870 – 1905	1969 – 2004	2068 – 2103
	2010	1894 – 1929	1993 – 2028	2092 – 2127
G225M	2186	2070 – 2105	2169 – 2204	2268 – 2303
	2217	2101 – 2136	2200 – 2235	2299 – 2334
	2233	2117 – 2152	2215 – 2250	2314 – 2349
	2250	2134 – 2169	2233 – 2268	2332 – 2367
	2268	2152 – 2187	2251 – 2286	2350 – 2385
	2283	2167 – 2202	2266 – 2301	2364 – 2399
	2306	2190 – 2225	2288 – 2323	2387 – 2422
	2325	2208 – 2243	2307 – 2342	2406 – 2441
	2339	2223 – 2258	2322 – 2357	2421 – 2456
	2357	2241 – 2276	2340 – 2375	2439 – 2474
	2373	2256 – 2291	2355 – 2390	2454 – 2489
	2390	2274 – 2309	2373 – 2408	2472 – 2507
	2410	2294 – 2329	2393 – 2428	2492 – 2527

Grating	Central wavelength setting (Å) ¹	Recorded wavelengths		
		Stripe A	Stripe B	Stripe C
G285M	2617	2480 – 2521	2596 – 2637	2711 – 2752
	2637	2500 – 2541	2616 – 2657	2731 – 2772
	2657	2520 – 2561	2636 – 2677	2751 – 2792
	2676	2539 – 2580	2655 – 2696	2770 – 2811
	2695	2558 – 2599	2674 – 2715	2789 – 2830
	2709	2572 – 2613	2688 – 2729	2803 – 2844
	2719	2582 – 2623	2698 – 2739	2813 – 2854
	2739	2602 – 2643	2718 – 2763	2837 – 2878
	2850	2714 – 2755	2829 – 2870	2945 – 2986
	2952	2815 – 2856	2931 – 2972	3046 – 3087
	2979	2842 – 2883	2958 – 2999	3073 – 3114
	2996	2859 – 2900	2975 – 3016	3090 – 3131
	3018	2881 – 2922	2997 – 3038	3112 – 3153
	3035	2898 – 2939	3014 – 3055	3129 – 3170
	3057	2920 – 2961	3036 – 3077	3151 – 3192
	3074	2937 – 2978	3053 – 3094	3168 – 3209
3094	2957 – 2998	3073 – 3114	3188 – 3229	
G230L	2635	1334 – 1733 ²	2435 – 2834	1768 – 1967³
	2950	1650 – 2050	2750 – 3150	1900 – 2100³
	3000	1700 – 2100	2800 – 3200	1950 – 2150³
	3360	2059 – 2458 ⁴	3161 – 3560 ⁵	2164 – 2361³

1. The central wavelength setting corresponds to the approximate midpoint of stripe B.
2. For central wavelength 2635 Å, the stripe A wavelengths are listed for completeness only (and in case a bright emission line falls onto the detector). The NUV detector's sensitivity at these wavelengths is extremely low. To obtain a low-resolution spectrum at wavelengths below ~ 1700 Å, we recommend the FUV grating G140L.
3. The values in shaded cells are wavelength ranges observed in second order. Their dispersion is twice that of the first-order spectrum. First-order flux, from wavelengths twice those of the listed range, will be present at the ~ 5% level.
4. Lyman α may be present in second order.
5. Longward of 3200 Å, second-order light may be present. No flux calibration is performed for these wavelengths.

Imaging with COS

In this chapter...

7.1 Introduction to COS Imaging / 61

7.2 Sensitivity / 63

7.3 Image Characteristics / 64

7.1 Introduction to COS Imaging

The COS NUV channel provides high spatial resolution across a narrow field of view. With a plate scale of 23.5 mas per pixel, its spatial sampling is the highest of any instrument aboard *HST*. [Figure 7.1](#) shows an image of Pluto and its moon Charon obtained with COS. COS images are fully corrected for the telescope's spherical aberration, though not for the zonal (polishing) errors on its primary and secondary mirrors ([Chapter 5](#)). Because the optics image the sky onto the detector, rather than the aperture, COS images extend to a radius of 2 arcsec, but suffer considerable vignetting at radii greater than 0.5 arcsec, as shown in [Figure 7.2](#).

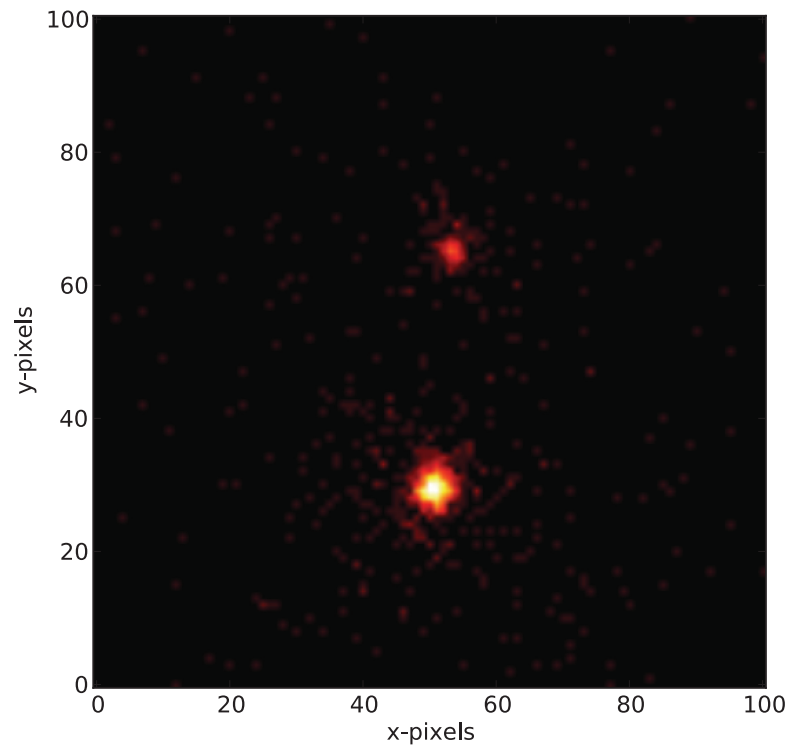
To request an imaging observation, specify `CONFIG = COS/NUV` and `MODE = TIME-TAG` or `ACCUM`. If `TIME-TAG` mode is selected, the minimum allowable `BUFFER-TIME` is 80 seconds, which may be longer than the expected exposure time. `ACCUM` mode is recommended for such short exposures. `MIRRORB` and/or the `BOA` can be used to obtain images of bright objects, but at some cost in spatial resolution; see [Section 8.4](#) for details.

To track motions of the optics selection mechanisms during `TIME-TAG` exposures longer than ~ 6 minutes, lamp flashes may be requested by setting `FLASH=YES`; a lamp flash in imaging mode will illuminate the WCA, whose position relative to the PSA is known. By default, `FLASH=NO` for all imaging modes.

COS imaging in `TIME-TAG` mode allows for high-speed NUV photometry with a temporal resolution of 32 msec. STIS is capable of much finer time resolution (125 microseconds), but at lower sensitivity.

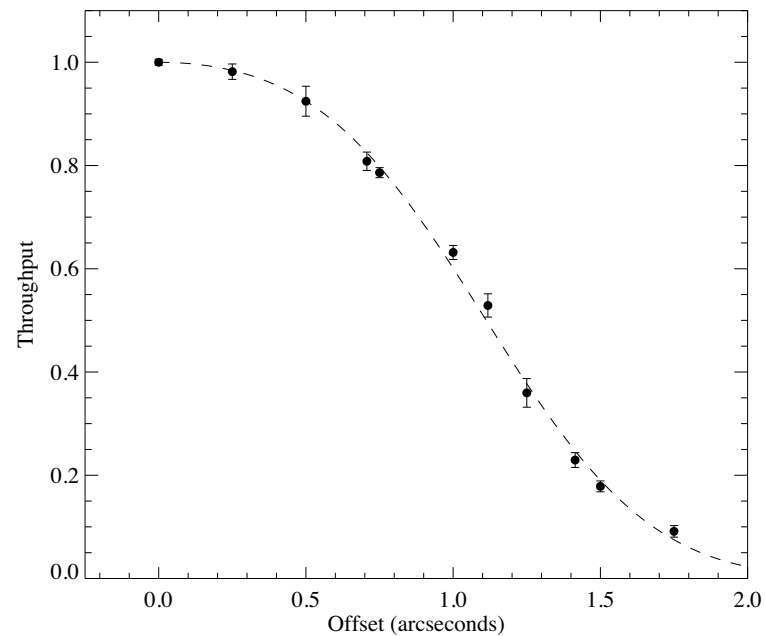
The minimum COS exposure duration is 0.1 seconds, as discussed in [Section 6.3](#).

Figure 7.1: Pluto and Charon Observed with COS



NUV exposure of Pluto and Charon, separated by $0.8''$. The exposure time is 25 seconds. Note that the pixels numbers refer only to this sub-section of the full image. Image courtesy of J. Green.

Figure 7.2: Relative Throughput of the COS PSA in NUV Imaging Mode



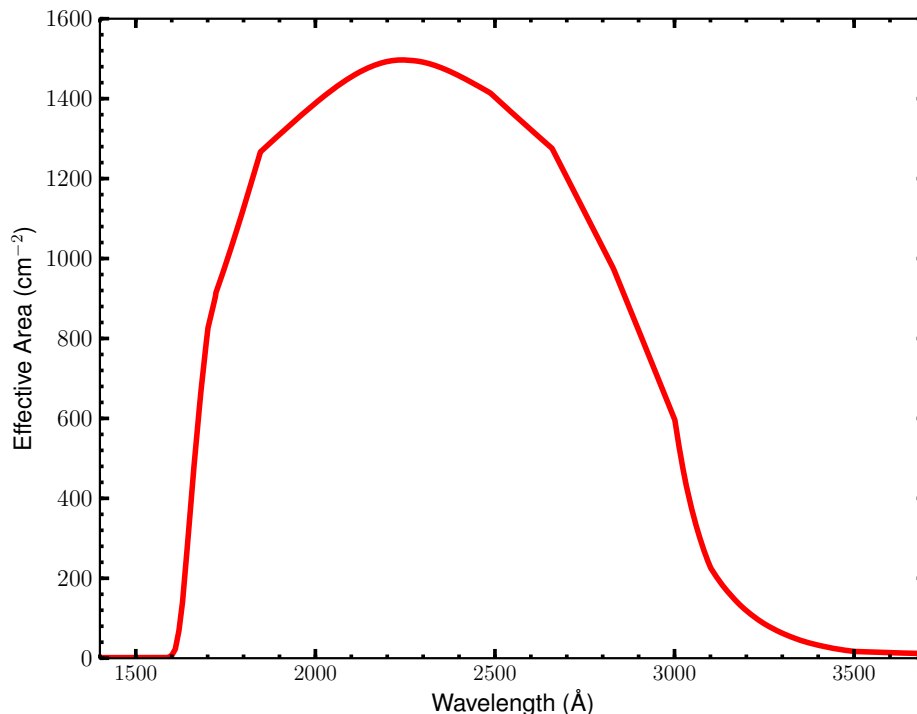
7.2 Sensitivity

In imaging mode, the COS effective area extends from about 1600 to 3300 Å, peaking at ~ 2300 Å (Figure 7.3). Care should be taken when observing cool stars ($T_{\text{eff}} < 5,000$ K) and other red objects, as high count rates at long wavelengths could damage the detector.

COS is a sensitive instrument, its imaging mode concentrates the target's NUV flux into a diffraction-limited image rather than dispersing the light. The local count rate limit for COS/NUV is 50 counts per pixel per second (Table 9.1), and that limit is easily reached, even for fairly faint objects. Observers should use the COS Exposure Time Calculator (ETC) to get an accurate estimate of expected count rates, but the following values will provide a guide. These have been calculated for a flat-spectrum source (flux independent of wavelength), and the limiting count rate is reached at the following approximate flux levels:

Aperture and Mirror	Flux Limit ($\text{erg cm}^{-2} \text{s}^{-1} \text{\AA}^{-1}$)
PSA + MIRRORA	2×10^{-15}
BOA + MIRRORA	4×10^{-13}
PSA + MIRRORB	3×10^{-14}
BOA + MIRRORB	6×10^{-12}

Figure 7.3: Effective Area for COS NUV Imaging with the PSA/MIRRORA



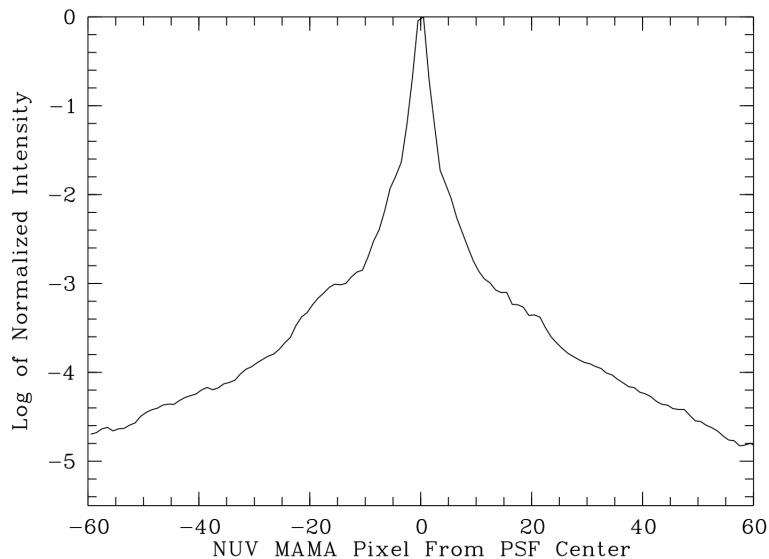
7.3 Image Characteristics

A two-dimensional Gaussian fit to a typical imaging PSF has a FWHM of 1.97 pixels (47.1 mas), with 13.4% of the light in the brightest pixel. Because the *HST* focus varies with orbital phase, FWHM values can range from 1.8 to 2.4 pixels.

As discussed in [Chapter 5](#), mid-frequency wavefront errors (MFWFEs) contribute significantly to the PSF wings at wavelengths $< 2500 \text{ \AA}$, so the spatial resolution of a point source will depend somewhat on its spectral energy distribution. For an M star, which has little flux at the shortest wavelengths, the image would be close to diffraction limited. For a hot white dwarf, the MFWFEs would have the maximum impact on the spatial resolution.

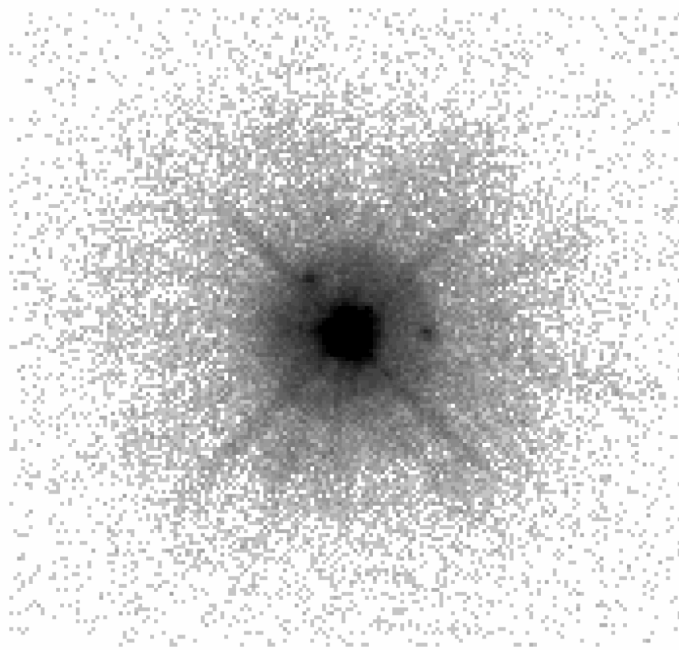
Deep images reveal the detailed shape of the COS imaging PSF. [Figure 7.4](#) shows the COS imaging PSF, averaged over 180 degrees of azimuth, and plotted on a log scale to reveal its extended wings. [Figure 7.5](#) shows a 2-dimensional grey-scale image of a deep imaging observation that reveals two low-level “ghosts” located approximately 20 pixels to the right and the upper left of the center of the PSF. The peak intensity of the brightest of the two ghosts is roughly 0.1% of that of the main PSF. These features may complicate the analysis of faint objects located in the wings of a brighter object.

Figure 7.4: Extended Wings in the COS Imaging PSF



Azimuth-averaged COS imaging PSF plotted with a logarithmic intensity scale.

Figure 7.5: Ghosts in COS NUV Images



Negative greyscale rendering of a deep COS NUV image of a point source. This figure is plotted with a logarithmic intensity scale and covers about 6.5 arcsec along each axis. Note the two ghost images to the right and upper left of the center of the PSF.

Target Acquisitions

In this chapter...

8.1 Introduction / 66
8.2 Target Acquisition Overview / 67
8.3 ACQ/SEARCH Acquisition Mode / 68
8.4 ACQ/IMAGE Acquisition Mode / 72
8.5 ACQ/PEAKXD Acquisition Mode / 74
8.6 ACQ/PEAKD Acquisition Mode / 75
8.7 Exposure Times / 76
8.8 Centering Accuracy and Data Quality / 77
8.9 Recommended Parameters for all COS TA Modes / 79
8.10 Special Cases / 81

8.1 Introduction

The COS apertures are 2.5 arcsec in diameter. An observation will yield high-quality data only if the target is properly centered in the desired aperture. This chapter discusses the available target-acquisition (TA) methods, demonstrates the dependence of data quality on centering accuracy, and recommends acquisition scenarios for various combinations of target coordinate accuracy and brightness. Recommended parameters for all COS TA modes are presented in [Section 8.9](#).

Based on recent improvements in the COS-to-FGS alignment, together with an analysis of the distribution of positional errors in the GSC2, we estimate that an *HST* guide-star acquisition will place a target in the COS aperture 98.5% of the time. As a result, we no longer require that all COS observations begin with an ACQ/SEARCH sequence if the uncertainty of the target coordinates is $\leq 0.4''$. We do, however, recommend that some sort of target acquisition be performed to center the target in the aperture. APT (the [Astronomer's Proposal Tool](#)) will issue a warning if an acquisition is omitted. Target acquisition is required only once for a series of observations in contiguous orbits (i.e., once per visit). Moving targets require an acquisition at the beginning of each orbit.

Bright Object Protection

The COS detectors are vulnerable to damage or performance degradation if exposed to too much light. Imaging acquisitions are a special risk because they concentrate the light of an object on a small area of the detector. Users of COS must demonstrate that their targets are safe. Information on bright-object protection and screening is in [Chapter 9](#).

8.2 Target Acquisition Overview

COS has four TA modes:

- **ACQ/SEARCH** performs a spiral search by executing individual exposures at each point in a square grid pattern on the sky (details are in [Section 8.3](#)). This mode can use either dispersed-light or imaging exposures.
- **ACQ/IMAGE** obtains an NUV image of the target field, moves the telescope to center the object, and obtains a second NUV image as confirmation (details are in [Section 8.4](#)). This is generally the fastest and most accurate method of target acquisition, but covers a limited area on the sky.
- **ACQ/PEAKXD** determines the centroid of the dispersed-light spectrum in the cross-dispersion (XD) direction and moves the telescope to center the object in the XD direction (details are in [Section 8.5](#)).
- **ACQ/PEAKD** centers the target in the along-dispersion (AD) direction by executing individual exposures at each point in a linear pattern along the dispersion axis (details are in [Section 8.6](#)). ACQ/PEAKXD should always precede ACQ/PEAKD, and the two should always be performed together.

Coordinate accuracy and target brightness will inform your choice of target-acquisition strategy and optional parameters. While these TA modes can be used in any order or even repeated, the recommended strategies are given in [Table 8.1](#).

Table 8.1: Basic COS Target Acquisition Strategies

Type	Step 1	Step 2	Step 3
Imaging (coordinates good to 0.4")	ACQ/IMAGE	none	none
Imaging	ACQ/SEARCH	ACQ/IMAGE	none
Dispersed-Light (coordinates good to 0.4")	ACQ/PEAKXD	ACQ/PEAKD	none
Dispersed-Light	ACQ/SEARCH	ACQ/PEAKXD	ACQ/PEAKD
Either Imaging or Dispersed-Light	ACQ/SEARCH	2 × 2 × 1.767 ACQ/SEARCH	none

Imaging acquisitions are fast and precise, but restrictions on the local count rate ([Chapter 9](#)) can prevent their use. We suggest evaluating the TA strategies in the following order:

1. NUV imaging target-acquisition sequence with the fastest allowable combination of aperture and mirror, even if the science to follow is performed with the FUV channel.
2. Dispersed-light acquisition using the same configuration as the first science exposure, if it will use less time overall.
3. Dispersed-light acquisition with a different configuration, if it will use less time overall.

The basic scenarios outlined here are for isolated point sources. See [Section 8.10](#) for additional information regarding crowded or complex fields and offset-target TAs.

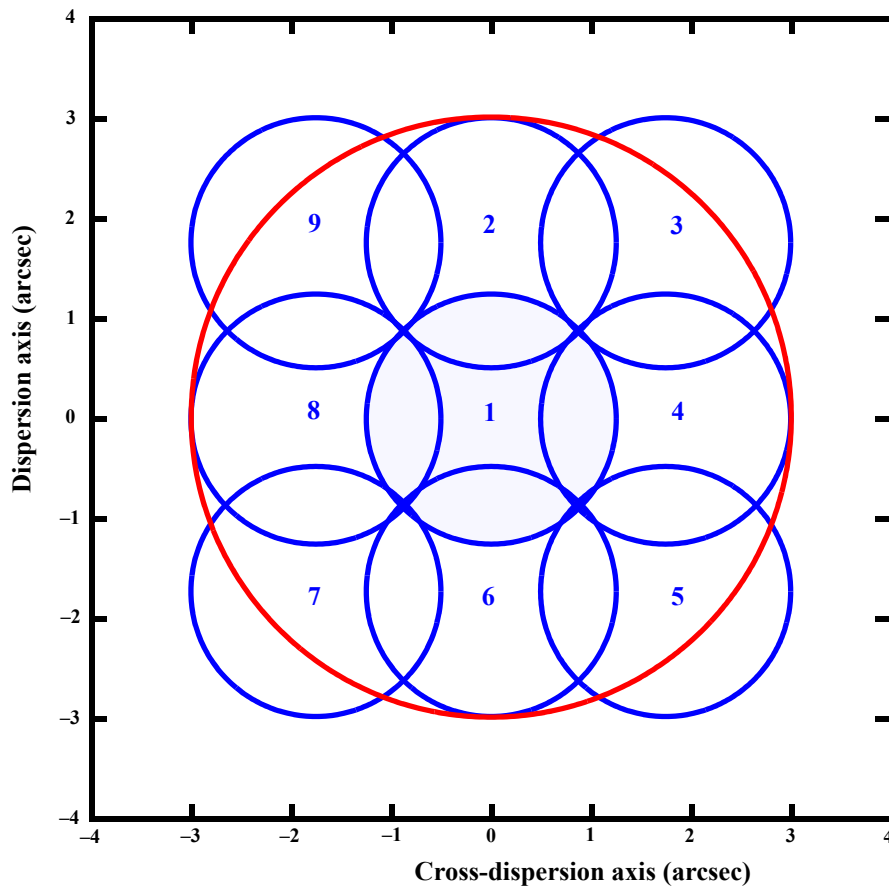
Please Note...

- It is the responsibility of the observer to provide coordinates and proper motions with the required accuracy. Observations that fail because of an inaccurate target position will not be repeated. STScI cannot be responsible for target-coordinate or proper-motion errors in published catalogs or in the literature. If there is any doubt that the available coordinates meet the required accuracy, then an ACQ/SEARCH should be performed.
- If a target falls near the edge of the aperture at the initial pointing, ACQ/IMAGE or ACQ/PEAKXD may achieve slightly degraded centering. Users who require the best possible photometric or absolute wavelength accuracy may wish either to begin with an ACQ/SEARCH to ensure that the target is reasonably well centered before the final stages of the acquisition are performed, or to perform an extra ACQ/IMAGE or ACQ/PEAKXD in case the observation at the initial pointing was partially vignetted.
- At the present time, the new central-wavelength settings for G130M (1055 and 1096 Å) cannot be used for target acquisitions.

8.3 ACQ/SEARCH Acquisition Mode

8.3.1 Description

In ACQ/SEARCH mode, the telescope is moved in a spiral pattern on the sky to cover a square grid up to 5×5 steps in size. At each scan point, the telescope stops and an integration is taken. A two-dimensional array containing the total counts measured at each dwell point is constructed. After completion of the full $n \times n$ pattern, the target position is calculated as described below, and the telescope is moved to center the target. A 3×3 ACQ/SEARCH is illustrated in [Figure 8.1](#).

Figure 8.1: Example of a 3×3 Spiral Search Pattern

This 3×3 spiral search was executed with the default STEP-SIZE of 1.767 arcsec. The blue circles represent the nine positions of the 2.5" diameter aperture, and the numbers show the sequence of steps. The large outer circle in red has a radius of ~ 3 arcsec. An initial pointing that was good to 1 arcsec (1σ) would result in a successful acquisition with a 3×3 pattern 99.5% of the time.

For an ACQ/SEARCH, the user must specify:

- The aperture to use, either PSA or BOA.
- The spectral element (grating or mirror) and the central-wavelength setting (if applicable). For a spectroscopic ACQ/SEARCH, these will generally be the grating and central wavelength of the initial science observation; however, an observer may use ACQ/SEARCH with a different grating and central-wavelength setting if there are advantages to doing so.
- The SCAN-SIZE, which is 2, 3, 4, or 5, corresponding to spiral patterns of 2×2 , 3×3 , etc.

- The `STEP-SIZE`, or spacing between grid points. It may be any value from 0.2 to 2.0 arcsec, but we strongly recommend using the default value of 1.767 arcsec. This value has been chosen so that no part of the sky is missed, given the 2.5 arcsec diameter aperture ($2.5''/\sqrt{2} = 1.767''$).
- The exposure time per dwell point.
- For FUV searches, users may choose to use just one of the segments, A or B, but the use of both (the default for all but G140L) is recommended.

Once the scan is complete, the flight software determines which point in the array contains the source. There are three centroiding options:

1. The first option is `CENTER=FLUX-WT`, which uses a flux-weighted centroiding algorithm to determine the center of light. It is the default for `SCAN-SIZE=2`.
2. A variation on `CENTER=FLUX-WT` is `CENTER=FLUX-WT-FLR`. In this case, a floor is subtracted from the counts at each dwell point before the centroid is computed. The floor is taken as the minimum number of counts seen in any one dwell point. `FLUX-WT-FLR` has the advantage of removing background counts, but leaves one or more points in the array with zero counts. As it can cause computational problems, `FLUX-WT-FLR` should not be used with `SCAN-SIZE=2`.
3. The last option for centering is `CENTER=BRIGHTEST`, which simply centers the dwell point with the most counts. This is straightforward but not as accurate as the other centroiding methods. `CENTER=BRIGHTEST` is appropriate if coordinates are uncertain and the `ACQ/SEARCH` is followed by a second `ACQ/SEARCH` using flux-weighted centering or an `ACQ/IMAGE`, or if the source is extended and it is only desired that the brightest point be in the aperture.

Table 8.2 presents the recommended `ACQ/SEARCH` parameters as a function of coordinate uncertainty. For all values of `SCAN-SIZE > 2`, we recommend `CENTER=FLUX-WT-FLR`, as it is slightly more accurate due to better sky and detector background suppression. Note that even `SCAN-SIZE` values (2 or 4) trigger additional overhead because of the telescope motion required to displace the aperture by half of a `STEP-SIZE` in both the dispersion and cross-dispersion directions, so that the overall pattern remains centered on the initial pointing.

8.3.2 Performance

The average `ACQ/PEAKD` and `ACQ/PEAKXD` centering maneuver is a good indicator of the centering accuracy following spectroscopic `ACQ/SEARCHs`, and the average `ACQ/IMAGE` centering maneuver is a good indicator of the centering accuracy following an imaging `ACQ/SEARCH`. For a large sample of `SMOV/Cycle 17 (C17)` acquisitions, the average post-spectroscopic `ACQ/SEARCH` centering move was $[AD, XD] = [0.005 \pm 0.122, 0.051 \pm 0.132]''$. The average post-imaging `ACQ/SEARCH` centering maneuver was $[AD, XD] = [0.107 \pm 0.266, 0.122 \pm 0.262]''$.

Table 8.2: Recommended ACQ/SEARCH Parameters as a Function of Coordinate Quality

Coordinate uncertainty (arcsec)	SCAN-SIZE	STEP-SIZE	CENTER
$\sigma \leq 0.4$	ACQ/SEARCH not required.		
$0.4 < \sigma < 0.7$	2	1.767 ^a	FLUX-WT
$0.7 < \sigma < 1.0$	3	1.767 ^b	FLUX-WT-FLR
$1.0 < \sigma < 1.3$	4	1.767 ^b	FLUX-WT-FLR
$1.3 < \sigma \leq 1.6$	5	1.767 ^b	FLUX-WT-FLR

^aThis is the default STEP-SIZE value and the largest to cover the search area without holes or gaps.

^bIf target coordinate uncertainty is on the lower edge of the given range, the STEP-SIZE may be reduced slightly (e.g., 1.5 arcsec) to improve target centering accuracy by sacrificing the total area of the sky covered by the search pattern.

These results indicate that ACQ/SEARCH places the target within the aperture, but that additional TA stages are necessary to refine the centering to achieve wavelength and photometric requirements. They are consistent with pre-launch estimates of the accuracy of the ACQ/SEARCH algorithm.

8.3.3 Effect of NUV Detector Background

Faint targets can be especially hard to acquire when using the COS NUV channel, as temporal fluctuations in the background level can confuse the ACQ/SEARCH algorithm. For NUV ACQ/SEARCH acquisitions requiring more than 35 s to reach $S/N = 40$, a 3×3 or larger ACQ/SEARCH with CENTER=FLUX-WT-FLR should be used. If more than 120 s is required to reach $S/N = 40$, then an NUV ACQ/SEARCH acquisition should be avoided. If the target coordinates are known to better than $0.4''$, then a simple ACQ/IMAGE should suffice. If a target is sufficiently bright in the FUV, then an FUV dispersed-light ACQ/SEARCH is an alternative. If the target's position relative to a nearby brighter object is well known, then an offset acquisition could be employed (Section 8.10.2)

If a target is too faint for any ACQ/SEARCH and also has a positional uncertainty greater than $0.4''$, then observers must obtain additional astrometric information before planning their COS observations.

8.4 ACQ/IMAGE Acquisition Mode

8.4.1 Description

In ACQ/IMAGE mode, COS obtains an NUV image of the target field, moves the telescope to center the object, and obtains a second NUV image as confirmation. ACQ/IMAGE may use either the primary science aperture (PSA) or the bright object aperture (BOA) and either MIRRORA or MIRRORB. All four combinations are illustrated in Figure 8.2. Note the additional structure present in images obtained with MIRRORB and the BOA: The secondary image produced by MIRRORB is half the intensity of the primary image and is displaced by 20 pixels (about 0.5 arcsec) in the along-dispersion (AD) direction. The BOA produces a chevron-like image whose peak is displaced in both the dispersion and cross-dispersion directions. When the BOA is used with MIRRORB, two distorted peaks result. In this configuration, there is some overlap between the wings of the primary and secondary peaks, but they are well enough separated to allow for reliable acquisitions.

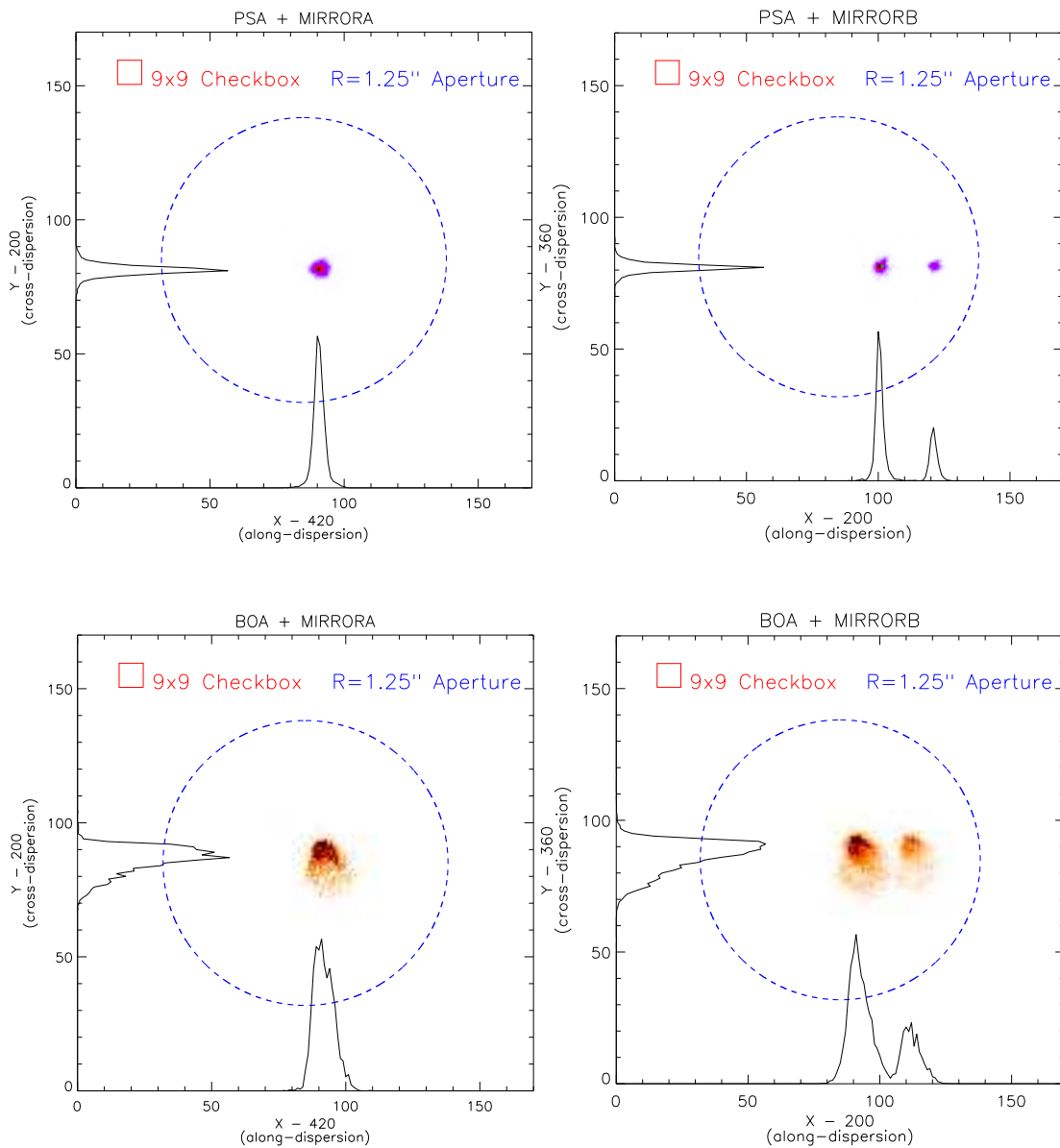
An ACQ/IMAGE exposure consists of the following steps:

1. An exposure of the internal Pt-Ne lamp is obtained through the WCA aperture. The onboard COS Flight Software (FSW) sets the exposure time for the lamp exposure automatically. The centroid of the WCA image is calculated by the FSW. Using the known offset between the center of the WCA and the science aperture (PSA or BOA), the location of the center of the science aperture on the detector is computed.
2. The shutter is opened and a TA image of the initial telescope pointing is obtained. The telescope is not moved, meaning that an acquisition using ACQ/IMAGE will be successful only if the target lies within or near the aperture. An area of 170×170 pixels, which corresponds to approximately 4×4 arcsec, centered on the aperture, is read out. This image is recorded and downlinked, and becomes part of the archived data package. (It is stored in the first extension of the `_rawacq` file.)
3. A 9×9 pixel checkbox array is then passed over the 170×170 pixel image. First, the checkbox with the most counts is identified. In the unlikely instance that two checkboxes have equal counts, the first one encountered is used. The brightest 9×9 array is then analyzed using a flux-weighted centroiding algorithm to calculate the target position.
4. Finally, *HST* is moved to place the calculated centroid at the center of the selected aperture. A second exposure, identical to the first, is taken and recorded for later downlink as a verification of the centering. (It is stored in the fourth extension of the `_rawacq` file.)

8.4.2 Performance

By comparing the final location of the targets in the confirmation images with the desired locations determined by the onboard algorithm, we can directly measure the centering accuracy of on-orbit ACQ/IMAGE exposures. The average [AD, XD] centering accuracy for all $S/N > 25$ ACQ/IMAGES in our sample of SMOV/C17 exposures was an impressive $[-0.006 \pm 0.015, -0.008 \pm 0.012]''$. This mean includes PSA, BOA, MIRRORA, and MIRRORB ACQ/IMAGES.

Figure 8.2: Point Sources Observed with all Four Aperture/Mirror Combinations



NUV images of point sources observed through the PSA (top) and BOA (bottom) using MIRRORA (left) and MIRRORB (right). The limits of each plot represent the 170×170 pixel image discussed in [Section 8.3](#). Also shown are the COS aperture (blue circle of radius $1.25''$) and the 9×9 checkbox used by ACQ/IMAGE. Histograms show the AD and XD profiles. The pointing is typical of that expected after an ACQ/SEARCH, but before additional peak-ups.

8.5 ACQ/PEAKXD Acquisition Mode

8.5.1 Description

An ACQ/PEAKXD sequence is used to improve centering in the cross-dispersion (XD) direction. The steps executed in an ACQ/PEAKXD sequence are

1. A short exposure of the Pt-Ne wavelength calibration lamp through the WCA aperture is obtained. The spectrum is collapsed along the dispersion direction, its centroid is calculated, and the center of the target aperture is computed.
2. A target spectrum is recorded for the user-specified time using a sub-array tailored to each grating and central wavelength (excluding edge effects and air-glow lines). The spectrum is collapsed along the dispersion direction.
3. The target XD location is assumed to be the median (NUV) or mean (FUV) of the collapsed spectrum.
4. The slew required to move the target spectrum in the XD direction to the center of the aperture is computed.
5. The telescope is slewed by the calculated offset to center the target in the XD direction.

The user must specify the aperture (PSA or BOA, typically the same as for the science exposure), the grating and central wavelength, and the exposure time. The use of MIRRORA or MIRRORB is not allowed. For NUV ACQ/PEAKXD acquisitions, the stripe (SHORT, MEDIUM, or LONG, corresponding to stripes A, B, or C) to be used in the computation may be specified; however, the default stripe B (MEDIUM) is recommended, as it achieves the best centering. For FUV ACQ/PEAKXD acquisitions, either segment A or B may be used, but use of the default (both, except for G140L) is recommended. For G140L, the default is segment A only.

8.5.2 Performance

By examining COS spectra, we can directly measure the final XD accuracies achieved by ACQ/PEAKXD. For the NUV channel, we find centering accuracies of 0.6 ± 1.14 pixels ($0.03''$) for the M gratings and 1.77 ± 0.82 pixels ($0.02''$) for G230L. For the FUV gratings, post ACQ/PEAKXD centerings average $0.023 \pm 0.125''$ (G130M), $0.247 \pm 0.177''$ (G160M), and $0.021 \pm 0.164''$ (G140L).

8.5.3 Effects of FUV Detector Distortions

The result of an FUV ACQ/PEAKXD is less accurate than an NUV result, because the FUV data are in raw coordinates (uncorrected for thermal and geometric distortions), and FUV segment B events must be mapped to the segment A coordinate system before a mean XD location is determined. In particular, until improvements in ACQ/PEAKXD parameters can be made, G160M ACQ/PEAKXD should be avoided for any COS observation that requires high photometric accuracy. Target acquisition with another grating or ACQ/IMAGE should be employed.

8.6 ACQ/PEAKD Acquisition Mode

8.6.1 Description

ACQ/PEAKD exposures are used to improve centering in the along-dispersion (AD) direction after an ACQ/PEAKXD. ACQ/PEAKD works much like ACQ/SEARCH except that, instead of a spiral, the spacecraft is moved linearly along the AD axis between exposures. An array containing the total counts at each dwell point is constructed. Its centroid is computed, and the telescope is moved to center the target in the aperture in the AD direction.

The user must specify the aperture, grating, central wavelength, and the exposure time at each dwell point. The use of MIRRORA or MIRRORB is not allowed. The number of steps, here called NUM-POS, may be 3, 5, 7, or 9. The STEP-SIZE is given in arcsec. There are three options for the centering algorithm, CENTER=FLUX-WT, FLUX-WT-FLR, and BRIGHTEST, and they work just as described in [Section 8.3](#).

For most applications, we recommend the use of NUM-POS=5, STEP-SIZE=0.9, and CENTER=FLUX-WT-FLR, as this combination is the least sensitive to high or variable background rates and covers a large area on the sky. Observers who wish to use NUM-POS=3 are advised to use STEP-SIZE=1.3 and CENTER=FLUX-WT. The special parameter CENTER=DEFAULT sets CENTER=FLUX-WT if NUM-POS=3 and CENTER=FLUX-WT-FLR if NUM-POS=5, 7, or 9. For FUV ACQ/PEAKD acquisitions, either segment A or B may be used, but use of the SEGMENT=DEFAULT (both, except for G140L) is recommended.

8.6.2 Performance

At present, it is not possible to ascertain how well a target is centered in the AD direction from an examination of its spectrum. Therefore, an alternative approach has been employed to characterize the accuracy of ACQ/PEAKD acquisitions. The full sample of SMOV/C17 ACQ/PEAKD exposures was combined to map the throughput-versus-offset profile for the COS PSA. Simulated ACQ/PEAKD exposures were constructed using this profile to determine the best ACQ/PEAKD parameter combinations.

We find that

- No CENTER=BRIGHTEST ACQ/PEAKD simulations were able to center observations to the required NUV or FUV accuracies.
- All CENTER=FLUX-WT-FLR simulations were able to center the target to the strictest NUV and FUV requirements for appropriate ranges of SCAN-SIZE. The best centerings were achieved with CENTER=FLUX-WT-FLR, SCANSIZE=7 or 9, and $0.4'' < \text{STEP-SIZE} < 0.8''$ ($0.6''$ recommended).
- The fastest procedure that meets the strictest centering requirements is CENTER=FLUX-WT-FLR, SCAN-SIZE=5, and $0.7'' < \text{STEP-SIZE} < 1.25''$ ($0.9''$ recommended).

- CENTER=FLUX-WT, SCAN-SIZE=3 and $1.2'' < \text{STEP-SIZE} < 1.5''$ simulations were also able to marginally exceed the NUV centering requirements for observations with good initial ACQ/SEARCH centerings in low-background (i.e., short and non-SAA) exposures (STEP-SIZE=1.3'' recommended).

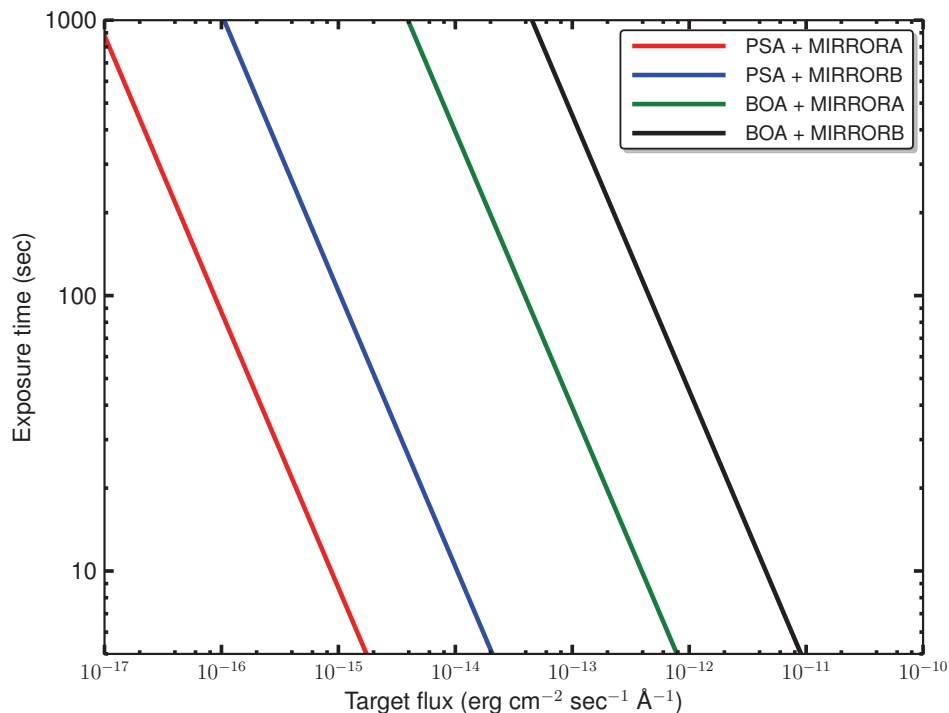
8.7 Exposure Times

While the figures in this section will help you to estimate exposure times for various acquisition scenarios, the COS Exposure Time Calculator (ETC) should be used for all proposal preparation.

8.7.1 Imaging Acquisitions

Acquisition images obtained through the PSA should strive for a minimum S/N of 40. Due to the complex shape of images obtained through the BOA, a S/N > 60 in the primary image is recommended to center the target in that aperture. The recommended S/N for MIRRORB acquisitions refers only to the primary image; the ETC performs this calculation appropriately. Figure 8.3 shows approximate exposure times needed to reach these S/N levels for various target fluxes. A flat source spectrum ($F_\lambda = \text{constant}$) is assumed.

Figure 8.3: Exposure Time Needed for an ACQ/IMAGE Acquisition

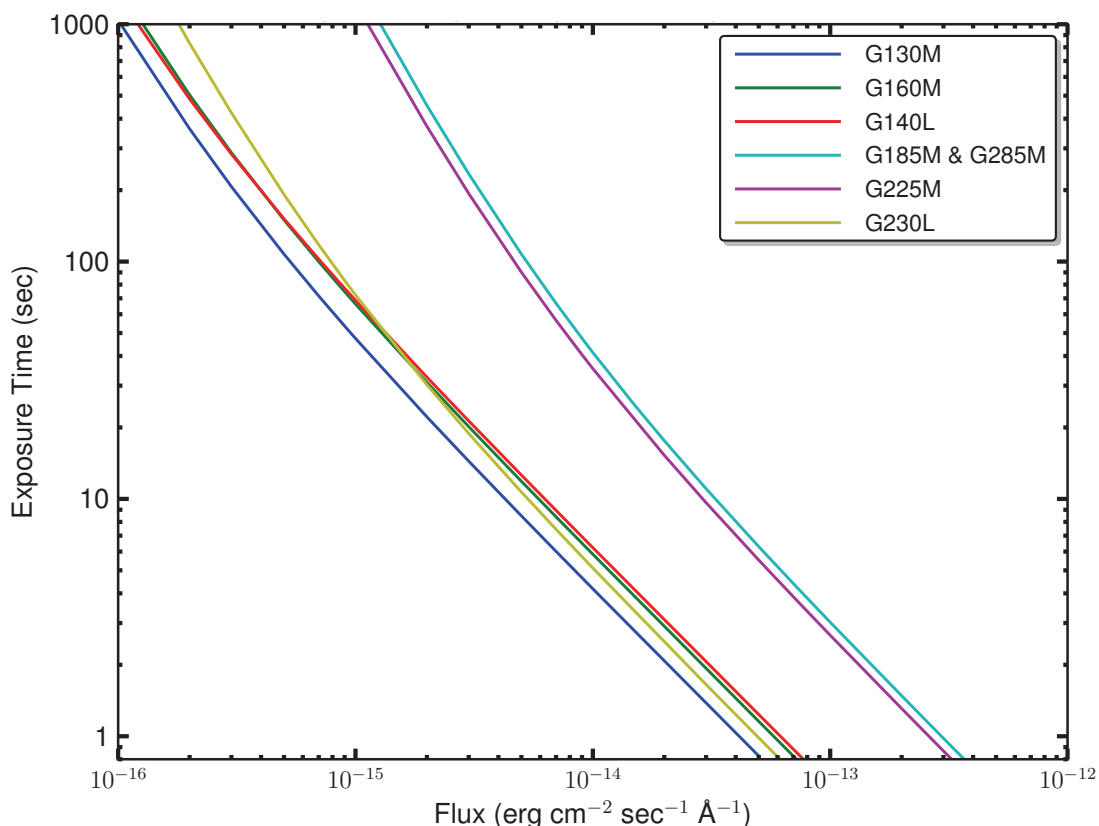


Approximate exposure time needed to achieve S/N = 40 (PSA) or 60 (BOA) as a function of target flux. This calculation assumes a flat source spectrum.

8.7.2 Dispersed-Light Acquisitions

We recommend a minimum S/N of 40 for all dispersed-light acquisition exposures. STScI calibration programs routinely use up to S/N=100 to minimize the influence of Poisson noise and background when very precise pointing is required. Figure 8.4 is a guide to the exposure time needed for a dispersed-light acquisition, assuming a flat source spectrum ($F_\lambda = \text{constant}$). Note that these exposure times apply to each separate dwell point of a pattern, which is the quantity entered into APT in Phase II.

Figure 8.4: Exposure Times for Dispersed-Light Acquisitions



Approximate exposure time needed to achieve a S/N of 40, assuming a flat source spectrum.

8.8 Centering Accuracy and Data Quality

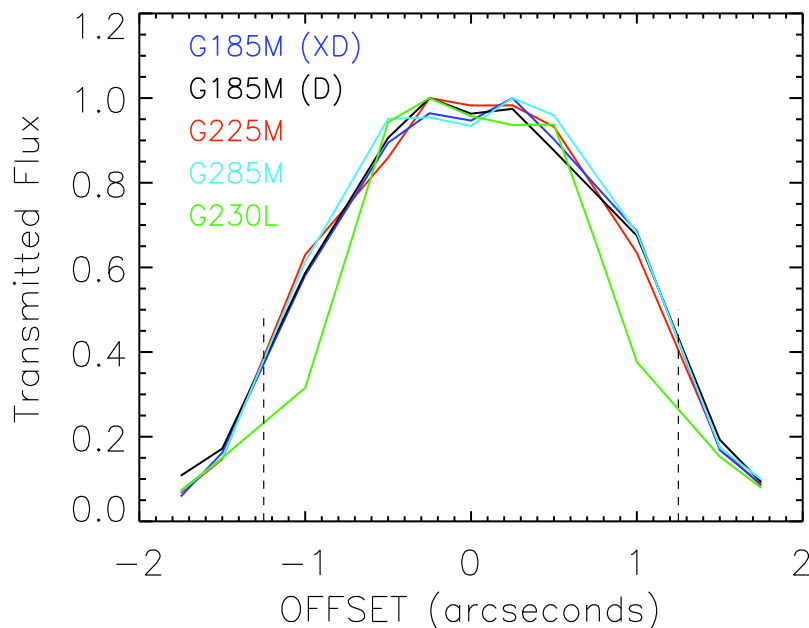
A centering accuracy of 0.3 arcsec in the cross-dispersion (XD) direction is required to achieve optimum photometric accuracy and spectral resolution. In the along-dispersion (AD) direction, the minimum accuracy is set by velocity requirements: ± 15 km/s for the medium-resolution modes, ± 150 km/s for G140L, and ± 175 km/s for G230L. Since the AD requirements are in units of km/s, they are detector and wavelength dependent. Assuming that the wavelength error budget is split evenly between the COS TA and wavelength scale accuracy, the strictest pointing requirements are $\pm 0.041''$ for the NUV channel and $\pm 0.106''$ for the FUV channel.

8.8.1 Centering Accuracy and Photometric Precision

Figure 8.5 shows the relative transmission of the PSA as a function of the displacement of a point source from the aperture center, as measured using each of the four NUV gratings. These and the corresponding FUV curves are nearly identical and show that the transmission of the COS apertures is essentially flat within the central ± 0.4 arcsec, then tails off in a non-linear but approximately symmetrical profile (COS ISR 2010-09).

The Gaussian FWHM of the XD profile ranges from approximately $0.2''$ to $2.0''$, depending on the wavelength and instrument configuration (grating and central wavelength); see Section 6.1.7. For configurations and wavelengths for which the FWHM of the XD profile is sufficiently small, two targets placed at locations up to ± 0.4 arcsec from the aperture center will receive essentially full throughput.

Figure 8.5: Relative Transmission of the COS PSA at NUV Wavelengths



Transmitted flux as a function of displacement from aperture center for all four NUV gratings. The dotted lines mark the edge of the aperture ($1.25''$). The two curves labeled D and XD refer to offsets along the dispersion and cross-dispersion axes, respectively. The other curves trace offsets in the cross-dispersion direction. For all gratings, the absolute transmission for a centered point source is at least 95%.

8.8.2 Centering Accuracy and Wavelength Accuracy

To achieve a wavelength accuracy of ± 15 km/s, the target should be centered to within about 0.04 – 0.07 arcsec for NUV observations and 0.1 – 0.2 arcsec for FUV observations (see Table 6.2). A single ACQ/SEARCH acquisition, whether spectroscopic or imaging, provides a centering accuracy of 0.3 arcsec only 75% of the time (see Section 8.3.2). Therefore, additional peak-up acquisitions in both the XD and AD directions are required.

The throughput of COS is not affected by centering errors of less than 0.4 arcsec, so high centering precision is not strictly necessary if science goals do not require that the wavelength zero point be well constrained. For example, the spectra of some objects may include foreground interstellar or inter-galactic absorption lines that can be used to establish the zero point of the wavelength scale.

8.8.3 Centering Accuracy and Spectroscopic Resolution

Targets placed within 0.4 arcsec of the aperture center will achieve maximum spectral resolution. Centering errors larger than 0.4 arcsec will lead to progressively poorer resolution. Targets at the edge of the aperture have approximately half the throughput and spectral resolution of well-centered targets.

8.9 Recommended Parameters for all COS TA Modes

As the result of our analysis of the target acquisition (TA) performance of COS during SMOV and Cycle 17, we have adjusted many COS TA parameters and have refined our recommendations and guidelines for routine COS TAs. We present these recommendations and guidelines in the previous sections and summarize the most significant changes below. [Table 8.3](#) provides our recommended values for optional parameters for each COS TA type.

- All TA modes provide good centering. For maximum wavelength accuracy, use NUV imaging mode; otherwise, use the mode that is fastest, based on ETC simulations.
- Signal-to-noise (S/N) is important. Use $S/N > 40$ for PSA TAs and $S/N > 60$ for BOA TAs.
- A single ACQ/SEARCH is not sufficient to center a COS point-source target in the aperture. Always follow the first ACQ/SEARCH with an ACQ/IMAGE, ACQ/PEAKXD+ACQ/PEAKD, or a second 2×2 ACQ/SEARCH.
- ACQ/SEARCH exposures are not required for targets with coordinate accuracies of ± 0.4 arcsec or better in the ICRS/GSC2 frame. Spending extra time to validate target coordinates is the best way to save TA time.
- NUV ACQ/SEARCH and ACQ/PEAKD acquisitions of faint sources may be affected by the detector background. An alternate acquisition strategy should be considered for CENTER=FLUX-WT-FLR targets requiring >120 sec to achieve $S/N = 40$ and for CENTER=FLUX-WT targets requiring >35 sec to achieve $S/N = 40$.
- If at all possible, use STRIPE=MEDIUM (stripe B) for NUV spectroscopic ACQ/PEAKXDs.
- Until improvements in ACQ/PEAKXD parameters can be made, FUV spectroscopic TAs should avoid G160M ACQ/PEAKXD for any COS target that requires high photometric accuracy. An ACQ/IMAGE or target acquisition with another grating should be employed instead.
- Use SCAN-SIZE=5, STEP-SIZE=0.9, and CENTER=FLUX-WT-FLR for most ACQ/PEAKD centerings. For the most accurate AD centering possible, use SCANSIZE=9, STEP-SIZE=0.6, and CENTER=FLUX-WT-FLR. Where a fast TA is required and lower centering accuracy can be tolerated, use SCAN-SIZE=3, STEP-SIZE=1.3, and CENTER=FLUX-WT.

Table 8.3: COS Acquisition Modes, Options, and Recommended Values

Acquisition Type	Description	SCAN-SIZE or NUM-POS	STEP-SIZE (arcsec)	Optional Parameters	Recommended Values	Recommended S/N
ACQ/ SEARCH	Spiral pattern; multiple exposures	2	1.767	CENTER= FLUX-WT, FLUX-WT-FLR, BRIGHTEST For FUV: SEGMENT= A, B, BOTH	FLUX-WT	40
		3 ¹			FLUX-WT-FLR	
		4			FLUX-WT-FLR	
		5			FLUX-WT-FLR	
ACQ/ IMAGE	Initial and confirmation images					40 (PSA) 60 (BOA)
ACQ/ PEAKXD	One exposure			For NUV: STRIPE= SHORT, MEDIUM, LONG For FUV: SEGMENT= A, B, BOTH	SEGMENT=BOTH STRIPE=MEDIUM (These are the default values.)	40 to 100
ACQ/ PEAKD	Linear pattern; multiple exposures	3	1.3	CENTER= FLUX-WT, FLUX-WT-FLR, BRIGHTEST, DEFAULT ² For FUV: SEGMENT= A, B, BOTH	FLUX-WT	40 to 100
		5 ¹	0.9		FLUX-WT-FLR	
		7	0.6		FLUX-WT-FLR	
		9	0.6		FLUX-WT-FLR	

1. Recommended number of acquisition steps.

2. For ACQ/PEAKD, use of the special parameter CENTER=DEFAULT is recommended. This parameter sets CENTER=FLUX-WT if NUM-POS=3 and CENTER=FLUX-WT-FLR if NUMPOS=5, 7, or 9.

8.10 Special Cases

8.10.1 Early Acquisitions and Preliminary Images

In some situations, an observer may need to obtain an independent ultraviolet image of a region in order to be sure that no objects violate safety limits and that the target to be observed can be acquired by COS successfully. Such an early acquisition should be included in the Phase I proposal, and the observation should not use a photon-counting detector. The UVIS channel on WFC3 is recommended, but observers are encouraged to consult with an STScI instrument scientist.

8.10.2 Offset Target Acquisitions

When targets are faint or lie in crowded fields, direct acquisition of the primary science target may be difficult or uncertain. In such cases, an offset acquisition, in which acquisition of a nearby field target is followed by a short slew to the primary science target, may be appropriate.

The size of the offset is limited by the requirement that the guide stars remain within the fields of view of their respective FGSs. Offset acquisition slews routinely involve displacements up to 1' and can be larger. Offset slews have a typical accuracy of $\pm 0.003''$. The centering of the initial offset target should be refined (via either ACQ/IMAGE or ACQ/PEAKXD+ACQ/PEAKD) before the offset maneuver. For offset acquisitions, bright-object considerations apply over the entire offset region. Refer to [Chapter 10](#) for a discussion of the modest overheads associated with the offset-acquisition spacecraft movement.

In unusual cases, including highly uncertain target coordinates or knotty, extended sources for which high wavelength accuracy is required, use of an offset TA scenario, followed by an additional ACQ/IMAGE or ACQ/PEAKXD+ACQ/PEAKD on the primary target, may be employed.

8.10.3 Acquisition Failure Actions and Diagnostics

Should any stage of the TA fail or a Local Rate Check (LRC) violation occur in a TA exposure, then the subsequent acquisition procedures in that visit (such as ACQ/PEAKXD or ACQ/PEAKD) will not be executed, but the science exposures will be. Note that *HST* will be left pointing at the last commanded position, which may differ substantially from the initial pointing.

Many quantities useful for evaluating the success of COS TAs are recorded in the COS TA data products (the `_rawacq` and `_spt` files). Table 5 of [COS ISR 2010-14](#) lists these keywords and their meanings.

Bright-Object Protection

In this chapter...

9.1 Introduction / 82
9.2 Screening Limits / 83
9.3 Screening versus Data-Rate Limits / 83
9.4 Source V or Flux Limits / 84
9.5 Policies and Procedures / 87
9.6 On-Orbit Protection Procedures / 90

9.1 Introduction

Both the FUV XDL and the NUV MAMA detectors are subject to damage or destruction by excessive illumination. An excessive local count rate can permanently reduce the sensitivity of the affected detector region; the most likely causes are a bright spectral emission line (XDL or MAMA) or a bright source observed in direct imaging (MAMA). A global over-illumination of the detector can result in its loss. To protect the detectors, onboard software monitors the local and global count rates, shuttering the instrument in case of a local violation, and lowering the high voltage if a global count-rate violation is detected. The local rate is checked before an exposure is begun, while the global rate is monitored continuously during the exposure. Under certain circumstances, damage could result despite the onboard safety measures, and in any event lowering the high voltage will disrupt the *HST* schedule and operations. Therefore, all proposed COS observations must meet count-rate screening limits with safety margins to allow for uncertainties. COS is currently the only *HST* instrument to use UV detectors for target acquisitions; such acquisitions must be screened, as well. It is the responsibility of the observer to screen all proposed targets and fields during Phase II preparation, and of STScI to check and enforce these limits. The COS Bright Object Protection (BOP) policies and procedures are described in this chapter.

Table 9.1: COS Count Rate Screening Limits

Detector	Source type	Type of limit	Limiting count rate (counts / sec)
FUV	predictable	global	15,000 per segment
		local	0.67 per pixel
	irregular	global	6,000 per segment
		local	0.67 per pixel
NUV	predictable	global	170,000 (imaging) or 30,000 per stripe (spectroscopic)
		local	50 per pixel ¹ (imaging) or 70 per pixel (spectroscopic)
	irregular	global	68,000 (imaging) or 12,000 per stripe (spectroscopic)
		local	50 per pixel (imaging) or 70 per pixel (spectroscopic)

1. For imaging acquisitions, a count rate of 360 cts/sec in the 9×9-pixel box surrounding the target (as computed by the COS Imaging Acquisition ETC) represents an equivalent safe upper limit.

9.2 Screening Limits

The global and local count-rate screening limits for each COS configuration are given in [Table 9.1](#). The limits are independent of observing mode (TIME-TAG or ACCUM). Compliance with these limits must be checked for all proposed COS targets by means of the Exposure Time Calculator (ETC), which issues warnings if they are exceeded. In Phase I, all proposed targets must be screened against these limits. In Phase II, the results of more detailed target and field checks must be submitted with the observing proposal; details are provided in [Section 9.5](#).

9.3 Screening versus Data-Rate Limits

It is useful to compare the BOP limits with the 30,000 counts/sec limit on TIME-TAG exposures discussed in [Section 6.2.1](#). In the FUV, a steep spectrum could exceed the BOP limit of 15,000 counts/sec per detector segment without exceeding the TIME-TAG limit. In the NUV, the BOP limit is considerably higher; a target that is perfectly safe could be far too bright to observe in TIME-TAG mode.

9.4 Source V or Flux Limits

In the following tables, the screening limits in Table 9.1 are converted into bright limits for a variety of source. They list V magnitudes for unreddened stellar spectral types and fluxes for other sources. These values are not meant to be a substitute for the ETC, but rather an indication of whether a given object may be near the limit. The most sensitive spectroscopic setting and rate limit (global or local) determine the listed values. Table 9.2 corresponds to spectroscopy through the PSA, Table 9.3 through the BOA, and Table 9.4 to NUV imaging for both apertures.

Table 9.2: V Magnitude Bright-Object Limits for PSA Spectroscopy

Spectral Class	FUV				NUV		
	G130M	G160M	G140L	G185M	G225M	G285M	G230L
O5 V	14.7	14.0	15.1	10.2	9.5	8.7	12.5
O7 V	14.5	13.8	14.9	10.0	9.5	8.6	12.4
O9 V	14.2	13.6	14.7	9.9	9.4	8.5	12.3
B0 V	14.2	13.5	14.6	9.8	9.3	8.4	12.2
B1 V	13.8	13.2	14.3	9.5	9.0	8.2	11.9
B3 V	12.8	12.5	13.4	8.8	8.4	7.8	11.3
B5 V	12.0	11.9	12.7	8.3	8.0	7.4	10.8
B8 V	10.9	11.0	11.5	7.5	7.2	6.7	10.0
A1 V	8.5	8.9	9.3	6.4	6.2	5.8	9.0
A3 V	6.4	7.8	8.3	6.1	6.0	5.6	8.7
A5 V	2.9	6.9	7.3	5.8	5.8	5.5	8.5
F0 V	-0.1	4.9	5.7	4.9	5.2	5.3	7.8
F2 V	-1.2	4.0	5.0	4.5	5.0	5.2	7.6
F5 V	-3.4	1.9	3.2	3.7	4.4	5.0	7.3
F8 V	-4.8	0.6	2.0	3.2	4.1	4.8	7.1
G2 V (Solar)	1.8	-0.5	3.4	1.4	2.7	4.4	6.8
G8 V (Tau Ceti)	3.0	-0.4	4.7	0.5	2.2	3.9	6.4
K2 V (Epsilon Eri)	4.0	-0.1	5.8	-0.7	1.1	3.2	6.1
KM III (Eta Ser)	-1.5	-1.4	0.2	-0.7	1.0	2.9	5.7
KM III (Alpha Boo)	-0.8	-2.3	0.9	-3.1	-1.1	0.9	4.7
KM III (Gamma Aql)	-2.3	-4.5	-0.5	-5.4	-3.9	-2.3	3.8
KM III (HD 146051)	-3.1	-5.0	-1.4	-7.0	-5.1	-3.1	3.3
KM III (Alpha Cet)	0.2	-1.5	1.9	-4.1	-1.9	-1.0	3.3
KM III (HD 123023)	0.0	-1.0	1.6	-3.2	-1.2	-0.3	3.7
KM III (Beta Gru)	-0.2	-0.6	1.5	-2.9	-1.0	0.7	3.4
T~50,000 Blackbody	14.6	14.0	15.0	10.1	9.5	8.6	12.5
$F_{\lambda} \sim \lambda^{-1}$	11.0	10.6	11.5	7.2	7.2	6.7	9.9
Flat limit surface brightness	11.1	10.9	11.8	7.8	8.1	7.7	10.7
Flat limit point source flux	9.4	9.2	10.0	6.1	6.4	5.9	9.0

Table 9.3: V Magnitude Bright-Object Limits for BOA Spectroscopy

Spectral Class	FUV				NUV		
	G130M	G160M	G140L	G185M	G225M	G285M	G230L
O5 V	9.4	8.5	9.8	4.6	3.8	2.8	6.9
O7 V	9.2	8.4	9.6	4.5	3.7	2.8	6.8
O9 V	9.0	8.2	9.4	4.3	3.6	2.7	6.7
B0 V	8.9	8.0	9.3	4.2	3.6	2.6	6.6
B1 V	8.5	7.7	9.0	3.9	3.3	2.4	6.2
B3 V	7.6	7.0	8.1	3.2	2.7	1.9	5.6
B5 V	6.7	6.5	7.4	2.7	2.2	1.5	5.1
B8 V	5.5	5.5	6.2	1.9	1.5	0.8	4.3
A1 V	3.1	3.4	3.8	0.8	0.4	-0.1	3.3
A3 V	1.0	2.2	2.8	0.5	0.2	-0.2	3.0
A5 V	-2.5	1.4	1.8	0.2	0.0	-0.4	2.8
F0 V	-5.6	-0.7	0.1	-0.8	-0.6	-0.7	2.0
F2 V	-6.7	-1.6	-0.6	-1.2	-0.8	-0.8	1.7
F5 V	-8.8	-3.7	-2.4	-1.9	-1.4	-1.0	1.4
F8 V	-10.2	-5.0	-3.6	-2.5	-1.7	-1.1	1.2
G2 V (Solar)	-3.6	-6.1	-1.9	-4.3	-3.1	-1.5	0.8
G8 V (Tau Ceti)	-2.3	-5.9	-0.6	-5.2	-3.6	-2.0	0.3
K2 V (Epsilon Eri)	-1.2	-5.6	0.5	-6.4	-4.7	-2.7	0.1
KM III (Eta Ser)	-6.9	-6.9	-5.2	-6.3	-4.8	-3.0	-0.4
KM III (Alpha Boo)	-6.1	-7.8	-4.4	-8.7	-6.9	-5.1	-1.3
KM III (Gamma Aql)	-7.6	-10.0	-5.9	-11.1	-9.7	-8.2	-2.2
KM III (HD 146051)	-8.5	-10.5	-6.8	-12.6	-10.8	-9.0	-2.8
KM III (Alpha Cet)	-5.1	-7.0	-3.4	-9.7	-7.7	-7.0	-2.8
KM III (HD 123023)	-5.4	-6.5	-3.7	-8.8	-7.0	-6.4	-2.3
KM III (Beta Gru)	-5.6	-6.1	-3.8	-8.6	-6.8	-5.2	-2.6
T~50,000 Blackbody	9.3	8.5	9.7	4.5	3.7	2.8	6.9
$F_{\lambda} \sim \lambda^{-1}$	5.7	5.1	6.2	1.6	1.4	0.8	4.2
Flat limit surface brightness	5.8	5.4	6.4	2.2	2.2	1.8	5.0
Flat limit point source flux	4.1	3.7	4.6	0.5	0.5	0.0	3.3

Table 9.4: V Magnitude Bright-Object Limits for Imaging

Spectral Class	PSA+MirrorA	PSA+MirrorB	BOA+MirrorA	BOA+MirrorB
O5 V	19.2	16.3	13.5	10.7
O7 V	19.1	16.2	13.4	10.5
O9 V	19.0	16.0	13.3	10.4
B0 V	18.9	15.9	13.2	10.3
B1 V	18.7	15.6	12.9	10.0
B3 V	18.1	15.0	12.4	9.3
B5 V	17.6	14.5	11.9	8.9
B8 V	16.9	13.7	11.1	8.0
A1 V	15.8	12.6	10.1	6.9
A3 V	15.6	12.3	9.9	6.6
A5 V	15.3	12.0	9.6	6.2
F0 V	14.7	11.3	8.9	5.5
F2 V	14.5	11.0	8.6	5.2
F5 V	14.0	10.6	8.1	4.7
F8 V	13.7	10.3	7.8	4.4
G2 V (Solar)	13.0	9.6	7.1	3.7
G8 V (Tau Ceti)	12.6	9.1	6.6	3.2
K2 V (Epsilon Eri)	11.8	8.3	5.8	2.4
KM III (Eta Ser)	11.4	8.0	5.5	2.0
KM III (Alpha Boo)	9.6	6.1	3.6	0.2
KM III (Gamma Aql)	7.1	3.6	1.1	-2.3
KM III (HD 146051)	6.2	2.7	0.2	-3.3
KM III (Alpha Cet)	8.0	4.6	2.1	-1.3
KM III (HD 123023)	8.7	5.2	2.7	-0.7
KM III (Beta Gru)	8.9	5.5	3.0	-0.4
T~50,000 Blackbody	19.2	16.2	13.5	10.6
$F_{\lambda} \sim \lambda^{-1}$	16.8	13.6	11.0	7.9
Flat limit point source flux	15.8	12.6	10.1	6.9
Flat limit surface brightness	9.8	7.0	4.1	1.3

9.5 Policies and Procedures

All proposers of COS observations are required to confirm that their targets (Phases I and II) and fields (Phase II) include no excessively bright sources. In Phase II, STScI will verify all targets and fields before any COS observations are scheduled.

STScI has developed a Bright Object Tool (BOT) to facilitate detailed field checking prior to COS program implementation. This tool is based on automated analysis of the fields by means of data from the second Guide Star Catalogue (GSC2) and displays of the Digital Sky Survey (DSS). GSC2 provides two magnitudes (photographic J and F), hence one color, for most fields down to about 22nd mag, which, combined with conservative spectral-type vs. color relationships, supports safety determinations for individual objects. In the best cases, these procedures allow expeditious target and field checks, but in some cases the GSC2 is inadequate because of crowding or the absence of one of the filters, for instance. In such cases, supplementary information must be provided by the proposers to support the BOP process. Always check the target in the ETC, using the more detailed information generally available there, rather than relying on the BOT field report. *When constructing your Phase II proposal with APT (the [Astronomer's Proposal Tool](#)), include the ETC exposure ID number to document your work and to facilitate the Phase II review.*

For Cycle 19, automated *GALEX* screening has been added as a selectable option in the BOT. The AIS (all-sky) sources are screened as unreddened O5 stars and reported as either safe or unsafe. This is a powerful tool, because it is based directly on UV fluxes; e.g., previously unknown hot companions to late-type stars will be revealed. The target should still be checked with the ETC, but if the field passes the BOT check, it is safe, subject to verification that the *GALEX* catalogue actually covers the field in question. Unsafe objects require further investigation; for example, *GALEX* fluxes represent upper limits in crowded regions because of the instrument's relatively low spatial resolution.

The *GALEX* detectors suffer local non-linear effects at high count rates. The fluxes and magnitudes in the current version of the *GALEX* catalog are not corrected for these effects and may be underestimated for the brightest stars. A preliminary correction is presented in Morrissey et al. (2007, ApJS, 173, 682). The BOT now applies this correction to the *GALEX* catalog. As a result, it may report *GALEX* magnitudes that are brighter than those given in the *GALEX* catalog itself.

The BOT is implemented within APT, using the Aladin interface, and reads target and exposure information from the proposal. Thus, the BOP procedures are conveniently accessible for General Observer (GO) use. Help files and training movies are available within APT. While the procedures may appear complex at first, their straightforward application rapidly become apparent. As proposers conduct BOP reviews of their targets and fields in conjunction with their Phase II preparations, they will become aware of any problems, such as the need for supplementary data, and thus avoid lengthy implementation delays following the Phase II deadline. (An exception is moving-target fields, which must be cleared after the scheduling windows have been

established.) To assist with these procedures, a COS Contact Scientist (CS) will be assigned to each COS program to interact with the GO as necessary during the Phase II preparations and through program execution.

Briefly, for a single default COS pointing with unconstrained orientation, a field of 43 arcseconds in diameter must be cleared. The APT/BOT reports on all GSC2 stars or *GALEX* sources within that field. If any displacements from the default pointing (e.g., acquisition scans, POS TARGs, patterns, or mosaics) are specified, the field to be cleared increases commensurately. POS TARG vectors and the enlarged, rotated field circles are conveniently displayed in APT/Aladin. Because both the PSA and BOA are exposed to the sky at all times, no unsafe or unknown star may lie within 7 arcseconds of either aperture. (The BOT automatically allows for the reduced throughput of the BOA aperture.) Orientation restrictions may be introduced to avoid bright objects in the field, but will constrain scheduling of the observation.

Light from a bright nearby source could scatter into the PSA. For example, even a target that is safe for the BOA may scatter enough light into the PSA to violate our screening limits. At present, the APT/BOT does not search for such objects, so they must be checked by hand. The region of concern is an annulus extending from 5 to 15 arcsec from the center of the PSA. Any field object falling in this annulus may not produce a global count rate in excess of 1×10^5 per segment for the FUV channel or 2×10^5 for the NUV, or a local count rate over 3.3 cts/sec/pixel in the FUV or 250 cts/sec/pixel in the NUV. Count rates must be estimated using the ETC as though the source were in the center of the aperture.

A COS GO must send to his/her CS, by the Phase II deadline, results of ETC calculations for each discrete target (including exposure ID numbers), and reports on any unsafe or unknown stars from APT/BOT for each field, either showing that the observations are safe or documenting any unresolved issues. In the latter case, including inadequacy of BOT/GSC2/*GALEX* to clear the observations, other photometric or spectroscopic data sources must be sought by the GO to clear the fields. Many of these are available directly through the APT/Aladin interface (although automatic BOP calculations are currently available only with GSC2 and *GALEX*), including the STScI Multimission Archive (MAST), which contains data from a number of FUV observatories. An existing UV spectrogram of the target or class may be imported directly into the ETC; *IUE* data must be low-resolution, large-aperture spectra. If model spectra are used, the original Kurucz (not Castelli & Kurucz) set should be used for early-type stars. None of the provided models is adequate for late-type stars, since the models lack chromospheric emission lines; actual UV data must be used for them. When importing data into the ETC, remember that it does not convolve spectra to the COS resolution. To be conservative, assume that the entire flux of an emission line falls within a single COS resolution element. In worst cases, new ground-based data or *HST* CCD UV exposures may be required to clear the fields for BOP; in general, the latter must be covered by the existing Phase I time allocation.

If a given star has only a V magnitude, it must be treated as an unreddened O5 star. (The older Kurucz O5 model with higher T_{eff} in the ETC should be used for BOP purposes.) If one color is available, it may be processed as a reddened O5 (which will

always have a greater UV flux than an unreddened star of the same color). If two colors are available, then the actual spectral type and reddening can be estimated separately. The APT/BOT clears automatically stars with only a single GSC2 magnitude, if they are safe based on the unreddened O5 assumption. Any other unknowns must be cleared explicitly.

In some cases, the 2MASS JHK may be the only photometry available for an otherwise “unknown” star. It is possible to estimate V and E(B-V) from those data on the assumption of a reddened O5 star, and thus determine its count rates in the ETC. Martins & Plez (2006, *A&A*, 457, 637) derive $(J-H)_0 = -0.11$ for all O stars and $(V-J)_0 = -0.67$, $(V-H)_0 = -0.79$ for early O types. (The K band should be avoided for BOP because of various instrumental and astrophysical complications.) Bessell & Brett (1988, *PASP*, 100, 1134), Appendix B, give relationships between the NIR reddenings and E(B-V). These data determine the necessary parameters. Note that the ETC also supports direct entry of observed J and H magnitudes with E(B-V).

It is not expected that all such issues will be resolved by the Phase II deadline, but they should at least be identified and have planned resolutions by then. One possible resolution is to change to a less sensitive instrumental configuration: one could use the BOA, MIRRORB, or both (though the BOA reduces image quality; see [Figure 8.2](#)), a higher-resolution grating, or a less-sensitive wavelength setting. Note that the medium-resolution gratings actually have higher throughput than G140L when the data are rebinned, but are subject to brighter limits.

Unlike any other *HST* instrument, for COS all target-acquisition exposures must also be cleared; acquisition fields may be relatively large because of the associated pointing steps. Any COS targets or fields that cannot be demonstrated to be safe to a reasonable level of certainty in the judgement of the CS will not be observed. In that case, it is possible that equivalent alternative targets may be approved upon request; but any observations that trigger the onboard safety mechanisms will not be rescheduled.

A related issue is COS pointing or configuration changes after the targets and fields have been cleared by the STSci BOP review. Any such changes must be approved by the COS Team on the basis of a specific scientific justification and a new BOP review by the GO, which may be submitted via the CS. In general, such requests should be avoided by ensuring that submitted COS specifications are final, to prevent a need for multiple BOP reviews.

GOs planning COS observations of unpredictably variable targets, such as cataclysmic variables, should be aware of the special BOP procedures in effect for them, including quiescence verification immediately preceding the COS observations, as detailed in [ACS ISR 2006-04](#), which applies to all *HST* detectors subject to BOP. Observations of flare stars are allowed with COS (and STIS) only if the Contact Scientist is convinced that the target would not violate BOP limits even in its brightest state.

9.6 On-Orbit Protection Procedures

Should an overly-bright object be observed with COS, on-board software will typically act to protect the instrument from damage. The most serious response is to reduce the high voltage of the affected detector; subsequent observations will not take place until COS undergoes a safe-mode recovery procedure that is run from the ground. Activating any of the instrument protection levels listed below is regarded as a serious breach of our health and safety screening procedures and is cause for an investigation. Observers are responsible for ensuring that their observations do not endanger the instrument.

FUV Bright Object Protection

There are five levels of protection for the COS FUV detector:

1. At the lowest level are the screening limits imposed on observers in order to provide a margin of safety for the instrument. The screening limits ([Table 9.1](#)) are set about a factor of two below actual risk levels, and we expect observers to work with us to ensure these limits are adhered to. They are determined by estimating the expected count rate from an object, both globally over the detector and locally in an emission line if appropriate. The COS ETC is the tool used for this check.
2. At the next level, within COS the “Take Data Flag” (TDF) is monitored during an exposure. If an event occurs that causes the TDF to drop (such as loss of lock on a guide star, which could lead to the telescope’s drifting), then the COS external shutter is not opened, and subsequent exposures in the visit are lost.
3. Next comes local rate monitoring. It is possible to permanently damage a localized region of the micro-channel plates without necessarily exceeding the global rate limits. This could occur if an object with bright emission lines were observed, for example. At the beginning of each exposure, the COS flight software bins the FUV spectrum by 4 pixels in x and 1024 in y ; if the count rate in any bin exceeds 1000 counts per 15 seconds, the external shutter is closed and the calibration lamps turned off. All subsequent exposures until the next grating change or target acquisition are lost.
4. Global rate monitoring is next. The COS flight software continuously monitors the total event rate for both FUV detector segments. If the rate for either segment exceeds 60,000 counts per second, the high voltage to both segments is turned off. Special commanding is required to turn on the FUV detector high voltage, so subsequent FUV observations will be lost, and the *HST* schedule will be disrupted.
5. At the highest level, the instrument is protected by software that senses an over-current condition in the high-voltage power supply; if triggered, the software shuts down the high voltage.

NUV Bright Object Protection

Similar protections also apply to the NUV detector:

1. At the lowest level are the screening limits imposed on observers to provide a margin of safety for the instrument. The screening limits ([Table 9.1](#)) are set at about a factor of two below actual risk levels, and we expect observers to work with us to ensure these limits are adhered to. They are determined by estimating the expected count rate from an object, both globally over the detector, and locally in an emission line if appropriate. The COS ETC is the tool used for this check.
2. At the next level, within COS the “Take Data Flag” (TDF) is monitored during an exposure. If an event occurs that causes the TDF to drop (such as loss of lock on a guide star, which could lead to the telescope’s drifting), then the COS external shutter is not opened, and subsequent exposures in the visit are lost.
3. Next comes local rate monitoring. It is possible to permanently damage a localized region of the micro-channel plates without necessarily exceeding the global rate limits. This could occur if an object with bright emission lines were observed, for example. At the beginning of each exposure, the flight software in COS analyzes the NUV spectrum and takes a short exposure to check for groups of pixels exceeding a threshold value (750 counts per second in an 8×8 -pixel area for imaging mode, 1300 counts per second in a 4×8 -pixel area for spectroscopic mode). This short exposure is not recorded. If the local rate limit is exceeded, the COS flight software closes the external shutter and turns off the calibration lamps. All subsequent exposures until the next grating change or target acquisition are lost.
4. Global rate monitoring is next. The COS flight software continuously monitors the total event rate for the NUV MAMA. If the total count rate exceeds 20,000 in 0.1 sec the high voltage to the MAMA is turned off, the external shutter is closed, and the calibration lamps are turned off. The NUV detector can resume operations only after a safe-mode recovery procedure, so subsequent NUV exposures will be lost, and the *HST* schedule disrupted.
5. At the highest level, the NUV MAMA is protected by the detector electronics. The Bright-Scene Detector (BSD) monitors the output of 2 of every 32 anode wires across the detector. The wires are parallel to the dispersion axis. If the total count rate exceeds 17,000 in 138 msec, then the high voltage is turned off. COS can resume operations only after a safe-mode recovery procedure. BSD differs from global-rate monitoring in two ways: it is done in hardware, not software, and what is measured is not a digitized count rate, but current in the anode grid wires.

Further information about these mechanisms can be found in [COS ISR 2002-01](#), although some details reported there have been superseded.

Overheads and Orbit Usage Determination

In this chapter...

10.1 Observing Overheads / 92
10.2 Generic Observatory Overheads / 93
10.3 Spectral Element Movement Overheads / 94
10.4 Acquisition Overheads / 95
10.5 Science Exposure Overheads / 95
10.6 First Exposure Overhead Adjustment / 96
10.7 Examples of Orbit Estimates / 97

10.1 Observing Overheads

Overheads are the times required to execute various instrumental functions that are over and above the actual exposure time. For example, mechanisms take a finite time to move into place, and electronic components must be configured properly for use.

This chapter helps you determine the total number of orbits that you need to request in your Phase I observing proposal. This process involves compiling the overheads for individual exposures or sequences of exposures, packing the exposure plus overhead time into orbits, and adding up the total number of orbits required. This will most likely be an iterative process as you modify exposures or their order to use orbital visibilities most efficiently.

The Phase I *Call for Proposals* includes information on the observatory policies and practices with respect to orbit time requests. The *HST Primer* provides specific advice on orbit determination. Below we provide a summary of the generic observatory overheads, the specific COS overheads, and several examples that illustrate how to calculate your orbit requirements for a Phase I proposal.

These numbers may be used in conjunction with the values in the *HST Primer* to estimate the total number of orbits for your Phase I proposal. After your *HST* proposal is accepted, you will be asked to submit a Phase II proposal to support scheduling of your approved observations. At that time, you will use the APT ([Astronomer's Proposal Tool](#)) scheduling software, which will contain the most up-to-date COS overheads. Allowing sufficient time for overhead in your Phase I proposal is important; additional time to cover unplanned or overlooked overhead will not be granted later.



Accounting properly for all the overheads involved in an observation can be complicated. The information provided here is meant only to be illustrative. Proposers are urged to use APT to derive a complete and accurate determination of overhead times.

10.2 Generic Observatory Overheads

The first time that you acquire an object, you must include a 6-minute overhead for the *HST* guide-star acquisition. In all subsequent orbits of the same visit, you must include the 4-minute overhead for the guide-star reacquisition; if you are observing an object in the Continuous Viewing Zone (CVZ), then no guide-star re-acquisitions are required.

You must allocate additional time for each deliberate movement of the telescope; e.g., if you are performing a target acquisition exposure on a nearby object and then offsetting to your target, or if you are taking a series of exposures in which you move the target on the detector (POS-TARG), then you must allow time for telescope motion. The time varies depending on size of the slew; see [Table 10.1](#).

Table 10.1: Generic Observatory Overhead Times

Action	Overhead type	Time needed
Guide star acquisition	Initial acquisition	6 min
	Re-acquisition	4 min per orbit
Spacecraft movements	10 arcsec < Offset < 1.5 arcmin ¹	60 sec
	1.25 arcsec ≤ Offset ≤ 10 arcsec	30 sec
	Offset < 1.25 arcsec	20 sec

1. Spacecraft motions larger than ~ 1.5 arcmin are likely to result in the loss of guide stars.

10.3 Spectral Element Movement Overheads

For any COS exposure, including target acquisition exposures, the overhead must be included for any change of spectral elements. Note that a transition from FUV to NUV requires movement of OSM1 to the NCM1 position, followed by a possible OSM2 movement. On the other hand, a transition from NUV to FUV requires only the movement of OSM1 from NCM1 to the desired FUV grating. Table 10.2 gives the times required for movement between OSM1 spectral elements and Table 10.3 gives the times for movement between OSM2 spectral elements.

Note that all COS visits start with OSM1 at the G130M position (with central wavelength 1309 Å) and OSM2 at the G185M position. These gratings are highlighted in Table 10.2 and Table 10.3. OSM1 and OSM2 move sequentially, so the total overhead is the sum of the two separate overheads. The time required to move from one optical element to another is independent of the initial and final central-wavelength and FP-POS settings.

Table 10.2: Overhead Times (seconds) for Motions Between OSM1 Spectral Elements

Movement times (seconds) from	to G140L	to G130M	to G160M	to NCM1
G140L	—	158	200	115
G130M	164	—	112	116
G160M	206	116	—	159
NCM1	121	109	154	—

Table 10.3: Overhead Times (seconds) for Motions Between OSM2 Spectral Elements

Movement times (seconds)	to G230L	to G185M	to G225M	to G285M	to MIRRORA	to MIRRORB
G230L	—	209	140	176	105	99
G185M	204	—	136	102	169	175
G225M	135	141	—	108	100	106
G285M	170	107	103	—	136	142
MIRRORA	100	174	105	141	—	71
MIRRORB	94	181	112	147	77	—

10.4 Acquisition Overheads

The various target-acquisition procedures are described in detail in [Chapter 8](#). The exposure overheads associated with each are given below:

ACQ/SEARCH: Add 20 seconds to the exposure time and multiply by the number of dwell points. Add the grating-change overheads from [Table 10.2](#) and [Table 10.3](#). Even `SCAN-SIZE` values (2 or 4) trigger an additional overhead because of the telescope motion required to displace the aperture by half of a `STEP-SIZE` in both the dispersion and cross-dispersion directions, so that the overall pattern remains centered on the initial pointing.

ACQ/IMAGE: The associated overhead is 120 seconds plus twice the specified exposure time; this includes OSM1 and OSM2 movements. The exposure time is doubled because, after *HST* is slewed to center the target, a confirmation image is obtained. Dumping the two images to memory requires an additional 58 seconds.

ACQ/PEAKXD: The overhead is 70 seconds (NUV) or 80 seconds (FUV) plus exposure time. Add the grating-change overhead from [Table 10.2](#) and [Table 10.3](#).

ACQ/PEAKD: Add 20 seconds to the exposure time and multiply by the number of dwell points. Add the grating-change overhead from [Table 10.2](#) and [Table 10.3](#). Add 39 seconds for memory readout.

10.5 Science Exposure Overheads

Science-exposure overheads are dominated by the time required to move OSM1 and OSM2 and to read out the on-board memory buffer at the end of each exposure. While the Phase II overheads computed by APT may be less than the values presented below, it is important to plan Phase I proposals using the conservative overheads given below to ensure adequate time for each exposure.

The full overhead calculation for science exposures depends upon a number of factors including generic exposure set-ups (which depend on the detector and observing mode), whether an aperture change is required, whether a grating change is required, whether the central wavelength setting for the grating is changed, and the directional sense of any required motion to implement an `FP-POS` change. [Table 10.4](#) lists these additional overheads.



When moving to a new grating, you may specify any combination of central wavelength and `FP-POS` setting with no additional overhead penalty. As a result, the `FP-POS` sequence 1,2,3,4 is more efficient than 3,4,1,2, because no backward motion is required.

Table 10.4: Science Exposure Overhead Times

Overhead times (sec)	FUV		NUV	
	TIME-TAG	ACCUM	TIME-TAG	ACCUM
Exposure set-up	71	79	36	38
Grating change	see Table 10.2		see Table 10.3	
Central wavelength change	72		75	
FP-POS forward ¹	3		3	
FP-POS backward ¹	70		70	
PSA – BOA Change	8		8	
WCS – BOA Change	10		10	
SEGMENT reconfiguration	330		N/A	
Memory readout ²	116	108 ²	116	48 ²

1. “Forward” refers to the preferred direction of motion of OSM1 or OSM2 and “backward” to the opposite direction. The preferred direction is toward larger FP-POS values.

2. ACCUM mode readout overheads can be hidden within subsequent exposures under certain circumstances, but the rules are complex. Use these values as safe upper limits for proposals.

To estimate the overhead for an exposure, round the desired exposure time up to the next whole second and add the generic exposure setup overhead from Table 10.4. If a grating change has occurred from the previous exposure, add the appropriate values from Table 10.2 and/or Table 10.3. If a central wavelength change is made, add the appropriate value from Table 10.4. If an FP-POS movement is made, add the appropriate value for motion in the preferred direction (toward larger FP-POS) or non-preferred direction. For FUV observations, both detector segments are powered by default. To turn one of them off, set SEGMENT to A or B and add the associated overhead. Lastly, add the appropriate detector memory readout overhead.

10.6 First Exposure Overhead Adjustment

To increase observing efficiency, a special feature of the COS instrument commanding allows a portion of the instrumental overheads for the first (and only the first) exposure of a visit to be performed during the initial guide-star acquisition. These will usually be target-acquisition exposures. As a result, up to 340 seconds of instrumental overheads (Table 10.2, Table 10.3, and Table 10.4) but *not* observatory or acquisition overheads (Table 10.1 and Section 10.4) may be hidden in this fashion. See Section 10.7 for examples.

10.7 Examples of Orbit Estimates

While the overhead rules presented in the previous sections may appear complex, the actual rules used by the *HST* scheduling software are even more so. It is thus imperative that you use APT to construct your Phase II proposal. In the examples that follow, we present both our overhead estimates using the rules in this chapter and the overheads computed by APT version 18.2.5. COS is a relatively new instrument, and the overhead rules will continue to evolve as we learn how to use it more efficiently. The version of APT available for constructing Cycle 19 Phase II proposals may well return values slightly different than those listed below.

10.7.1 FUV Acquisition plus TIME-TAG

In this example, we start with an FUV ACQ/SEARCH, followed by ACQ/PEAKXD and ACQ/PEAKD target acquisitions, then add an FUV TIME-TAG exposure with G140L and SEGMENT=A.

Table 10.5: Overhead Values for FUV Acquisition and FUV TIME-TAG Science

Action	APT Time (s)	Phase I Time Estimate	Comment
Initial guide star acquisition	333	360 sec = 6 min	Required at start of a new visit
FUV ACQ/SEARCH, G130M at 1309 Å, 3 × 3 pattern, 15 sec exp.	481	$9 \times (20 + 15) = 315$ sec = 5.3 min	COS starts from G130M 1309 Å on OSM1 so no initial move; 9 ACQ/SEARCH sub-exposures, so overhead includes 9 slews (20 sec each) plus 9 exposures (15 sec each)
First exposure overhead adjustment	-50	0 min	No instrument movements prior to first exposure in this example
FUV ACQ/PEAKXD, G130M at 1309 Å, 20 sec exp.	169	$80 + 20$ sec = 100 sec = 1.7 min	PEAKXD overhead; exp time
FUV ACQ/PEAKD, G130M at 1309 Å, 5 steps, 25 sec exp.	331 + 39 (dump)	$5 \times (20 + 25) + 39 = 264$ sec = 4.4 min	5 slews plus 5 exposures; memory readout
FUV G140L at 1280 Å, TIME-TAG, FLASH=YES, FP-POS=3, SEGMENT=A, 1500 sec exp.	300 (reconfig) + 1730 + 116 (dump)	$71 + 164 + 330 + 116 + 1500 = 2181$ sec = 36.3 min	Generic FUV TIME-TAG setup; OSM1 grating change (164 sec); SEGMENT reconfiguration change; TIME-TAG memory readout; exposure time
Total science time	1500	1500 sec = 25 min	
Total time used in orbit	3449	3220 sec = 53.7 min	

10.7.2 NUV Acquisition plus TIME-TAG

In this example, we start with an NUV ACQ/IMAGE target acquisition, then add two NUV TIME-TAG exposures that use the same grating but different central wavelengths, both utilizing the default FP-POS setting and FLASH=YES.

Table 10.6: Overhead Values for NUV TIME-TAG

Action	APT Time (s)	Phase I Time Estimate	Comment
Initial guide star acquisition	334	360 sec = 6 min	Required at start of a new visit
NUV ACQ/IMAGE with 2 sec exposure time	419 + 58 (dump)	116 + 169 + 120 + 4 + 58 = 467 sec = 7.8 min	COS starts at G130M on OSM1, so move to NCM1 requires 116 sec. OSM2 home position is G185M, so move to MIRRORA takes 169 sec; Add 2 min ACQ/IMAGE setup, twice the exposure time, and memory readout.
First exposure overhead adjustment	-334	-(116 + 169) sec = -285 sec = -4.8 min	OSM1 and OSM2 movements may be hidden in guide star acquisition.
NUV G185M at 1850 Å, TIME-TAG, FLASH=YES, FP-POS=3, 1200 sec exp.	1403 + 116 (dump)	36 + 174 + 116 + 1200 = 1526 sec = 25.6 min	Generic NUV TIME-TAG setup; change from MIRRORA to G185M (174 sec); TIME-TAG memory readout; exp time
NUV G185M at 1817 Å, TIME-TAG, FLASH=YES, FP-POS=3, 600 sec exp.	704 + 116 (dump)	36 + 75 + 116 + 600 = 827 sec = 13.8 min	Generic NUV TIME-TAG exposure setup; central wavelength change (75 sec); TIME-TAG memory readout; exp time
Total science time ¹	1800	1800 sec = 30 min	
Total time used in orbit	2816	2895 sec = 48.25 min	

1. The indicated science time was chosen to be the orbit visibility period less the various overheads.

10.7.3 NUV plus FUV TIME-TAG

In this example, we start with an NUV ACQ/SEARCH followed by an ACQ/IMAGE target acquisition, then add an NUV TIME-TAG exposure followed by a switch to the FUV channel and an FUV TIME-TAG exposure.

Table 10.7: Overhead Values for NUV ACCUM with FUV TIME-TAG

Action	APT Time (s)	Phase I Time Estimate	Comment
Initial guide star acquisition	333	360 sec = 6 min	Required at start of a new visit
NUV ACQ/SEARCH, MIRRORA, 3 × 3 pattern, 10 sec exp.	686	$116 + 169 + 9 \times (20 + 10) = 555$ sec = 9.3 min	COS starts at G130M on OSM1, so move to NCM1 requires 116 sec; OSM2 home position is G185M, so move to MIRRORA takes 169 sec; 9 ACQ/SEARCH sub-exposures, so overhead includes 9 slews (20 sec each) plus 9 exposures (10 sec each)
First exposure overhead adjustment	-300	$-(116 + 169)$ sec = -285 sec = -4.8 min	OSM1 and OSM2 movements may be hidden in guide star acquisition.
NUV ACQ/IMAGE with 10 sec exposure time	148 + 58 (dump)	$120 + 2 \times 10 + 58 = 198$ sec = 3.3 min	No OSM2 movement; ACQ/IMAGE setup, twice exp time, and memory readout
NUV G225M at 2250 Å, TIME-TAG, FLASH=YES, FP-POS=3, 1200 sec exp.	1334 + 116 (dump)	$36 + 105 + 116 + 1200 = 1457$ sec = 24.3 min	Generic NUV TIME-TAG setup; change from MIRRORA to G225M (105 sec); TIME-TAG memory readout; exp time
FUV G130M at 1309 Å, TIME-TAG, FLASH=YES, FP-POS=3, 600 sec exp.	775 + 116 (dump)	$71 + 109 + 116 + 600 = 896$ sec = 14.9 min	Generic FUV TIME-TAG setup; OSM1 move from NCM1 to G130M (109 sec); TIME-TAG memory readout; exp time
Total science time	1800	1800 sec = 30 min	
Total time used in orbit	3266	3181 = 53.0 min	

10.7.4 FUV TIME-TAG with BOA and FLASH=NO

In this example, we start with an NUV ACQ/IMAGE, followed by a switch to the FUV channel and an FUV TIME-TAG science exposure using G160M, a non-default FP-POS=1, the BOA, and, as required with the BOA, FLASH=NO. The science exposure will be followed automatically by a 12-second wavecal (see Table 6.3). The next orbit begins with a longer science exposure using the same set-up as for the first orbit. Because more than 40 minutes will have elapsed since the first wavecal, a wavecal will be inserted automatically following this science exposure, as well.

Table 10.8: Overhead Values for FUV TIME-TAG Using the BOA

Action	APT Time (s)	Phase I Time Estimate	Comment
Initial guide-star acquisition	334	360 sec = 6 min	Required at start of a new visit
NUV ACQ/ IMAGE with 2 sec exposure time	419 + 58 (dump)	$116 + 169 + 120 + 4 + 58 = 467$ sec = 7.8 min	OSM1 starts at G130M, so move to NCM1 requires 116 sec. OSM2 starts at G185M, so move to MIRRORA takes 169 sec; Add 2 min ACQ/ IMAGE setup, twice the exposure time, and memory readout.
First exposure overhead adjustment	-334	$-(116 + 169)$ sec = -285 sec = -4.8 min	OSM1 and OSM2 movements may be hidden in guide star acquisition.
FUV G160M at 1600 Å, TIME-TAG, BOA, FLASH=NO, FP-POS=1, 1800 sec exp.	2016 + 116 (dump)	$71 + 154 + 8 + 116 + 1800 = 2149$ sec = 35.8 min	Generic FUV TIME-TAG setup; NUV to FUV adds no overhead; change from NCM1 to G160M (154 sec); non-preferred direction (3 to 1); aperture change from PSA to BOA (8 sec); TIME-TAG memory readout; exposure time
FUV G160M at 1600 Å, TIME-TAG, AUTO WAVECAL, WCA, FP-POS=1, 12 sec exp.	88 + 40 (dump)	$71 + 10 + 116 + 12 = 209$ sec = 3.5 min	AUTO WAVECAL to be inserted, since FLASH=YES is not allowed with BOA; generic FUV TIME-TAG setup; no grating, central wavelength, or FP-POS change; aperture change from BOA to WCA (10 sec); TIME-TAG memory readout; exposure time
Total science time in orbit 1	1800	1800 sec = 30 min	
Total time used in orbit 1	2737	2900 sec = 48.3 min	
Guide star re-acquisition	222	240 sec = 4 min	Required at start of additional orbit
FUV G160M at 1600 Å, TIME-TAG, BOA, FLASH=NO, FP-POS=1, 2400 sec exp.	2470 + 116 (dump) - 10 (hidden)	$71 + 10 + 116 + 2400 = 2597$ sec = 43.3 min	Generic FUV TIME-TAG setup; continue at same grating, central wavelength, and FP-POS; aperture change from WCA to BOA (10 sec); TIME-TAG memory readout; exposure time
FUV G160M at 1600 Å, TIME-TAG, AUTO WAVECAL, WCA, FP-POS=1, 12 sec exp.	88 + 40 (dump)	$71 + 10 + 116 + 12 = 209$ sec = 3.5 min	Another AUTO WAVECAL required as more than 40 min have elapsed since last one; again generic FUV TIME-TAG exposure setup; aperture change from BOA to WCA (10 sec); TIME-TAG memory readout; exposure time
Total science time in orbit 2	2400	2400 sec = 40 min	
Total time used in orbit 2	2926	3046 sec = 50.8 min	

10.7.5 FUV TIME-TAG with Multiple FP-POS

In this example, we start with an NUV ACQ/IMAGE exposure, followed by a switch to the FUV channel for a set of 900-second exposures, one at each FP-POS position. We will again use TIME-TAG, FLASH=YES, and G130M, but at central wavelength 1327 Å. To avoid backward motion of OSM1, we will execute the individual FP-POS exposures in the order FP-POS=1, 2, 3, and 4.

The desired exposures will not fit into a single orbit, so some must be performed in a second orbit. As the second orbit is not completely filled, the observer would typically add additional exposures (not shown here) to fill it.

Table 10.9: Overhead Values for FUV TIME-TAG at FP-POS=1, 2, 3, 4

Action	APT Time (s)	Phase I Time Estimate	Comment
Initial guide star acquisition	334	360 sec = 6 min	Required at start of a new visit
NUV ACQ/IMAGE with 10 sec exposure time	435 + 58 (dump)	116 + 169 + 120 + 20 + 58 = 483 sec = 8.1 min	OSM1 starts at G130M, so move to NCM1 requires 116 sec. OSM2 starts at G185M, so move to MIRRORA takes 169 sec; Add 2 min ACQ/IMAGE setup, twice the exposure time, and memory readout.
First exposure overhead adjustment	-334	-(116 + 169) sec = -285 sec = -4.8 min	OSM1 and OSM2 movements may be hidden in guide star acquisition.
FUV G130M at 1327 Å, TIME-TAG, FLASH=YES, FP-POS=1, 900 sec exposure	1075 + 116 (dump)	109 + 71 + 116 + 900 = 1196 sec = 19.9 min	Move OSM1 from NCM1 to G130M (109 sec); generic TIME-TAG set-up (71 sec); TIME-TAG memory read-out (116 sec); exposure time
FP-POS=2, 900 sec exposure	969 + 116 (dump)	71 + 3 + 116 + 900 = 1090 sec = 18.2 min	Second exposure of FP-POS sequence: generic TIME-TAG set-up (71 sec); move to FP-POS=2 (3 sec); TIME-TAG memory read-out (116 sec); exposure time
Total science time in orbit 1	1800	1800 sec = 30 min	
Total time used in orbit 1	2769	2844 sec = 47.4 min	
Guide star re-acquisition	222	240 sec = 4 min	Required at start of next orbit
FP-POS=3, 900 sec exposure	969 + 116 (dump) - 5 (hidden)	71 + 3 + 116 + 900 = 1090 sec = 18.2 min	As for FP-POS=2
FP-POS=4, 900 sec exposure	969 + 116 (dump)	71 + 3 + 116 + 900 = 1090 sec = 18.2 min	As for FP-POS=2
Total science time in orbit 2	1800	1800 sec = 30 min	
Total time used in orbit 2	2387	2420 sec = 40.3 min	

Exposure-Time Calculator (ETC)

In this chapter...

11.1 The COS Exposure Time Calculators / 102
11.2 Imaging Observations of Red Objects / 103
11.3 Sensitivity, Count Rate, and S/N / 104
11.4 Detector and Sky Backgrounds / 104
11.5 Extinction Correction / 111
11.6 Examples / 112

11.1 The COS Exposure Time Calculators

To help with proposal preparation, four COS Exposure-Time Calculators (ETCs) are available on the COS Web pages:

<http://www.stsci.edu/hst/cos/software/planning/etc/>

These calculators model spectroscopic and imaging exposures for both target acquisitions and scientific observations. They estimate count rates for given source and background parameters and calculate either the signal-to-noise ratio for a given exposure time or the exposure time needed to achieve a desired signal-to-noise ratio. If you have a calibrated spectrum of your source, you can upload it to the Exposure Time Calculators. The ETCs warn if your observations exceed local or global brightness limits (see [Table 9.1](#)). They have extensive online help that explains how to use them and provides the details of the calculations.

A unique exposure ID is assigned to each calculation performed by the ETCs, allowing results from previous calculations to be retrieved easily. This number should be included as a comment in your Phase II proposal to document your work and to facilitate Phase II review. Proposers are urged to check the [COS ETC Web page](#) for any updates or issues related to the COS ETCs before performing any ETC simulation.

The spectroscopic ETC can display the input spectrum, a simulated one-dimensional output spectrum, and the S/N and number of counts per resolution element for the selected COS configuration and source. These outputs can also be downloaded by the user in ASCII format.

The imaging ETC is simple, because COS has only a single imaging mode. However, it does allow the selection of either the PSA or BOA and either MIRRORA or MIRRORB. The ETC reports the count rate in the brightest pixel, total counts in the detector, and S/N per resolution element.

The target acquisition ETCs return the acquisition exposure time to be entered in APT (the [Astronomer's Proposal Tool](#)) for both imaging and spectroscopic acquisitions. Target acquisition is described in [Chapter 8](#).

11.2 Imaging Observations of Red Objects

As shown in [Figure 7.3](#), the COS NUV channel is sensitive to wavelengths above 3200 Å, an important consideration when imaging red objects. For stars with effective temperatures above 6000 K, the effect is negligible, but it grows to about 20% at 5000 K, and below 5000 K it quickly becomes large.

If you upload a spectrum into the ETC to calculate exposure time of an imaging exposure, whether for a target acquisition or a scientific observation, be sure that the spectrum spans the full range of wavelengths to which the NUV channel is sensitive, from about 1600 Å to 12,000 Å. Failure to do so can produce a misleading result.

The COS ETC expects input spectra to extend out to 12,000 Å and will return a warning message (“Partial overlap between instrument throughput band and input spectrum”) if they do not.

11.3 Sensitivity, Count Rate, and S/N

A complete theoretical discussion of the exposure time as a function of instrument sensitivity and signal-to-noise ratio is given in Chapter 6 of the *STIS Instrument Handbook* and will not be repeated here. However, COS has several characteristics that simplify signal-to-noise calculations.

Both COS detectors are photon counters, which means that they have no read noise. COS is optimized for point sources, and in this case the signal-to-noise ratio is given by

$$\frac{S}{N} = \frac{C \cdot t}{\sqrt{C \cdot t + N_{\text{pix}}(B_{\text{sky}} + B_{\text{det}}) \cdot t}},$$

where

C = the signal from the astronomical source, in counts s^{-1}

t = the integration time, in seconds

N_{pix} = the total number of detector pixels integrated to achieve C

B_{sky} = the sky background, in counts $\text{s}^{-1} \text{pixel}^{-1}$

B_{det} = the detector dark count rate, in counts $\text{s}^{-1} \text{pixel}^{-1}$

With no detector read noise, the signal-to-noise ratio is proportional to the square root of the exposure time whether the target is bright or faint compared to the backgrounds and dark count.

Note that the detector dead-time effects discussed in [Section 4.1.8](#) and [Section 4.2.5](#) are not included in the ETC, which will over-predict the count rates and resulting S/N ratios for bright targets.

11.4 Detector and Sky Backgrounds

The background sources that affect COS observations include

- Detector dark count,
- Earthshine,
- Zodiacal light, and
- Geocoronal emission.

The ETC allows the user to select among several levels of intensity for each of the sky backgrounds, corresponding to different observing environments.

11.4.1 Detector dark background

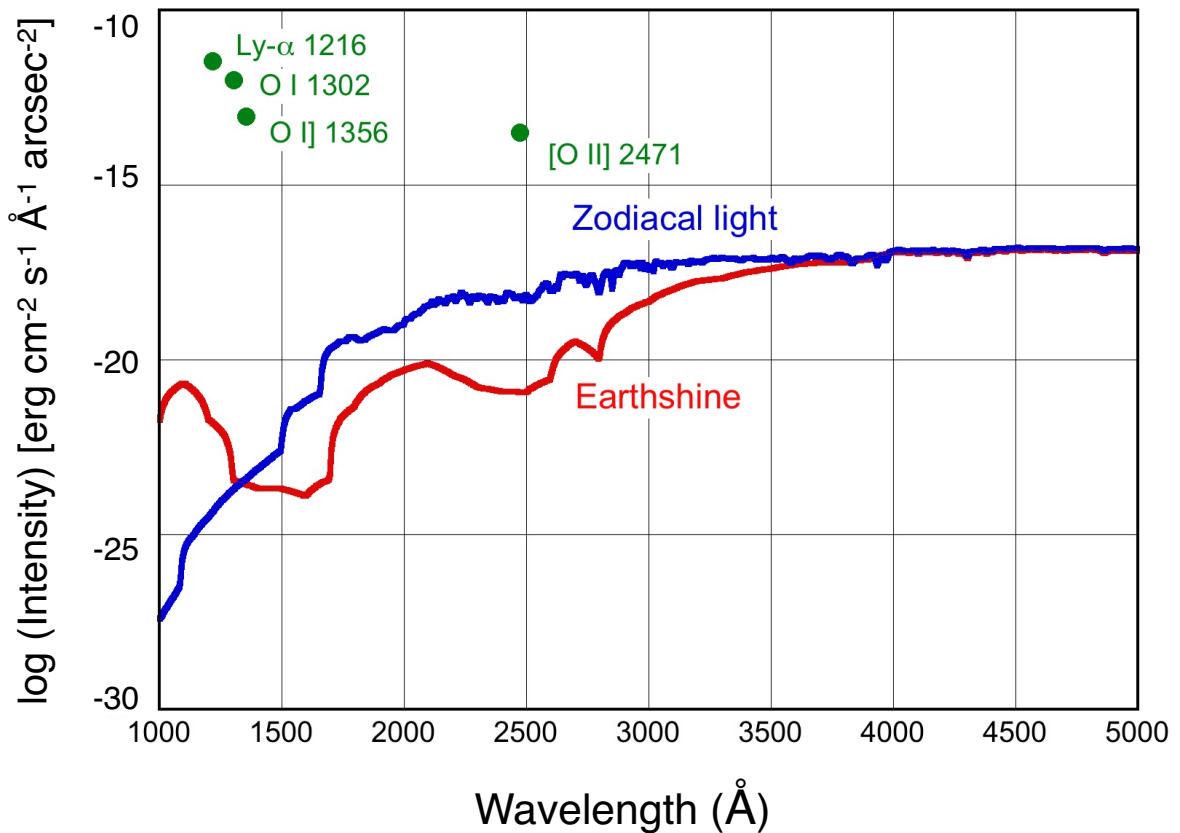
[Table 11.1](#) lists the dark count rate and read-noise characteristics of the COS detectors as used by the ETC. The FUV values were measured in 2010 September, while the NUV values are projections for mid-Cycle 19 (2012 April).

Table 11.1: Detector Background Count Rates

Detector:	FUV XDL	NUV MAMA
Dark rate (counts s ⁻¹)	1.25 per cm ² 1.8 × 10 ⁻⁶ per pixel 1.1 × 10 ⁻⁴ per resel	117 per cm ² 7.3 × 10 ⁻⁴ per pixel 6.6 × 10 ⁻³ per resel
Read noise	0	0

Here we assume that a resolution element, or “resel,” spans 6×10 pixels on the FUV XDL and 3×3 pixels on the NUV MAMA. The dark rate in the FUV detector is truly small, due in part to its windowless design. The NUV detector has a window and thus a higher dark rate.

Figure 11.1: Sky Background Intensity as a Function of Wavelength

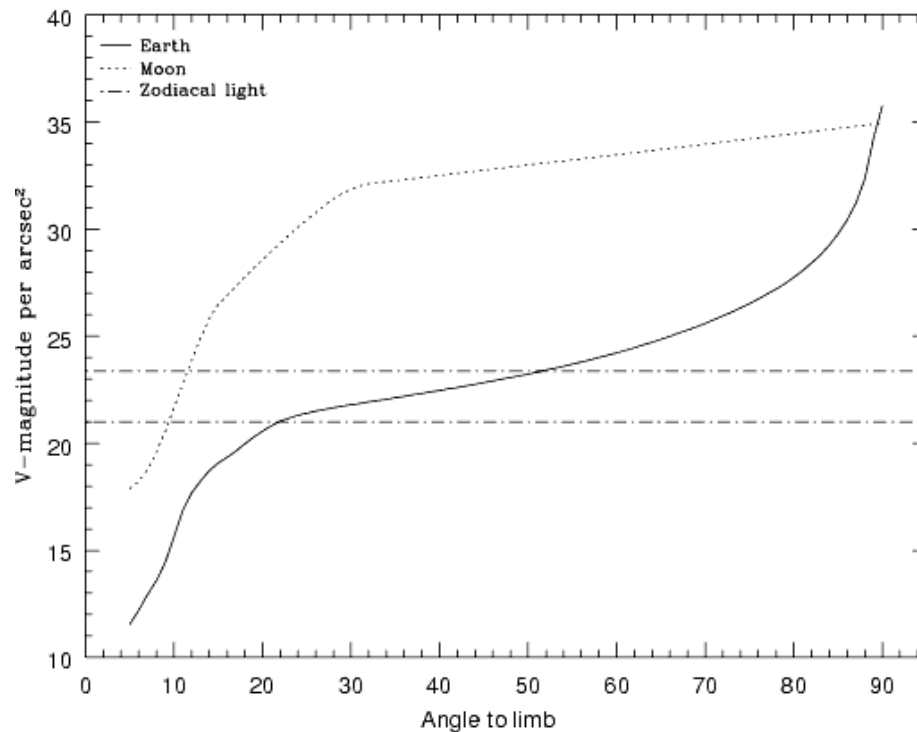


Earthshine for a target 24° above the limb of the sunlit Earth, corresponding to the “high” level in the ETC. Use [Figure 11.2](#) to estimate background contributions at other angles. The zodiacal light level ($m_V = 22.7$ per arcsec², the “average” level in the ETC) corresponds to a heliocentric latitude and longitude of 30° and 180° , respectively. The geocoronal line intensities are integrated fluxes, corresponding to the “Day” level in [Table 11.4](#). The upper limit to the [OII] 2471 intensity is shown.

11.4.2 Earthshine

Four earthshine intensity levels, with scaling factors of (*none, average, high, extremely high*) = (0.0, 0.5, 1.0, 2.0), are available in the ETC. Earthshine intensity is a strong function of the angle between the target and the bright Earth limb. The earthshine surface brightness for a target 24° degrees above the limb, corresponding to the “high” level, is shown in Figure 11.1. The limb angle is approximately 24° when *HST* is aligned toward its orbit pole (i.e., the center of the CVZ). The variation of earthshine with limb angle is shown in Figure 11.2.

Figure 11.2: Background Contributions from the Moon, Earth, and Zodiacal Light



The values are V magnitude per square arcsec due to the moon and the sunlit Earth as a function of angle between the target and the limb of the bright Earth or moon. Zodiacal light levels range between $m_V=22.1$ and $23.3 \text{ mag arcsec}^{-2}$.

11.4.3 Zodiacal Light

Away from the airglow lines, at wavelengths between about 1300 and 3000 Å, the sky background is dominated by zodiacal light, which is generally fainter than the intrinsic detector background, especially for the NUV detector. Figure 11.1 shows the zodiacal light for the “average” level in the ETC. Table 11.2 gives the variation of the zodiacal background as a function of helioecliptic longitude and latitude. For a target near $(50^\circ, 0^\circ)$ or $(-50^\circ, 0^\circ)$, the zodiacal light is relatively bright at $m_V = 20.9 \text{ mag arcsec}^{-2}$, about 9 times the polar value of $m_V = 23.3 \text{ mag arcsec}^{-2}$. These limits are plotted in Figure 11.2. The intensity levels and the factors by which they are scaled in

the ETC are (*none, low, average, high*) = (0.0, 0.576, 1.0, 1.738), corresponding to $m_V = (\text{none}, 23.3, 22.7, 22.1) \text{ mag arcsec}^{-2}$.

Observations of the faintest objects may need the special requirement LOW-SKY in the Phase II observing program. LOW-SKY observations are scheduled during the part of the year when the zodiacal background is no more than 30% greater than the minimum possible value for the given sky position. LOW-SKY also invokes the restriction that exposures will be obtained at angles greater than 40° from the bright Earth limb to minimize earthshine and the UV airglow lines. The LOW-SKY requirement limits the times at which targets within 60° of the ecliptic plane will be scheduled and limits visibility to about 48 minutes per orbit.

Table 11.2: Approximate Zodiacal Sky Background ($V \text{ mag arcsec}^{-2}$) as a Function of Heliocentric Coordinates

Heliocentric Longitude (deg)	Heliocentric Latitude (deg)						
	0°	15°	30°	45°	60°	75°	90°
180°	22.1	22.4	22.7	23.0	23.2	23.4	23.3
165°	22.3	22.5	22.8	23.0	23.2	23.4	23.3
150°	22.4	22.6	22.9	23.1	23.3	23.4	23.3
135°	22.4	22.6	22.9	23.2	23.3	23.4	23.3
120°	22.4	22.6	22.9	23.2	23.3	23.3	23.3
105°	22.2	22.5	22.9	23.1	23.3	23.3	23.3
90°	22.0	22.3	22.7	23.0	23.2	23.3	23.3
75°	21.7	22.2	22.6	22.9	23.1	23.2	23.3
60°	21.3	21.9	22.4	22.7	23.0	23.2	23.3
45°	SA	SA	22.1	22.5	22.9	23.1	23.3
30°	SA	SA	SA	22.3	22.7	23.1	23.3
15°	SA	SA	SA	SA	22.6	23.0	23.3
0°	SA	SA	SA	SA	22.6	23.0	23.3

Note: A value of “SA” denotes positions in the solar avoidance zone

The ETC provides the user with the flexibility to adjust both the zodiacal (*none, low, average, high*) and earthshine (*none, average, high, extremely high*) sky background components to determine if the use of LOW-SKY is advisable for a given program. However, the absolute sky levels that can be specified in the ETC may not be achievable for a given target. As shown in Table 11.2, the minimum zodiacal background level for an ecliptic target is $m_V = 22.4$, which is brighter than both the low and average options with the ETC. By contrast, a target near the ecliptic pole would always have a zodiacal = *low* background in the ETC. The user is cautioned to consider sky levels carefully, as the backgrounds obtained in *HST* observations can span a significant range.

11.4.4 Geocoronal Airglow Emission

In the ultraviolet, the sky background contains important contributions from airglow lines, which vary from day to night and as a function of *HST* orbital position. Airglow lines may be an important consideration for spectroscopic observations at wavelengths near the lines.

Background due to geocoronal emission originates mainly from hydrogen and oxygen atoms in the exosphere of the Earth. The emission is concentrated in a very few lines. The brightest line by far is Lyman α at 1216 Å. The strength of the Lyman α line varies between about 2 and 20 kilo-Rayleighs (i.e., between 6.3×10^{-14} and 6.3×10^{-13} erg s⁻¹ cm⁻² arcsec⁻², where 1 Rayleigh = 10^6 photons s⁻¹ cm⁻² per 4π steradians, which equates to 3.15×10^{-17} erg s⁻¹ cm⁻² arcsec⁻² at Lyman α) depending on the time of the observation and the position of the target relative to the Sun. The next strongest line is the O I line at 1302 Å, which rarely exceeds 10% of Lyman α . The typical strength of the O I 1302 Å line is about 2 kilo-Rayleighs (about 7×10^{-14} erg s⁻¹ cm⁻² arcsec⁻²) on the daylight side and about 150 times fainter on the night side of the HST orbit. The O I] 1356 Å and [O I] 2471 Å lines may appear in observations on the daylight side of the orbit, but these lines are at least 10 times weaker than the O I 1302 Å line. The widths of the lines also vary, but a representative value for a temperature of 2000 K is about 3 km s⁻¹. The geocoronal emission lines are essentially unresolved at the resolution of COS, but the emission fills the aperture in the spectral and spatial directions. For the FUV modes, the aperture width is approximately 114 pixels, or 1.12, 1.36, and 9.46 Å for G130M, G160M, and G140L, respectively. For the NUV modes, the aperture width is approximately 105 pixels, or 3.87, 3.46, 4.18, and 41.21 Å for G185M, G225M, G285M, and G230L, respectively.

The COS ETC provides four airglow intensity levels (*none, low, average, high*) whose scaling factors depend on the airglow line considered: (0.0, 0.1, 0.5, 1.0) for Lyman α , (0.0, 0.0667, 0.5, 1.0) for O I λ 1302, (0.0, 0.006, 0.5, 1.0) for O I] λ 1356, and (0.0, 0.005, 0.5, 1.0) for [O I] λ 2471.

It is possible to request that exposures be taken when *HST* is in the umbral shadow of the earth to minimize geocoronal emission (e.g., if you are observing weak lines at 1216 Å or 1302 Å) using the special requirement SHADOW. Exposures using this special requirement are limited to roughly 25 minutes per orbit, exclusive of the guide-star acquisition (or reacquisition) and can be scheduled only during a small percentage of the year. SHADOW reduces the contribution from the geocoronal emission lines by roughly a factor of ten, while the continuum earthshine is essentially nil. If you require SHADOW, you should request it in your Phase I proposal (see the [Call for Proposals](#)).

An alternate strategy for reducing the effects of geocoronal emissions is to use time-resolved observations, so that any data badly affected by geocoronal emission can simply be excluded from the final co-addition. This can be done either by doing the observations in TIME-TAG mode, the default for all COS observations if the target is not too bright, or by taking a series of short (~ 5 min) ACCUM mode exposures over the course of each orbit.

As noted, geocoronal Lyman α is by far the strongest airglow feature to contend with. Despite this, we estimate that on the day side of *HST*'s orbit, when Lyman α is at its strongest, it will produce a net count rate of 20 counts s⁻¹ resel⁻¹, well below rates at which bright lines are a safety concern.

11.4.5 Tabular Sky Backgrounds

Table 11.3 lists the *high* sky background numbers as plotted in Figure 11.1. The *high* sky values are defined as the earthshine at 24° from the limb and by the typical zodiacal light of $m_V = 22.7$. The quoted values represent the zodiacal and earthshine backgrounds (excluding the contributions from geocoronal emission lines) averaged over each wavelength interval. The line widths and intensities of some important geocoronal emission lines in the COS bandpass are listed in Table 11.4.

Table 11.3: Earthshine and Zodiacal Light in the COS PSA

Wavelength (Å)	Earthshine	Zodiacal Light	Total
1000	6.48 E-7	1.26 E-12	6.48 E-7
1100	1.66 E-6	6.72 E-11	1.66 E-6
1200	4.05 E-7	6.23 E-10	4.06 E-7
1300	2.66 E-8	3.38 E-9	2.99 E-8
1400	2.28 E-9	1.32 E-8	1.54 E-8
1500	1.95 E-9	2.26 E-7	2.28 E-7
1600	1.68 E-9	1.14 E-6	1.14 E-6
1700	6.09 E-8	3.19 E-5	3.19 E-5
1800	6.19 E-7	6.63 E-5	6.69 E-5
1900	2.30 E-6	1.05 E-4	1.07 E-4
2000	5.01 E-6	2.07 E-4	2.12 E-4
2100	6.97 E-6	5.95 E-4	6.02 E-4
2200	3.94 E-6	9.82 E-4	9.86 E-4
2300	1.83 E-6	9.67 E-4	9.69 E-4
2400	1.27 E-6	1.05 E-3	1.05 E-3
2500	1.37 E-6	1.01 E-3	1.01 E-3
2600	6.33 E-6	2.32 E-3	2.32 E-3
2700	2.66 E-5	4.05 E-3	4.08 E-3
2800	3.79 E-5	3.67 E-3	3.71 E-3
2900	2.17 E-4	7.46 E-3	7.68 E-3
3000	4.96 E-4	8.44 E-3	8.94 E-3
3100	1.04 E-3	9.42 E-3	1.05 E-2
3200	1.72 E-3	1.10 E-2	1.27 E-2
3300	2.18 E-3	1.34 E-2	1.56 E-2
3400	3.12 E-3	1.30 E-2	1.62 E-2
3500	4.06 E-3	1.31 E-2	1.72 E-2

Table 11.3: Earthshine and Zodiacal Light in the COS PSA

Wavelength (Å)	Earthshine	Zodiacal Light	Total
3600	5.15 E-3	1.24 E-2	1.77 E-2
3700	5.89 E-3	1.49 E-2	2.18 E-2
3800	6.19 E-3	1.41 E-2	2.03 E-2
3900	7.80 E-3	1.39 E-2	2.17 E-2
4000	1.14 E-2	2.07 E-2	3.21 E-2
4250	1.13 E-2	2.17 E-2	3.40 E-2
4500	1.33 E-2	2.53 E-1	3.86 E-2
4750	1.35 E-2	2.57 E-2	3.92 E-2
5000	1.30 E-2	2.50 E-2	3.80 E-2

These rates correspond to the *high* level in the ETC and are listed in units of 10^{-15} erg cm^{-2} s^{-1} Å^{-1} for the total COS PSA, which is 4.91 arcsec² in area.

Table 11.4: Typical Strengths of Important Ultraviolet Airglow Lines

Airglow features	Intensity					
	Day			Night		
	Rayleighs	10^{-15} erg cm^{-2} s^{-1} arcsec ⁻²	10^{-15} erg cm^{-2} s^{-1} per PSA	Rayleighs	10^{-15} erg cm^{-2} s^{-1} arcsec ⁻²	10^{-15} erg cm^{-2} s^{-1} per PSA
O I λ 911	17	0.7	3.5	8.3	0.35	1.7
O I λ 989	161	6.2	30	0.6	–	–
H I λ 1026	571	21	105	2.7	–	–
O I λ 1027	64	2.4	12	0	–	–
O I λ 1152	28	0.93	4.6	0	–	–
H I λ 1216	20,000	630	3100	2,000	63	310
O I λ 1302	2,000	59	290	13	0.38	1.9
O I λ 1356	204	5.8	28	12.5	0.35	1.7
O I λ 2471	45	0.70	3.4	1	–	–

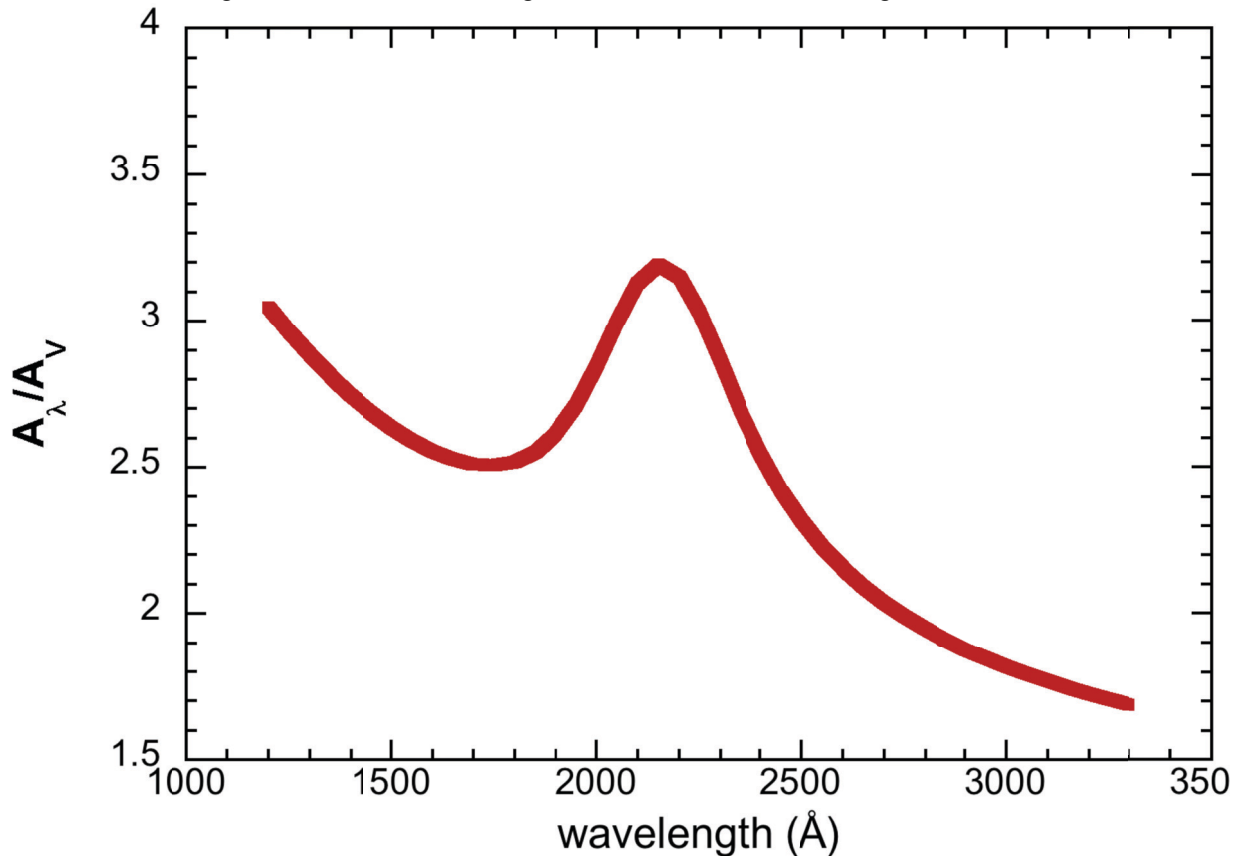
11.5 Extinction Correction

Extinction can dramatically alter the counts expected from your source, particularly in the ultraviolet. Figure 11.3 shows A_λ/A_V values applicable to our Galaxy, taken from Cardelli, Clayton, & Mathis (1989, ApJ, 345, 245). A value of $R = 3.1$ was used. This corresponds to the “Average Galactic” selection of the ETC.

Extinction curves have a strong metallicity dependence, particularly at ultraviolet wavelengths. Sample extinction curves can be seen in Koornneef and Code [1989, ApJ, 247, 860 (LMC)], Bouchet et al. [1985, A&A, 149, 330 (SMC)], and Calzetti et al. [1994, ApJ, 429, 582 (starburst galaxies)], and references therein. At lower metallicities, the 2200 Å bump that is so prominent in the Galactic extinction curve disappears, and $A_\lambda/E(B-V)$ increases at shorter UV wavelengths.

The ETC allows the user to select among a variety of extinction curves and to apply the extinction correction either before or after the input spectrum is normalized.

Figure 11.3: Extinction in Magnitude as a Function of Wavelength



The Galactic extinction model of Cardelli et al. (1989) is shown, computed for $R = 3.1$.

11.6 Examples

In this section, we present a few examples of the way in which the COS ETCs may be used. They illustrate the information that is returned by the ETCs and how they can be used to plan your observations.

11.6.1 A Flat-spectrum Source

One often does not know the exact spectrum shape of the object to be observed, so the answer to a simple question is desired: How long will it take to achieve a given signal-to-noise ratio at a given wavelength if the flux at that wavelength is specified? The easiest way to determine this is to use a flat spectrum as input. How long will it take to achieve $S/N=10$ per resolution element at 1320 \AA with a source flux of $10^{-15} \text{ erg cm}^{-2} \text{ s}^{-1} \text{ \AA}^{-1}$, using a medium resolution grating?

Only the G130M grating covers the desired wavelength at medium resolution, but several choices of central wavelength are available. We select a setting of 1309 \AA . We enter these values into the spectroscopic ETC, select the Primary Science Aperture (PSA), select “Exposure time needed to obtain a S/N ratio of 10.0,” and enter the specified wavelength of 1320 \AA . For the spectrum distribution, choose a flat continuum in F_λ . Make sure the reddening, $E(B-V)$, is set to 0. Normalize the target to $10^{-15} \text{ erg cm}^{-2} \text{ s}^{-1} \text{ \AA}^{-1}$. The zodiacal light, earthshine, and airglow were not specified, so we choose average values.

When this case is computed with the ETC, we find the required time is 12,586 seconds; the total count rates are 57 and 276 counts s^{-1} in detector segments A and B, respectively, well below the safety limit; the count rate in the brightest pixel is 0.104 counts s^{-1} , also well within the safe range (but see below); and the buffer time indicated by the ETC is 7704 seconds.

What if somewhat higher S/N were desired and one were willing to devote 5 *HST* orbits to the observation? Assuming that each orbit allows 50 minutes of observing time (ignoring the acquisition time here), we find that in 15,000 seconds we will get $S/N = 11.4$ per resel. Note that $(15,000/12,586)^{1/2} = (10.9/10.0)$. That is, the S/N ratio scales as $t^{1/2}$, as stated in [Section 11.3](#).

If a low-resolution observation is acceptable, then one could switch to the G140L grating. With a grating setting of 1105 \AA and $S/N = 10$ per resel, we find the required exposure time is 2178 seconds, considerably less than the medium-resolution case required.

Note that the sensitivity of G130M is higher than that of G140L once resolving power is taken into account. In other words, a G130M spectrum that is rebinned to the same resolution as a G140L spectrum can be obtained in less time for a given S/N , although, of course, with diminished wavelength coverage. If only a limited portion of the source’s spectrum is of interest, using G130M is more efficient than using G140L.

These cases also illustrate that the earthshine and zodiacal light are completely negligible in the FUV, unless the target flux is much lower than that considered here. This is also true of the airglow if the wavelength of interest is far from the airglow

lines. Of course, the airglow cannot be ignored in terms of the total count rate on the detector, or the local count rate if the source contributes at the same wavelengths as the airglow lines.

This is a toy example. For most targets, a more realistic model spectrum would be used to estimate exposure times and test for bright-object violations.



If only a limited portion of the source's spectrum is of interest, using G130M is more efficient than using G140L.

11.6.2 An Early-type Star

We wish to observe an O5 star at medium spectral resolution at a wavelength of 1650 Å. We know that the star has a magnitude of $V = 16$. How long will it take to obtain $S/N = 15$?

We select the G160M grating with a central wavelength of 1623 Å. We select a Kurucz O5 stellar model and set the normalization to be Johnson $V = 16$. We find that the required exposure time is 784 seconds.

Suppose this star is reddened, with $E(B-V) = 0.2$. We select the *Average Galactic* extinction law, which is shown in Figure 11.3. We must now decide if this extinction is to be applied before or after the normalization. Since the star has a measured magnitude, we want to apply the reddening before normalization. Otherwise, the extinction would change the V magnitude of the stellar model. Making this selection, we find that $S/N = 15$ can be obtained in 1840 seconds. The ETC returns a `BUFFER-TIME` of 2313. To be conservative, we scale it by 2/3 to get 1542 s.

11.6.3 A Solar-Type Star with an Emission Line

We want to observe a solar-type star with a narrow emission line. Consider the Si II $\lambda 1810$ feature with the following parameters: $\text{FWHM} = 30 \text{ km s}^{-1}$ or 0.18 \AA at 1810 Å, and integrated emission line flux of $1 \times 10^{-14} \text{ erg cm}^{-2} \text{ s}^{-1}$. The measured magnitude of the star is $V = 12$. The desired exposure time is 1000 seconds.

In the ETC we select a G2V star and an NUV grating, G185M, set to a central wavelength of 1817 Å. We request an exposure time of 1000 s and specify that the S/N be evaluated at 1810 Å. We add an emission line with the line center at 1810 Å, $\text{FWHM} = 0.18$, and an integrated flux of $10^{-14} \text{ erg cm}^{-2} \text{ s}^{-1}$. We specify the normalization as Johnson $V = 12$. We set the zodiacal and earthshine to be *average*.

The ETC returns $S/N = 16.6$ per resel. The local and global count rates are within safe limits. The recommended buffer time is 7477 seconds. This `BUFFER-TIME` exceeds the exposure time of 1000 s, so the `BUFFER-TIME` should be set to 1000.

11.6.4 A Faint QSO

An important science goal for the design of COS was to obtain moderate S/N spectra of faint QSOs in the FUV. In the ETC, use the FOS-based QSO spectrum and choose G130M at 1309 Å, S/N = 20, and a continuum flux of 10^{-15} erg cm⁻² s⁻¹ Å⁻¹ at 1320 Å. The indicated exposure time is 45,557 seconds, or about 14 orbits. The source count rate is 0.002 (counts per second), with a background rate of 1.06×10^{-4} counts per second, 20 times lower than the source. The background is completely dominated by the dark current of the detector. The count rate over the entire detector is 350, well below any safety limits, and the maximum BUFFER-TIME is 6743 seconds. Scaling by 2/3 yields 4495 seconds for the BUFFER-TIME.

Data Products and Data Reduction

In this chapter...

12.1 Overview / 115
12.2 COS Data Files / 116
12.3 Additional COS Files / 117

12.1 Overview

Raw COS data are processed through the STScI **OPUS** pipeline. Data first undergo Generic Conversion, by which bits from individual exposures are unpacked and combined into files containing raw, uncalibrated data. Next, the raw files are processed through the COS calibration pipeline, **calcos**, which performs image and spectroscopic reduction to produce output files useful for scientific analysis. Finally, the data are ingested into the Hubble Data Archive through the Data Archive and Distribution System (DADS). This system populates a database containing header keywords that is accessible to users via the Multimission Archive at STScI (MAST). Both calibrated and uncalibrated data are then available for distribution by MAST to the user.

12.2 COS Data Files

When data are taken in TIME-TAG mode (the default), the raw data are in the form of a table of photon events containing the arrival time, x and y pixel coordinates, and pulse height (for FUV data) for each photon detected. Raw ACCUM data are in the form of a 2-D image. For FUV data, there will be two raw files for each exposure, one file for segment A and one for segment B. For NUV data, there will be one raw file for each exposure, whether imaging or spectroscopic.

The calibrated data have the same general format for both FUV and NUV, although there are differences in detail. There will be a “corrtag” file (the file name contains the string “corrtag”) containing a corrected events table. The corrtag table includes all of the columns from the raw data file, plus these additional columns: a weight that accounts for the flat-field and dead-time corrections, a data-quality column, and a column that gives the pulse-height amplitude of each event. (Codes for the DQ flags are listed on the [COS Web page](#).) The corrtag file provides several sets of corrected pixel coordinates for each event. These include X[Y]CORR, which are corrected for thermal drifts in the detector electronics and geometric distortions in the detector; XDOPP, which are the X coordinates corrected for orbital Doppler motions; X[Y]FULL, which are the XDOPP and YCORR coordinates recast into a coordinate system defined by the WAVECAL spectrum; and WAVELENGTH, which provides the wavelength corresponding to the XFULL coordinate. For ACCUM data, the corrtag table has the same format, but all the values in the TIME column are a constant, half the exposure time. There is one row in this pseudo-TIME-TAG table for each count in the raw ACCUM image.

Additional calibrated files include the `flt` and `counts` images, which are created by binning the events in the corrtag table. Both images have units of counts s^{-1} , but the `flt` image may also be corrected for flat-field and dead-time effects. For spectroscopic data, a 1-D extracted spectrum (or three spectra, for NUV exposures) will be written to an `x1d` file for each exposure. For data in an association (whereby multiple exposures are processed together—the usual case), the 1-D spectra for separate exposures will be averaged and written to an `x1dsum` table. If multiple FP-POS settings are used, there will be one `x1dsum` file for each FP-POS (`x1dsum[1, 2, 3, 4]`), even if only one spectrum was obtained at each position. The distinction between the `x1d` and `x1dsum` files in such cases is that the data-quality weights, the `DQ_WGT` column of the `x1d` files, are used to eliminate bad or suspect data (such as the FUV grid-wire shadows). The `x1dsum` file without a number is the final sum of all of the exposures. It can be a weighted mean of all the `x1dsum[n]` files or, if a single exposure was obtained at a single FP-POS setting, a copy of the `x1d` file with the `DQ_WGTs` applied.

While `calcos` will average data taken at different FP-POS settings, data taken at different central wavelengths or with different gratings will not be combined. A new association is created when either the grating or central wavelength is changed, and `calcos` only averages data within an association. In IRAF/PyRAF there is a “splice” task in the `ctools` package for averaging spectra. This task was written for STIS

data, but it can be run on COS data, though not all of the input columns will be preserved.

Wavelength calibration can be performed in either of two ways. The default (specified as FLASH=YES) is to take line-lamp exposures (“wavecal” exposures) simultaneously with the science data. In this case, the wavecal spectra will be extracted and saved in lampflash tables. The alternative is to take separate wavecal exposures interspersed with the science exposures. These wavecals will be calibrated in the same way as science exposures, except that the calibrated wavecal data (`corrtag`, `flt`, `counts`, `x1d`) will not be corrected for the offset of the spectrum from the template, and no `x1dsum` file will be created for a wavecal.

12.3 Additional COS Files

Several additional files are used in the processing of COS data. These include association files (`asn`), which are used to control calibration processing; engineering support files (`spt`), which contain information used in the pipeline processing; and lampflash files (`lampflash`), which contain extracted wavelength calibration spectra used in the processing of TIME-TAG data with FLASH=YES. For a full description of these and other files, see the *COS Data Handbook*.

The COS Calibration Program

In this chapter...

13.1 Introduction / 118
13.2 Ground Testing and Calibration / 119
13.3 SMOV4 Testing and Calibration / 119
13.4 Cycle 17 Calibration Program / 120
13.5 Cycle 18 Calibration Program / 122

13.1 Introduction

In this chapter, we provide a brief guide to the calibration observations obtained during ground testing and on-orbit through Cycle 18. Potential Cycle 19 observers should assume that all of these calibrations will be completed by the time that Cycle 19 begins.

Observers wishing to use instrument configurations that are not addressed by these calibration plans should assess their specific calibration needs and include time in their Phase I proposal for any additional calibrations that are required. Proposers who believe that more extensive calibration observations or analysis may be of general benefit to the COS user community should consider submitting a Cycle 19 Calibration Outsourcing Proposal (see the [Cycle 19 “Call for Proposals”](#) for details).

13.2 Ground Testing and Calibration

The COS Instrument Definition Team (Principal Investigator, James Green, University of Colorado) was responsible for the ground testing and ground calibration of COS. Most of the ground test data was obtained in 2003 and 2006 during thermal vacuum testing at Ball Aerospace and Goddard Space Flight Center, respectively. These tests characterized the basic properties of the optics, the detectors, and the mechanisms. While some measurements (e.g., FUV full-detector flat-field images) cannot be repeated in orbit, most of the ground-test data have been superseded by on-orbit measurements obtained during SMOV4.

13.3 SMOV4 Testing and Calibration

The primary goal of Servicing Mission 4's Orbital Verification program (SMOV4) was the timely commissioning of *HST* for normal science operations. For the newly-installed COS, this included testing the focus (internal and external), verifying the target-acquisition procedures, monitoring instrument stability (both in terms of image motions and sensitivity), and measuring plate scales, line-spread functions, and other instrument parameters. SMOV4 observations were completed in 2009 October, and a series of Instrument Science Reports (ISRs) detailing the results of their analysis have been published. Those ISRs and the observing programs on which they are based are listed in [Table 13.1](#).

Table 13.1: COS ISRs Resulting from SMOV Calibration Programs

Number	Title	Author	Associated SMOV Programs
2009-01	Preliminary Characterization of the Post-Launch Line Spread Function of COS	Ghavamian et al.	11489, 11476
2010-01	SMOV Absolute Flux Calibration of the COS NUV Mode	Massa et al.	11479
2010-02	SMOV Absolute Flux Calibration of the COS FUV Modes	Massa et al.	11492
2010-03	COS Near-UV Flat Fields and High S/N Determination from SMOV Data	Ake et al.	11478, 11481
2010-04	SMOV: COS NUV On-Orbit Optical Alignment	Hartig et al.	11468, 11469
2010-05	SMOV: COS NUV Wavelength Calibration	Oliveira et al.	11470, 11474, 11475
2010-06	SMOV: COS FUV Wavelength Calibration	Oliveira et al.	11485, 11488, 11487
2010-07	SMOV: COS FUV Focus Determination	Lennon et al.	11484
2010-08	NUV Spectroscopic Performance	Beland & Ghavamian	11476, 11477
2010-09	FUV Spectroscopic Performance	Ghavamian et al.	11489, 11490
2010-10	SMOV: COS NUV Imaging Performance	Goudfrooij et al.	11473
2010-11	FUV Darks	Sahnou et al.	11356, 11482, 11484, 11895
2010-12	NUV Darks	Sahnou et al.	11355, 11466, 11894
2010-13	NUV/FUV Structural and Thermal Stability	Smith & Keyes	11480, 11493
2010-14	COS Target Acquisition Guidelines, Recommendations, and Interpretation	Keyes & Penton	11471, 11472, 11486
2010-15	Early Results from the COS Sensitivity Monitoring Programs	Osten et al.	11492, 11494, 11897
2010-16	FUV Flats	TBD	11491, 11494

13.4 Cycle 17 Calibration Program

The Cycle 17 calibration program continued the testing begun during SMOV. It included long-term programs to monitor the sensitivity and wavelength scale of both the NUV and FUV detectors. Midway through Cycle 17, additional calibration programs were added. Brief descriptions of these programs are presented in [Table 13.2](#).

Table 13.2: Cycle 17 Calibration Programs

Program ID	Title	Desired Accuracy	Products
11894	NUV Detector Dark Monitor	1%	ISR, Reference file
11896	NUV Spectroscopic Sensitivity Monitor	< 1%	COS ISR 2010-15, Reference file
11899	NUV Imaging Sensitivity	1% from counting stats, 5% overall accuracy of sensitivity formula	ISR, Reference file
11900	NUV Internal/External Wavelength Scale Monitor	1-3 pixel wavelength zero-point accuracy	ISR, Reference file
11895	FUV Detector Dark Monitor	Obtain a few counts per exposure.	ISR, Reference file
11897	FUV Spectroscopic Sensitivity Monitor	< 1%	COS ISR 2010-15, Reference file
11997	FUV Internal/External Wavelength Scale Monitor	3-4 pixel wavelength zero-point accuracy	ISR, Reference file
12010	COS FUV Line Spread Function	S/N = 10 near 1530 Å	COS ISR 2009-01, Reference file
12052	COS NUV Grating Efficiency Test	Determine temporal trends to $\pm 2\%$	ISR
12080	G140L Focus Sweep	± 100 focus steps	Flight software change, ISR
12081	COS Flux Calibration Below 1150 Å with G140L/1280	3% for 900-1150 Å, 10% for 300-700 Å	ISR, Reference file
12082	Extending COS/ G130M Coverage Down to 905 Å with Two New Central Wavelengths	Resolution and sensitivity to 10%, wavelength scale to 100 km/s	ISR, Reference file
12083	G140L/1280 Wavecal Template	N/A	Reference file
12084	G140L/1280 Internal-to-External Wavelength Scales	0.2-pixel wavelength zero-point accuracy	Reference file
12085	STIS/E230M Data to Determine Internal-to-External Offsets in COS/G230L	0.2-pixel wavelength zero-point accuracy	Reference file
12086	Generation of 1-D Fixed-Pattern Templates	2%	Reference file
12096	COS FUV Detector Lifetime Position Test	N/A	ISR

13.5 Cycle 18 Calibration Program

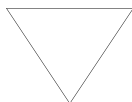
The Cycle 18 calibration program, currently under development, will continue the routine calibration and monitoring observations performed in Cycle 17. The draft Cycle 18 calibration programs are listed in [Table 13.3](#).

Table 13.3: Cycle 18 Calibration Programs

NUV MAMA Fold Distribution
NUV Detector Dark Monitor
NUV Spectroscopic Sensitivity Monitor
NUV Internal/External Wavelength Scale Monitor
NUV Detector Recovery After Anomalous Shutdown
FUV Detector Dark Monitor
FUV Spectroscopic Sensitivity Monitor
FUV Internal/External Wavelength Scale Monitor
FUV Detector Recovery After Anomalous Shutdown
COS Observations of Geocoronal Lyman-Alpha Emission
COS FUV Sensitivity Characterization
COS FUV Detector Gain Sag vs. High Voltage
A DB White Dwarf as a Fundamental Calibrator for G130M

13.6 Cycle 19 Calibration Plans

The Cycle 19 calibration plans for COS will continue the routine calibration and monitoring observations performed in Cycles 17 and 18. The priorities assigned to the calibration of various COS modes will be determined by the approved GO programs in each cycle.



If your program requires calibrations beyond those described here and that are of direct benefit to other COS users, then you should apply directly for this calibration in your Phase I proposal.

Spectroscopic Reference Material

In this chapter...

14.1 Introduction / 123
14.2 Using the Information in this Chapter / 124
14.3 Gratings / 127
14.4 Line-Spread Functions / 152

14.1 Introduction

The information in this chapter will help you to select a detector, grating configuration, and observing aperture and to develop your observing plan. For each grating, the following information is provided:

- A brief description of the grating, with special considerations for its use.
- Grating parameters, including the dispersion and plate scale.
- Plots showing the available central-wavelength settings and the range of wavelengths covered by each setting and (for the FUV gratings) FP-POS position.
- Plots and tables of sensitivities and effective areas as a function of wavelength.
- Plots of signal-to-noise ratio as a function of STMAG, F_{λ} , and exposure time.
- Line-spread functions as a function of wavelength.

Note that the quoted sensitivities are estimates for mid-Cycle 18 (2011 April). The COS Exposure Time Calculator (ETC) will be updated with Cycle 19 estimates in time for the Cycle 19 Phase II deadline. See the [COS Web site](#) for the latest information.

14.2 Using the Information in this Chapter

14.2.1 Grating Parameters

For each grating, the resolving power and dispersion are taken from [Table 6.1](#). Plate scales are derived from data obtained during SMOV.

14.2.2 Wavelength Ranges

For each grating, we plot the wavelengths sampled by each central-wavelength setting. For the NUV gratings, the central wavelength is the approximate midpoint of stripe B. For the FUV gratings, the central wavelength is (approximately) the shortest wavelength recorded on segment A. Wavelength ranges for each central wavelength at FP-POS=3 are provided in tabular format in [Table 6.4](#) and [Table 6.5](#).

For the FUV gratings, the wavelength ranges sampled at each FP-POS position are plotted separately. For the NUV gratings, the total wavelength range sampled by all FP-POS positions is plotted for each central-wavelength setting.

14.2.3 Grating Sensitivities and Effective Areas

This section presents sensitivities and effective areas as a function of wavelength for each grating. The target is assumed to be a point source centered in the PSA. For both the FUV and NUV detectors, the total systemic¹ *spectroscopic point-source sensitivity*, S_{λ}^p , has units of counts $\text{pix}_{\lambda}^{-1} \text{sec}^{-1}$ per incident $\text{erg cm}^{-2} \text{sec}^{-1} \text{\AA}^{-1}$, where

- pix_{λ} = a pixel in the dispersion direction, and
- counts refer to the total counts from a point source integrated over the PSF in the direction perpendicular to the dispersion.

The count rate per pixel is simply the product of the target flux and the point-source sensitivity at a given wavelength. To estimate the S/N ratio achieved at a given count rate and exposure time, follow the directions in [Section 11.3](#) or use the S/N plots in this chapter.

The effective area has units of cm^2 .

14.2.4 Signal-to-Noise Plots

For each grating, a plot is provided to help you estimate the signal-to-noise ratio (S/N) that can be achieved from a point source observed at a fiducial wavelength near the peak of the effective-area curve. The fiducial wavelength is indicated in the ordinate label of each plot. To estimate S/N at other wavelengths, scale your source flux or magnitude by the relative sensitivities at the wavelength of interest and at the fiducial. The plots show S/N as a function of F_{λ} and of STMAG for a range of

1. COS plus *HST* Optical Telescope Assembly (OTA).

exposure times. $STMAG_{\lambda}$ is the color-dependent correction from V magnitude to STMAG at wavelength λ . Values of $STMAG_{\lambda}$ for various stellar and extragalactic sources are presented in [Table 14.1](#) and [Table 14.2](#), respectively. In producing these plots, we assumed an average sky background (as described in [Chapter 11](#)) and the dark current appropriate for each detector. These plots should be used only for rough estimates of exposure times. When constructing your proposal, use the COS Exposure Time Calculator (ETC) to estimate S/N values.

Note the following:

- The point source S/N has been calculated per resolution element and has been integrated over the PSF to contain all of the flux in the cross-dispersion direction.
- The symbols in the S/N figures delineate regions of parameter space where the dark current contributes more than half the source counts.
- The vertical shaded area indicates the bright-object screening limit given in [Table 9.1](#).

Follow these steps to use the S/N plots:

1. Look up in [Table 14.1](#) the effective temperature and wavelength region of interest (e.g., 5000 K @ 2000 Å). Interpolate in the table to get $STMAG_{\lambda}$.
2. Add the V magnitude of the target to get STMAG.
3. Find the appropriate plot for the desired grating and locate STMAG on the horizontal axis. Read off the S/N for the desired exposure time, or vice-versa. Alternatively, use F_{λ} directly on the horizontal axis.
4. To get accurate values for repeated or FP-POS exposures, use the sub-exposure time when consulting the plot, and then multiply the resulting S/N by \sqrt{N} , where N is the number of sub-exposures to be averaged.

For example, consider a $V=15$ star of spectral type B0 V, for which we want to derive the S/N achieved in a 100 sec exposure using the NUV grating G230L. The S/N calculations for G230L are presented in [Figure 14.24](#), where we learn that the fiducial wavelength for this grating is 3000 Å. Assuming an effective temperature of 30,000K, we obtain $STMAG_{\lambda} \sim -2.1$ at 3000 Å from [Table 14.1](#), making $STMAG = 12.9$. Returning to [Figure 14.24](#), we find this value on the horizontal axis. For an exposure time of 100 seconds, the $S/N \sim 9.5$.

Table 14.1: $STMAG_{\lambda}$ as a Function of Wavelength for Stellar Objects

Temp (K)	Wavelength (\AA)									
	1000	1200	1500	2000	2500	3000	3500	4000	4500	5000
45000	-5.87	-5.46	-4.79	-3.87	-3.02	-2.36	-1.76	-1.27	-0.79	-0.37
30000	-5.38	-4.92	-4.37	-3.50	-2.70	-2.13	-1.56	-1.23	-0.76	-0.35
20000	-3.90	-3.38	-3.45	-2.73	-2.14	-1.66	-1.18	-1.13	-0.72	-0.33
15000	-1.68	-1.24	-2.68	-2.08	-1.53	-1.21	-0.83	-1.05	-0.68	-0.31
10000	9.18	6.27	-0.72	-0.68	-0.26	-0.21	-0.03	-0.88	-0.62	-0.29
9000	12.84	8.67	1.81	-0.19	0.15	0.05	0.16	-0.75	-0.58	-0.26
8000	17.10	11.79	6.33	0.51	0.58	0.21	0.24	-0.56	-0.46	-0.20
7000	20.97	15.07	9.29	1.86	1.26	0.36	0.24	-0.34	-0.32	-0.12
6000	N/A	19.44	14.17	5.50	2.92	0.94	0.47	0.02	-0.15	-0.04
5000	N/A	N/A	20.15	9.80	6.24	2.74	1.24	0.50	0.04	0.10
4000	N/A	N/A	N/A	14.74	9.70	5.53	2.37	0.97	0.24	0.58
3000	N/A	N/A	N/A	17.85	11.46	5.69	2.22	0.71	0.25	0.82

Table 14.2: $STMAG_{\lambda}$ as a Function of Wavelength for Non-Stellar Objects

Spectrum	Wavelength (\AA)								
	1500	2000	2500	3000	3500	4000	4500	5000	
Elliptical	3.35	3.19	4.17	2.92	1.60	0.70	0.17	0.15	
S0	4.63	3.95	3.27	2.23	1.61	0.71	0.18	0.13	
Sa	2.64	2.27	2.39	1.78	1.31	0.36	0.12	0.07	
Sb	1.70	2.59	2.04	1.32	1.12	0.43	0.17	0.10	
Sc	-0.18	0.44	-0.17	-0.68	-0.67	-0.51	-0.44	-1.25	
Starburst, $E(B-V) < 0.1$	-1.71	-1.15	-0.68	-0.43	-0.13	-0.42	-0.23	-1.24	
Starburst, $0.25 < E(B-V) < 0.35$	-0.95	-0.87	-0.33	-0.10	0.08	-0.19	-0.19	-0.28	
Starburst, $0.51 < E(B-V) < 0.60$	-0.40	-0.18	0.01	0.23	0.03	-0.14	-0.12	-0.36	
Starburst, $0.61 < E(B-V) < 0.70$	0.05	0.31	0.31	0.15	0.27	-0.17	-0.13	-0.11	

The $STMAG_{\lambda}$ values of Table 14.1 are derived from the stellar models of Castelli and Kurucz (2003, 2004), assuming solar metallicity ($[Fe/H] = 0.0$) and a surface gravity $\log(g) = 4.5$. The $STMAG_{\lambda}$ values of Table 14.2 are based on observed spectra of each object type.

14.3 Gratings

For each COS grating, we present the resolving power, dispersion, plate scales, the wavelength ranges covered at each central wavelength setting and (for the FUV gratings) FP-POS position, sensitivities, effective areas, and a tool for estimating S/N. Advice on use is provided where appropriate.

Note that the quoted sensitivities are estimates for mid-Cycle 18 (2011 April). The COS Exposure Time Calculator (ETC) will be updated with Cycle 19 estimates in time for the Cycle 19 Phase I deadline.

Wavelengths in this handbook and in COS data products are always measured in vacuum.

Gratings:

- ["FUV Grating G130M," page128.](#)
- ["FUV Grating G130M with CENWAVE=1055 or 1096," page131.](#)
- ["FUV Grating G160M," page134.](#)
- ["FUV Grating G140L," page137.](#)
- ["NUV Grating G185M," page140.](#)
- ["NUV Grating G225M," page143.](#)
- ["NUV Grating G285M," page146.](#)
- ["NUV Grating G230L," page149.](#)

FUV Grating G130M

Description

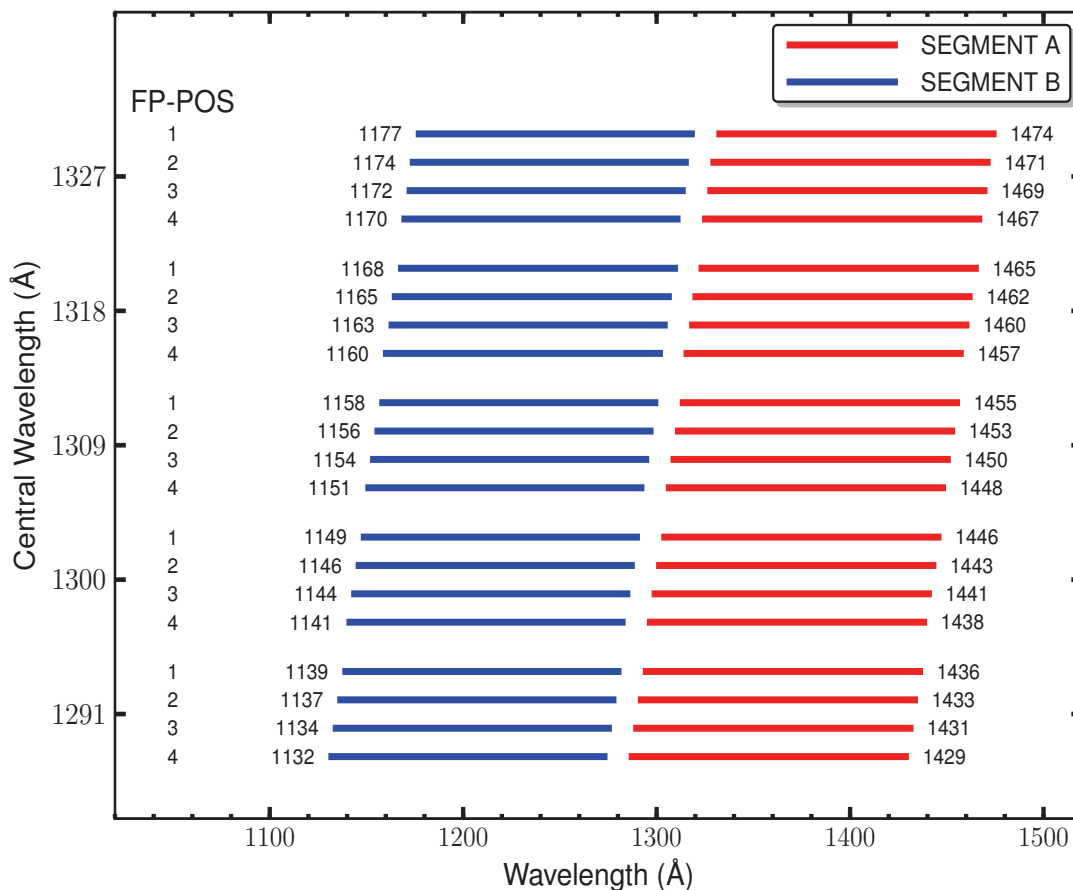
The G130M grating samples wavelengths between about 1150 and 1450 Å. (Its use at shorter wavelengths is discussed below.) It offers higher resolution and effective area than the G140L grating, but less spectral coverage.

Special Considerations

The gap between segments A and B spans 14.3 Å. To fill this gap requires exposures separated by two central-wavelength settings.

Grating	Resolving Power $R = \lambda/\Delta\lambda$	Dispersion (mÅ pixel ⁻¹)	Plate Scale (milliarcsec pixel ⁻¹)		FP-POS Step (Å step ⁻¹)
			Disp. Axis	Cross-Disp. Axis	
G130M	16,000 - 21,000	9.97	22.9	100	2.5

Figure 14.1: Wavelength Ranges for the G130M Grating

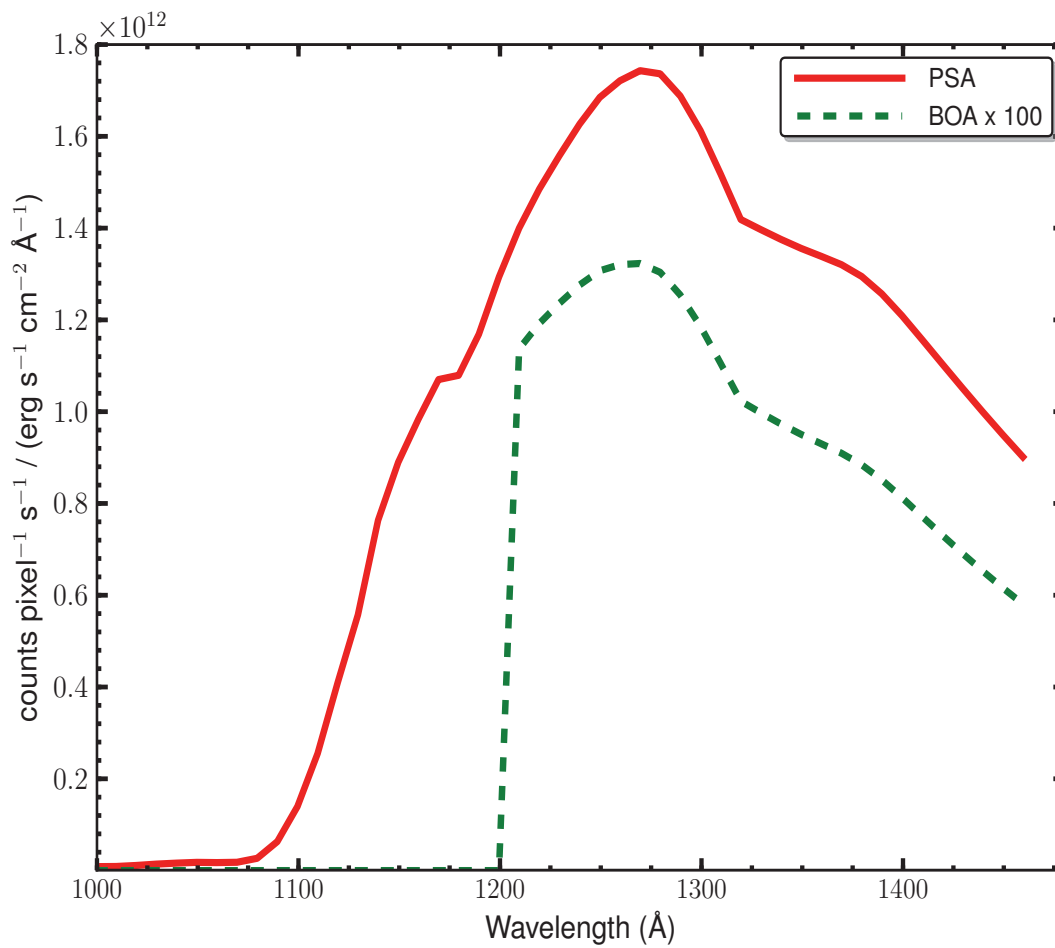


G130M Sensitivities

Table 14.3: G130M Sensitivities and Effective Areas for a Point Source Centered in the PSA

Wavelength (Å)	Sensitivity (counts pixel ⁻¹ sec ⁻¹ per erg cm ⁻² sec ⁻¹ Å ⁻¹)	Effective Area (cm ²)
1150	8.9E11	1.55E03
1200	1.3E12	2.16E03
1250	1.7E12	2.69E03
1300	1.6E12	2.47E03
1350	1.4E12	2.00E03
1400	1.2E12	1.72E03
1450	9.5E11	1.30E03

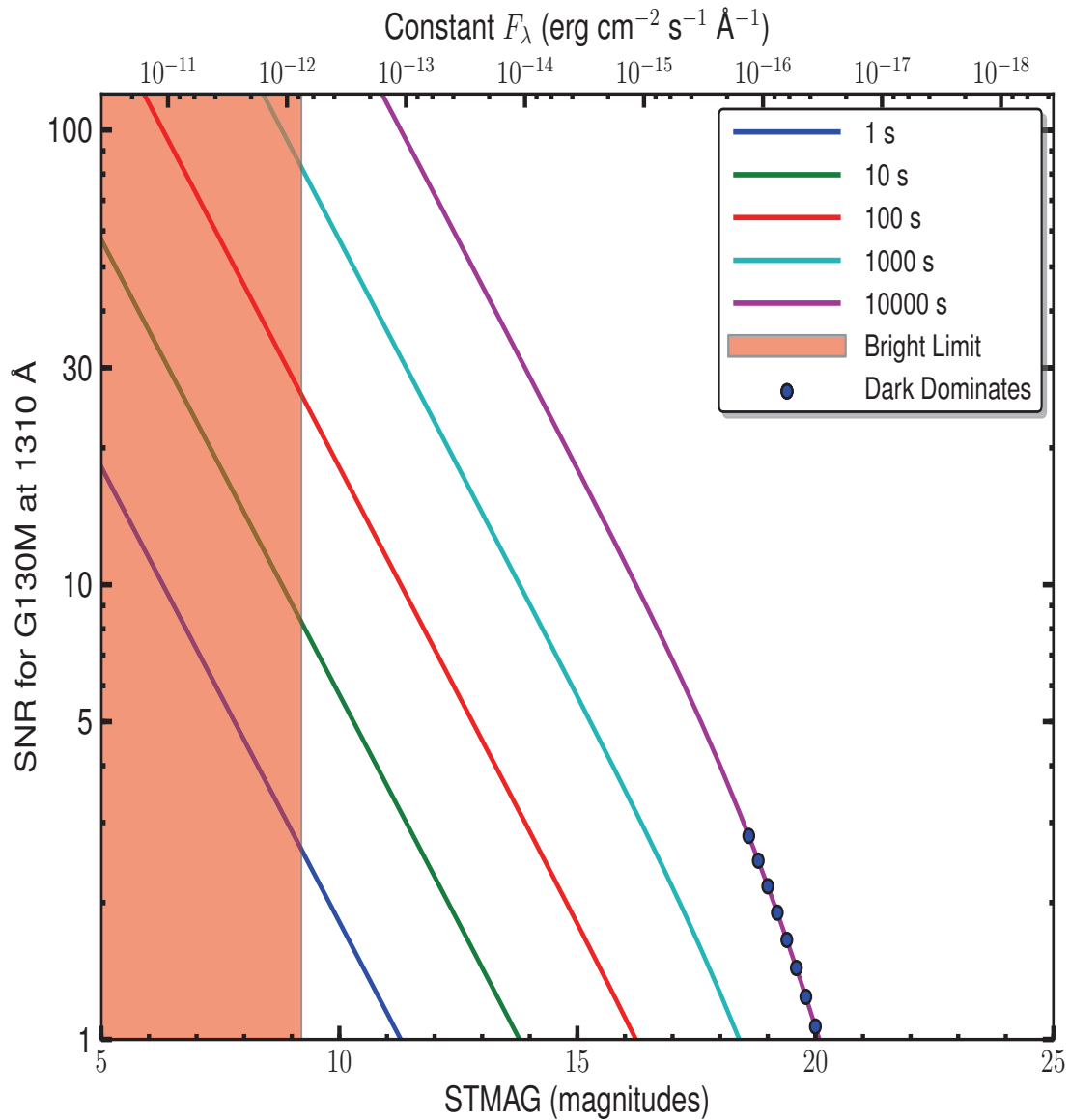
Figure 14.2: G130M Point Source Sensitivity for PSA and BOA



The throughput of the BOA is poorly characterized below 1200 Å and close to zero below 1150 Å.

G130M Signal-to-Noise Ratio

Figure 14.3: Point Source Signal-to-Noise as a Function of STMAG for G130M at 1310 Å



The top axis displays constant F_λ values corresponding to the STMAG units ($V+STMAG_\lambda$) on the bottom axis. Recall that $STMAG=0$ is equivalent to $F_\lambda = 3.63E-9 \text{ erg cm}^{-2} \text{s}^{-1} \text{\AA}^{-1}$. Colors refer to exposure times in seconds. The edge of the shaded area corresponds to the bright-object screening limit. Use of the PSA is assumed.

FUV Grating G130M with CENWAVE=1055 or 1096

Description

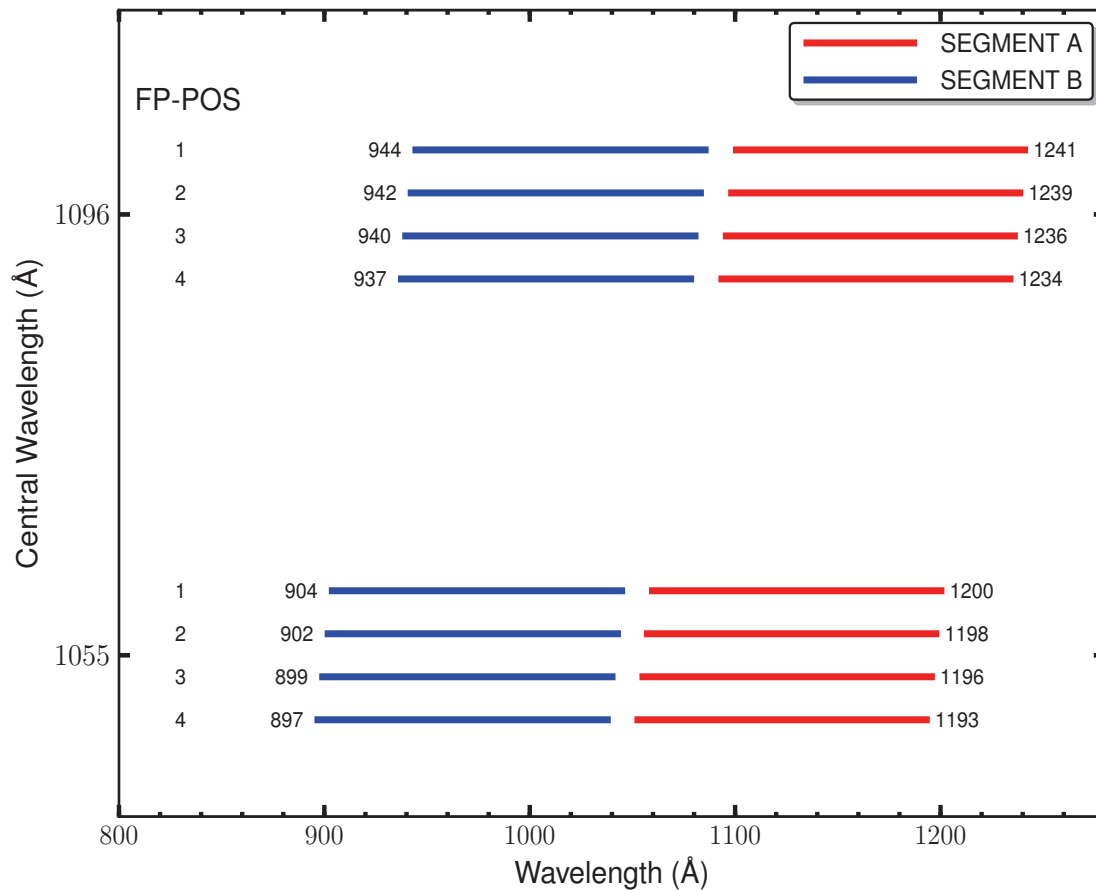
When used with a central wavelength of 1055 or 1096 Å, grating G130M samples wavelengths between about 900 and 1200 Å. Its resolution and effective area are higher than those of the G140L grating, but lower than those of G130M when used at longer wavelengths.

Special Considerations

The COS sensitivity rises steeply between 1070 and 1150 Å. To observe bright targets near the Lyman limit, turn off detector segment A and use only segment B.

Grating	Resolving Power $R = \lambda/\Delta\lambda$	Dispersion (mÅ pixel ⁻¹)	Plate Scale (milliarcsec pixel ⁻¹)		FP-POS Step (Å step ⁻¹)
			Disp. Axis	Cross-Disp. Axis	
G130M	3000 - 1000	9.97	22.9	100	2.5

Figure 14.4: Wavelength Ranges for the G130M Grating

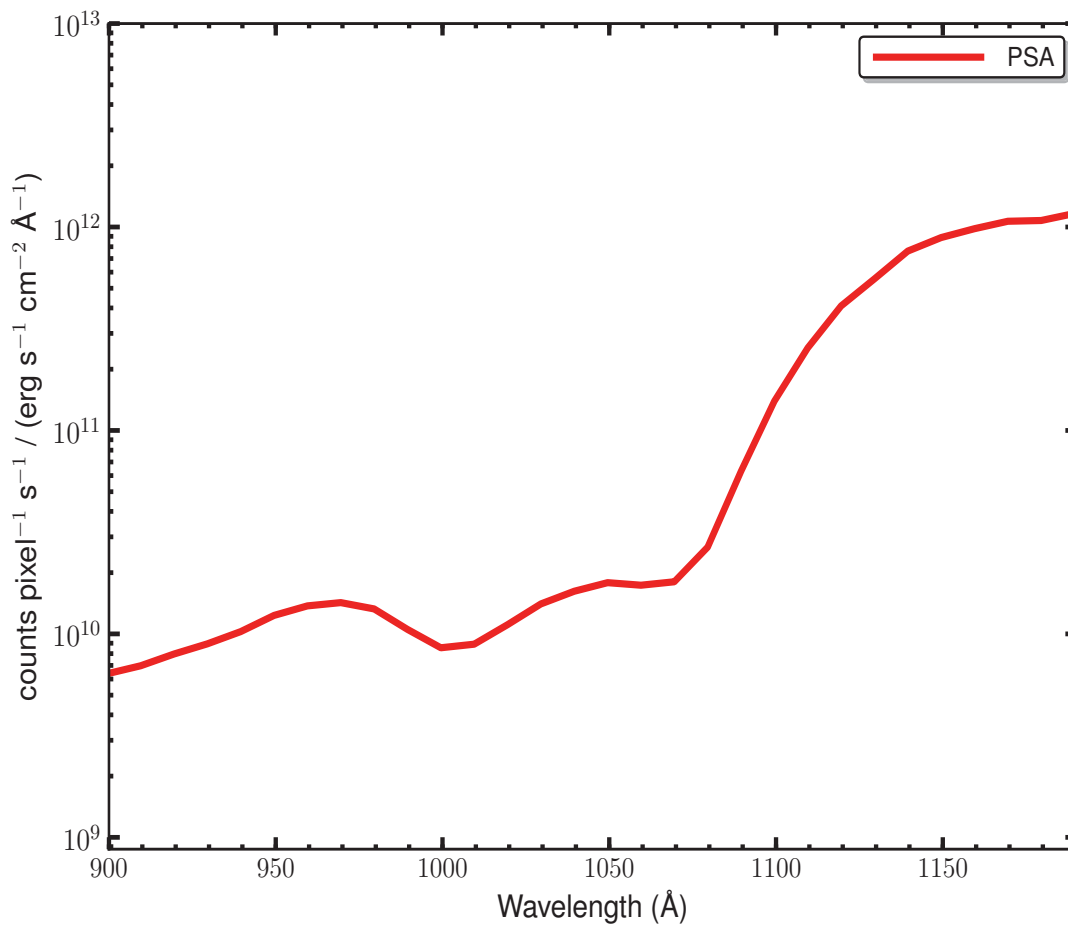


G130M Sensitivities

Table 14.4: G130M Sensitivities and Effective Areas for a Point Source Centered in the PSA

Wavelength (Å)	Sensitivity (counts pixel ⁻¹ sec ⁻¹ per erg cm ⁻² sec ⁻¹ Å ⁻¹)	Effective Area (cm ²)
900	6.4E09	1.42E01
950	1.2E10	2.61E01
1000	8.5E09	1.70E01
1050	1.8E10	3.40E01
1100	1.4E11	2.61E02
1150	8.9E11	1.55E03
1200	1.3E12	2.16E03

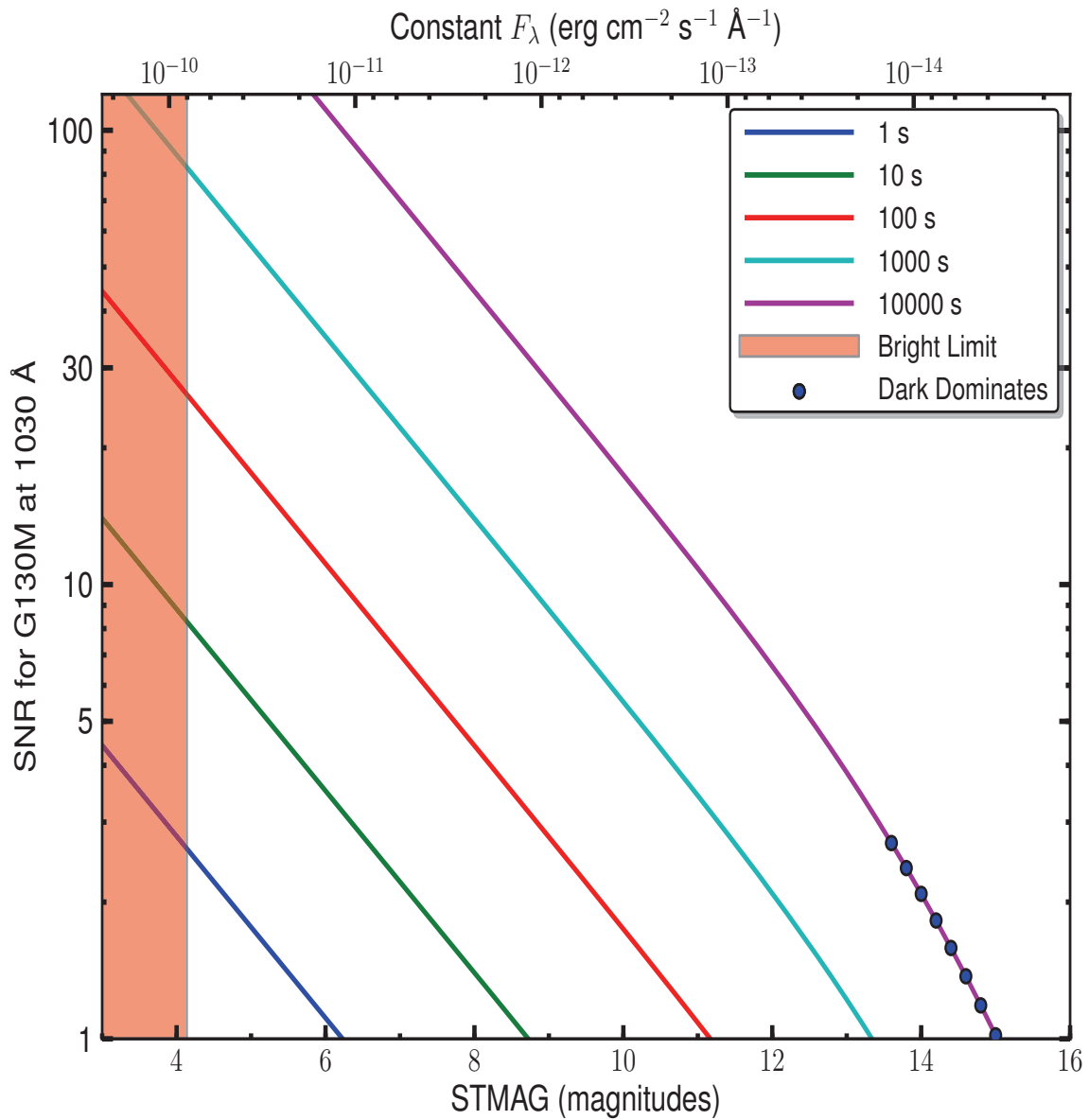
Figure 14.5: G130M Point Source Sensitivity for PSA and BOA



The sensitivity through the BOA is not shown, as its MgF₂ filter is opaque at these wavelengths.

G130M Signal-to-Noise Ratio

Figure 14.6: Point Source Signal-to-Noise as a Function of STMAG for G130M at 1030 Å



The top axis displays constant F_λ values corresponding to the STMAG units ($V+STMAG_\lambda$) on the bottom axis. Recall that $STMAG=0$ is equivalent to $F_\lambda = 3.63E-9 \text{ erg cm}^{-2} \text{ s}^{-1} \text{ \AA}^{-1}$. Colors refer to exposure times in seconds. The edge of the shaded area corresponds to the bright-object screening limit. Use of the PSA is assumed.

FUV Grating G160M

Description

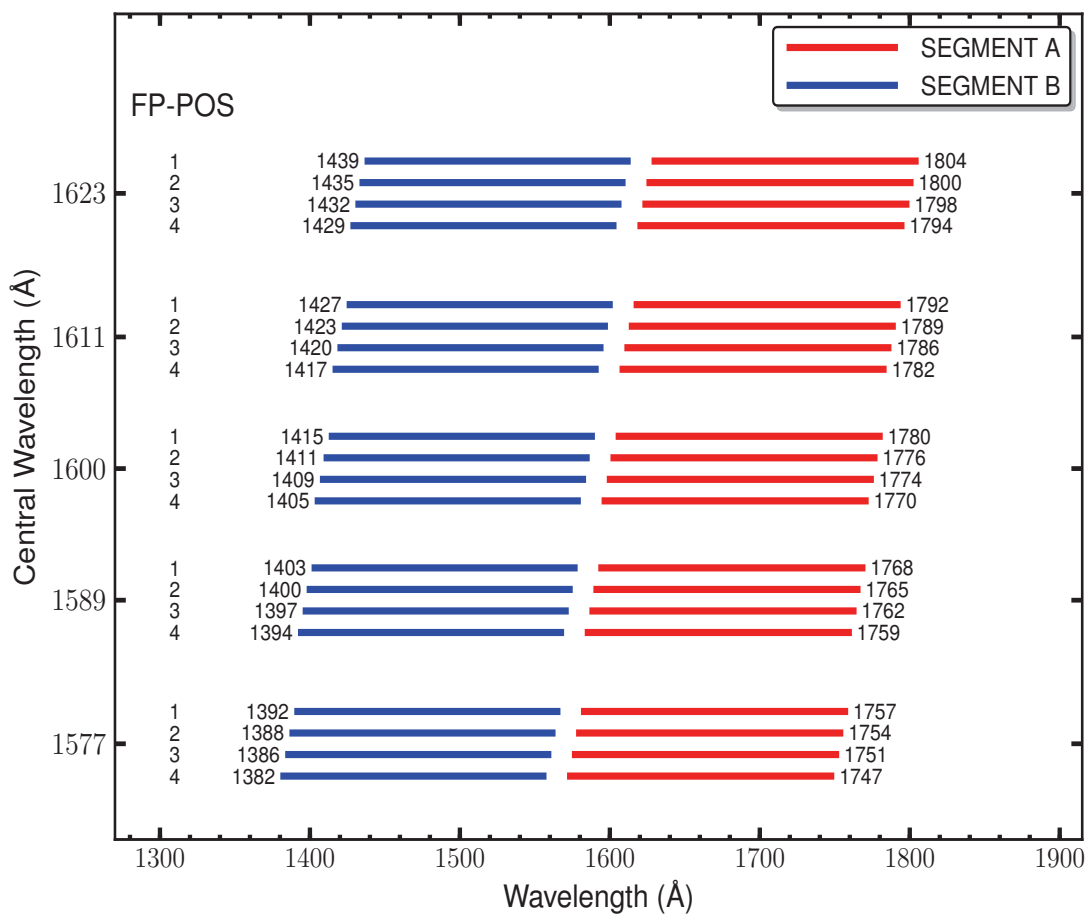
The G160M grating samples wavelengths between about 1405 and 1775 Å. It offers higher resolution and effective area than the G140L grating, but less spectral coverage.

Special Considerations

The gap between segments A and B spans 18.1 Å. To fill this gap requires exposures separated by two central-wavelength settings.

Grating	Resolving Power $R = \lambda/\Delta\lambda$	Dispersion (mÅ pixel ⁻¹)	Plate Scale (milliarcsec pixel ⁻¹)		FP-POS Step (Å step ⁻¹)
			Disp. Axis	Cross-Disp. Axis	
G160M	16,000 - 21,000	12.23	24.3	90	3.2

Figure 14.7: Wavelength Ranges for the G160M Grating

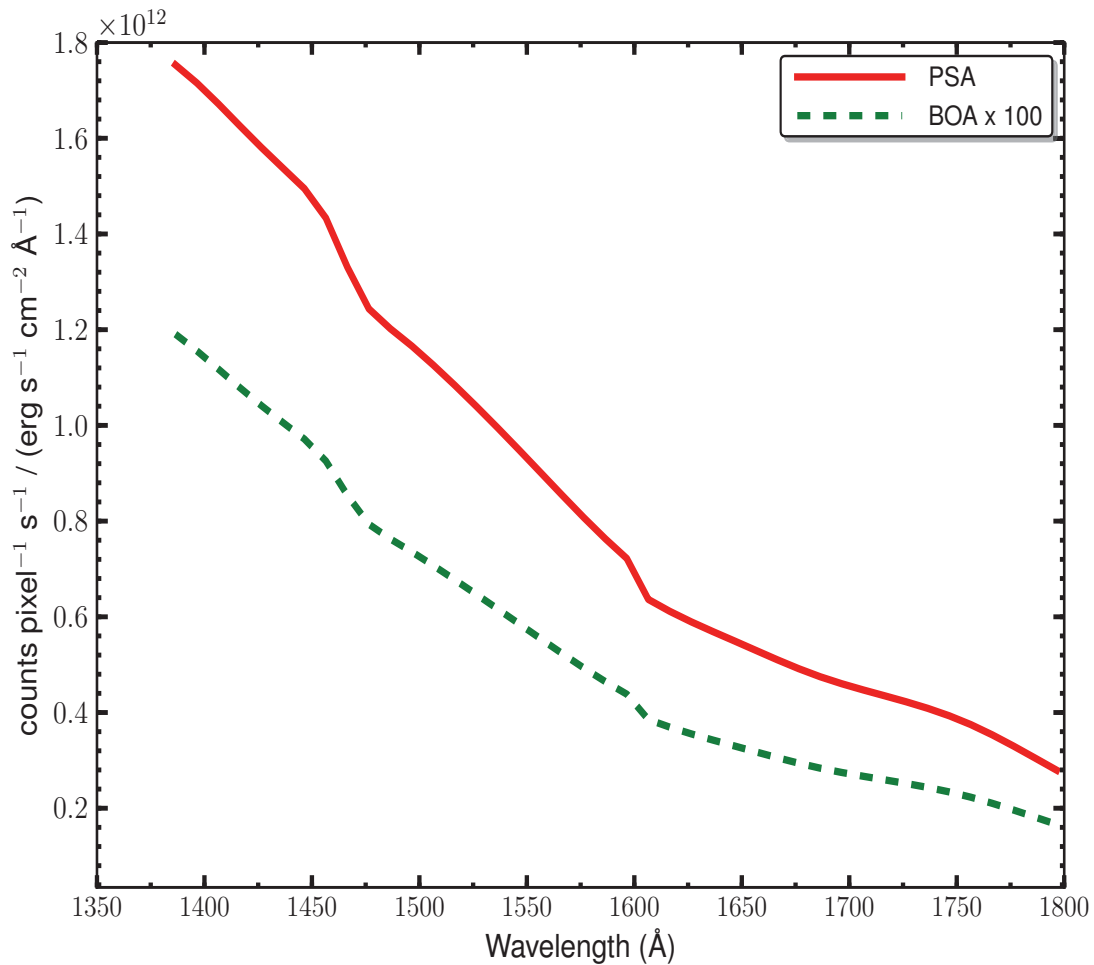


G160M Sensitivities

Table 14.5: G160M Sensitivities and Effective Areas for a Point Source Centered in the PSA

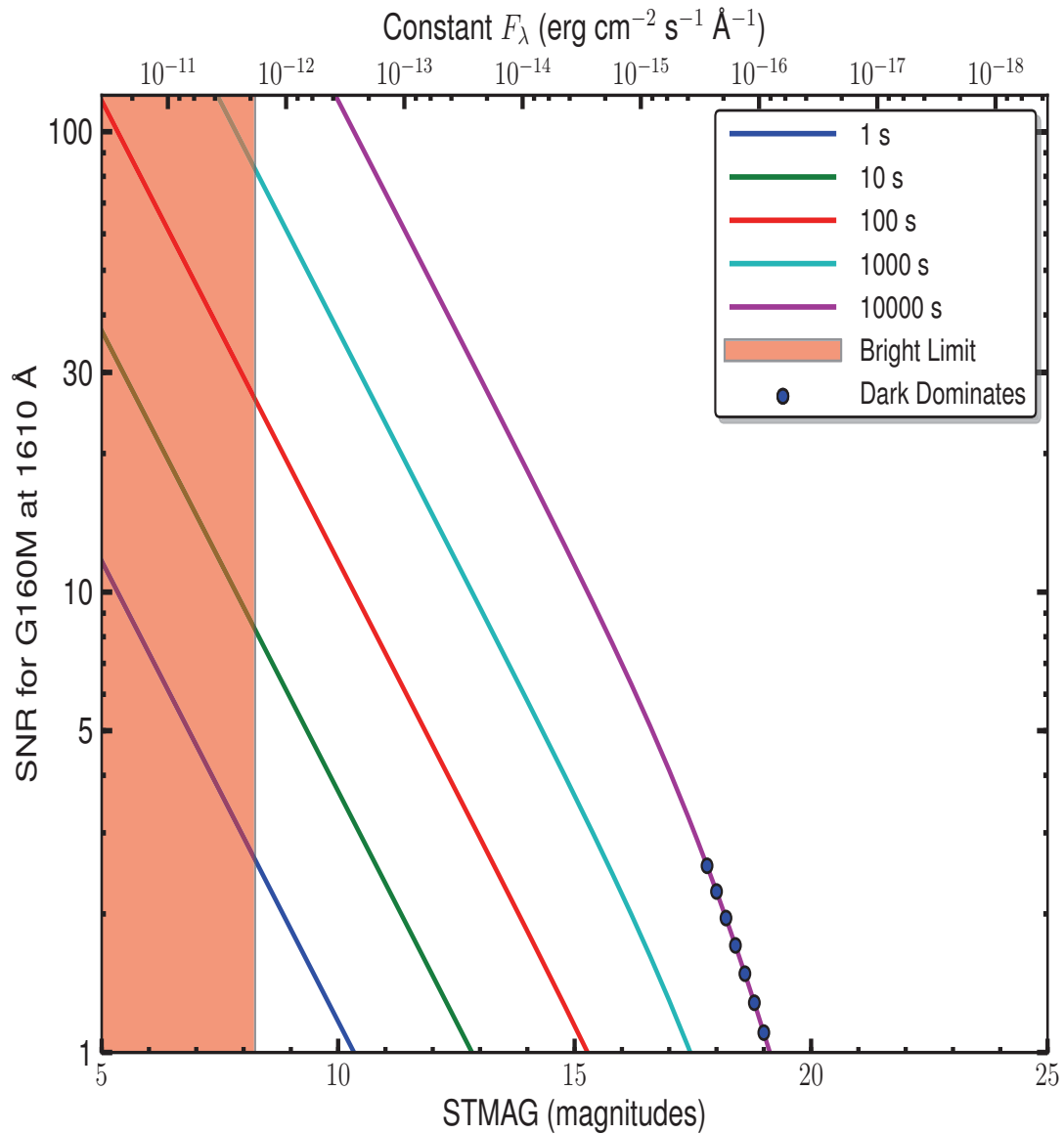
Wavelength (Å)	Sensitivity (counts pixel ⁻¹ sec ⁻¹ per erg cm ⁻² sec ⁻¹ Å ⁻¹)	Effective Area (cm ²)
1400	1.7E12	1.97E03
1450	1.5E12	1.65E03
1500	1.2E12	1.25E03
1550	9.3E11	9.76E02
1600	7.1E11	7.19E02
1650	5.4E11	5.34E02
1700	4.6E11	4.35E02
1750	3.9E11	3.59E02

Figure 14.8: G160M Point Source Sensitivity for PSA and BOA



G160M Signal-to-Noise Ratio

Figure 14.9: Point Source Signal-to-Noise as a Function of STMAG for G160M at 1610 Å



The top axis displays constant F_λ values corresponding to the STMAG units ($V+STMAG_\lambda$) on the bottom axis. Recall that $STMAG=0$ is equivalent to $F_\lambda = 3.63E-9$ erg cm⁻² s⁻¹ Å⁻¹. Colors refer to exposure times in seconds. The edge of the shaded area corresponds to the bright-object screening limit. Use of the PSA is assumed.

FUV Grating G140L

Description

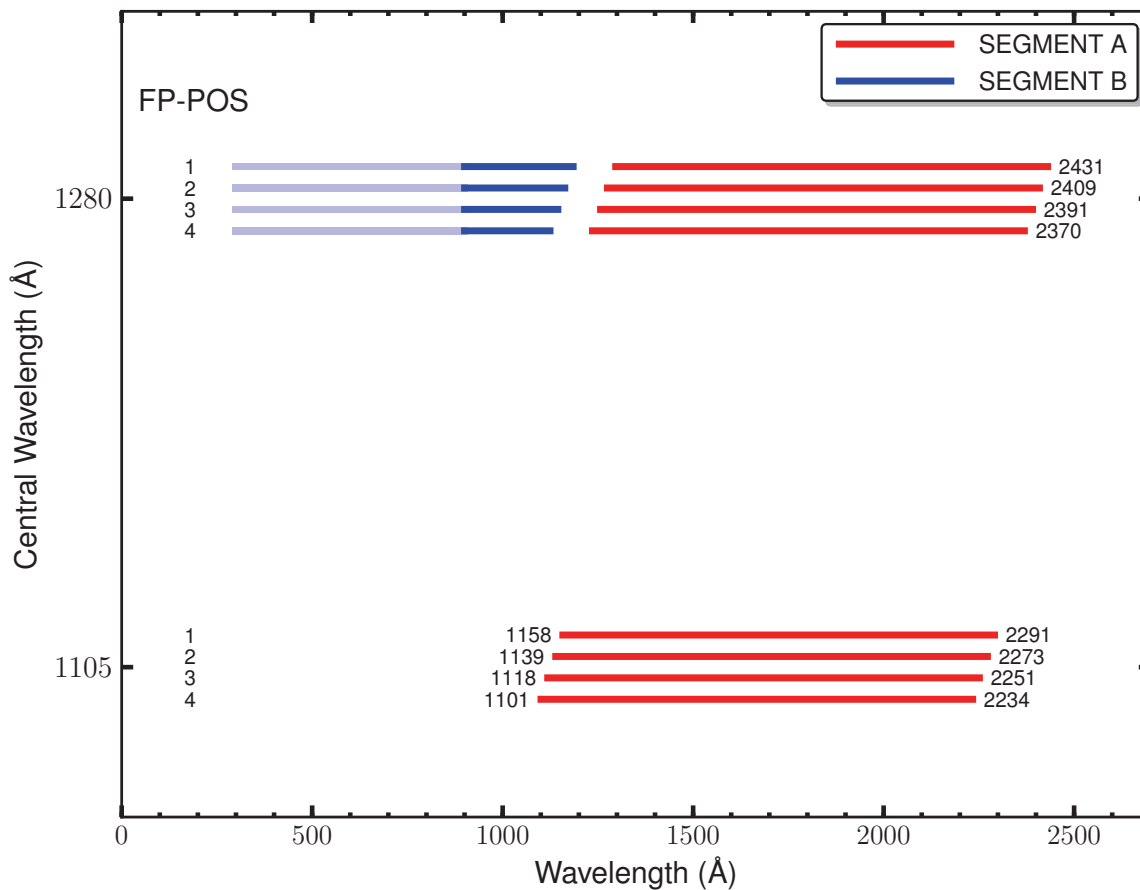
G140L is a low-resolution grating ($R \sim 2,000$) with wavelength coverage extending to 900 \AA —and perhaps below. Its sensitivity at EUV wavelengths—marked in light blue in Figure 14.10—has not yet been calibrated. The grating has two central-wavelength settings, 1105 and 1280 \AA .

Special Considerations

The gap between segments A and B spans 105 \AA . To fill this gap requires exposures at both central-wavelength settings. When setting 1105 is used, the high voltage on Segment B must be lowered to avoid a dangerously high count rate from zero-order light. Wavelengths longer than 2150 \AA may be contaminated by second-order light.

Grating	Resolving Power $R = \lambda/\Delta\lambda$	Dispersion (m\AA pixel^{-1})	Plate Scale ($\text{milliarcsec pixel}^{-1}$)		FP-POS Step (\AA step^{-1})
			Disp. Axis	Cross-Disp. Axis	
G140L	1,500 - 4,000	80.3	23.0	90	19.6

Figure 14.10: Wavelength Ranges for the G140L Grating



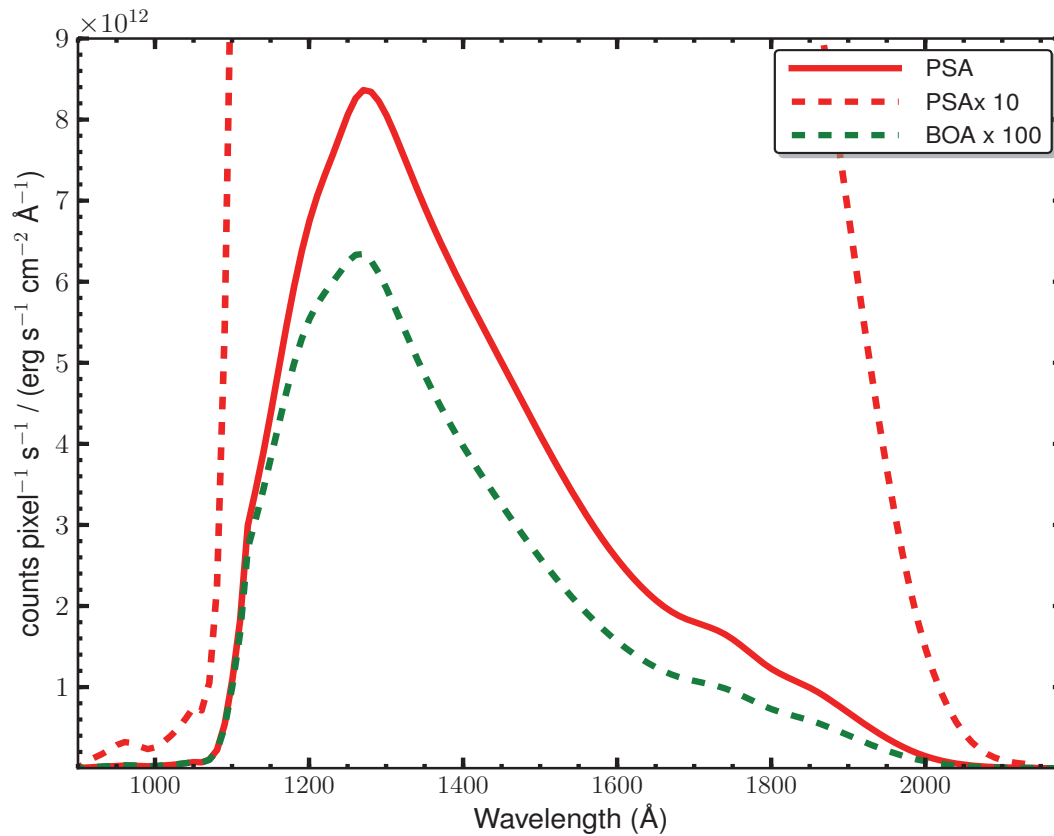
The COS sensitivity at EUV wavelengths (marked in light blue) is not yet known.

G140L Sensitivities

Table 14.6: G140L Sensitivities and Effective Areas for a Point Source Centered in the PSA

Wavelength (Å)	Sensitivity (counts pixel ⁻¹ sec ⁻¹ per erg cm ⁻² sec ⁻¹ Å ⁻¹)	Effective Area (cm ²)
950	2.8E10	7.44E00
1000	2.5E10	6.35E00
1100	1.1E12	2.42E02
1200	6.7E12	1.40E03
1300	8.1E12	1.55E03
1400	5.9E12	1.06E03
1500	4.1E12	6.85E02
1600	2.6E12	4.03E02
1700	1.8E12	2.65E02
1800	1.2E12	1.71E02
1900	6.9E11	9.02E01
2000	1.5E11	1.86E01
2100	9.9E09	1.18E00

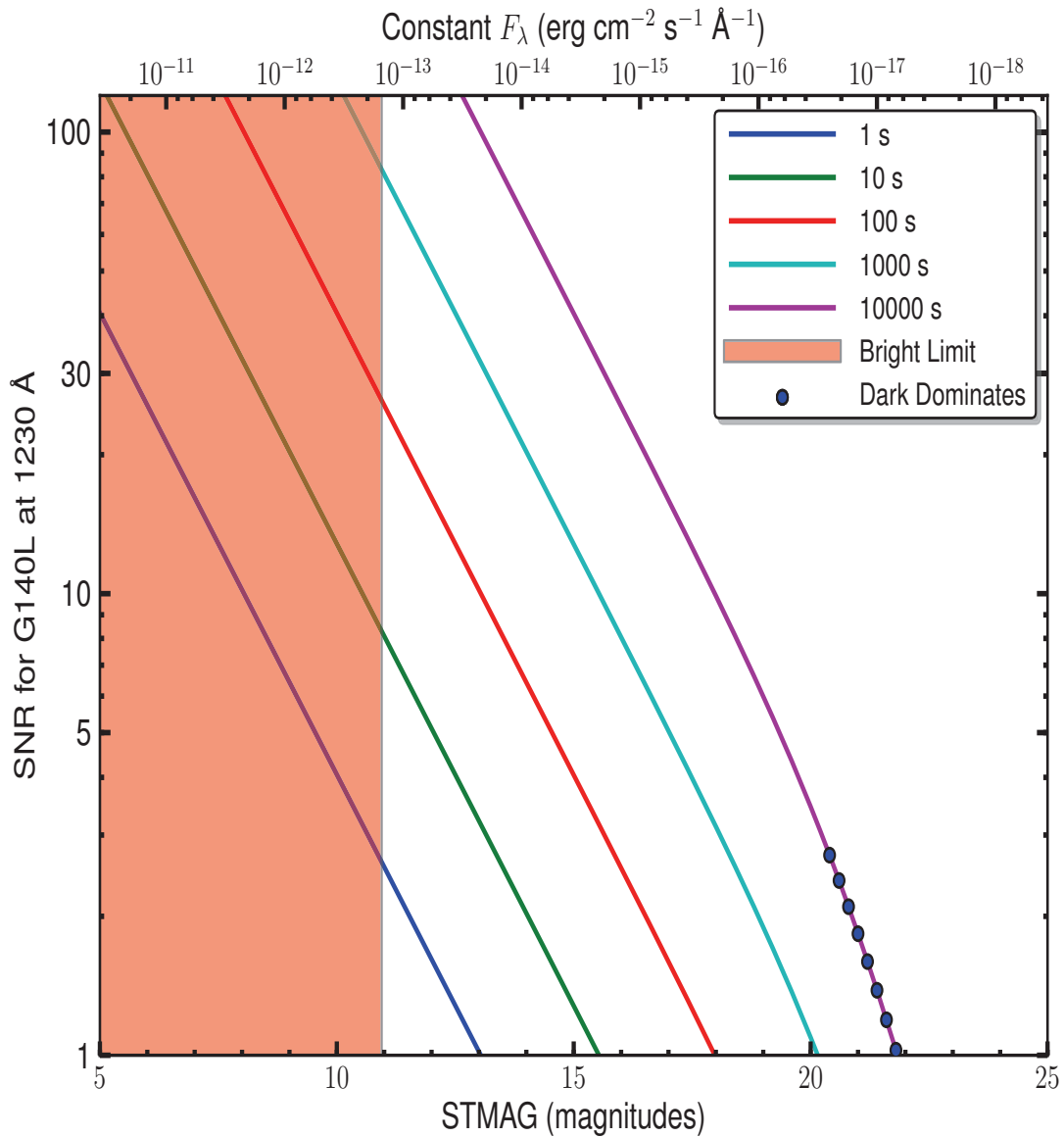
Figure 14.11: G140L Point Source Sensitivity for PSA and BOA



PSA × 10 is plotted to show sensitivity below 1100 Å.

G140L Signal-to-Noise Ratio

Figure 14.12: Point Source Signal-to-Noise as a Function of STMAG for G140L



The top axis displays constant F_λ values corresponding to the STMAG units ($V+STMAG_\lambda$) on the bottom axis. Recall that $STMAG=0$ is equivalent to $F_\lambda = 3.63E-9 \text{ erg cm}^{-2} \text{s}^{-1} \text{\AA}^{-1}$. Colors refer to exposure times in seconds. The edge of the shaded area corresponds to the bright-object screening limit. Use of the PSA is assumed.

NUV Grating G185M

Description

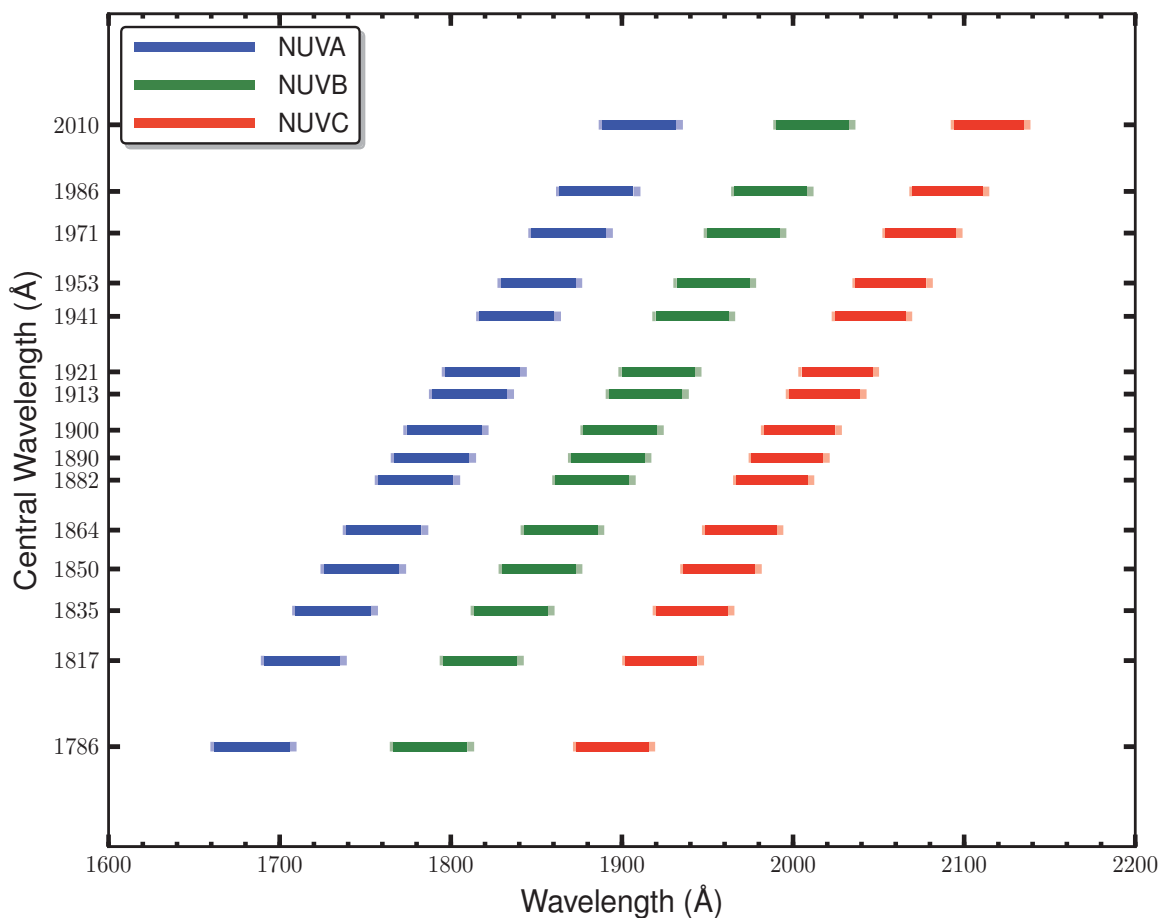
The G185M grating samples wavelengths between about 1700 and 2100 Å. The grating has 15 central wavelength settings.

Special Considerations

G185M spectra consist of three 35-Å stripes separated by two 64-Å gaps. To acquire a complete spectrum requires the use of six central-wavelength settings.

Grating	Resolving Power $R = \lambda/\Delta\lambda$	Dispersion (mÅ pixel ⁻¹)	Spatial Resolution (milliarcsec pixel ⁻¹)	Plate Scale (milliarcsec pixel ⁻¹)		FP-POS Step (Å step ⁻¹)
				Disp. Axis	Cross-Disp. Axis	
G185M	16,000 - 20,000	37	75 ± 4	24.3	23.8	1.9

Figure 14.13: Wavelength Ranges for the G185M Grating

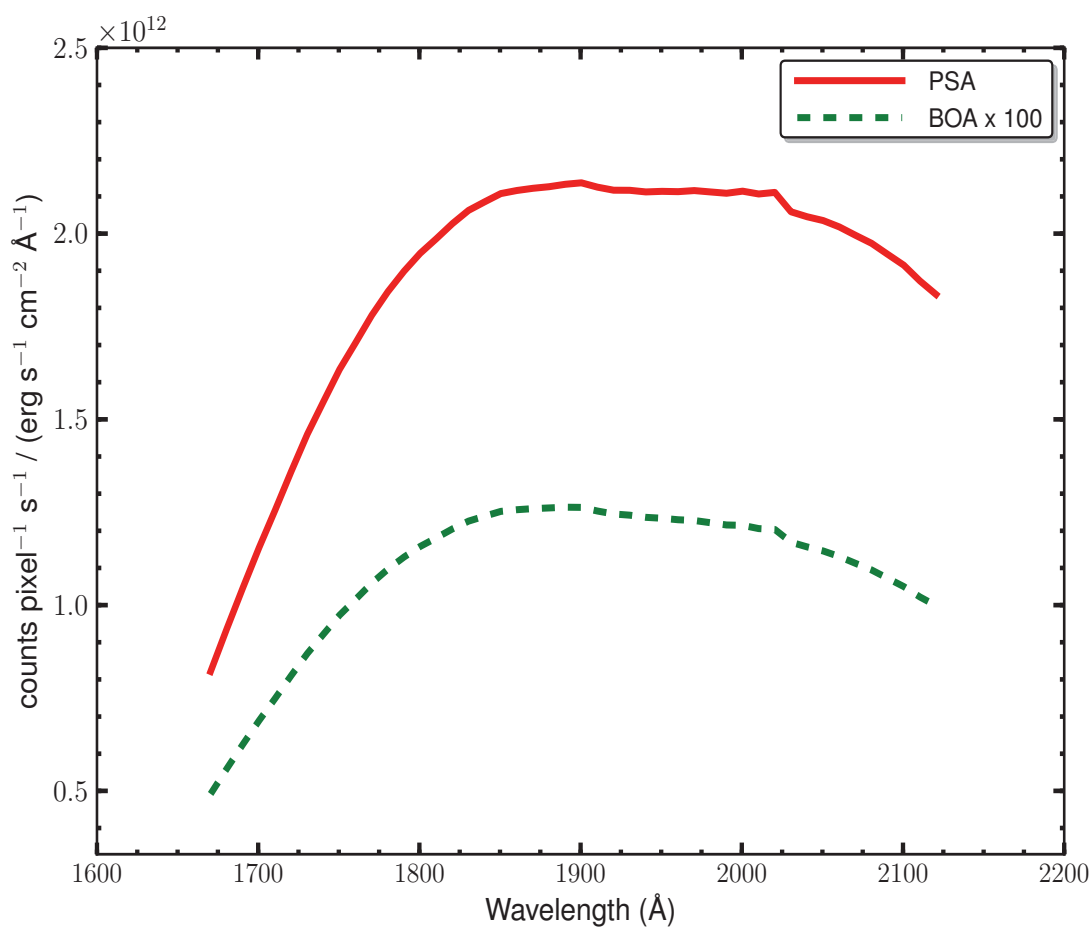


Dark lines represent wavelengths sampled by all four FP-POS positions.

Table 14.7: G185M Sensitivities and Effective Areas for a Point Source Centered in the PSA

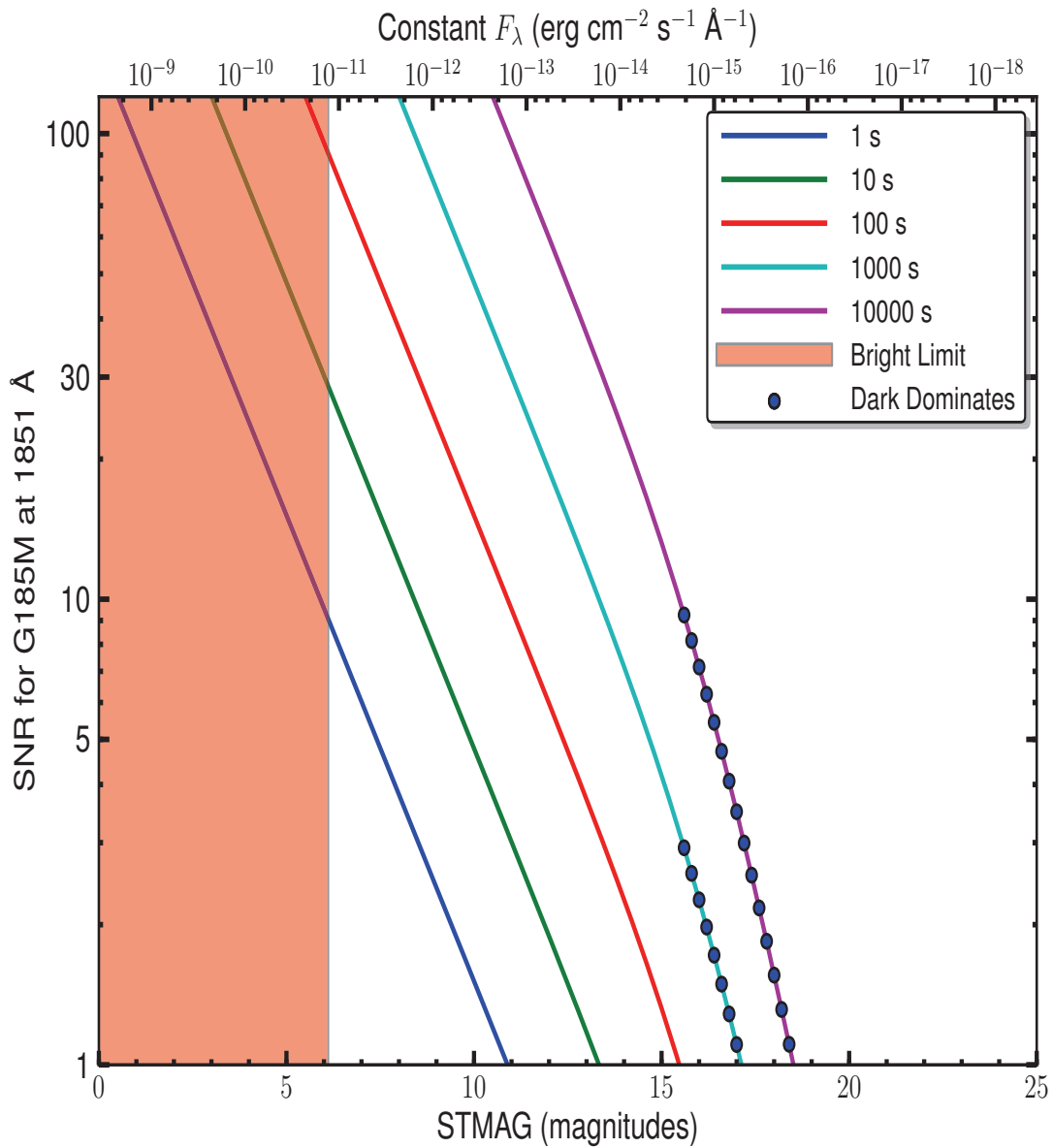
Wavelength (Å)	Sensitivity (counts pixel ⁻¹ sec ⁻¹ per erg cm ⁻² sec ⁻¹ Å ⁻¹)	Effective Area (cm ²)
1670	4.5E11	1.45E02
1700	1.1E12	3.67E02
1750	1.6E12	5.06E02
1800	1.9E12	5.87E02
1850	2.1E12	6.19E02
1900	2.1E12	6.11E02
1950	2.1E12	5.89E02
2000	2.1E12	5.74E02
2050	2.0E12	5.40E02
2100	1.9E12	4.96E02

Figure 14.14: G185M Point Source Sensitivity for PSA and BOA



G185M Signal-to-Noise Ratio

Figure 14.15: Point Source Signal-to-Noise as a Function of STMAG for G185M



The top axis displays constant F_λ values corresponding to the STMAG units ($V+STMAG_\lambda$) on the bottom axis. Recall that $STMAG=0$ is equivalent to $F_\lambda = 3.63E-9 \text{ erg cm}^{-2} \text{ s}^{-1} \text{\AA}^{-1}$. Colors refer to exposure times in seconds. The edge of the shaded area corresponds to the bright-object screening limit. Use of the PSA is assumed.

NUV Grating G225M

Description

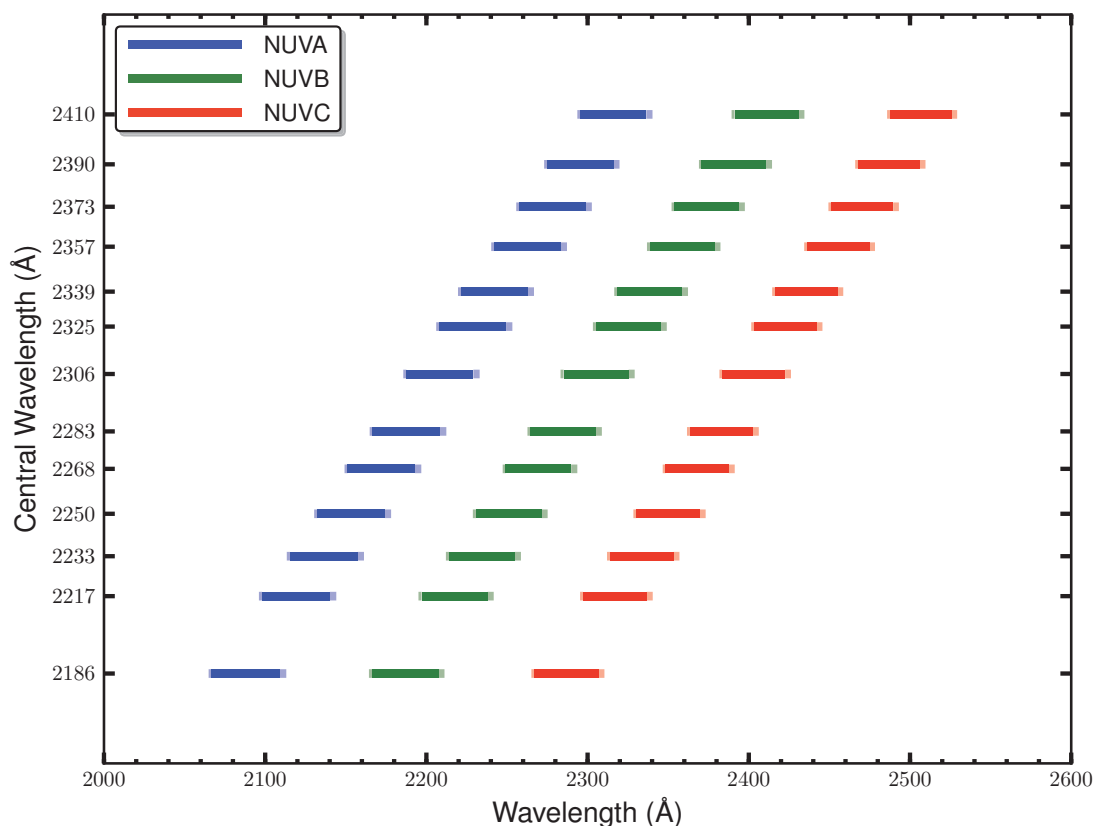
The G225M grating samples wavelengths between about 2100 and 2500 Å. The grating has 13 central wavelength settings.

Special Considerations

G225M spectra consist of three 35-Å stripes separated by two 64-Å gaps. To acquire a complete spectrum requires the use of six central-wavelength settings.

Grating	Resolving Power $R = \lambda/\Delta\lambda$	Dispersion (mÅ pixel ⁻¹)	Spatial Resolution (milliarcsec pixel ⁻¹)	Plate Scale (milliarcsec pixel ⁻¹)		FP-POS Step (Å step ⁻¹)
				Disp. Axis	Cross-Disp. Axis	
G225M	20,000 - 24,000	33	58 ± 2	24.3	23.1	1.7

Figure 14.16: Wavelength Ranges for the G225M Grating



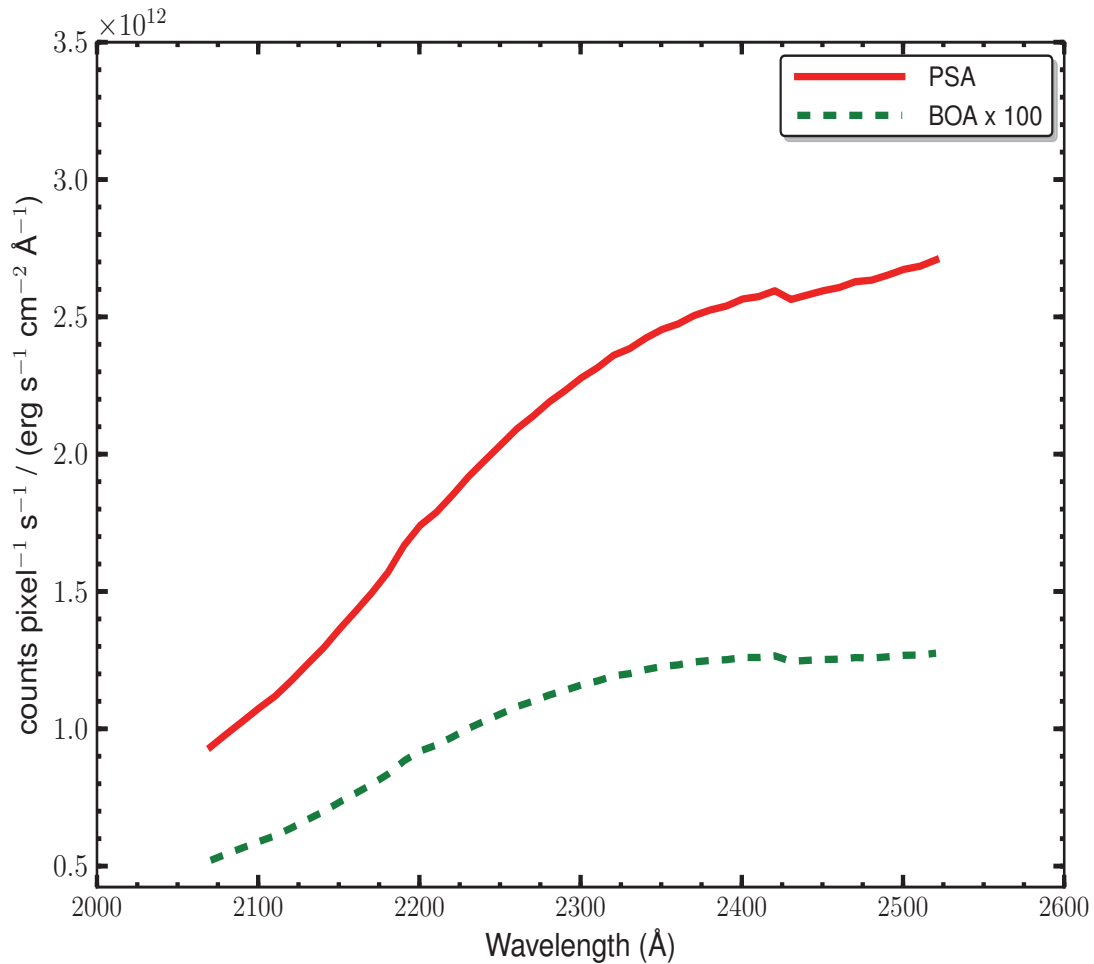
Dark lines represent wavelengths sampled by all four FP-POS positions.

G225M Sensitivities

Table 14.8: G225M Sensitivities and Effective Areas for a Point Source Centered in the PSA

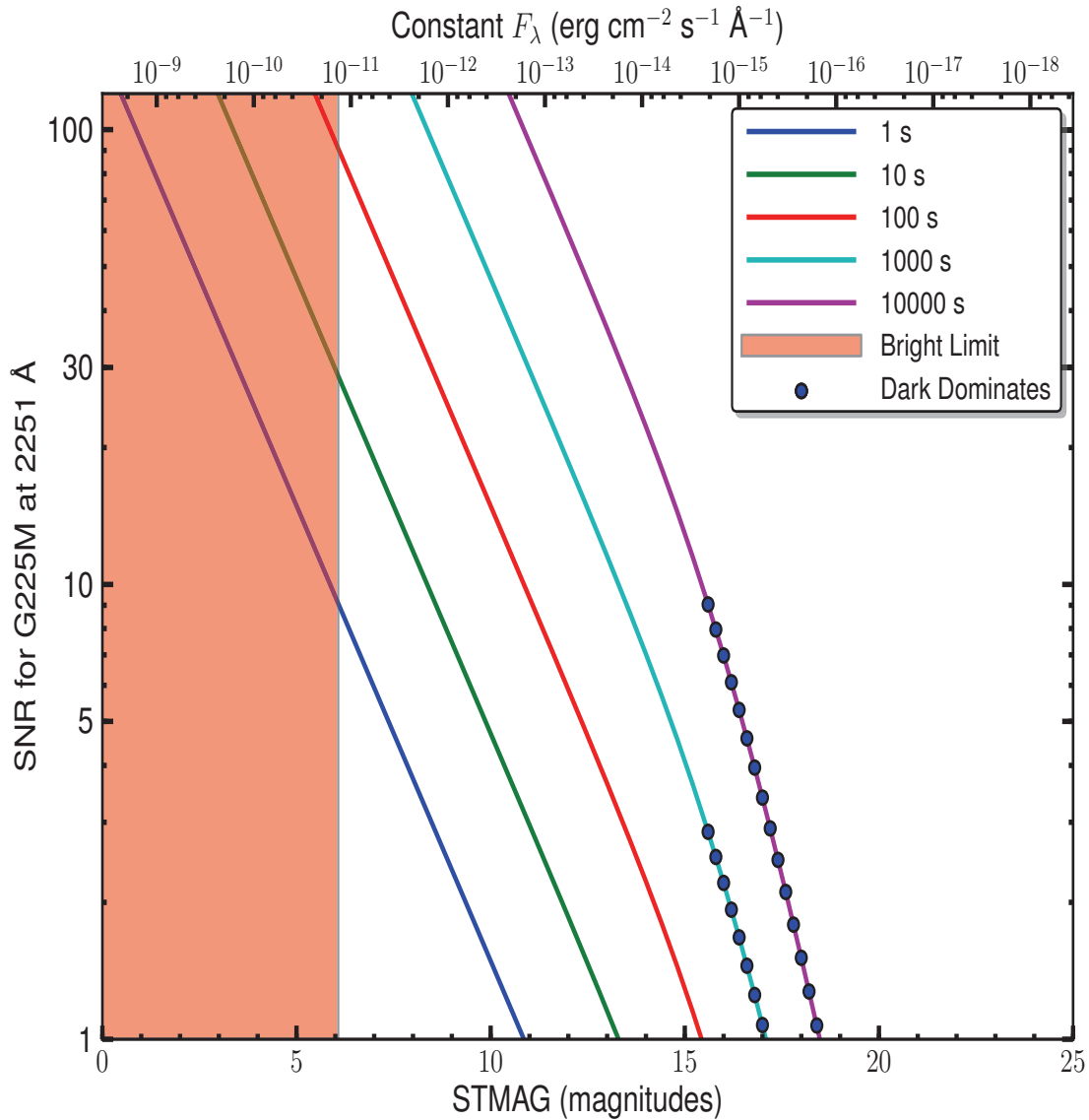
Wavelength (Å)	Sensitivity (counts pixel ⁻¹ sec ⁻¹ per erg cm ⁻² sec ⁻¹ Å ⁻¹)	Effective Area (cm ²)
2100	1.1E12	2.96E02
2150	1.4E12	3.66E02
2200	1.7E12	4.57E02
2250	2.0E12	5.22E02
2300	2.3E12	5.73E02
2350	2.5E12	6.04E02
2400	2.6E12	6.18E02
2450	2.6E12	6.13E02
2500	2.7E12	6.18E02

Figure 14.17: G225M Point Source Sensitivity for PSA and BOA



G225M Signal-to-Noise Ratio

Figure 14.18: Point Source Signal-to-Noise as a Function of STMAG for G225M



The top axis displays constant F_λ values corresponding to the STMAG units ($V+STMAG_\lambda$) on the bottom axis. Recall that $STMAG=0$ is equivalent to $F_\lambda = 3.63E-9 \text{ erg cm}^{-2} \text{ s}^{-1} \text{ \AA}^{-1}$. Colors refer to exposure times in seconds. The edge of the shaded area corresponds to the bright-object screening limit. Use of the PSA is assumed.

NUV Grating G285M

Description

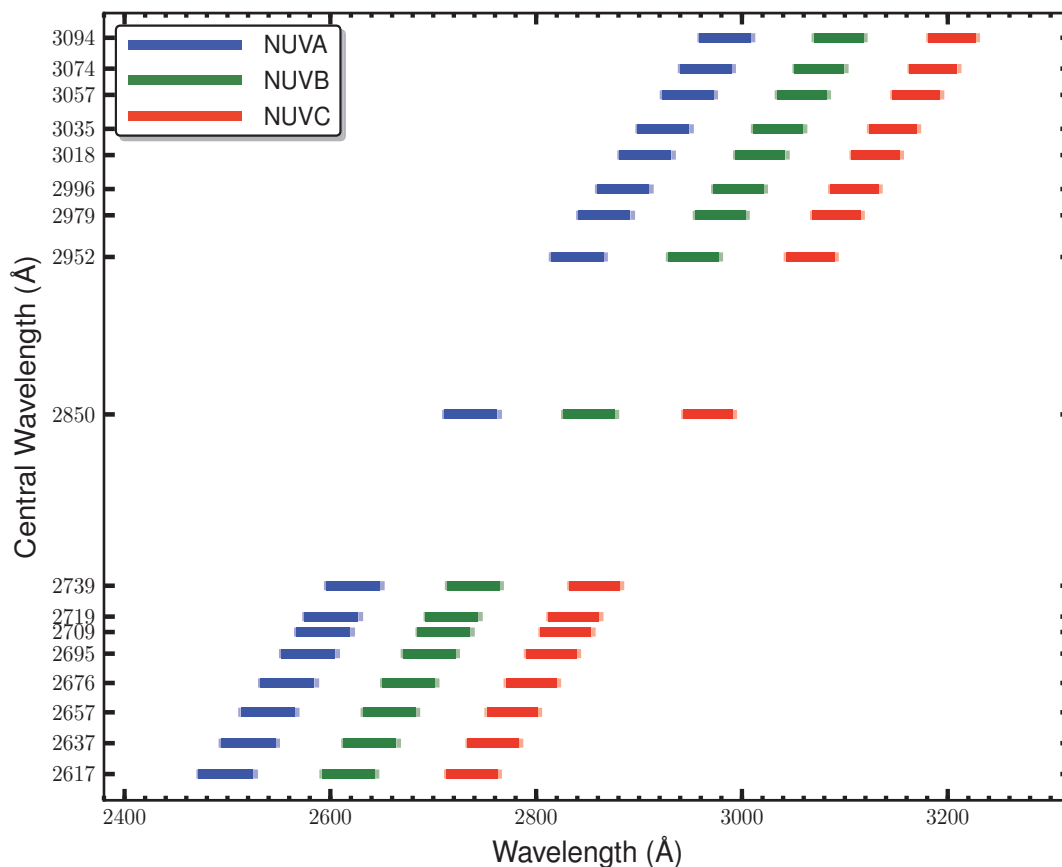
The G285M grating samples wavelengths between about 2500 and 3200 Å. The grating has 17 central wavelength settings.

Special Considerations

G285M spectra consist of three 41-Å stripes separated by two 74-Å gaps. To acquire a complete spectrum requires the use of eight central-wavelength settings.

Grating	Resolving Power $R = \lambda/\Delta\lambda$	Dispersion (mÅ pixel ⁻¹)	Spatial Resolution (milliarcsec pixel ⁻¹)	Plate Scale (milliarcsec pixel ⁻¹)		FP-POS Step (Å step ⁻¹)
				Disp. Axis	Cross-Disp. Axis	
G285M	20,000 - 24,000	40	56 ± 1	24.3	24.4	2.1

Figure 14.19: Wavelength Ranges for the G285M Grating



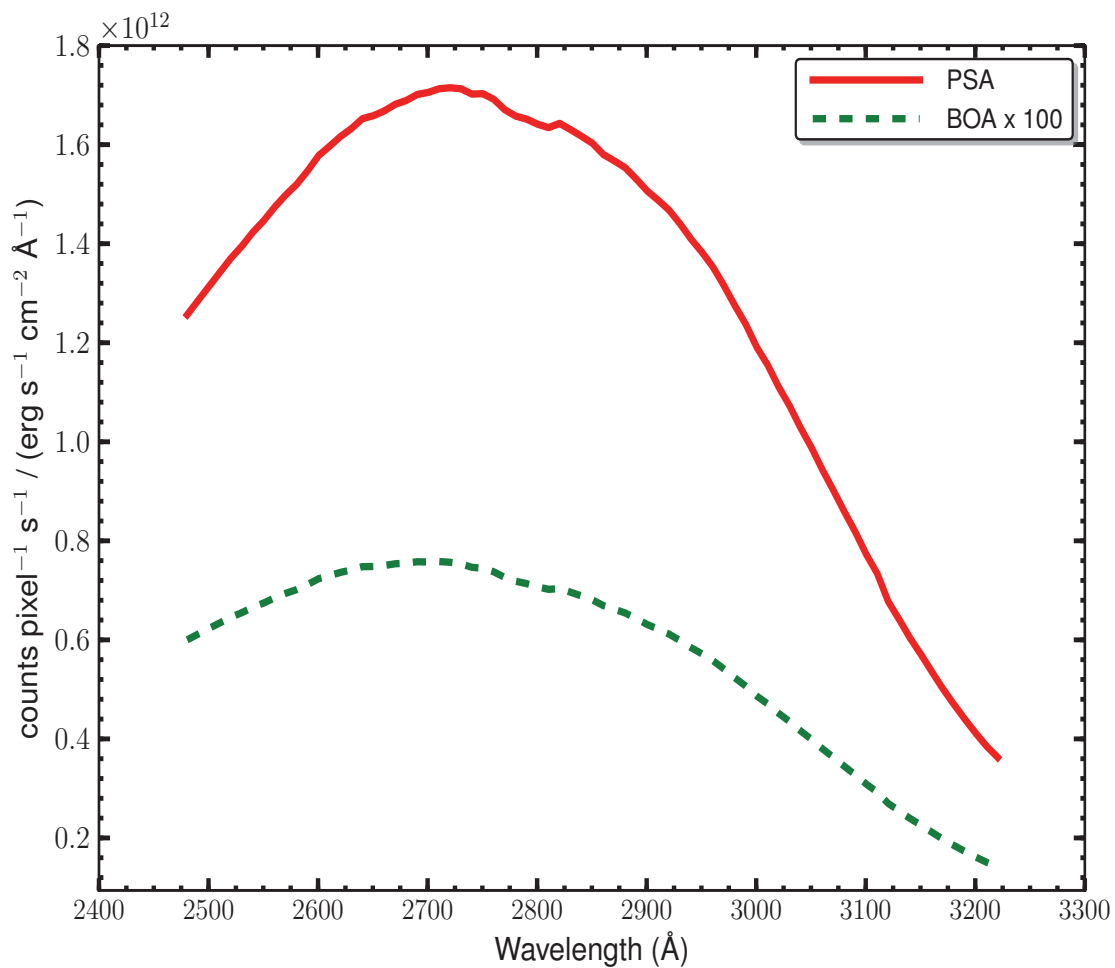
Dark lines represent wavelengths sampled by all four FP-POS positions.

G285M Sensitivities

Table 14.9: G285M Sensitivities and Effective Areas for a Point Source Centered in the PSA

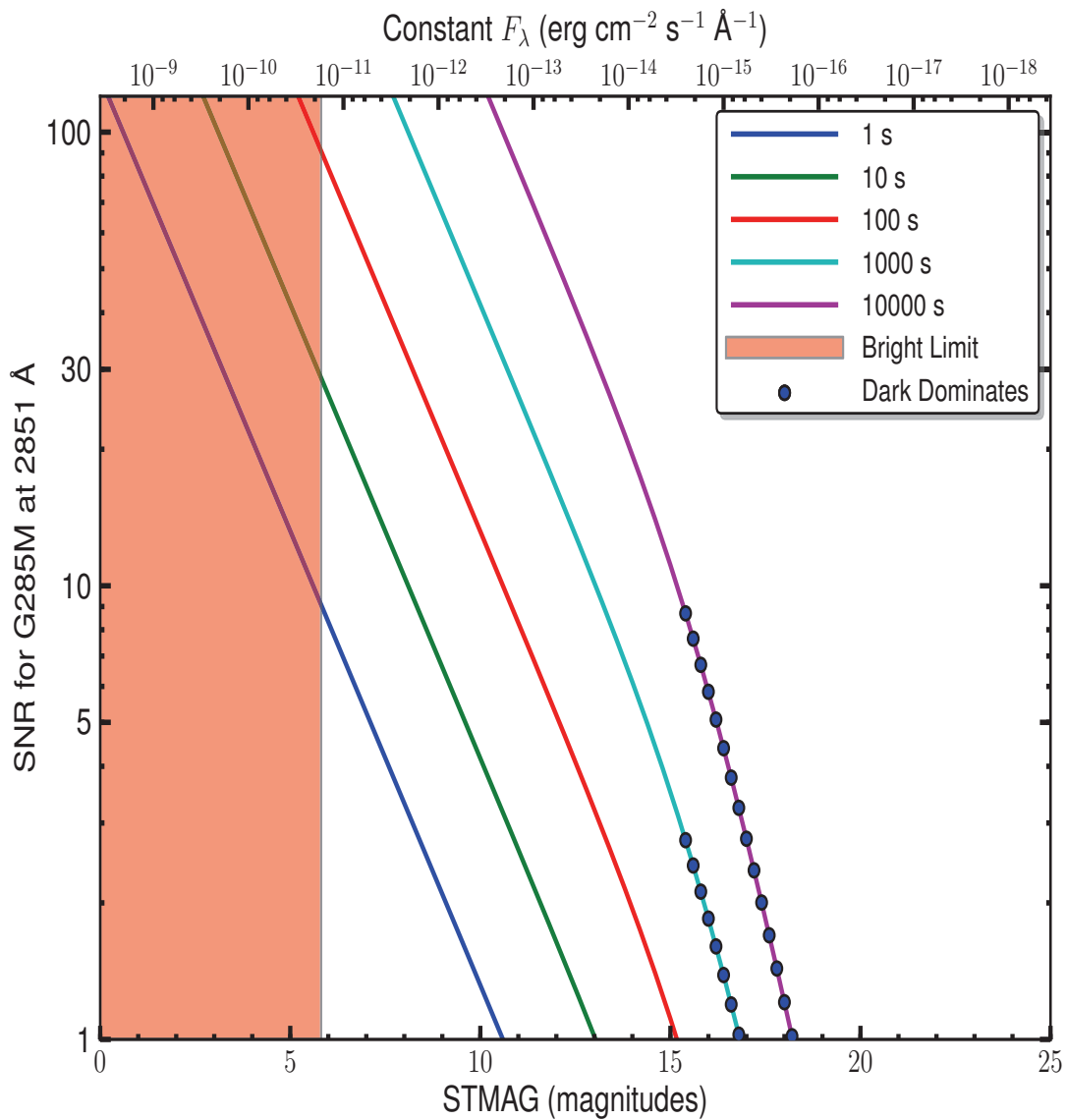
Wavelength (Å)	Sensitivity (counts pixel ⁻¹ sec ⁻¹ per erg cm ⁻² sec ⁻¹ Å ⁻¹)	Effective Area (cm ²)
2500	1.3E12	2.57E02
2600	1.6E12	2.97E02
2700	1.7E12	3.09E02
2800	1.6E12	2.87E02
2900	1.5E12	2.54E02
3000	1.2E12	1.95E02
3100	7.7E11	1.22E02
3200	4.1E11	6.31E01

Figure 14.20: G285M Point Source Sensitivity for PSA and BOA



G285M Signal-to-Noise Ratio

Figure 14.21: Point Source Signal-to-Noise as a Function of STMAG for G285M



The top axis displays constant F_λ values corresponding to the STMAG units ($V+STMAG_\lambda$) on the bottom axis. Recall that $STMAG=0$ is equivalent to $F_\lambda = 3.63E-9$ erg cm⁻² s⁻¹ Å⁻¹. Colors refer to exposure times in seconds. The edge of the shaded area corresponds to the bright-object screening limit. Use of the PSA is assumed.

NUV Grating G230L

Description

G230L is a low-resolution grating ($R \sim 3000$) with wavelength coverage extending from about 1650 to 3200 Å. The grating has four central-wavelength settings.

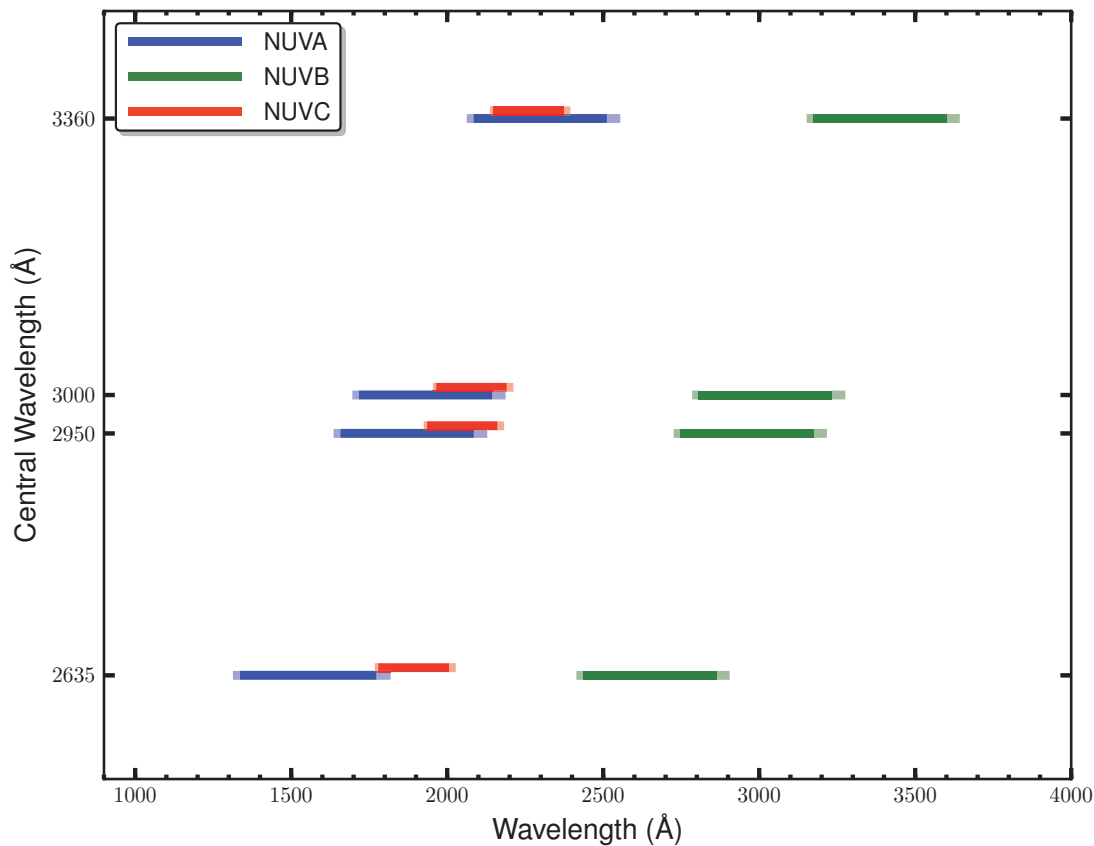
Special Considerations

G230L spectra consist of three 400-Å stripes separated by two 700-Å gaps. To acquire a complete spectrum requires the use of all four central-wavelength settings.

Only stripes A and B record first-order light, and even they may be contaminated by second-order light when central wavelength 3360 is used. See [Table 6.5](#).

Grating	Resolving Power $R = \lambda/\Delta\lambda$	Dispersion (mÅ pixel ⁻¹)	Spatial Resolution (milliarcsec pixel ⁻¹)	Plate Scale (milliarcsec pixel ⁻¹)		FP-POS Step (Å step ⁻¹)
				Disp. Axis	Cross-Disp. Axis	
G230L	2,100 - 3,900	390	81 ± 1	24.3	24.0	20.3

Figure 14.22: Wavelength Ranges for the G230L Grating



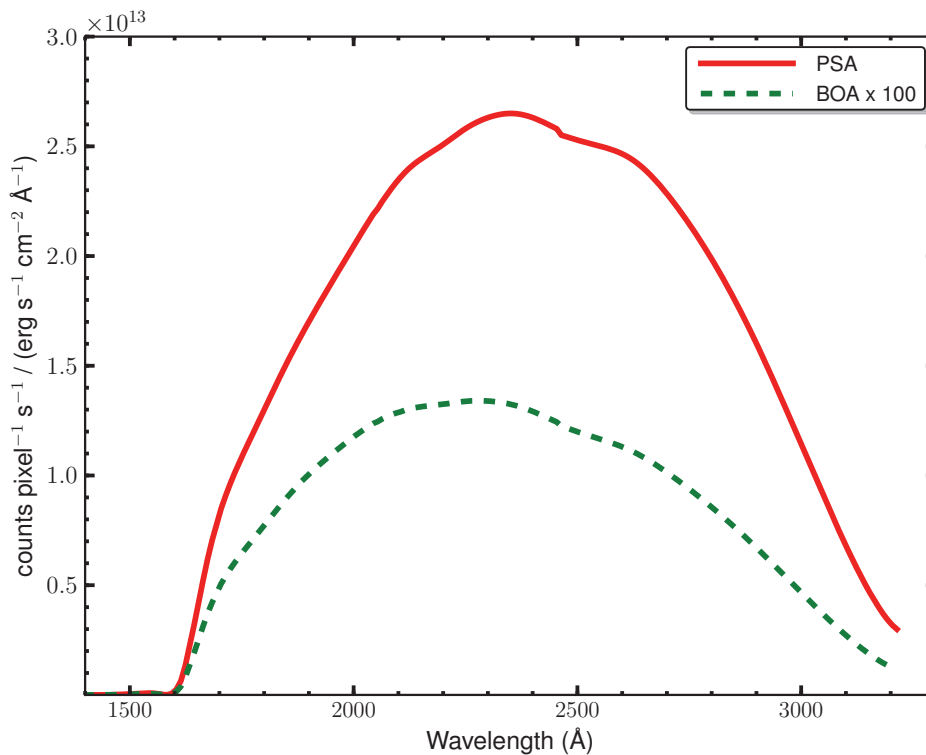
Dark lines represent wavelengths sampled by all four FP-POS positions. Wavelengths above 3200 Å may be contaminated by second-order light.

G230L Sensitivities

Table 14.10: G230L Sensitivities and Effective Areas for a Point Source Centered in the PSA

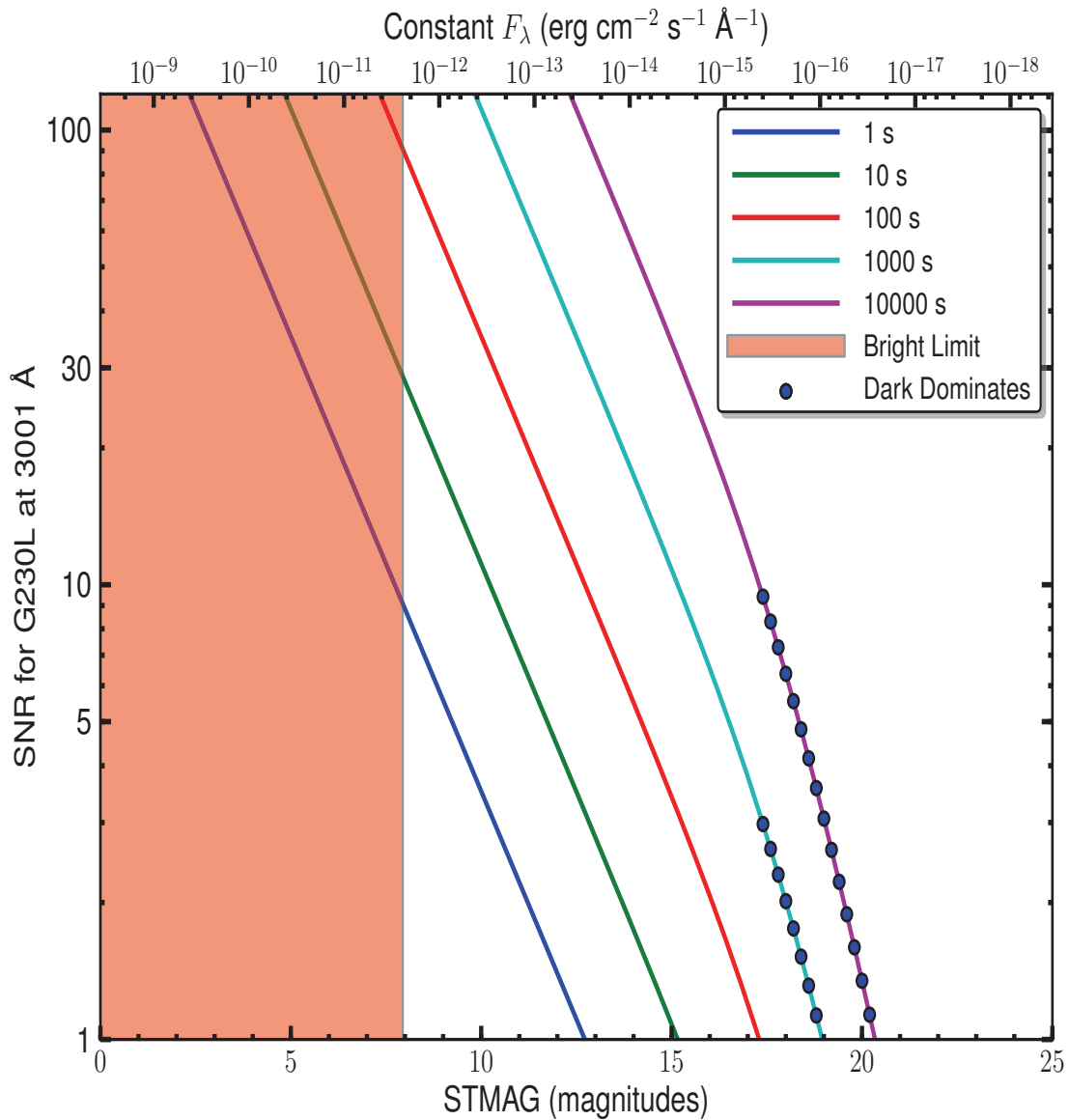
Wavelength (Å)	Sensitivity (counts pixel ⁻¹ sec ⁻¹ per erg cm ⁻² sec ⁻¹ Å ⁻¹)	Effective Area (cm ²)	Wavelength (Å)	Sensitivity (counts pixel ⁻¹ sec ⁻¹ per erg cm ⁻² sec ⁻¹ Å ⁻¹)	Effective Area (cm ²)
1600	1.6E11	6.10E00	2600	2.5E13	5.77E02
1700	8.2E12	2.92E02	2700	2.3E13	5.14E02
1800	1.3E13	4.39E02	2800	2.0E13	4.31E02
1900	1.7E13	5.44E02	2900	1.6E13	3.36E02
2000	2.0E13	6.22E02	3000	1.1E13	2.31E02
2100	2.3E13	6.80E02	3100	6.8E12	1.33E02
2200	2.5E13	6.93E02	3200	3.3E12	6.19E01
2300	2.6E13	6.95E02	3300	5.0E12	9.14E01
2400	2.6E13	6.66E02	3400	8.1E12	1.45E02
2500	2.5E13	6.15E02			

Figure 14.23: G230L Point Source Sensitivity for PSA and BOA



G230L Signal-to-Noise Ratio

Figure 14.24: Point Source Signal-to-Noise as a function of STMAG for G230L



The top axis displays constant F_λ values corresponding to the STMAG units ($V+STMAG_\lambda$) on the bottom axis. Recall that $STMAG=0$ is equivalent to $F_\lambda = 3.63E-9 \text{ erg cm}^{-2} \text{s}^{-1} \text{\AA}^{-1}$. Colors refer to exposure times in seconds. The edge of the shaded area corresponds to the bright-object screening limit. Use of the PSA is assumed.

14.4 Line-Spread Functions

Model Line-Spread Functions (LSFs) for the COS gratings have been computed from the expected aberration of the COS + *HST* optical telescope assembly (OTA) system, the OTA pupil geometry, the OTA mid-frequency wavefront errors (as determined by Krist & Burrows 1995), and estimates of the point response function of the detectors.

The FUV LSF models were calculated at the nominal central wavelength setting of each FUV medium-resolution grating (1309 Å and 1600 Å respectively, for G130M and G160M) and at intervals of 50 Å over the full range of wavelengths covered by each grating. While the aberrations change slightly as the grating is moved to other settings, changes to the LSF at different grating positions are expected to be small.

The NUV optical models assume no variation between gratings or central wavelength settings, since we are dealing with planar gratings used in a collimated beam. The LSFs were computed at intervals of 100 Å over the full spectral range covered by the COS NUV gratings.

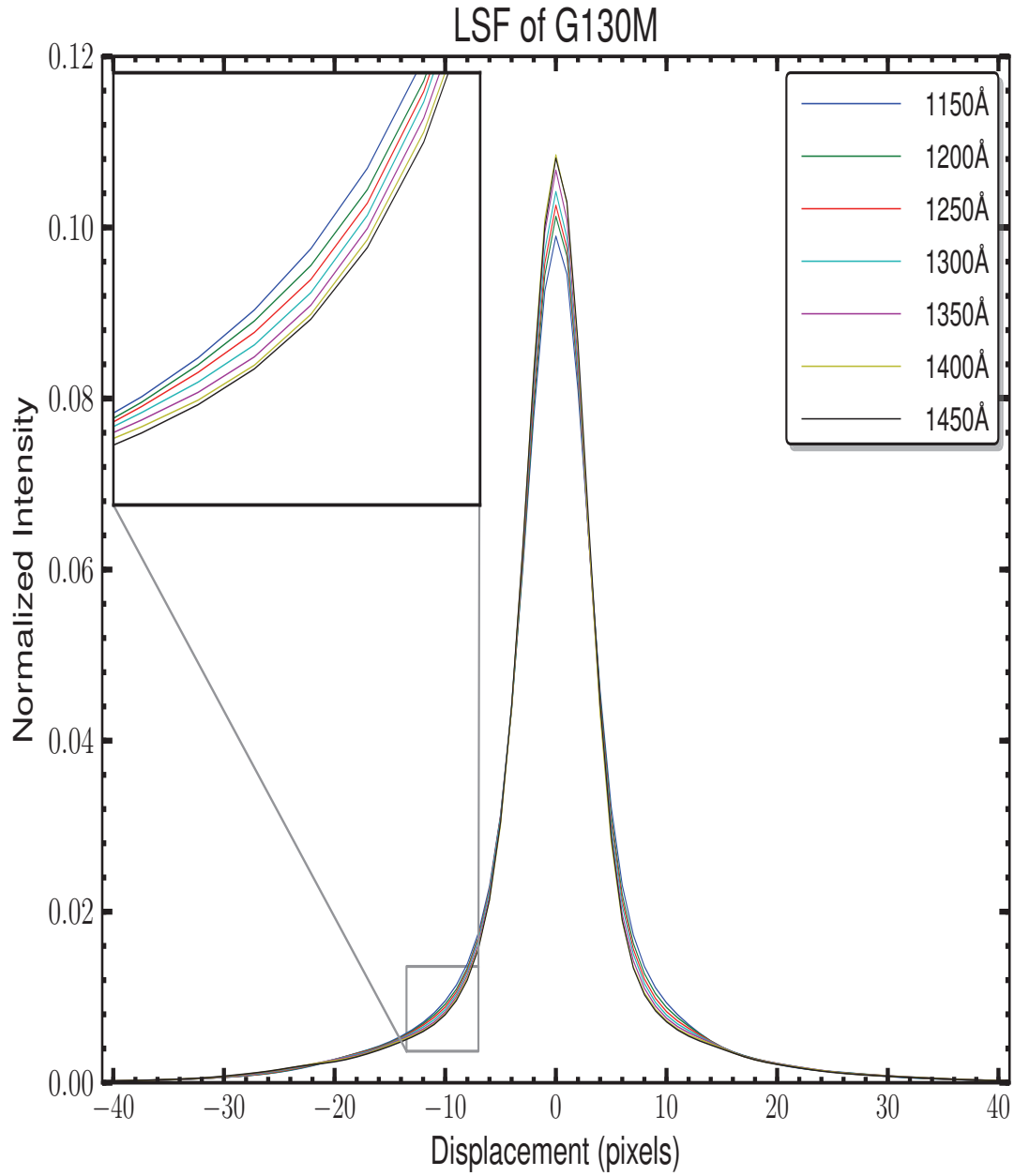
More detailed descriptions of the COS LSF are available in [COS ISR 2009-01](#).

Line Spread Functions:

- ["G130M," page153.](#)
- ["G160M," page154.](#)
- ["G140L," page155.](#)
- ["NUV Gratings," page156.](#)

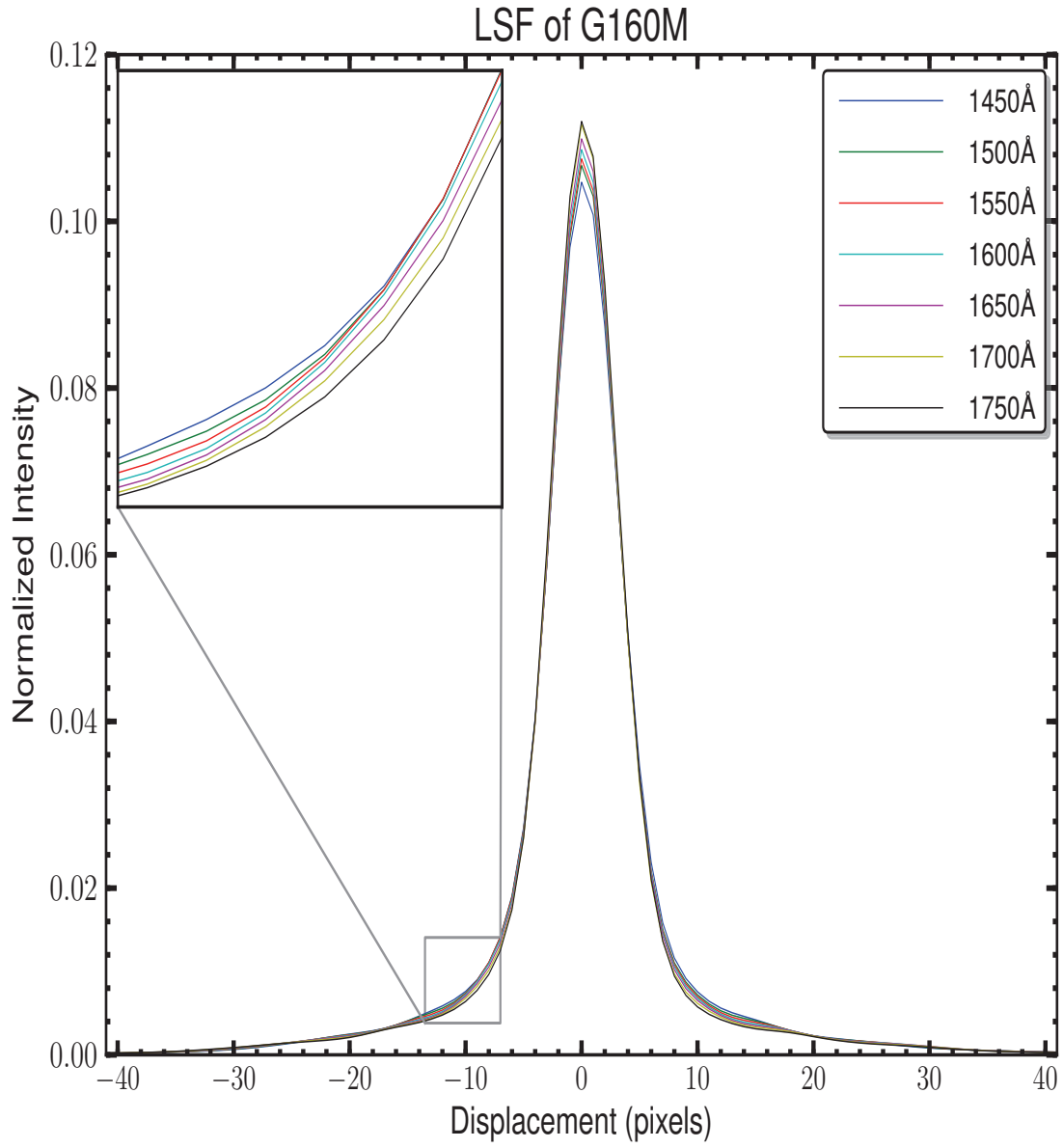
G130M

Figure 14.25: Line Spread Functions of G130M as a function of wavelength.



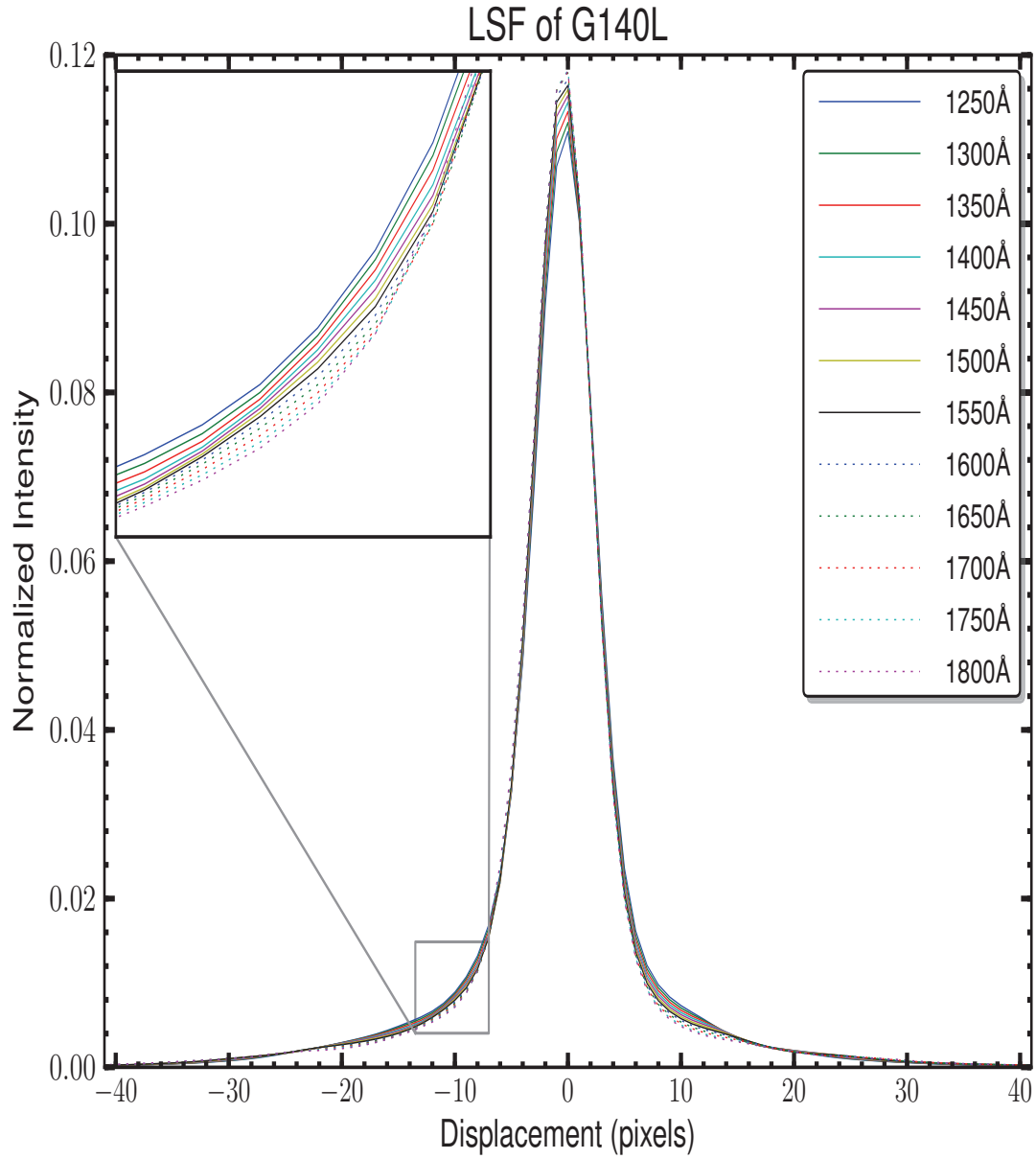
G160M

Figure 14.26: Line Spread Functions of G160M as a function of wavelength.



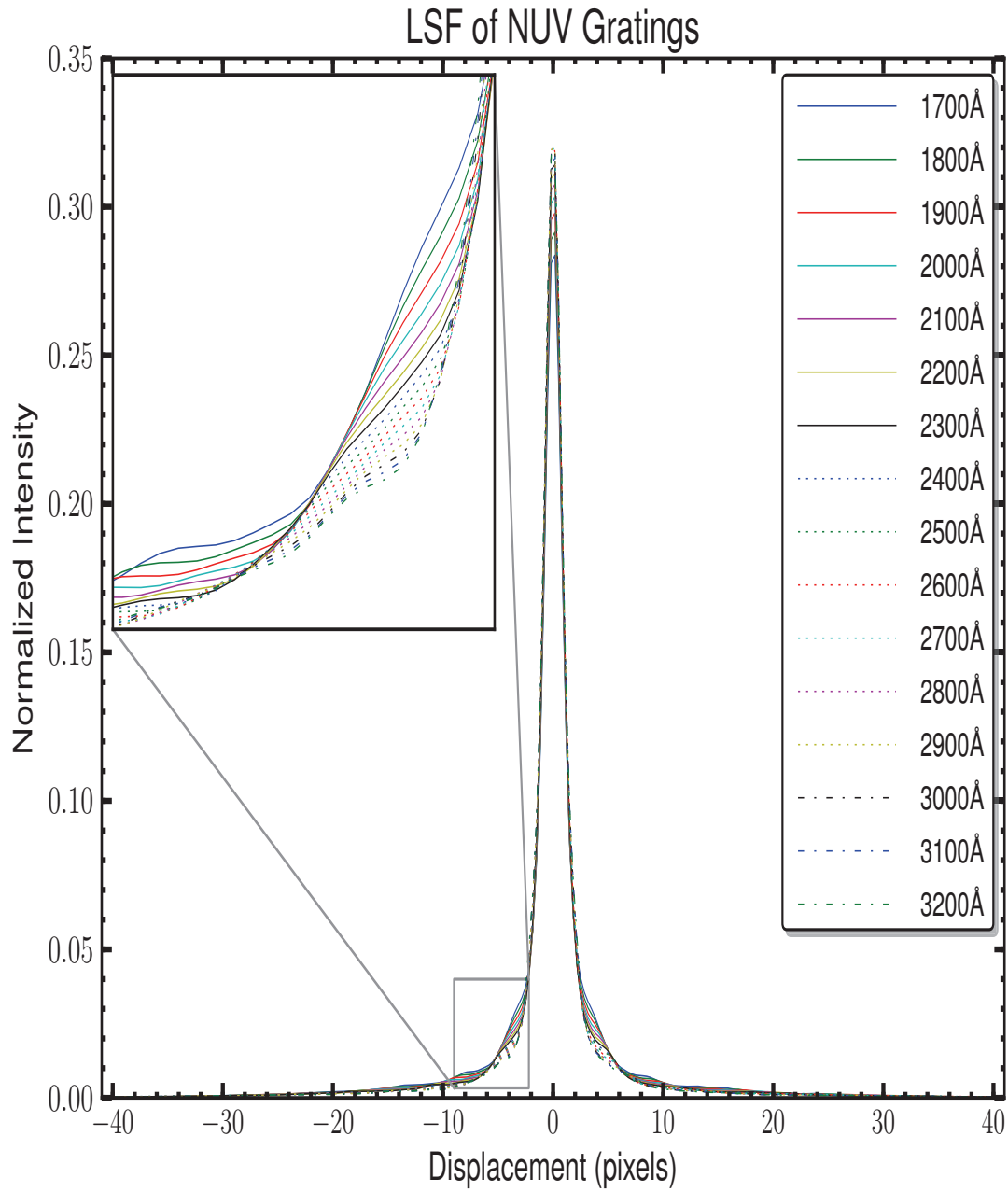
G140L

Figure 14.27: Line Spread Functions of G140L as a function of wavelength.



NUV Gratings

Figure 14.28: Line Spread Functions of NUV Gratings as a function of wavelength.



Spectrograph Design Parameters

In this chapter...

A.1 FUV Channel / 157
A.2 NUV Gratings / 158

A.1 FUV Channel

Table A.1 presents design parameters of the FUV spectrograph and gratings. The FUV gratings are concave and have holographically-generated grooves to provide dispersion and correct for astigmatism. The gratings have aspherical surfaces to correct for *HST*'s spherical aberration. The FUV “M” gratings have been ion etched to produce triangular groove profiles for better efficiency. The G140L grating has grooves with a laminar profile. All FUV gratings are coated with MgF₂ over aluminum.

The surface of the optic is a sphere of the quoted radius, but with a deviation of $\Delta z = a_4 r^4 + a_6 r^6$, where z is measured along the vertex normal. The quantities γ , δ , r_c , and r_d are the standard positions of the recording sources as defined in Noda, Namioka, and Seya (1974, J. Opt. Soc. Amer., 64, 1031).

Table A.1: Design Parameters for the FUV Spectrograph and Gratings.

Dimension	G130M	G160M	G140L
secondary mirror vertex to aperture (z , mm)	6414.4		
V_1 axis to aperture (mm)	90.49		
aperture to grating (mm)	1626.57		
α (degrees)	20.1	20.1	7.40745
β (degrees)	8.6466	8.6466	-4.04595
$\alpha - \beta$ (degrees)	11.4534		
grating to detector (mm)	1541.25		
detector normal vs. central ray (degrees)	9.04664		
nominal groove density (lines mm^{-1})	3800	3093.3	480
radius of curvature (mm)	1652	1652	1613.87
a_4	1.45789×10^{-9}	1.45789×10^{-9}	1.33939×10^{-9}
a_6	-4.85338×10^{-15}	-4.85338×10^{-15}	1.4885×10^{-13}
γ (degrees)	-71.0	-62.5	10.0
d (degrees)	65.3512	38.5004	24.0722
r_c (mm)	-4813.92	-4363.6	3674.09
r_d (mm)	5238.29	4180.27	3305.19
recording wavelength (\AA)	4880		

A.2 NUV Gratings

Table A.2 presents design parameters of the NUV gratings. The NUV gratings are flat and were not constructed holographically. The NUV MAMA has low but measurable sensitivity at FUV wavelengths, and with some gratings second-order light could contaminate the spectrum. To minimize this effect, the coated optics are optimized for wavelengths above 1600 \AA . Given the four reflections used in the NUV channel, wavelengths below 1600 \AA , including geocoronal Lyman α , are effectively eliminated. In addition, gratings G230L and G285M have order-blocking filters mounted directly on them to block the second-order spectra below 1700 \AA . Even with these filters, it is possible for second-order light with G230L to appear on the NUV MAMA, especially in the long-wavelength stripe.

Table A.2: Design Parameters for the NUV Gratings.

Dimension	G185M	G225M	G285M	G230L
groove density (mm ⁻¹)	4800	4800	4000	500
α (degrees)	27.24	33.621	35.707	5.565
β (degrees)	25.85	32.23	34.32	1.088
coating	Al + MgF ₂	Al only	Al only	Al + MgF ₂

Glossary

A Glossary of Terms and Abbreviations

ACCUM

Operating mode for COS in which only the locations of detected photons are recorded; no time information is recorded. ACCUM mode is designed for brighter object with higher count rates. See also TIME-TAG.

Along Dispersion (AD)

The dispersion direction, corresponding to the X axis on both the FUV and NUV detectors.

Aperture Mechanism (ApM)

The Aperture Mechanism is used to place either the BOA or PSA into position as the science aperture. The ApM is also moved to place the FCA into position if a flat-field exposure is to be taken.

APT

The Astronomer's Proposal Tool, software provided by STScI for writing Phase I proposals and Phase II programs. The use of APT is encouraged in all cases, even for Phase I proposals, because it provides an accurate estimate of the actual time needed to obtain an observation. For more information, go to

<http://apt.stsci.edu>

BOA

Bright Object Aperture, which is 2.5 arcsec in diameter with a neutral-density filter that attenuates flux by a factor of about 200.

calcos

The COS calibration pipeline, a software package that performs image and spectroscopic data reduction to produce output files useful for scientific analysis.

central wavelength

For the NUV gratings, the central wavelength is the approximate midpoint of the stripe B spectrum. For the FUV gratings, the central wavelength refers to the shortest wavelength recorded on segment A (though that value is subject to change as the instrument calibration improves).

channel (FUV or NUV)

One of the two COS optical systems, FUV and NUV, including mirrors, gratings, and detectors.

ETC

Exposure Time Calculator, software provided by STScI to estimate exposure times needed to achieve, say, a given signal-to-noise level on a source. Although information is provided in this handbook on exposure estimation, the ETC provides the most accurate way to determine the exposure times required to acquire or observe an object. The ETC is used together with the APT to plan *HST* observations. For more information, go to

<http://www.stsci.edu/hst/cos/software/planning/etc>

FCA

Flat-field Calibration Aperture, the aperture through which the on-board deuterium lamps illuminate the COS optical system.

FGS

Fine Guidance Sensor. By tracking guide stars, the three FGSs can maintain the pointing stability of *HST* with a precision of 2 mas or less.

FP-POS

A command used to move the spectrum on the detector (in the dispersion direction) to reduce the effects of fixed-pattern noise.

FUSE

Far Ultraviolet Spectroscopic Explorer, a moderate-resolution ($R \sim 15,000$), far-UV spectrograph that used micro-channel plate detectors similar to those employed by the FUV channel of COS.

FUV

Far ultraviolet, the channel of COS that spans wavelengths from less than 900 to 1800 Å.

Galex

Galaxy Evolution Explorer, a NASA mission observing the sky in two ultraviolet bandpasses. *Galex* data are useful for determining the UV fluxes of COS targets. For more information, go to

<http://www.galex.caltech.edu/>

GSC2/IRCS

Guide Star Catalog II / International Celestial Reference System. The GSC2 is an all-sky optical catalog based on 1" resolution scans of the photographic Sky Survey plates from the Polomar and UK Schmidt telescopes. The ICRS is the fundamental celestial reference system adopted by the International Astronomical Union for high-precision astrometry. Uncertainties in this system are dominated by the 0.3" uncertainty of the GSC2.

GTO

Guaranteed Time Observer, a member of the COS science team who has been granted a share of telescope time as part of their involvement in designing and building COS.

home position

The default position for a mechanism. COS is reconfigured at the start of each visit, and mechanisms are returned to their home positions. For the ApM, the home is the PSA; for OSM1, home is G130M, CENWAVE=1309; and for OSM2, home is G185M, CENWAVE=1850.

IDT

Instrument Development Team, NASA's term for the group that proposed and built COS.

LSF

Line Spread Function, the shape of a spectral feature emitted by a monochromatic point source.

MAMA

Multi-Anode Micro-channel Array, a photon-counting UV detector, used in the NUV channel.

MAST

The Multi-mission Archive at Space Telescope, which makes available data from a number of NASA missions, including *HST*. Go to

<http://archive.stsci.edu>

MCP

Micro-Channel Plate, a resistive glass plate with 10-15 micron-sized holes used within both the XDL and MAMA detectors to amplify photo-electrons into charge pulses large enough for downstream electronic processing.

MIRRORA, MIRRORB

MIRRORA and MIRRORB are used for NUV imaging in COS. MIRRORA provides the highest throughput. MIRRORB uses a reflection off of the order-sorting filter of MIRRORA to get lower throughput, which can be helpful when observing brighter targets.

NUV

The near ultraviolet channel of COS. It spans wavelengths from ~1650 to 3200 Å.

OSM1, OSM2

The Optics Select Mechanisms on COS that place gratings or mirrors in the optical path.

OTA

Optical Telescope Assembly, *HST*'s optical system of primary and secondary mirrors, plus the structure that holds them and maintains alignment.

pixel

The basic stored unit of data. In the NUV channel, MAMA pixels correspond to physical portions of the detector. In the FUV channel, the position of a detected event is assigned to a pixel based on calculations, but there are no physical pixels as such.

PHD

Pulse-Height Distribution, a histogram of the charge cloud sizes collected in a particular exposure or portion thereof. The PHD is a useful measure of data quality and is recorded as a data product for FUV exposures. PHD data are not available for NUV exposures.

POS TARG

The “POS TARG X, Y,” special requirement is used to request a target offset in APT. POS TARG offsets are specified in the COS user coordinate system, which is used in all COS data products ([Section 3.2](#)). Note that the POS TARG coordinates represent motion of the target in the aperture; the telescope moves in the opposite direction.

PSA

Primary Science Aperture, a circular aperture 2.5 arcsec in diameter and completely open.

PSF

Point Spread Function, the two-dimensional distribution of light produced by the *HST*+COS optics.

resel

Resolution element of a spectrum or image. For spectra, a resel corresponds to the FWHM of a narrow wavelength-calibration line. Using pre-flight data, resels were determined to be roughly 6 pixels wide (dispersion direction) by 10 tall for the FUV channel and 3×3 pixels for the NUV. On-orbit data suggests that the FUV resel is somewhat larger than this, while the NUV resel is somewhat smaller. Note that spectra are recorded in pixel units and that any rebinning into resels is performed on the ground during data reduction.

segment

The COS FUV detector consists of two independent segments. In all spectroscopic modes, the long-wavelength end of the spectrum falls on segment A, and the short-wavelength end on segment B.

SMOV

Servicing Mission Observatory Verification, the period immediately following a servicing mission in which *HST*'s instruments are activated, tested, and made ready

for science observing. Only a minimal set of calibrations are done in SMOV to confirm instrument performance; more detailed calibrations are performed in the ensuing cycle.

stim pulse

Artificially-induced events on each segment of the FUV detector. The stim pulses allow for the correction of thermal distortion and aid in determining the dead-time correction.

STMAG

In this system, the flux density is expressed per unit wavelength, and the reference spectrum is flat in F_λ . $STMAG = -2.5 \log F_\lambda - 21.10$.

stripe

To accommodate the NUV detector format, COS NUV spectra are split into three non-contiguous stripes, each of which covers a relatively small range in wavelength.

TAGFLASH

Use of TIME-TAG mode with FLASH=YES selected. This adds wavelength calibration spectra at periodic intervals during a PSA TIME-TAG observation so that any drifts of the spectrum due to residual motion of the optics can be removed.

TIME-TAG

A COS observing mode in which the locations (pixels) and times (to the nearest 32 msec) are recorded for each detected photon. Doing this consumes memory but allows great flexibility in reducing and analyzing the data.

wavecal

A wavelength calibration exposure; i.e., an exposure of the Pt-Ne wavelength calibration lamp through the WCA.

WCA

Wavelength Calibration Aperture, which is illuminated by a Pt-Ne wavelength calibration lamp.

XD

Cross-dispersion direction, corresponding to the Y axis on both the FUV and NUV detectors.

XDL

Cross Delay Line, the type of detector used in the FUV channel of COS.

Index

A

- ACCUM mode 16, **46**
 - Doppler correction 46
 - pulse-height data 46
- ACQ 68
- acquisitions 16, **66–81**
 - ACQ/IMAGE 72
 - ACQ/PEAKD 75
 - ACQ/PEAKXD 74
 - ACQ/SEARCH 68
 - spiral pattern 69
 - centering accuracy and photometry 77
 - early (preliminary images) 81
 - exposure time
 - dispersed-light 77
 - imaging 76
 - offset target 81
 - overhead times 95
 - recommended parameters (table) 80
- airglow - see background rates
- apertures 11–12
 - BOA 11
 - FCA 12
 - PSA 11
 - table 11
 - WCA 11
- ApM - see mechanisms, ApM

B

- background rates 104–110
 - airglow 105, 108
 - detector 104
 - Earthshine 106
 - geocoronal 108

- Moon 106
 - second-order light 39
 - tables 109
 - zodiacal 106
 - zodical 105

- BOA - see apertures, BOA
- bright-object protection 82–89
- BUFFER-TIME estimation 47

C

- calibration accuracies 18
- calibration observations 118–122
 - Cycle 17 120
 - Cycle 18 122
 - Cycle 19 122
 - ground testing 119
 - SMOV 119
- Cardelli extinction model 111
- COS
 - compared to STIS 4–6
 - focal plane schematic 9
 - optical design 10–15
 - team members ix
- Cycle 17 calibration observations 120
- Cycle 18 calibration observations 122
- Cycle 19 calibration observations 122

D

- dark rate 18, **105**
- data products 115–117
- dead time
 - FUV 25
 - NUV 28

detector non-linear effects - see dead time
 detector plate scale 17
 Doppler correction
 ACCUM mode 46
 TIME-TAG mode 45

E

Earthshine - see background rates
 effective area
 FUV point source 37
 NUV imaging 63
 NUV point source 37
 ETC 102–114
 examples
 observing sequences 97–101
 using the ETC 112–114
 exposure time
 acquisitions
 dispersed-light 77
 imaging 76
 estimating with ETC 112–114
 valid values 47
 wavecal exposures 47
 Exposure Time Calculator - see ETC
 EXTENDED optional parameter 57
 extinction 111
 Cardelli model 111

F

FCA - see apertures, FCA
 flat-field quality 53
 flux precision 42
 FP-POS optional parameter 55
 Frequently-Asked Questions 2
 FUV channel
 detector 20–26
 bright-object protection procedures 90
 characteristics (table) 18
 count-rate limits 18
 dark rate 18, **105**
 dead time 25
 dead-time constant 18
 format 21
 photocathode 18

 pulse-height distribution 23
 quantum efficiency 18
 segment gap coverage 49
 sensitivity adjustments 26
 single-segment observations 50
 stim pulses 23
 effective area 37
 grating parameters 36
 optical design 13
 structure in dark images 25
 wavelength settings and ranges 58

G

G130M grating 128
 new CENWAVE settings 131
 G140L grating 137
 G160M grating 134
 G185M grating 140
 G225M grating 143
 G230L grating 149
 G285M grating 146
 Gain Sag 24
 Galactic extinction - see extinction
 geocoronal emission - see background rates
 grating parameters 36
 ground testing 119

H

HST
 apertures and focal plane 7–9
 wavefront errors 29

I

Instrument Development Team (IDT) members
 ix

L

line-spread function **29–31**, 152

M

mechanisms
 ApM 11
 OSM1 12

OSM2 14
 shutter 10
 MIRRORA 14
 MIRRORB 14

N

Number_of_Iterations optional parameter 46
 NUV channel
 detector 26–28
 bright-object protection procedures 91
 characteristics (table) 18
 count-rate limits 18
 dark rate 18, **105**
 dead time 28
 dead-time constant 18
 format 27
 MAMA properties 26
 photocathode 18
 point-spread function 31
 quantum efficiency 18
 spectral gap coverage 49
 effective area 37
 grating parameters 36
 imaging 61–65
 optical design 14
 vignetting 44
 wavelength settings and ranges 59

O

OSM1 - see mechanisms, OSM1
 OSM2 - see mechanisms, OSM2
 overhead times 92–101
 acquisitions 95
 first-exposure adjustment 96
 generic observatory times 93
 OSM1 movements 94
 OSM2 movements 94
 science exposures 95

P

photometric precision 42
 plate scale - see detector plate scale
 point-spread function 29–31
 of NUV MAMA 31

PSA - see apertures, PSA
 pulse-height distribution 23

R

resolution
 imaging 64
 spatial 41
 spectroscopic 31, 40
 (table) **36**
 temporal (TIME-TAG mode) 45
 resolution element (resel) 15
 resolving power 40

S

Scattered light, internal 43
 second-order light 39
 SEGMENT optional parameter 50
 sensitivity 124
 shutter - see mechanisms, shutter
 signal-to-noise ratio
 estimating 104
 improving 53
 plots 124
 see also exposure time, estimating
 SMOV calibration observations 119
 SNAP programs 4
 spectrograph design parameters 157–158
 spectroscopic modes - see grating parameters
 stim pulses 23
 STIS compared to COS 4–6
 STMAG system 124
 STScI Help Desk ii

T

TAGFLASH 51
 exposure durations 52
 target acquisitions - see acquisitions
 TIME-TAG mode 16, **45**
 BUFFER-TIME estimation 47
 Doppler correction 45
 pulse-height data 45

U

units and conventions 2

User Support ii

W

wavecal - see wavelength calibration

wavelength accuracy

specifications 42

wavelength calibration 50–53

AUTO 51

TAGFLASH 51

user-specified 53

wavelength settings and ranges (table) 58

wavelengths, units and convention 2

WCA - see apertures, WCA

X

XDL - see FUV channel

Z

zodiacal light - see background rates